# An Investigation into the Effects of Resonant Acoustic Mixing on Energetic Materials

Jordan Marie Homan
Imperial College London, Department of Shock Physics

A thesis submitted for the degree of Doctor of Philosophy

November 2019

**Declaration of Originality**

This study is comprised of my own research. Any research conducted by other people has been credited.

**Copyright Declaration**

**Acknowledgements**

This research could not have been conducted without the support of both the Royal Commission of the Great Exhibition of 1851 and QinetiQ. My sincerest thanks to both organisations. Additionally, thank you to the Weapons Science Technology Centre (WSTC) for their support with the Mix Theory experimentation.

There are several people I would like to thank and acknowledge. At Imperial College London, thank you to my supervisor Bill Proud for your technical expertise and guidance throughout this process. Thank you also to David Sory, who conducted the data analysis for the high strain rate testing.

At QinetiQ there are countless people I could thank and acknowledge. Firstly, my industrial supervisor Dave Tod whose expertise helped me work out the answer to many a technical question. Paul Steward who has suffered through countless conversations, giving great advice and convincing me to use the streak camera on the VoD experiments. Nick Johnson for his all-round technical experience and finally, Doug Furze.

# Abstract

Energetic materials are highly complicated composite materials, designed to produce tailored outputs. A large part of their behaviour depends on the sample being a homogeneous material. As such, the processing of energetic materials is critical to optimise performance. Traditional methods are based around intrusive blade mixers, which take time, and due to safety considerations, do not necessarily produce a consistent material. Resonant acoustic mixing (RAM) is a novel non-intrusive technique which propagates acoustic vibrations into a sealed sample vessel. It is more efficient in both time and material, and opens up avenues for mixing novel materials.

This programme is a comparative study designed to determine if RAM impacts energetic materials in comparison to a planetary mixed baseline. Starting with two-phase inert composites the composition was scaled up to a mimic PBX and then to a live PBX. A variation of characterisation was conducted; mechanical testing was conducted via dynamic mechanical analysis, hardness testing and split Hopkinson pressure bar. Thermal characterisation was conducted by thermo mechanical analysis and differential scanning calorimetry/thermogravimetric analysis. Chemical analysis was conducted by nuclear magenetic resonance and density testing was conducted by pycnometry. In addition, hazard testing and functionality testing was conducted on the explosive samples.

The research found that mixing via RAM did not impact the material; however, it also highlighted a potential limitation. Several of the RAM compositions demonstrated significantly weaker mechanical properties due to poor curing of the binder caused by inconsistent distribution of the isocyanate through the material.

# List of Contents

# Table of Figures

# Table of Tables

# Table of Equations

# List of Abbreviations

| | |
|---|---|
| AFM | Atomic Force Microscopy |
| AN | Ammonium Nitrate |
| ANOVA | Analysis of Variance |
| AO | Antioxidant |
| AP | Ammonium Perchlorate |
| API | Active Pharmaceutical Ingredient |
| ARDEC | Army Research, Development and Engineering Centre |
| DCPD | Dicyclopentadiene |
| DMA | Dynamic Mechanical Analysis |
| DOA | Dioctyl Adipate |
| DOS | Dioctyl Sebacate |
| DSC | Differential Scanning Calorimetry |
| DSR | Dynamic Shear Rheometer |
| DSTL | Defence Science and Technology Laboratory |
| EM | Energetic Materials |
| EMTAP | Energetic Material Testing Assessment |
| ESD | Electrostatic Discharge |
| F of F | Figure of Friction |
| F of I | Figure of Insensitive |
| FID | Free Induction Decay |
| GC | Gas Chromatography |
| GIM | Group Interaction Modelling |
| GPC | Gel Permeation Chromatography |
| HMX | High Melting-Point Explosive |
| HTCE | Hydroxyl Terminated Caprolacetone |

| | |
|---|---|
| HTPB | Hydroxyl Terminated Polybutadiene |
| IDP | Isodecyl Perlargonate |
| IM | Insensitive Munitions |
| IPDI | Isophorone Diisocyanate |
| KN | Potassium Nitrate |
| MDI | Methylenediphenyl Diisocyanate |
| NIR | Near Infrared |
| NMR | Nuclear Magnetic Resonance Spectroscopy |
| NQ | Nitroguanadine |
| PBX | Polymer Bonded Explosives |
| PCB | Polychlorinated Biphenyls |
| PEPT | Positron Emission Particle Tracking |
| RAM | Resonant Acoustic Mixing |
| RDX | Research Development Explosive |
| RSD | Relative Standard Deviation |
| SAW | Surface acoustic waves |
| SEM | Scanning Electron Microscopy |
| SHPB | Split Hopkinson Pressure Bar |
| T of I | Temperature of Ignition |
| TDI | Toluene Diisocyanate |
| TGA | Thermogravimetric Analysis |
| TMA | Thermo Mechanical Analysis |
| TMD | Theoretical Maximum Density |
| TNT | Trinitrotoluene |
| TriPhyBi | Triphenyl Bismuth |
| UV | Ultraviolet |
| VOD | Velocity of Detonation |

# 1 Introduction

Energetic materials, also known as explosives, are materials that can release a large amount of stored energy over a very short duration. They are used in a range of applications, from demolition and entertainment through to military applications and each application requires a specific output and behaviour. Energetics is an umbrella classification with multiple sub-categories having specific chemical, behavioural and performance related characteristics [Teipel, 2005] [Agrawal, 2010] [Akhavan, 2004]. A diagram detailing the categories is found in Figure 1.

The sub-categories are as follows:

1. High explosives
2. Low explosives or propellants
3. Pyrotechnics

The defining feature for a high explosive is that detonation occurs at a very high reaction rate and produces high pressure. They produce a detonation wave ranging from 3000 to 9500$s^{-1}$. There are three main types; primary, secondary and tertiary. Primary explosives are very sensitive to a huge range of stimuli; in particular, mechanical, static and thermal stimuli. As such, primary explosives are typically used as ignitors or detonators. Many primary explosives used are lead or silver azide or styphnate compositions; due to new environmental regulations there is a requirement to phase out lead based materials.

Secondary explosives, in comparison, are less sensitive and require sufficient shock to produce a detonation. High explosives tend to be contained molecules which do not require additional materials for detonation. Common secondary explosives include; trinitrotoluene (TNT), research development explosive (RDX) and high melting-point explosive (HMX). To use these materials in a military application, they are modified either through the addition of binders, stabilisers or performance enhancers. These modifiers have different purposes: binders are used to provide an increase in physical stability and a reduction in the vulnerability properties. Explosive vulnerability is a property related to how a material reacts when subjected to an external stimuli. Stabilisers are used to improve the shelf life and delay the ageing mechanisms of explosives, either through reacting with degradation products or providing alternate options for oxidation. Performance enhancers typically improve the blast properties and can either be additional energetic material or metal powders.

These modified energetics are also classed as secondary explosives and there are four key types; melt cast materials, plastic explosives, polymer bonded explosives and pressed materials. All of these materials are particulate composites. The plastic explosives, polymer bonded explosives and pressed explosives all have polymer matrices with solid loadings of typically over 80% mass of HE powders. The melt cast materials have lower solid loading as the matrix is also explosive, usually TNT.

Tertiary explosives are mostly oxidisers such as ammonium nitrates and perchlorates. They are less sensitive than the secondary explosives and have a reduced output unless combined with fuels. When transporting and storing these materials they are classed as oxidisers instead of explosives. They are used as part of a larger complex composition.

Low explosives or propellants are designed to deflagrate or burn, as opposed to detonate and as such have different characteristics, requirements and applications. They produce a large quantity of gas to drive the projectile. There are three main composition types; single base, based on nitrocellulose, double base with nitrocellulose and nitroglycerine and composite, which are comparable to PBXs with a lower solid loading. Propellants are combustible materials with all the oxygen required within the system.

Pyrotechnics are mixtures containing fuels and oxidisers, typically with a binder to provide stability properties. They are designed for combustion and the optimisation of specific outputs, such as sound, light or heat. These are dependent on the final application.

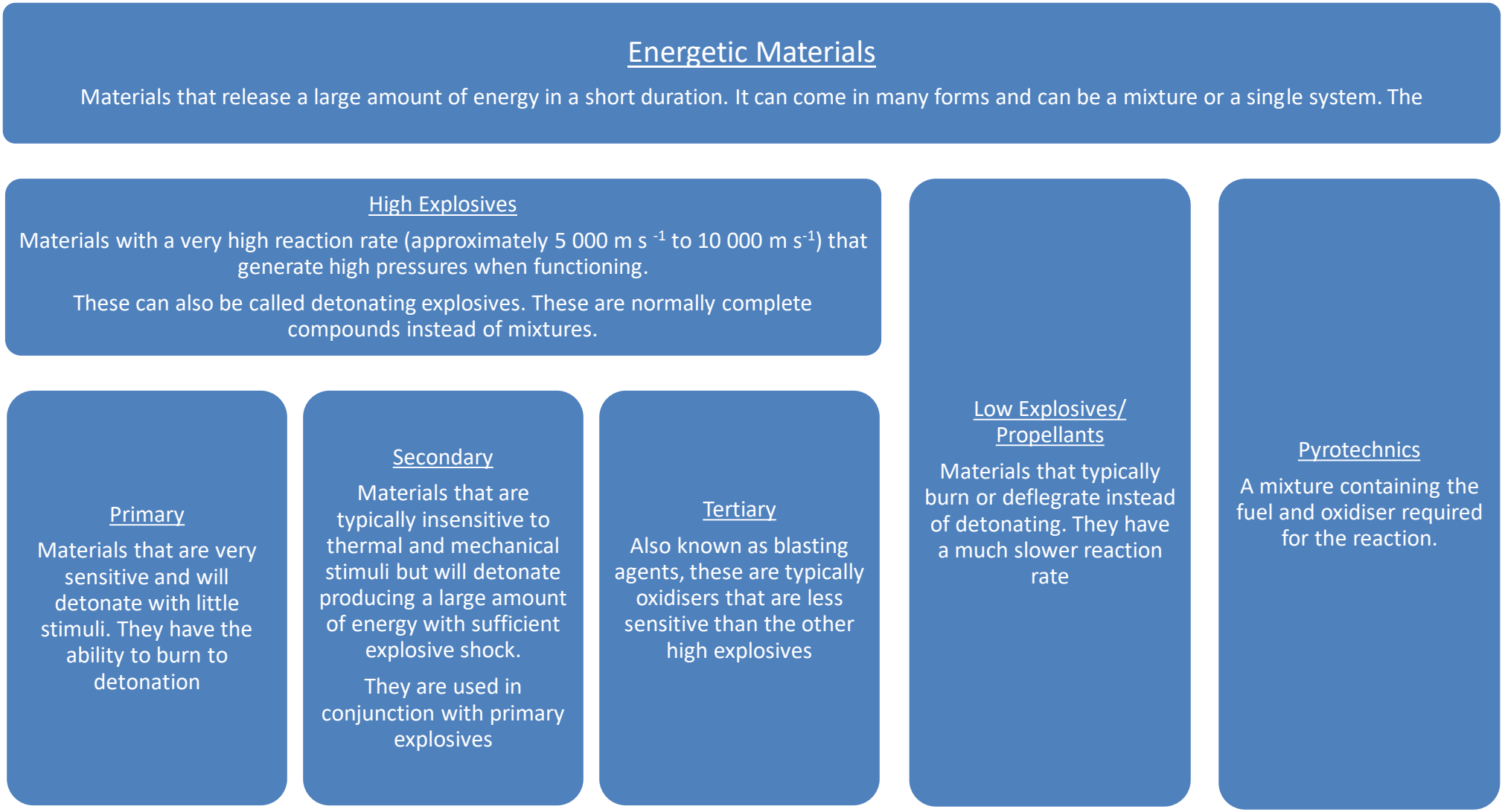


*Figure 1. A diagram demonstrating the explosives classification and explaining the energetic material types*

As mentioned, in order to use the majority of the energetic materials discussed above in a military application requires careful tailoring of the materials behaviour and performance. The energetic substance will be used in a larger material system in order to have successful functionality and in-service materials have highly complex composite compositions with multiple components. As these samples depend on high levels of homogeneity to function as intended it is important to understand and optimise the manufacturing processes.

In terms of mixing explosives, the current processes are based around intrusive blade mixers. These mixers use metal blades that move through the mixture, in a very similar manner to home food mixers. Greater explanation is provided in Chapter 2.2.

Although these techniques are well established, there are limitations. Handling and mixing energetics is a hazardous activity, as such the clearance between the metal blades and the metal bowl has to be increased. Too small a clearance could cause inadvertent initiation through either metal-on-metal contact, and the resulting sparking, or pinching of the explosive crystal which can cause damage and fracture, both are unacceptable. However, by increasing the clearance to a safe amount the “dead zones” increase where mixing does not occur. This is particularly noticeable in the corners of the bowl and along the bottom [Andrews et al, 2020] [Tekchandaney, 2012] [Charles Ross & Son Company, 2011].

In addition, mixing can take multiple days and the sample requires post-processing. Material needs to be decanted from the mix bowl into its intended receptacle which increases processing time and costs, limits the viscosity to enable successful transfer and usually requires machining.

Resonant acoustic mixing is attracting interest within the industry as it can address some of these issues. RAM is a novel mixing method for explosives which utilises acoustic waves to initiate flow within a sample sealed in a mix vessel. This technique provides four key benefits compared to current mixing methods:

1. Mix duration is dramatically shorter when compared to alternative mixing methods. The use of macro- and micro-mixing zones increases mix efficiency, the rate at which a sample is mixed so that there is a consistent distribution of the component parts throughout the sample, and therefore reduces the duration required for mixing. A typical mix period for planetary mixing is an hour whereas LabRAM can have a mix period of 10 to 15 minutes. Multiple mix periods are required for the production of these complex compositions.

2. Planetary mixing is an intrusive technique which uses blades within the sample to induce flow within the sample. Due to the hazardous nature of explosives, mixers are required to have a large blade-bowl clearance to eliminate the risk of pinching or crushing explosive crystals. LabRAM is non-intrusive and theoretically could increase the efficiency of mix.
3. LabRAM samples are sealed in containers clamped onto the RAM base plate; as long as the maximum mass capability of the mixer is not exceeded, there is no limitation on the containers. This provides the opportunity to mix in-case eliminating the requirement for post-processing and reducing wastage.
4. As well as reducing post-processing and wastage, mixing in-case enables an increase in the solid loading and viscosity of potential materials. Materials previously considered hard or impossible to process could be feasible using this mixing technique. This is also the same for complicated geometries that would not be possible to manufacture by casting or machining.

Resodyn produce a range of acoustic mixers and LabRAM was first produced in 2006 [Resodyn, 2016]. As stated, the technique uses acoustic vibrations to encourage flow within the sample propagating vibrations through a base plate into a sample container clamped onto the plate, in Figure 2. Resodyn reports that the acoustic vibrations, at the resonance frequency of the sample container and base plate, ensures that a good mix is achieved through the production of micro-mixing zones. They also state that unlike conventional planetary mixing, the LabRAM mixer has no “dead zones”, areas where little or no mixing is achieved, as the vibrations will propagate throughout the entire system. The resonance frequency, nominally 60 Hz, is determined by a feedback system in the mixer and can vary by ± 3 Hz.

The LabRAM is a bench top mixer that is controlled by the Resodyn software [Resodyn, 2015]. There are two controlling settings: either the power percentage or the acceleration, measured in G. As a side note, the units for acceleration will be consistently capitalised during this study to eliminate confusion with the units for grams. The power percentage and the acceleration can either be modified during mixing or set as a recipe prior to mixing. An in-situ mix chart is produced which plots the mixers input acceleration and power percentage and the frequency of the entire system over time.

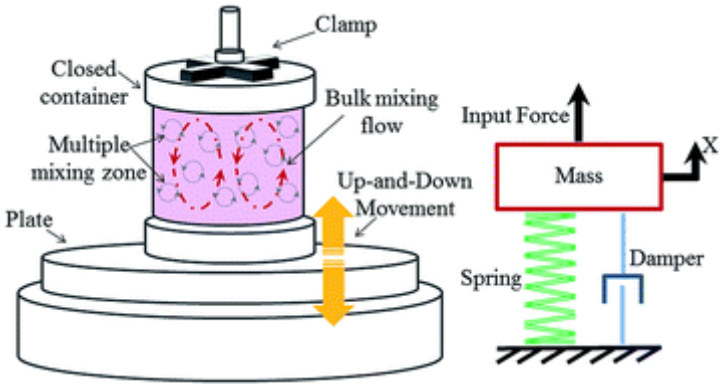


*Figure 2. Diagram demonstrating how LabRAM operates. On the left hand side, the sample is sealed in a vessel that is clamped to the vibrating base plate causing flow within the sample. On the right hand side is the theoretical set up, with a spring and damper causing the mass to move [Tanaka et al, 2016]*

This research and the majority of current published research within the field utilises the LabRAM, which is small scale limited to less than 1kg of material. An area of interest that is outside the scope of this programme is the potential scale up applications. To use this in a manufacturing environment it has to be functional on a larger scale. In terms of scale up, Resodyn do produce larger mixers and have published research comparing three different sized mixers [Coguill et al, 2014]. The materials produced had comparable mechanical properties. However, there has been nothing published on the potential limitations that need to be overcome; these include noise, which would be negated through the requirement to mix remotely, and thermal controls. Temperature increase is a concern for energetic mixing and has been proven to occur when mixing via RAM [Hope et al, 2015]. When mixing, large bulks of polymer based composites have poor thermal dissipation properties; the concern is that the temperature will rise and not be able to dissipate potentially leading to an ignition.

## 1.1 Programme Purpose and Design

The research conducted on RAM has been investigated in Chapter 2.3, however, it can be divided into three groups; technique analysis [Lucon, 2009] [NavSea, 2015], mixing effectiveness [Vanarase et al, 2010] [Hope et al, 2015] and materials characterisation [Bluestone et al, 2010] [Coguill et al, 2014] [Nelson et al, 2012] [Rumeau et al, 2015] [Wilgeroth et al, 2018]. The majority of the research has been conducted by Resodyn who manufacture the mixers. However, the independent research within the energetics industry focuses on functionality and low strain mechanical testing. The papers treat the characterisation separately and do not use a cohesive material science approach, limiting the understanding of the impact of resonant acoustic mixing on the overall material.

This research programme is designed to use the material science approach to answer whether mixing via RAM impacts the material and to fill in gaps in testing, primarily the high strain rate testing and investigating the ageing characteristics. The programme investigated the materials characterisation of a range of inert composites and an energetic composition manufacture by RAM and planetary mixing, and the influences of mixing parameters. A diagram detailing the programme can be found in Figure 3.

Polymer bonded explosives (PBXs) and composite propellants were used as the focus of this research. They have similar compositions; a polymeric binder system with plasticisers, stabilisers and additional processing agents, with energetic fillers ranging upwards of 60% mass solid loading for propellants and 80% for PBXs, and then a curative to chemically cure the binder system. These were chosen due to their complex composition and homogeneity requirement, high chemical and physical stability and low sensitiveness and vulnerability properties. This means there is a smaller risk of initiation due to unintended stimuli.

This programme was a direct comparison to determine whether the mixing method impacted the material. As such, the approach taken to mixing and the mixing parameters remained consistent between the two methods. It was based on the methodology already used with the planetary mixer.

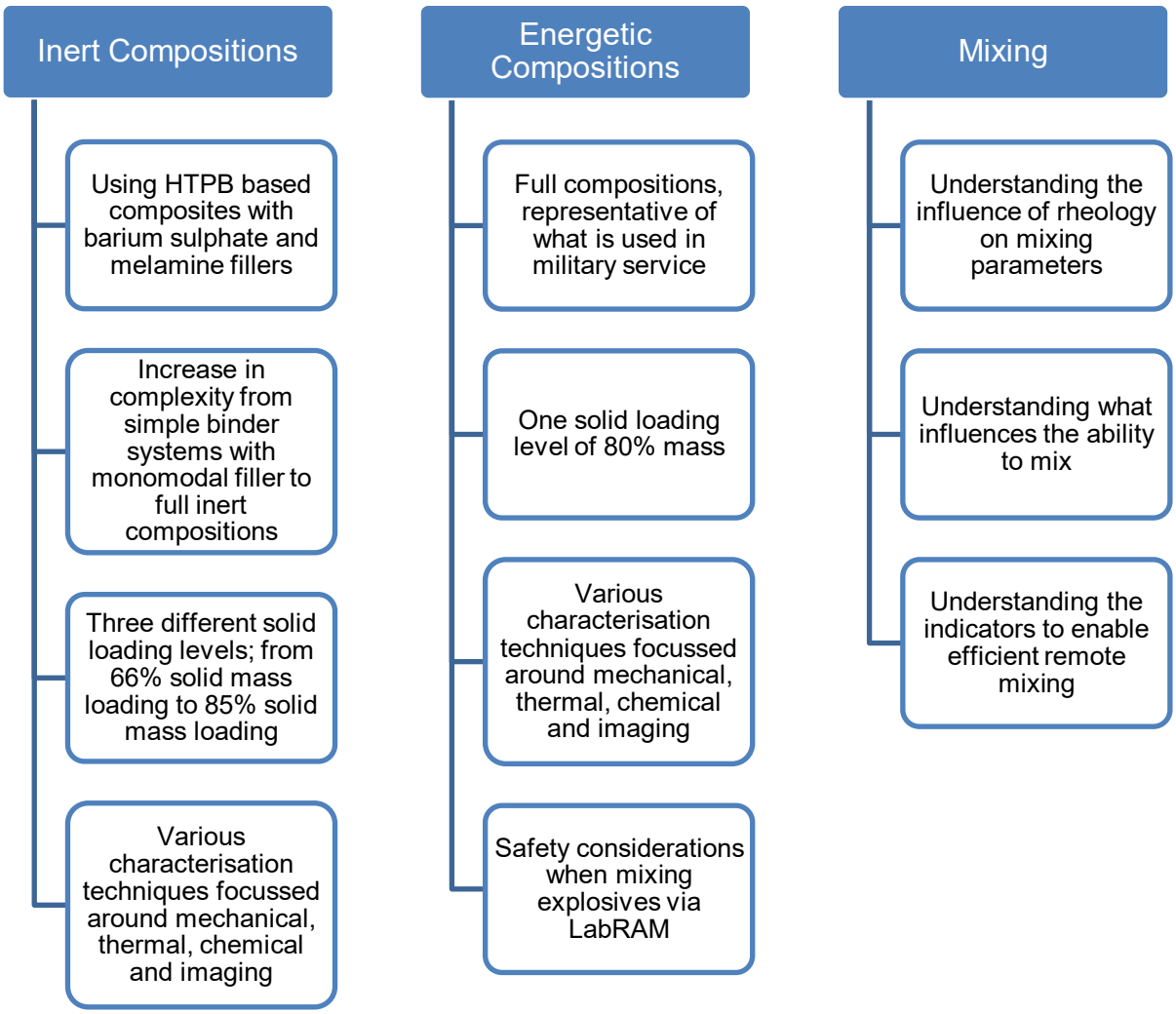


*Figure 3. Diagram demonstrating the three research strands of this programme; inert compositions, energetic composition and mixing theory.*

## 1.2 Programme Structure

The structure of the thesis is as follows:

- Chapter 3- HTPB-Melamine
    - Manufacturing HTPB binder and melamine filler composites
    - Characterisation through dynamic mechanical analysis, differential scanning calorimetry, nuclear magnetic resonance and optical microscopy
- Chapter 4- HTPB-Melamine-Barium Sulphate
    - Manufacturing HTPB binder and melamine and barium sulphate filler composites. The barium sulphate is the fine filler component.
    - Characterisation through dynamic mechanical analysis, hardness testing, density testing, thermomechanical analysis and optical microscopy
- Chapter 5- HTPB-DOS-Melamine-Barium Sulphate
    - Manufacturing HTPB and DOS binder and melamine and barium sulphate filler composites. DOS is a plasticiser which reduces the glass transition temperature and improves the mechanical behaviour
    - Characterisation through dynamic mechanical analysis, split Hopkinson pressure bar testing, moisture diffusion and optical microscopy
- Chapter 6- Full Inert Composition
    - Manufacture HTPB, DOS and AO binder and melamine and barium sulphate filler composites. AO is added to reduce the oxidation of the binder system and extend the shelf life of the material.
    - Characterisation through dynamic mechanical analysis, split Hopkinson pressure bar, differential scanning calorimetry/ thermogravimetric analysis, nuclear magnetic resonance, density, moisture diffusion and optical microscopy
- Explosive Formulation
    - Manufacture of explosive composition. Using a HTPB and DOS binder system and a bimodal distribution of RDX explosive powder.
    - Risk analysis of explosive mixing via RAM
    - Characterisation through hazard testing, dynamic mechanical analysis, nuclear magnetic resonance, density, hardness and functionality testing
- Mixing Theory
    - Analysis of mix behaviour
    - Influence of mass, vacuum and acceleration on mixing
    - Diffusion experimentations

# 2 Literature Review

## 2.1 Introduction

This review covers three topics; methodology and limitations of mixing and processing energetic materials, prior research on the LabRAM mixer and statistical analysis. Each area highlights research within the field, identifies gaps and situates this study.

## 2.2 Processing

Over the last century energetic materials have become highly engineered, using formulations and designs that tailor properties to specific outputs and performance. This can be undermined by inconsistent samples; heterogeneous materials have variation in performance and safety due to either component rich or deficient areas. Large quantities of energetic crystals in contact can cause an initiation. Although traditional material processing is well understood, considerations and modifications are needed for energetics. Traditional methods include planetary mixing, extrusion and melt casting.

### 2.2.1 Planetary Mixing

Planetary mixing is the most common mixing method. It is an intrusive technique using a metal bowl and two spinning blades; one blade remains fixed in the centre of the bowl and the second orbits around it. It is easily recognisable as the design of many at-home food processors. Considerations are made for explosive mixing; bowl-blade clearance is the prime one with increased clearances to reduce both the risk of pinching or crushing explosive crystals and metal-on-metal sparking. Both could cause initiation of the energetic material. The mix blade set up is pictured in Figure 4. This technique is derived from a paddle or propeller mixer. The behaviour depends on the blades; paddle mixers extend between 66 to 90% of the diameter of the vessel typically and rotate between 15 and 45 rpm whereas planetary mixers occupy less of the bowl due to the combination of the moving and stationary blade. The majority of mixing occurs close to the edge and the tips of the blades which cause turbulent flow. By having this second blade rotating around the mixing vessel the turbulent motion around the edges of the blades is increased; depending on the set up of the mixer this can be a result of the possible overlap between the two blades. As the material within the vessel is mainly circulated through the blade movement, it causes centrifugal movement of bulk material out and up the mixing vessel walls and inward and downwards at the surface. Some minor mixing is attributed to shearing motion between the vessel wall and blade. The

paddle mixer is more suitable to liquid-liquid mixing, whereas the planetary mixing can be utilised for pastes and solid-solid compositions. Generally these are all vertical mixers. Horizontal mixers have different properties and behaviours [Matthews, 1982].

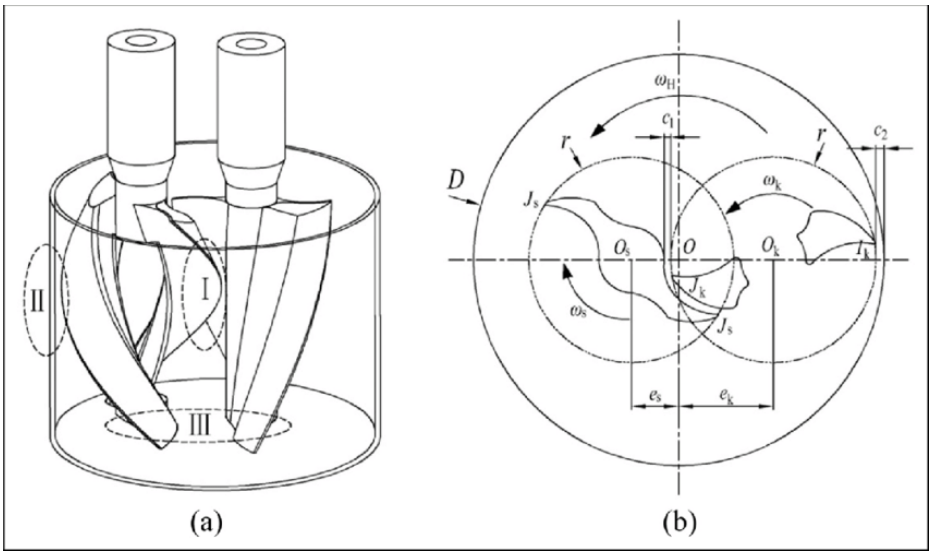


*Figure 4. Diagram demonstrating the layout and movement of planetary mixer blades from a side on (a) and aerial (b) view [Liang et al, 2016]*

Considerations for this technique have been well summarised by Jayesh Tekchandaney [Tekchandaney, 2012]. Concerns like clearance between the blades and the container have already been mentioned; however, other considerations are highlighted. These include blade speed, as the speed needs to be sufficient to ensure the blades do not stall but not too quick to impart excessive energy into the explosive mixture, heat transfer, to ensure that the sample can dissipate heat out and not risk reaching the ignition temperature, vacuum operation, vacuum helps degas the sample but filters need to be sufficient to ensure that the system is not contaminated, and mixer seals, which have to be chemically compatible with the explosive mixture. Further analysis [Charles Ross & Son Company, 2011] using adhesives show that, in comparison to multi-shaft mixers and stationary agitators, planetary mixing offers greater mixing and kneading, with little consideration required of the material's flow properties, interacting with material throughout the entire pot and not just the periphery. With a multi-shaft mixer, if the low-speed anchor cannot produce adequate flow it will carve a path through the material and form high-temperature zones near the dispenser and the rotor assembly. This is unacceptable for explosives. What is of particular interest in this research is the order of material addition; the author recommends starting with the solids and then gradually adding liquids stating that the higher the viscosity, the greater the shear that the material will experience.

Planetary mixing is a batch technique, usually followed by vacuum casting. Mixing efficiency is poor, particularly for energetics due to the increased mechanical clearances. There has been little development in the recent years to the technique, and as such any literature is usually utilising the technique for other areas of research; such as burning rates [Patil et al, 2011] or characterisation of an energetic material [Hamshere, 2003] [Prakash et al, 2004] [Vadhe et al, 2015] [Simic et al, 2013].

Papers, dated pre-2000s, cover processing issues of energetics and planetary mixing. Much of this research [Muthiah et al, 1993] [Muthiah et al, 1996] uses sigma mixers which use a similar principle as a horizontal mixer but with a different type of blade, applying greater shear [Teipel, 2005]. As this study focuses on the vertical planetary mixers these are not relevant. For research specific to planetary mixing a publication from 1990 [Perez et al, 1990] investigated the reasons for variations between batches on PBAN/AP/Al propellant mixed by a Baker Perkins Vertical Planetary Mixer. Part of the discrepancies between batch burning rate was due to propellant being stored before adding the unnamed curing agent. When storing the propellant for 24 hours there was a significant increase in the burning rate; continued storage after this point did not impact the behaviour. A relationship between mechanical behaviour and mixing duration was also reported. Using a baseline of 3 hours of mixing, any additional mixing time produced an increase in the maximum tensile stress. Similarly to the burning time, it reaches what can be considered as a maximum influence of mixing duration to mechanical behaviour; however, the mechanism that causes this was not explained or discussed.

### 2.2.2 Extrusion

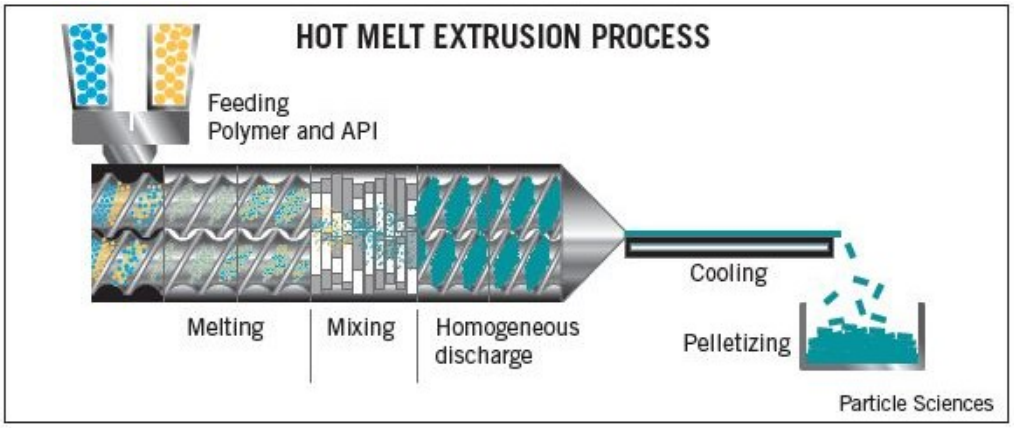


*Figure 5. Hot melt extruder diagram detailing the processing steps [Fenner, 1970]*

Extrusion is the act of pushing material out of a die for a specified cross-section, see Figure 5. It can be a continuous or a batch process. Batch processing uses a set amount of material throughout the entire process; whereas continuous processing continuously feeds material in [Fenner, 1970]. There are two methods of forcing the material out of the die; using a ram or a rotating screw. A rotating screw is commonly used within polymer processing; pellets are introduced at the feed and melted whilst being transported by either a single or double screw down the barrel [Callister Jr, 2007]. It is a popular process for molten polymeric materials because of their good flow properties [Fenner, 1970]. Although traditionally the clearance between the screw and the barrel is small, extruders designed for explosives, in a similar way to planetary mixers, will have an increased clearance. Within the barrel, the mixing is both dispersive and distributive; where dispersive breaks up agglomerations and distributive distributes them through the system. Dispersive mixing depends on the stresses within the system, whereas distributive is the total deformation of the mixture.

A thesis published in 2012 [Tucker, 2012] from Cranfield University investigates the effect of solvent free extrusion on double base rocket propellant. The process was described as mixing then rolling and reworking the material before finally extruding the sample. The authors acknowledged that extrusion submits the material to high thermal and mechanical stresses, which causes mechanical and physical changes to polymeric materials. A homogeneous propellant was produced, attributed to the rolling and reworking phases, although the sample contained what would be considered an above average amount of plasticiser, ~45%. The sample was extruded from a star shaped die with a ~72 mm diameter. A surface sample was taken at a 5 mm depth in the propellant; however, variations could occur within that 5 mm depth. Recommended further research by the author was to investigate smaller steps across the grain in order to gain a more accurate representation. As well as homogeneity in the final sample, they reported a variation of crystalline structure through x-ray measurements. This was mainly attributed to the nitrocellulose.

Further research undertaken in 2015 [Dombe et al, 2015] described continuous extrusion as having a few advantages over batch mixing; there is a limited amount of energetic materials handled within the processing platform at any one point and the complete automation helps provide increased productivity. Constant monitoring and greater surface to volume ratios provide improved heat transfer and more intensive mixing leading to improved quality. Highly filled energetic materials, due to the high viscosity, do not exhibit turbulence or eddy diffusion and do not experience significant molecular diffusion due to time limiting factors. To achieve homogeneous mixing they rely on both distributive mixing and dispersive mixing, also known as macro-mixing and micro-mixing respectively. These mechanisms were studied using

diagnostic techniques such as particle tracking, x-ray or positron emission based, residence time or shear distribution and numerical simulation. Residence time distribution analyses the dispersive and distributive mixing and is expressed in terms of various age distribution functions. A tracer is included and measured at various points. Residence shear distribution determines the shear history inside the extruder, characterised by polymeric micro-capsules containing an organic dye rupturing at predefined shear stresses. This also allows characterisation of shear stresses, which can help with the optimisation of screw geometry and process parameters.

### 2.2.3 Casting

Casting is the solidification of a liquid based material into a mould. Melt casting, where the material is molten, and vacuum casting, where the material is cast under a vacuum, are the primary ones for explosives. Melt casting is popular within the metal industry. Casting is another well-established technique, with known parameters and processes. It is a simple, cheap and flexible method which can scale up for mass production. Voidage can occur with highly loaded viscous materials due to their poor rheological properties. It is not uncommon for charges to have a density of less than 95% of the theoretical density. This affects the output of the charge. Cracking can be a by-product of the solidification process of the material; solidification is usually associated with a decrease in volume and as such material experiences an overall shrinkage and contraction [Akhavan, 2004]. Research [Zhang et al, 2008] assessed the solidification process in-situ through the use of ultrasonics; ultrasonic attenuation identifies the density of the explosive and can detect voids and cracks. A final issue with casting is the risk of inhomogeneous samples, as separation of solid ingredients can occur throughout the solidification process dependent on the relative masses and densities of the components [Akhavan, 2004].

Melt casting is primarily used with Trinitrotoluene (TNT) due to its low melting temperature, 80.4 °C, and high decomposition temperature, around 300 °C. Most high explosives are unstable in their liquid form TNT is not, making it a perfect candidate for melt casting. Research Department Explosive (RDX) and High Melting-Point Explosive (HMX) are now commonly added to improve the performance. TNT is melted by steam heating and additional energetic material is added into the molten TNT in a seeding process. As with most materials, TNT contracts whilst cooling, with an average shrinkage of 11-12%, potentially causing cracking and de-bonding. This causes new burn surfaces, reducing the safety of the material and modifying the energetic output. To address the shrinkage issue, controlled cooling methods can be used and excess material is added to gain a continuous, crack free

sample. TNT/RDX/HMX mixes are the traditional melt cast materials; however, more materials have been developed that are suitable for this process.

Vacuum casting for PBXs is used for moderate solid loadings of high explosives such as RDX or HMX in a polymeric binder system. An example in literature of vacuum casting is PBXN-109, where several moulds were filled sequentially. The vacuum was repeatedly applied and released in order to degas the samples; this was supported by applied vibrations in order to remove any potential air pockets that were trapped within the material [Hamshere et al, 2003]. It has been argued by U.S. Army Research, Development and Engineering Centre (ARDEC) that vacuum casting provides the best mechanical behaviour in comparison to melt cast or pressed materials; however, the other mixing processes did not use a cross linker and are dependent on mechanical force or solidification to bind the material [Cook et al, 2016]. Like planetary mixing, vacuum casting is a technique that is utilised in other research [Turker, 2016].

### 2.2.4 Pressing

Pressing is an alternative technique for materials with too high viscosity for casting. It is used quite commonly with pyrotechnics, as they are typically powdered materials, or very highly loaded materials where there is limited binder system to ensure cohesion. Although pressing has the capability of producing more highly loaded materials compared to casting, the samples can have greater variation in comparison. There is an inherent safety risk with the metal drift and container, which have a small clearance between to keep material within the press increasing the likelihood of initiation. This risk is greater than the risk with mixing and casting [Akhavan, 2004]. There are several variations of this technique; unidirectional, dual directional and hydrostatic or isostatic. Unidirectional pressing applies the force on one face; it is a simple and effective method but can cause some variation in the sample density depending on material amount. Dual direction reduces the likelihood of density gradients as the force is applied on the top and bottom faces, applying pressure towards the middle of the sample. A dual direction press is seen in Figure 6. Hydrostatic and isostatic pressing applies pressure to all available faces of the sample, producing a homogeneously pressed sample; however, it is a much more complicated method. Pressed materials do not need a cross-linker.

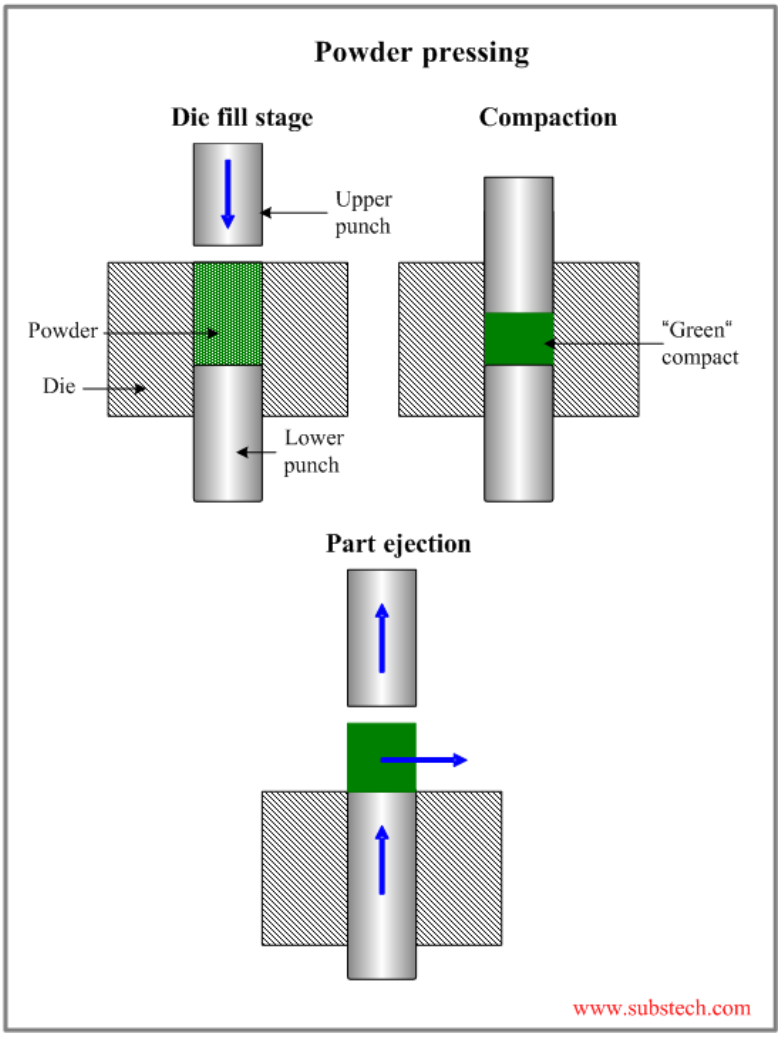


*Figure 6. Diagram demonstrating powder pressing in three steps. The first step is the introduction of the powder and the lowering of the upper punch, the second is the compaction of the powder and the third is the removal of the pressed pellet [Substech.com, 2020]*

Research [Watt et al, 1998] was conducted on TNAZ, and the material was not consistently melt cast, attributed to its complicated crystallization process. However, they produced a pressed TNAZ charge which achieved 99% of its theoretical maximum density (TMD). The sample material when manufactured by melt casting could not reach over 90% density. The pressed TNAZ was believed to be partially melted and sintered, producing high quality pellets.

A study was conducted on the influence of pressing intensity on PBX9501 [Peterson et al, 2003] with particular attention on the microstructure. PBX9501 is highly loaded with almost 95% solid loadings and was pressed into 3 different cylinders of 25.4 mm diameter and 25.4 mm depth. Each cylinder was pressed at a different pressure; 5000, 15000 and 30000 psi with a 100 ton heated steel die press. Pressing occurred at 90 °C under vacuum for two 3-minute durations with a rest period of 3 minutes between. It was found that the average crystal size decreased with an increase in pressing intensity; this is seen between the

different pressing loads and within the sample itself, where towards the centre of the sample there is semi-protected material.

### 2.2.5 Mix stability

Mix stability is dependent on material, composition and properties of individual components. Although mix method is important as it determines conditions and stresses that material is exposed to, it will not have the same impact on every material; hence the reason the composition is the dominating factor. The key indications of mixture instability are dramatic temperature changes and agglomeration or separation of components, forming an inhomogeneous mixture. Mechanisms of inhomogeneity include: creaming, sedimentation, flocculation, phase inversion, coalescence and Ostwald ripening [Tadros, 2013]. Figure 7 demonstrates the different mechanisms schematically; although these are primarily for a liquid-liquid emulsion. Creaming and sedimentation are simple; applied external forces, such as gravitational or centrifugal, exceed the Brownian motion of the filler, dependent on density. Sedimentation is a key concern in polymeric based explosives; curing can take up to a week and powders with too great a density difference can separate from the matrix. Flocculation is the formation of multiple agglomerations, as the van der Waals forces overcomes the repulsive forces. Phase inversion is unlikely to occur without external conditions, as it is the reversal of the discrete filler and continuous binder phase. With regards to solid-liquid and solid-solid mixes, as are used in this research, possible concerns would be evaporation of various liquid components, or breakdown of solid components. Coalescence where liquid droplets merge, arguably, is of little relevance in this research as the focus is on the solid-liquid compositions that then cure to become solid-solid. Similarly, ostwald ripening is of little interest, as the smaller crystals dissolve and redeposit onto larger crystals.

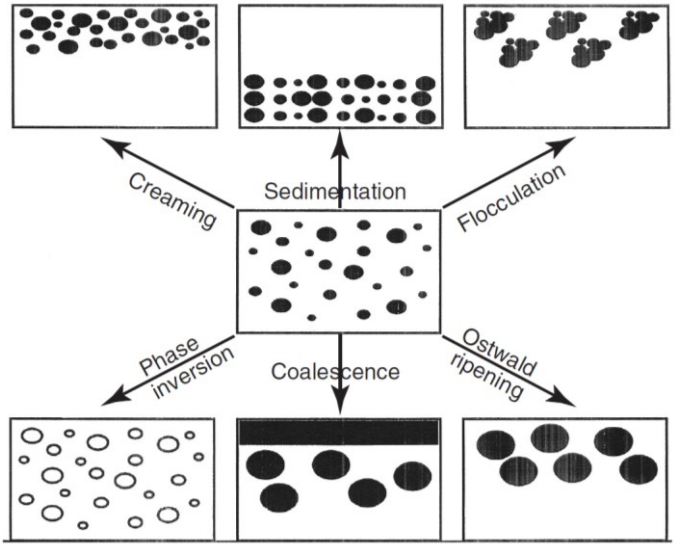


*Figure 7. Diagram indicating the various instabilities in a mixture [Tadros, 2013]*

Determining whether a sample is mixed or not is key to ensuring the homogeneity of a sample; as previously discussed, the materials of interest for this research programme are complex composites with multiple components. Their behaviour, performance and reliability is highly dependent on whether the sample is mixed effectively.

There is no universal definition for key phrases with regards to mixing; however, key ideas reoccur within the literature [Daumann et al, 2008] [Edward et al, 2004] [Harnby et al, 1992] [Sturman, 2012] [Teipel, 2005] [Kang et al, 2012]. The difficulty arises when different phrases can mean very much the same thing. Phrases such as intensity of segregation, mixing quality and information entropy, which both relate to the distribution and segregation of components within the mixture, are good examples of that. There are several methods for determining whether the distribution of the components within the mixture are consistent or not; a visible tracer, particle tracking to determine where particles from various components move through the sample, torque and other measurements from the mix process to determine any rheological transitions in the mixture, image analysis, and probes measuring the composition at any one point.

A visible tracer uses a small amount of material with specific characteristics, such as a dye, to track the distribution within the mixture [Harnby et al, 1992]. It provides a visual aid for determining how components are moving through the sample and is an easy qualitative assessment. Tracers can be used in conjunction with other techniques; one example is using an IR tracer in a sample that does not produce a strong IR signal.

Particle tracking tracks produces a particle distribution at the end of the mix; the more uniform this particle distribution the more mixed the sample. This technique requires flow analysis of the mixer to obtain the velocity field, the particle tracking and then mixing quantification from the obtained particle distribution. Depending on the tracking method, a tracer material may be used. This is a very quantitative method, but does require additional equipment and analysis to fully understand the results [Kang et al, 2012].

Using torque, or other related properties, is a useful method as it can indicate transitions or variation in the rheological behaviour of the mixture. As a sample is mixed the behaviour will transition; when the sample is fully mixed it is expected that the behaviour will remain consistent and any variation seen in the mixing properties will plateau [Teipel, 2005]. Although it is a crude method, it can be highly effective and will give an understanding of the behaviour in real-time. Most mixers already some read out already installed so this methodology does not require additional equipment.

Probes can use a range of characterisation techniques [Harnby et al, 1992], although mainly focus around the infrared. They try to make conclusions about the compositional analysis and any changes over time with the expectation that as the sample is mixed consistently the probe with measure a plateau. Probes can only detect in a finite sampling volume so any changes on a finer scale will not be appropriately detected. As such, it is important to have a sampling volume that detects consistent to the degree that is required.

## 2.3 LabRAM and acoustic mixing

Research in resonant acoustic mixing has three focuses; an analysis of the technique, the effectiveness of the mixing capability and the effect on the material. For most of the published research, the main focus is on the functionality and the mechanical behaviour of the material.

### 2.3.1 Technique Analysis

Analysis of the technique has primarily been conducted by Resodyn. Obviously there are benefits and drawbacks to this; as the main manufacturer Resodyn has a unique understanding of the technology, but the publications are sales documentation.

The technique uses low-frequency acoustic fields, with a frequency around 60 Hz with an applied amplitude of less than 0.3 inches. Designed to operate at mechanical resonance with the system, it is reported that it results in a “virtually lossless transfer” of acoustic energy into the sample, in the form of an acoustic pressure wave. This is internally sensed and controlled to gain the optimum mixing performance for potential materials and mixes. For fluid

compositions, the dominant mixing method is acoustic streaming which forms multiple intense mixing zones with a 50 micron diameter. Solid systems instead depend on particle collisions with the mixing vessel and other particles, causing chaotic motion and bulk mixing [Bickley, 2009]. It differs from ultrasonic mixing which operates at above the audible range, ~20 kHz [Mukdadi, 2004]. Resodyn report that as the frequency is an order of magnitude lower, it has a greater potential scale-up. This would be beneficial as it provides the opportunity to mix in-situ [Resodyn, 2017]; however, there appears to be limited demonstration of this in literature so far.

Early research in 2009 [Lucon, 2009] described the technique, systems mixed, its applications and scalability potential. The technology was developed to address the challenge for a mixer that goes “beyond mechanical and costing considerations, with the primary consideration being how to best achieve the key process objectives” [Paul et al, 2004]. Although there is a lot of repetition from earlier discussed research [Bickley, 2009], six different capabilities were discussed: powder mixing and coating, liquid-liquid mixing, gas-liquid dispersion, viscous solid-liquid mixtures, mixing in case and scale up. Particle coating, using powder, was achieved after mixing for 10 minutes at unknown G level, producing a uniformly-coated powder. The base was a 40 micron polymeric powder and the coating was a 50 nm micron oxide powder, which had an average size of 30 microns when agglomerated. Achieving a well-mixed sample with these different particle sizes in 10 minutes would be unlikely in conventional mixing and although the G level has not been stated it is reasonable to assume that it is at the mid-level of the LabRAM capability. Powder mixing has an advantage over mixing materials like composites, as there is not a viscous matrix that the filler phase has to be distributed through. As such, de-bonding from the sample vessel, which can occur at the higher acceleration levels, is not a concern and could aid the mixing process. Following on from that research, 30 nm iron oxide powder was blended with and dispersed throughout 45 micron polymer powder. Scanning Electron Microscopy (SEM) images show that the mixing technique successfully broke down the agglomerations of the nanopowder and distributed the material. The mixing parameters were not included, but it would be a fair assumption to suspect that they are comparable to the previous powder mix. Viscous liquid-liquid systems required an acceleration of 100 G for a thorough mix. It is not stated whether liquid flow was not observed until these higher G levels, or that the higher G levels provided a greater rate of flow; from personal experience, there is a dependency on other factors, such as the application of a vacuum, the vessel geometry and fill level. Pure liquid systems require a much greater input than the solid systems; this is not seen on the conventional, intrusive mixers. Gas dispersion in liquid was briefly mentioned and was described as comparable to

powder mixing; this implies that by having a liquid sample that is not degassed mixing could occur at lower inputs. Viscous solid-liquid systems were demonstrated by a “typical” 120 L mix of 80,000,000 cP viscosity in 2 minutes at 80 G. These materials are the most difficult materials to mix, as the solid filler has to be dispersed throughout the viscous liquid matrix without separation or agglomeration of the components. Previous personal experience has shown that these materials risk de-bonding from the vessel at the higher energy levels, causing poor energy transfer into the material. As a result of this poor energy transfer into the material, the filler does not successfully distribute throughout the matrix and the sample is non-homogeneous. Specific details of the materials and mixing observations were not provided so it is not possible to conclude whether the sample was mixed effectively. However, previous experience shows that with most viscous solid-liquid systems, there is a notable temperature rise due to internal friction and the reported temperature rise from the 2 minute mix was around 15 °C. As such, it is expected that these materials were successfully mixed. The capability of mixing in various containers, most importantly in-situ, was discussed. This has obvious benefits and uses within the energetics industry; mixing and curing in complicated shapes without the need for casting reduces the risk of voids and poor fill quality. Most research undertaken so far is in cylindrical vessels, so this is a topic to watch. The final area of interest is scale up. The majority of the research discussed below uses the LabRAM, which is the laboratory scale version. For intrusive techniques there is a relationship between mixing duration and mixing quantity for the same level of input. With resonant acoustic mixing there is an apparent scale up, it will take the same duration to mix different quantities of material; however, there is a proportional relationship between mass of material and energy input for the same acceleration. This was modelled by a lumped mass acoustic model and verified by experimentation on the efficiency of mixing powder-powder and liquid-powder compositions on a range of particle sizes.

In 2015 a one-page report [NavSea, 2015] issued by NavSea, the US Naval Sea Systems Command, discussed their objective to have a small munitions production process utilising resonant acoustic mixing at NSWC IHEODTD, as well as having a certified production process for the Mk 152 warhead. The technology was developed and patented under a SBIR (Small Business Innovation Research), which led to a total Mantech investment of just under $1.5 million from July 2014 to December 2017. Laboratory scale investigations have already been undertaken at various military labs in the States, and various partnerships are being instigated. The benefits are explained; safety, faster production, reduced costs, reduced footprint and new capabilities. The estimated labour costings for using this technique for

manufacture is $1400 per warhead, resulting in a saving of $100 each. Using the current production levels it is expected to save $1 million a year for the new Mk 152 production.

A report released by the Munition Safety Information Analysis Centre (MSIAC), a group within NATO, provided an analysis of the research that has been conducted and the safety implications and cases that have been developed throughout the industry [Andrews et al, 2020]. A survey was conducted on nine RAM users in the energetic industry. The safety cases focused on the following areas: electrostatic discharge, thermal, impact and pressure and then the mitigation through the facility and system. Electrostatic discharge is the largest concern due to the expectation of charge build up through mixing via RAM; testing after mixing did detect a change in the charge of the mix vessel but grounding did successfully dissipate this charge. Temperature measurement appears to be the preferred option over thermal control, due to the short mix time and limited payload capability of the various RAM mixers. Having some kind of thermal tracking was important to all respondents though, due to RAMs noted temperature increase and the sensitiveness of explosives to thermal runaway and thermal ignition. Impact and pressure was considered worth analysing by a few respondents, as shock to detonation is a common mechanism to function explosives. Various calculations, on a single perfect RDX crystal, reported by MSIAC require impacts thousands of time greater than that calculated by RAM. Real material will have interactions between materials and defects to be considered, but this is still a large safety margin. In addition, there is the consideration of adiabatic compression of gas bubbles within the liquid phase. Calculations using nitroglycerine and estimating the highest cyclic pressures are approximately an order of magnitude smaller than required for initiation. For installation of the equipment for energetic mixing, there was typically a power interlock or kill switch to ensure remote operation and that the mixer could not be used when the mixer was operational. Resodyn has produced the LabRAM II (H) which is compliant to the electrical regulations for working with explosives. Continual checks were also found to be important to using this equipment with energetics, particularly ensuring the grounding was intact, the vessel was clamped appropriately and test runs were used before mixing explosives.

Additional research has been conducted on the potential of this technique for material processing aside from mixing. Milling is a key one that is mentioned, particularly in the pharmaceutical industry. Nanosuspensions [Li et al, 2016] were prepared by LabRAM for 96 minutes with a power percentage of 40% upwards. They were typically coarser and slower to break then samples produced via other wet milling methods. A patent was applied for by Merck Sharp and Dohme [Merck Sharp & Dohme Corp, 2015]

### 2.3.2 Mixing Effectiveness

Mixing effectiveness is the key concern with regards to mixing techniques. As such, it is only appropriate that there have been independent research published on this issue. This research varies on scale, material properties, input and vessels. As the different types of materials have different mixing methods, they have been grouped by material type.

In 2010, a paper presented at WM2010 [Lattin et al, 2010], a waste management conference in Phoenix, focused on successfully utilising the resonant acoustic mixing technology in a contaminated waste pilot plant; polychlorinated biphenyls (PCBs) are required to be processed into a non-liquid form in order to adhere to regulations. 1% of the waste drums had the excess liquid on the top surface; the remainder had the liquid inaccessibly dispersed within the inner bag, between the inner bag and the drum liner or between the drum liner and the drum. This lack of access proved problematic. The process previously used was a mechanical shaker-table that was slow and most effective for liquid within the inner bag. It used the vibrations to collapse the internal voids where excess liquid was typically located; this liquid would then either be consolidated within the bulk material or forced to the surface of the waste. Other methods included manually removing the liquid through either draining or tipping; however, it was manually intensive and exposed workers to radioactive contamination. Acoustic mixing was investigated due to its flexibility and the availability of larger mixing containers; the 30-galleon RAM was chosen for this research. It should be noted, that this is one of the few papers that look at larger scale. Utilising resonant technology, the mixer can provide 100 Gs of acceleration on a 226.8 kg mass with 30 kW of power. Characterisation proved that mixing for 4 minutes at 40 to 50 G produced a uniform blending. However, the drums were constructed of 1.2 mm steel and modelling limited the maximum acceleration to 56 G; a de-rating factor of 0.3 was required due to the folded seams connecting the drum walls to the lid and base. The overall experimentation proved the capability of the resonant acoustic technology to mix materials of different viscosities; however, the effect of the technology on the material, even the quality of the mix, was not of concern and as such no assessment was undertaken.

Lithium-ion batteries have a significant issue with powder blending during manufacture; lithium carbonate and manganese carbonate are mixed and heated to form a $LiMn_2O_4$ spinel. However, the powders have significantly different bulk densities causing the material to be susceptible to segregation or separation and resulting in component-rich areas. Using conventional mixing processes the duration can be up to 6 hours, using the LabRAM this process took one minute with an input acceleration of 80 G [Resodyn, 2010]. The samples

were electrochemically characterised, and exhibited efficient and stable cycling, implying high quality materials; which implies the mixing is stable and the material is undamaged.

Continuing with powder mixing, samples consisting of 90 wt% of coarse material, 100 µm Fast Flo Lactose, and 10 wt% fine powder, 45 µm Acetaminophen were tested in two vessel with fill levels of, 25% and 75%, accelerations of 47 G and 82 G and sampling times at 0.17, 0.5, 1, 2 and 4 minutes [Vanarase, 2010]. These were compared with double-cone blended samples with fill levels of 25% and 65% and mixer speed of 30 RMP. The sampling times were at 1, 2, 4 and 8 minutes. The mix uniformity was determined by near infrared (NIR) with 18 to 36 10 mg samples. It was assessed through the concentration of Acetaminophen and the relative standard deviation (RSD), which is shown in Figure 8. Having a lower RSD indicates more effective mixing, so the LabRAM samples showed potentially more efficiently mixed samples; however, it varied depending on the G level and the fill percentage. The double cone mixer was consistent across percentage fill level. However, despite the variation in RSD, the most effectively mixed LabRAM samples had a greater uniformity than the double-cone blended samples. This reinforces that the potential of this technique is impressive, but that parameters need to be optimised. What is of note in this research is the utilisation of a low G level. For powder mixing, high levels of acceleration are used; however, these results show that a lower G level may give a more consistent mixture in the same duration.

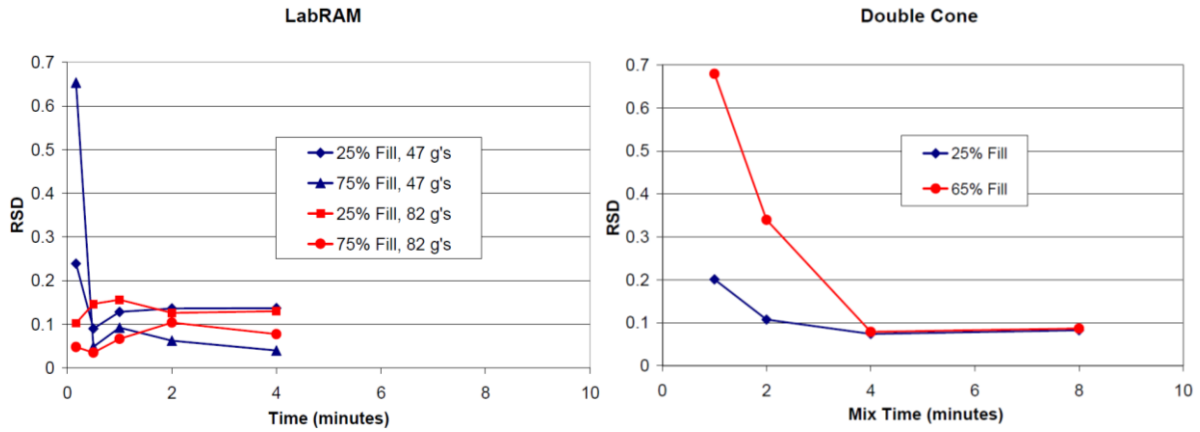


*Figure 8. Graph showing the relative standard deviation of samples mixed by LabRAM and Double Cone using different parameters [Vanarase et al, 2010]. A lower RSD indicates a more consistent sample*

A report to C&EN in 2014 [Webb, 2014] investigated the production of pharmaceutical cocrystals. This usually requires the use of solutions or mechanical processing methods. Avoiding the use of solvents has environmental advantages. However, mechanical methods

such as grinding are limited in production size; it won't achieve the multi-kilogram scale that is required. The initial research, undertaken by Nalas Engineering Services, provided proof of concept with carbamazephine and nicotinamide quantities of 100 mg, 1.5 g and 22 g mixed on the LabRAM for an hour. The intensity level was not included in the article; however, the cocrystals that were produced were reportedly of equivalent quality to those manufactured and processed by other methods. Further study needs to be undertaken into scale up and applicability for a range of compounds.

The full paper [Ende et al, 2014] details the mixing procedure; the powders were mixed in the LabRAM at 30% intensity for 5 minutes and solvents were then added, 20 µL for every 100 mg of solid material. The wetted material was initially mixed at 90% intensity for 2 hours; this was later altered to 80% for 1 hour, providing an acceleration of 80 to 90 G. At the beginning of the mixing period the wetted powders exhibited fluid properties; the end of mixing saw a solidified material at the bottom of the vessel.

Co-crystallisation was undertaken on two separate energetic compounds; NTO and nitroguanidine (NQ) [Hope et al, 2015]. They were mixed for an hour, and the experiments are detailed in Table 1. Depending on the parameters, co-crystals were successfully formed at a shorter duration and with less solvent required compared to the other methods.

*Table 1. Table detailing the parameters for RAM experiments on co-crystallisation by the University of Edinburgh [Hope et al, 2015]*

| Energetic | Crystal | G level | Water | Comments |
|---|---|---|---|---|
| NTO | 4ATZ | 50 | yes | small amounts of co-crystals formed |
| | | | no | agglomerates of 4ATZ coated in NTO:4ATZ salt |
| | | 100 | yes | small amounts of co-crystals formed |
| | | | no | agglomerates of 4ATZ coated in NTO:4ATZ salt |
| | 44BP | 50 | yes | co-crystals were formed |
| | | | no | no co-crystals formed |
| | | 100 | yes | co-crystals were formed but less than at 50 G |
| | | | no | no co-crystals formed |
| NQ | H5NP | 50 | yes | co-crystals were formed |
| | | 70 | yes | co-crystals were formed |

In 2015 an evaluation of resonant acoustic mixing for powder mixing [Osorio et al, 2015] was based around fractional factorial experimentation to determine the effect of the processing parameters on the samples. Using the standard 1 pint LabRAM with a 236 mL mixing vessel,

the variables included particle size, vessel fill, acceleration or mixing intensity and blending duration for API and lubricants. The materials were micronized, semi-fine and granulated acetaminophen, caffeine, microcrystalline cellulose and magnesium stearate. The fractional factorial design reduced the required experiments from 243 to 27 with the chosen parameters detailed in Table 2 below.

*Table 2. Table detailing the experimental parameters for RAM powder mixes reported in Powder Technology 2015 [Osorio et al, 2015]*

| | | | |
|---|---|---|---|
| Particle size | 28 μm | 45 μm | 195 μm |
| Vessel fill | 25% | 50% | 75% |
| Acceleration | 30 G | 60 G | 90 G |
| Duration | 1 minute | 2 minute | 4 minute |

Mixing performance was characterised by taking 1 mL aliquots at various points through the mixing cycle. Once samples were taken, the bulk sample was scrapped and a fresh sample was started as it was decided that the volume of the sample vessel was not sufficient to prevent significant perturbation. NIR was used to quantify the concentration of the various components, with a spectrum from 4000 $cm^{-1}$ to 10000 $cm^{-1}$. The results are neatly summarised below in Figure 9. With an increase in percentage fill level and input acceleration there was a decrease in mean sample variance. This publication contrasts with the previous one; a relationship can be observed with a decreasing level of variance with an increasing G level. The powder size has a greater range in comparison with the previous work; however, it would not be expected to make a significant difference.

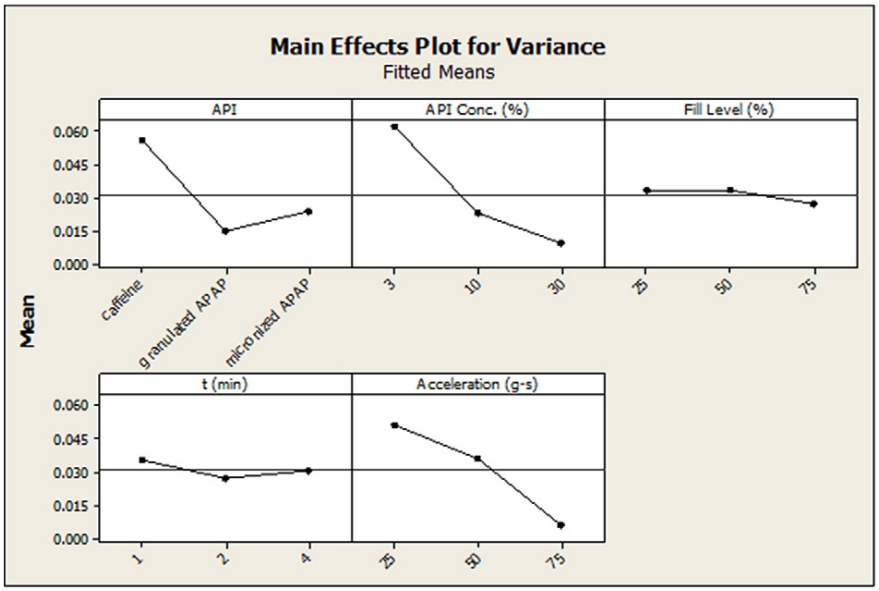


*Figure 9. Diagram illustrating the effect of the variables on blend uniformity using the normalised variance [Osorio et al, 2015]*

A pharmaceutical study in 2017 [Tanaka et al, 2017] demonstrated the capability of live assessing of the mixing process. Powders that were sieved through an 850 µm mesh screen were mixed in a glass vessel and near-infrared scans were run every second with a 10 ms integration time. Near-infrared sits between visible and infrared light. In this area there can be overlap in the wavelengths which can make identification of adsorption peaks difficult; however, using multivariate analysis can quantify these. The authors believe that LabRAM works by throwing the powder into the air and mixing as it free falls back down, see Figure 10. Calibration samples consisting of lactose, potato starch and theophylline were mixed in 50mL glass containers by LabRAM at 100 G for 300 seconds. Further experimentation included the same compositions mixed at 40 G, 60 G, 80 G or 90 G. They reported that the powders were successfully mixed in 12 seconds and that the mixing was monitored in real-time.

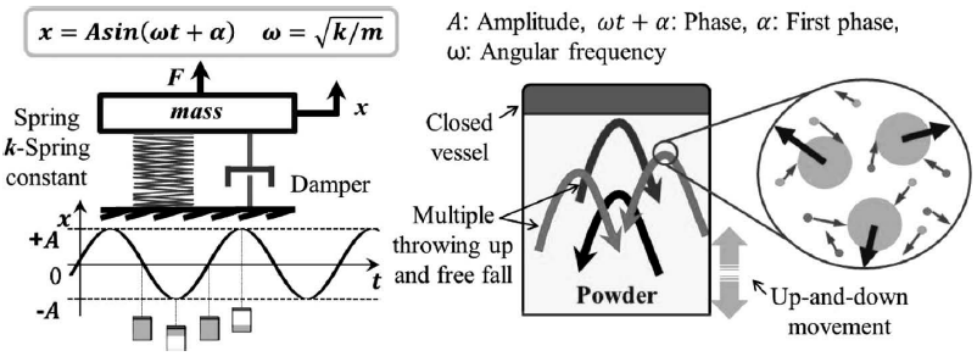


*Figure 10. Diagram showing the design of the resonant acoustic mixing system with a demonstration of the mechanisms of powder mixing [Tanaka et al, 2017]*

Resodyn published research on the influence of vessel geometry and the fluid properties [Coguill et al, 2012]. Uncured inert PBX samples using an HTPB binder system and an 84.7% solid filler loading of gypsum, sugar and hollow glass were mixed using a LabRAM. The samples were mixed in polycarbonate tubes; the dimensions are set out in Figure 11. The mixing behaviour was either characterised as mixing, no mixing or transition mixing. The diameter of the mixing vessel was plotted against the Reynolds number divided by diameter showing a negative exponential relationship.

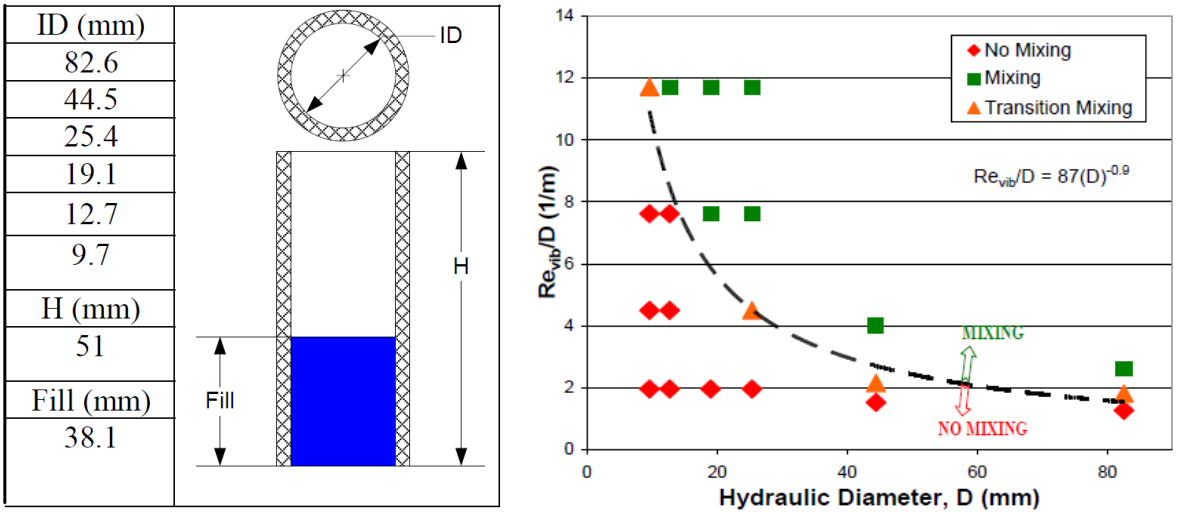


*Figure 11. Diagram demonstrating the mix vessel geometry and how the Reynolds number and diameter impacts the mix/ no mix boundary [Coguill et al, 2012]*

Further research undertaken by Roxel, presented at the Early Careers Symposium 2016 [du Plessis, 2016] highlighted a different approach. Mixing an HTPB based composite, they utilised the high intensities, roughly 80 to 90%, and reported that they experienced the expected de-bonding from the vessel wall as the material clumped and bounced in the pot. However, the material eventually slumped into a slurry and flowed. Their research at the time faced an issue with continuity as samples were not reliable. Further research was being undertaken in order to gain an understanding of this.

### 2.3.3 Material Characterisation

Material characterisation is most relevant to this body of research. The main focus has been on functionality; examples include combustion and pharmaceutical behaviour. Mechanical testing was also consistently undertaken throughout the different research papers as it gives an overview of the behaviour; typically, any deviations in the material can be seen through mechanical testing.

Nanothermites are an effective way of storing and delivering a high quantity of energy; however, processing methods are not optimum. Ultrasonic mixing is primarily used; nanopowders are wetted with solvents and the liquid phase is agitated by ultrasonic vibrations. Although this provides a well dispersed mix, drying large amounts of residual liquid can cause separation and settling of the solid phases. Increasing the solid loading reduces this issue but poses problems of its own, as ultrasonic agitation produces high levels of localised energy which could cause reactivity of the particles. Experiments [Nellums et al, 2013] were undertaken on aluminium-bismuth(III) oxide, produced from 0.8693 g of bismuth(III) oxide, particle size 90-210 nm, from Sigma Aldrich and 0.1307 g nano aluminium, particle size 80 nm with 77% active aluminium, from Novacentrix. They were mixed on the LabRAM in 10 mL plastic syringes, at 80% intensity for 16 minutes. At 8 minutes the testing was stopped and the sample was flipped and left for a minute before mixing resumed. The LabRAM samples were compared to ultrasonically mixed compositions and they were characterised by electrostatic discharge (ESD) sensitivity, combustion analysis and SEM imaging. The results were consistent between the conventionally mixed baseline samples and the LabRAM samples.

Developing new pharmaceutical drugs is costly, time consuming and heavily regulated. At the beginning of the drug development process there can be a limited amount of active pharmaceutical ingredients (API), which also have poor physiochemical properties. That makes targeting the appropriate receptor to evaluate efficiency and toxicity challenging. The typical formulations that are used during this early testing phase can cause misleading poor results; as such nanoparticles are being investigated. Suspensions with drug particles with typically <400 nm diameter suspended in an aqueous solution can achieve improved results. Utilising nanosuspensions in these early stages has been successfully developed and enabled commercialisation of several drugs due to the increased solubility and dissolution in the gastro region. However, nanosuspensions pose their own difficulty through processing. As such resonant acoustic mixing was investigated [Leung et al, 2014]. The suspension was approximately 90% of the total volume of the container, and was first mixed with a spatula to ensure the API was thoroughly wetted. It was mixed for 90 minutes at 40% intensity, equating to a nominal 50 G acceleration, and aliquots were taken every 30 minutes. Using acoustic mixing, it was reported that the mixing had a dramatic time-saving benefit, and due to its homogeneity it also required a smaller sample. Therefore, potential drugs were screened at a much greater rate. It was also reported that the lower stresses produce more physically stable suspensions with a lower risk of agglomerations.

Purdue University has acquired a LabRAM mixer, which was used in 2010 to develop new formulations of composite solid propellants based off a dicyclopentadiene (DCPD) binder [Bluestone et al, 2010]. Current binder systems are hydrocarbons; HTPB is standard due to its good mechanical performance. Prior to being used in propellants and explosives, HTPB was used commercially as a sealant which also makes it affordable. However, DCPD has superior mechanical properties and has been commonly used in various applications, including car bumpers and snowmobile hoods. It melts at 90 °C to form a low viscosity clear liquid. The low viscosity is beneficial as it can potentially increase the solid loading; however, the low viscosity can result in particle separation if not constantly agitated. Initial investigations used a Ross Dual Planetary Mixer but the long mixing durations made it unsuitable as the DCPD has a short polymerisation period, or 'pot life'. Without a suitable inhibitor, DCPD and Grubbs' 1$^{st}$ Generation catalyst will gel in 30 seconds; using an inhibitor or a less effective catalyst can extend this duration to several hours. LabRAMs shorter mixing period therefore makes it more appropriate. A temperature conditioning box was constructed as the DCPD needs to be processed above 90 °C, and the LabRAM did not have a heating jacket. The planetary mixer had 1 US-quart mixing capability and LabRAM had 1 US-pint capability, half that of the planetary mixer. No further mixing parameters were supplied. Tensile testing was undertaken and results were within the suspected range. No issues were highlighted as a result of the mixing technique; however, no comparison was undertaken and it was based around author's assumptions and past experiences. A comparison with an alternative mixing technique for this material would be an interesting follow up; however, the lack of this so far implies that Purdue University has confidence with resonant acoustic mixing.

Resodyn presented on mixing PBXs and the scale up potential of the technique at the 40$^{th}$ International Pyrotechnics Seminar [Coguill et al, 2014]. Using an inert formulation with 83% solid loading, the samples mixed in the LabRAM, RAM 5 and RAM 55. LabRAM mixed 0.2 kg of composition in 12 minutes, RAM 5 mixed 20 kg in 12 minutes and RAM 55 mixed 200 kg in 14 minutes. Tensile testing was then undertaken, and the variation in each batch was plotted in Figure 12. As can be seen, the LabRAM samples showed the least variation, of around 2%; but the scale up to 200 kg had reasonable sample quality with less than 4% variation. There is no indication of the variation that would be expected with these materials when mixed by conventional mixing techniques, so no comparison can be made to determine whether the variation is within the expected range; however, when compared to other literature the variation tends to either be equivalent or less. This research indicates that the potential is

promising and supports the implementation of this technology in a small munitions plant in the United States.

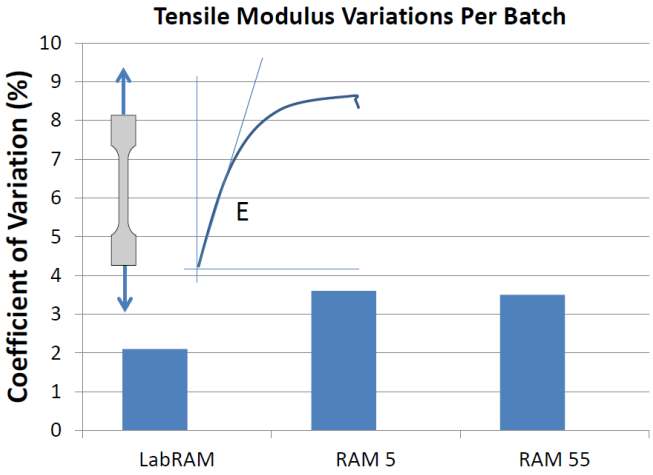


*Figure 12. Graph demonstrating the variation in tensile modulus in PBX mimics manufactured through either LabRAM, RAM 5 or RAM 55 [Coguill et al, 2014]*

One of the two of the most comprehensive materials research in the public domain was published by NavAir, the US Naval Air Systems Command in 2012 [Nelson et al, 2012], on a brief comparison between various energetic mixtures manufactured with the LabRAM, by hand or conventional planetary mixing. These ranged from 1 to 450 g sample vessels made of plastic and metal. Initial differential scanning calorimetry (DSC) tests compared hand mixed compositions with LabRAM samples and consisted of a polymer, a plasticizer and a nitramine in unknown proportions, totalling 1 g or 5 g. The LabRAM mixing schedule ramped from 0% to 100% intensity in increments of 10%, and held at 100% for 10 minutes. The difference between hand mixing and acoustic mixing for the DSC onsets were less than 5 °C and on average 2.1 °C. No graphs were supplied so no comment can be made on the thermogram. This indicates that the degradation point is not dramatically changed by using acoustic mixing. The DSC testing parameters were ambient to 350 °C with a ramp of 5 °C $min^{-1}$. Hand mixing would be softer on the material than using a planetary mixer, and so it can be assumed that in this scenario, with these compositions, the LabRAM, which reached and held at maximum percentage power input, was not a damaging technique. Further experimentation was undertaken on mixed propellant. These were hydroxyl-terminated caprolactone ether (HTCE), ammonium perchlorate (AP) and aluminium compositions and were either acoustically mixed for a total of 30 minutes with an input of 40 to 50 G or planetary mixed for 100 minutes. The burning rate was comparable and the tensile properties, tested at room temperature with a cross-head speed of 2 in $min^{-1}$ and 20 in $min^{-1}$, demonstrated slightly greater stress for RAM samples but similar moduli. This is a good demonstration of the potential of LabRAM, as the

overall mixing time was half that in comparison with planetary mixing; however, the functionality and mechanical behaviour does not appear to be compromised. The final set of experiments reported tested the ability to mix highly loaded polybutadiene based PBX; using particles with surface areas of 0.021 $m^2$ $g^{-1}$, 0.165 $m^2$ $g^{-1}$ and 1.65 $m^2$ $g^{-1}$. The particle size 0.021 $m^2$ $g^{-1}$ was used as a baseline and mixed in a planetary mixer; 0.165 $m^2$ $g^{-1}$ and 1.65 $m^2$ $g^{-1}$ were mixed in a LabRAM, not under vacuum. The 0.165 $m^2$ $g^{-1}$ sample was mixed at 100% intensity for a total of 120 minutes, 75% for a further 20 minutes, 30% for 10 minutes, 50% for 8 minutes and finally 20% for 3 minutes. The 1.65 $m^2$ $g^{-1}$ sample was mixed at 100% intensity for 100 minutes and 50% for 60 minutes. Microscopy images shown below, in Figure 13, were taken from the paper and show broken surfaces of the various explosives. The final samples visually appear homogeneous without any noticeable agglomerations.

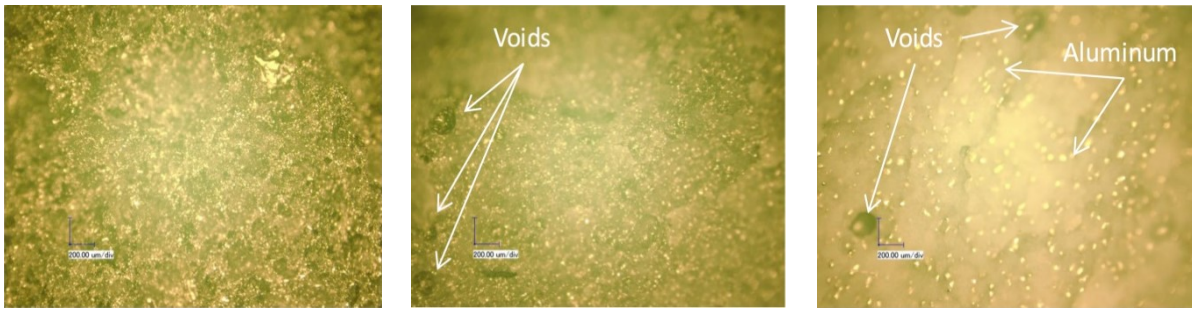


*Figure 13. Microscopy images of exposed broken surfaces of explosives with particle surface area of (from L to R) 0.021 $m^2$ $g^{-1}$, 0.165 $m^2$ $g^{-1}$ and 1.65 $m^2$ $g^{-1}$ [Nelson et al, 2012]*

NavAir concluded that the energetics tested were not compromised by the LabRAM; they had similar ballistic and mechanical properties when compared to planetary mixed samples and the technique could mix highly viscous materials. This research is promising for the field; at a top level the material is functional and stable and so far has not highlighted any issues or reasons to be concerned. More in depth research would hopefully validate this, and provide a greater level of confidence in order to fully utilise this in the production of energetic materials.

Roxel have purchased the 1-pint LabRAM mixer and by 2015 they had mixed several inert compositions; these include epoxy, silicone and polyester inhibitors, highly loaded thermal insulators, polyurethane liners and inert simulants of ignition powders. The paper [Rumeau et al, 2015] focused on the epoxy inhibitor which was characterised mechanically through tensile testing and thermally through dilatometry. The sample consisted of titanium oxide, a hardener heated at 50 °C and epoxy resin weighing a total of 180 g. A vacuum of 26 inHg was applied 2 minutes prior to mixing to degass the sample and held throughout. Mixing comprised of 30 seconds at 10% intensity, 90 seconds at 15%, 180 seconds at 40% and 60 seconds at 45%,

resulting in a rough acceleration of 25 G. Throughout the mixing a 4 °C temperature rise was noted. The tensile testing parameters were 50 mm $min^{-1}$ at 20 °C. Dilatometry used nitrogen gas and held the sample at 80 °C for 15 minutes, cooled to -70 °C at a rate of 2°C $min^{-1}$, held at -70 °C for 15 minutes, heated to 80 °C at 2 °C $min^{-1}$ at held at 80 °C for 5 minutes. The mechanical results were within the tolerances for the material and had a smaller deviation when compared to conventional mixing, in Figure 14 and Figure 15.

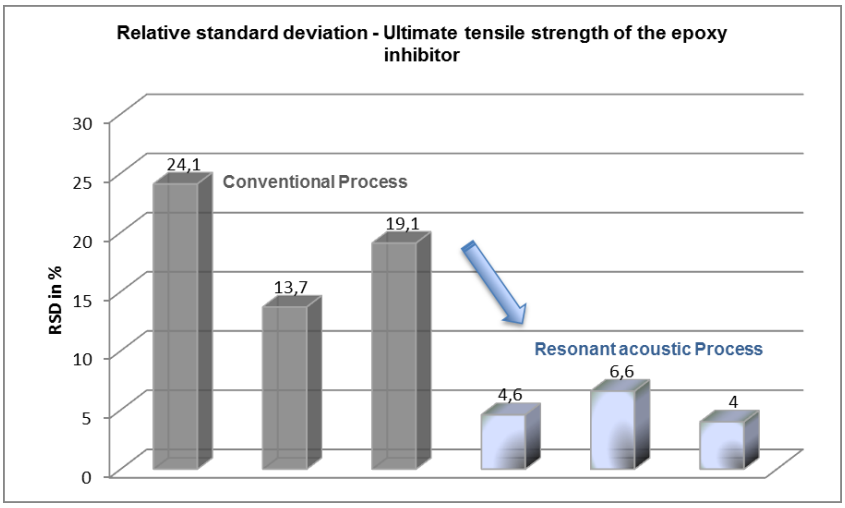


*Figure 14. Graph demonstrating a lower relative standard deviation for the ultimate tensile strength of epoxy inhibitors mixed by RAM when compared to traditional mixing methods [Rumeau et al, 2015]*

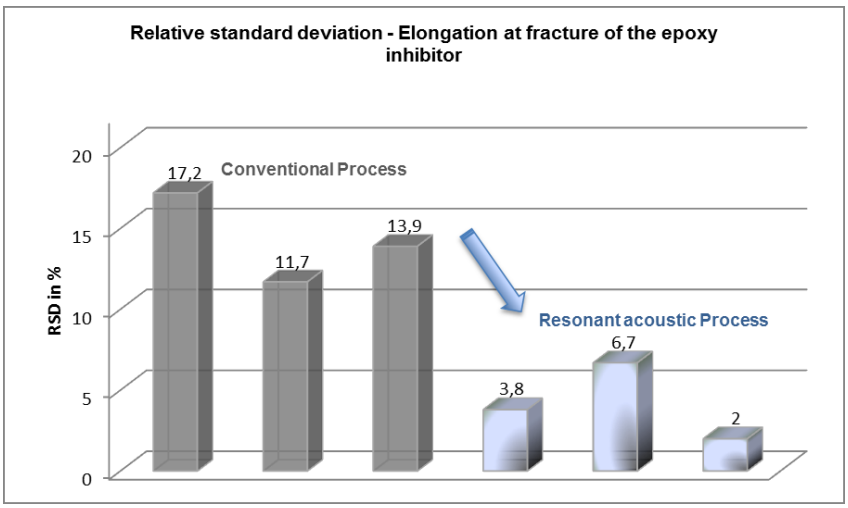


*Figure 15. Graph demonstrating a lower relative standard deviation for the elongation at fracture of epoxy inhibitors mixed by RAM when compared to traditional mixing methods [Rumeau et al, 2015]*

Alongside mechanical behaviour, AFM (Atomic Force Microscopy) was undertaken; these produced topographical maps of surface roughness, adhesion and modulus of the RAM samples and conventionally mixed samples. The results indicated a much higher surface roughness for conventionally mixed samples at micron and sub-micron scale. This may indicate that the surface has a greater proportion of binder for the LabRAM samples and less in the bulk material, in comparison to the planetary mixed samples; however, this has not been discussed or tested.

At NTREM (New Trends in Research of Energetic Materials) in 2015, the University of Edinburgh presented a paper on applicability of RAM for energetic materials [Hope et al, 2015]. The three areas of research were thermal activity, particle damage and co-crystallisation. Thermocouple measurements were first taken in an empty plastic vessel mixed for 15 minutes. There was no significant change in comparison to ambient temperature. The thermocouple was then placed into contact with the inside vessel wall with freedom of movement to indicate any potential friction induced heat with the vessel. A 10 minute mix cycle was used, and a temperature rise of 5 °C was noted. The mix acceleration was not reported for either set of experimentation. The next stage tested 25 g of sand mixed for 60 minutes at 100 G which provided a 21 °C increase, before reportedly plateauing at 45 °C to 50 °C. However, the graph provided in the paper, Figure 16, does not appear to plateau, instead reaches a steady rate of temperature increase before the test ends.

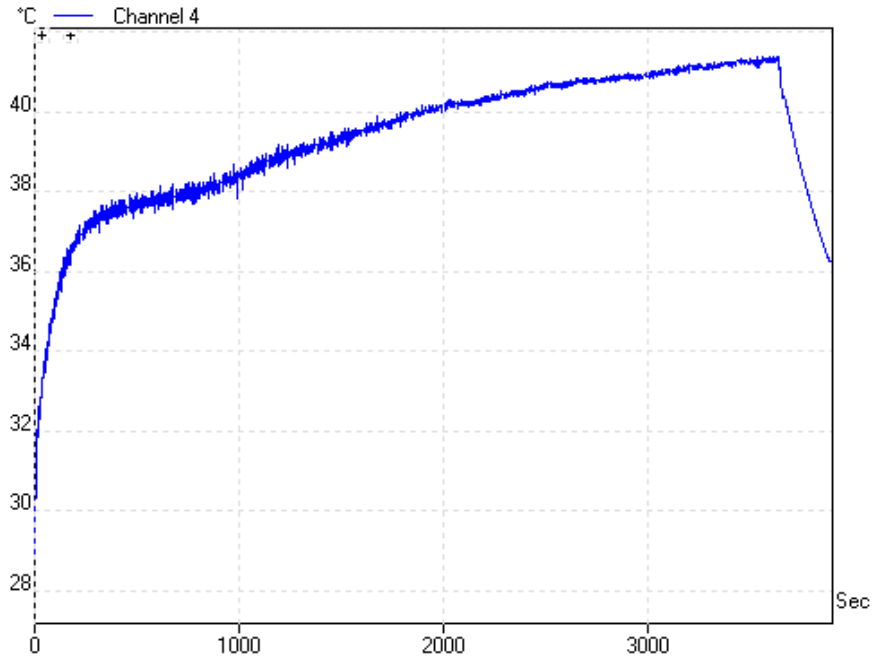


*Figure 16. Temperature measurements of sand mixed by RAM for 60 minutes at 100 G with a reported plateaus at 45 °C to 50 °C [Hope et al, 2015]*

Additional testing using powders with known melting points and mixing was conducted to determine thermal increase. Powders with a melting point of around 26 °C melted fully whereas powders with a melting points of approximately 40 °C partially melted around the edges of the mix vessel. They then crystallised when mixing stopped. Powders with melting points of 57 °C did not have any visual indication of melting. Viscous materials were mixed to compare the thermal changes; they exhibited a greater increase in temperature in comparison to the powders, plateauing at 84 °C when mixed at 80 G; this G level is consistent with previous literature.

Particle damage was assessed by visual techniques; optical microscopy was undertaken on sucrose with a scale of 10 µm. 15 g of sucrose, filling half of a plastic tube, undergoing an hour of mixing on the LabRAM with varying acceleration levels from 10 to 100 G. When the mixed sample was visually compared to the control sample it exhibited an increased agglomeration on crystal surfaces but no evidence of crystal fracture or shearing. This was confirmed by a triboluminescence experiment, which measures the luminescent emissions caused by severe crystal damage.

An HTPB-RDX based shape charge was manufactured in-case [Wilgeroth et al, 2018] with 89% solid loading. Mixing occurred in three stages; the wetting stage was 3 minutes at 30 G with no vacuum, the mixing stage was 8 minutes for 60 G with partial vacuum of 550 mbar and the last stage was the degassing which was 6 minutes at 30 G with a vacuum of 350 mbar. Thermal controls kept the mixture at 60 °C. The density and hardness were consistent throughout the measured charges as were the thermal transitions, measured by Differential Scanning Calorimetry (DSC). The shape charges were tested alongside planetary mixed charges, and the penetration depth was measured using mild steel witness plates. The LabRAM charges had a greater penetration depth and produced more circular penetration marks; however, they had a much greater variation ranging from 0.96 plates to 2.13 plates.

Additional experimentation from BAE [Davey et al, 2019] tested PBXs and LOVA (low vulnerability propellant) manufactured by planetary mixers and RAM. A three stage mixing regime was employed, with the samples being wetted at a low G for 2 minutes, mixed at accelerations between 30 and 80 G for up to 40 minutes and degassed, again at a low G for 5 minutes. Thermal analysis was conducted by DSC and DMA demonstrating consistent thermal transition points. Additionally, the density, measured by liquid displacement, were consistent between the planetary mixer and the RAM samples mixed with vacuum. The RAM samples with no vacuum had large variation both with like samples and with the other mixing methods. Hardness testing demonstrated an interesting feature, where the higher the

acceleration used for mixing, the more consistent the hardness results. However, when compared with planetary mixed samples the RAM samples were softer, see Figure 17.

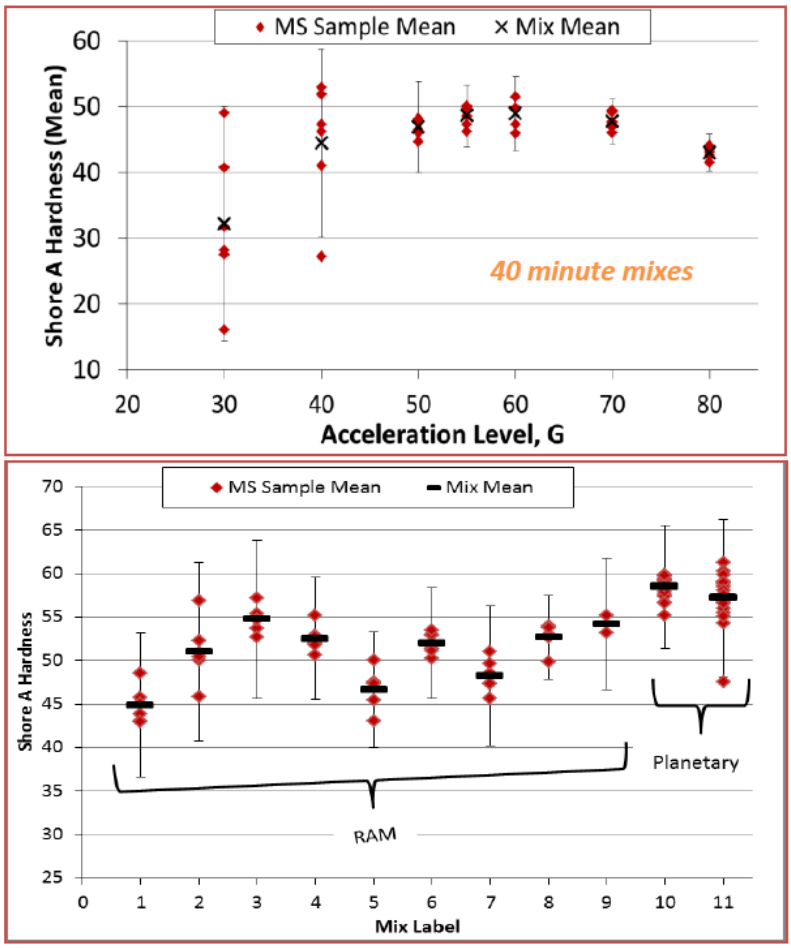


*Figure 17. Hardness results of composite explosives mixed by BAE. The top graph is purely RAM samples, demonstrating high consistency in the hardness results when using a higher acceleration. Comparisons with the planetary mixed samples demonstrated decreased hardness for the RAM samples [Davey et al, 2019]*

The remainder of the mechanical testing was compression testing; when mixing via RAM the materials properties where improved and more consistent when mixing occurred at greater than 50 G attributed to poor isocyanate distribution. When comparing the RAM and the planetary mixed samples, the RAM samples experienced greater stress to fracture. Functionality tests were conducted, consisting of hazard testing and velocity of detonation. The results remained consistent between the mixing methods. Chemical analysis was utilised and demonstrated no significant variation between the two mixing methods; the analysis technique was described as a multi-stage solvent extraction and no additional information was provided.

The Australians have also conducted research on the technique to try and determine whether it lives up to its promised potential [Smith et al, 2019]. Mixing an aluminised ammonium perchlorate composite propellant on the RAM II (H) it took 20% of the time taken to manufacture by conventional planetary mixing. As with the BAE report [Wilgeroth et al, 2018] the RAM samples had a greater range but did have samples which exhibited improved properties when compared to the planetary mixed samples. The sensitiveness testing, which consisted of impact, friction, thermal and electrostatic stimuli, demonstrated no significant variation between the 2 galleon mixer and the RAM samples. Ballistic testing consisted of measuring the burning rate, which remained consistent between the mixing methods. The mechanical testing demonstrated the greatest variation; tensile testing was conducted at 25 °C, -54 °C and 74 °C. Across all three temperatures the RAM samples exhibited significantly greater max strain and lower modulus.

So far, the research in this field has shown a few distinct trends. Mixing has tended to use high G levels, regardless of the material and its properties. No mixing observations have been reported determining how the material flows within the sample vessel, but the results indicate that a reasonable mix has been achieved. Mechanical tests have been used on the tested samples, and the results have shown either equal or less variation when compared to conventional mixing; however, there is only a limited amount of data available. Some analysis on material damage has been undertaken and this has shown that so far there is no evidence to suspect that the material has been compromised as a result of this technique. However, there is only a limited amount of research available in this area on the use of resonant acoustic mixing and how it compares to conventional mixing, and as such, with the exception of the US, there is no indication that this technique has the confidence to be utilised in energetic production.

## 2.4 Statistical Analysis

The null hypothesis for this study was that processing via RAM did not affect material properties. The planetary mixed samples were defined as the baseline. Although repeats were conducted on every experiment the sample sizes were small, therefore a student's T-test was used. This test is an analysis of variance (ANOVA) test which determines the significance of any difference between two sample sets, identifying whether any deviation is due to the changed variable or due to chance. The test is considered an independent T-test, as the samples are from two independent batches. Using Equation 2-1 with the variables explained in Table 3, a t-value is produced, which determines the size of difference relative to variation within sample data. A greater t-value provides more evidence against the null

hypothesis. Using data tables, the t-value and the number of samples, the p-value is found; a small p-value, of less than 0.05, means the null hypothesis is rejected. This is also called the alpha level. Statistics in this study were conducted by Microsoft Excel 2016 t-test function with two tails, and an equal variance.

$$t = \frac{\mu_A - \mu_B}{\sqrt{\left[\frac{\left(\Sigma A^2 - \frac{(\Sigma A)^2}{n_A}\right) + \left(\Sigma B - \frac{(\Sigma B)^2}{n_B}\right)}{n_A + n_B - 2}\right] \cdot \left[\frac{1}{n_A} + \frac{1}{n_B}\right]}}$$

*Equation 2-1. Independent Student T-Test equation*

*Table 3. Table explaining the variables for the Independent Student T-Test equation*

| Symbol | Variable |
|---|---|
| t | t-value |
| $\mu_x$ | Mean of sample x |
| A | Data Set A |
| B | Data Set B |
| Σ | Sum of |
| n | Number of sample |

# 3 HTPB-Melamine

This study investigated the impact of resonant acoustic mixing on the properties of energetic materials. Due to their hazardous nature, initial research was conducted on simple two-phase HTPB-Melamine composites. A single modal filler system reduces the complexity of the sample and limits the maximum filler loading. Three loading levels were manufactured and are described as mass decimals; 0.66 solid loading is 66% of the compositions mass as solid filler. This terminology is used throughout this study. The three loadings represent different materials; 0.66 solid loading is a composite propellant, 0.80 solid loading is a polymer bonded explosive (PBX) and 0.73 solid loading is an intermediate step. The samples in this study are cast into finger moulds, seen in Figure 18, as they have correct dimensions for the characterisation. These are the largest samples required, and eliminate the need for machining which can be hazardous, time consuming and costly. Although machining samples provides more precise test pieces and reduces variability, the time and cost implication significantly reduce the amount of testing possible that can be conducted through this programme. All sets of samples were treated in the same manner, and as it is a direct comparison any effect would be consistent.

In this study the definition of “significant” changes between samples is based around material specifications for Qualified explosives. Materials such as PBXN-109 and PBXN-110, are commonly used aluminised and non-aluminised castable PBX compositions, which allow for a range of ~10% in their characterised behaviour. As such, significant behaviour in this programme is considered to be ±10% change from the planetary mixed samples.

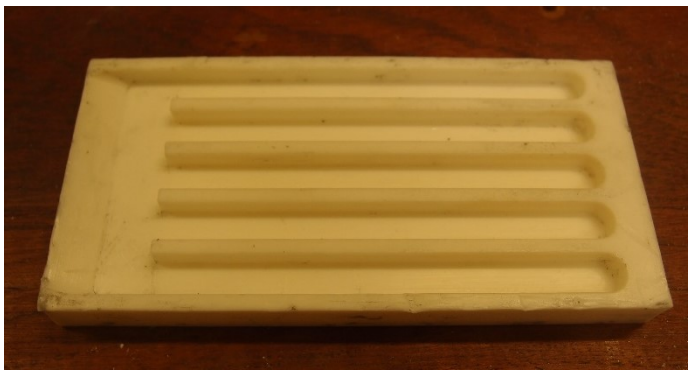

*Figure 18. Finger mould used within this research programme, with each of the five fingers having the correct width and depth measurements to produce DMA samples*

## 3.1 Materials

The energetic materials of interest in this study are composites. The binder system provides structural integrity to the HE crystals, and provides low vulnerability properties, a requirement for modern munitions and materials. The binder system is a viscous fluid that is chemically cured to form a solid matrix. The filler particles are entrapped in the binder system and not chemically bonded.

### 3.1.1 Binder System

As the simplest composition in this study, the binder system is cured hydroxyl-terminated polybutadiene (HTPB) with no modifiers. HTPB is commonly used in energetic formulations to form a polyurethane binder system, popular due to its high temperature stability, resilience and good mechanical properties [Mahanta et al, 2012] [Daniel, 2006]. It is chemically stable and compatible with a range of explosives. HTPB is the prepolymer, which when cured forms a polyurethane; however, the nomenclature is used for both the uncured and the cured material. The HTPB used in this study is Cray Valley R45 HTLO. Before use, the HTPB was dried via a vacuum line overnight to reduce moisture.

HTPB has three possible isomers; vinyl, cis and trans as seen in Figure 19; these are formed during synthesis dependent on the polymerisation conditions. They affect the mechanical properties; greater vinyl content leads to an increase in viscosity and weaker mechanical properties whereas a higher proportion of trans form has stronger mechanical behaviour [Dey et al, 2017]. There are also three options within the vinyl microstructure. Most commercial HTPBs have a mixture of these three different structures randomly distributed throughout the sample. HTPB R45 HTLO consists of 60% trans, 20% vinyl and 20% cis, see Figure 20.

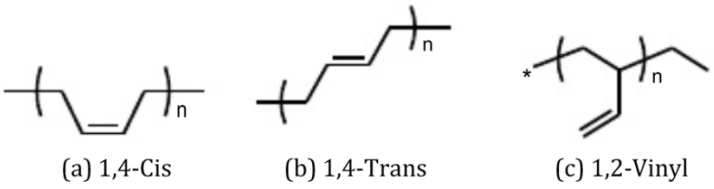


*Figure 19. The chemical structure of the three potential HTPB isomers: cis, trans and vinyl [Dey et al, 2017]*

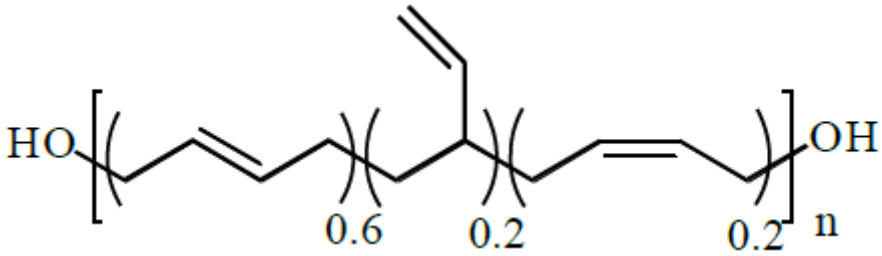


*Figure 20. Chemical structure of the HTPB R45 HTLO variant [Cray Valley, 2018]*

To form a structurally sound solid, various curing methods are available; thermal, UV or chemical. HTPB is chemically cured using an isocyanate. Isocyanates are components with an isocyanate group (-NCO) that react with alcohol groups, such as HTPB to produce polyurethane plastics. They are available in solid or liquid form; liquid isocyanate is a hazardous substance, can be carcinogenic or a sensitizer and is usually an irritant to the respiratory system. However, solid isocyanate does not distribute as well throughout the sample and can produce a highly uneven cure. Three commonly used isocyanates in the energetics industry are isophorone diisocyanate (IPDI), toluene diisocyanate (TDI) and methylenediphenyl diisocyanate (MDI). IPDI was chosen which has two functional NCO groups, seen in Figure 21. IPDI was chosen due to its long pot life; the HTPB and IPDI takes several hours before curing starts to impact its behaviour which allows sufficient time for the sample to be cast and processed. Too short a pot life the greater the risk that the sample starts to cure within the mixer and cause poor homogeneity. The longer the pot life the greater the risk of sedimentation and an inhomogeneous sample. Catalysts can be used to increase the pot life but have not been used in this study. A ratio of 1:10 of HTPB: IPDI has been used consistently throughout this entire study; this was calculated by Equation 3-1 [Wingborg, 2004]. The material properties are in Table 4.

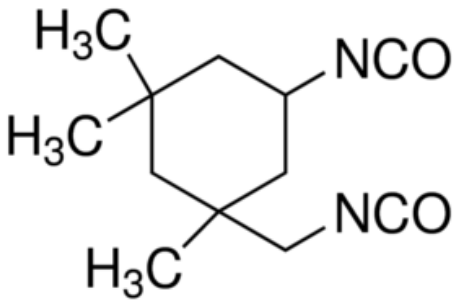


*Figure 21. IPDI chemical structure [Sigmaaldrich, 2016(b)]*

$$m_{NCO}\frac{f_{NCO}}{M_{NCO}} = m_{HTPB}\frac{f_{HTPB}}{M_{HTPB}}$$

*Equation 3-1. Calculation to determine the HTPB and isocyanate ratio required to successfully chemically cure the HTPB [Wingborg, 2004]*

*Table 4. Table detailing the functionality and molecular weight of HTPB and IPDI which is required to calculate the HTPB and IPDI ratio [Crayvalley, 2018] [Sigmaaldrich, 2016(b)]*

| **Component** | HTPB | IPDI |
|---|---|---|
| **Functionality ($f_x$)** | 2.5 (average 2.4 to 2.6) | 2 |
| **Molecular Weight ($M_x$)** | 2800 g $mol^{-1}$ | 222.3 g $mol^{-1}$ |

### 3.1.2 Filler Component

Melamine is the filler component discussed in this chapter and is used during production of plastics. It is most commonly known as the durable plastic found in a range of homewares in the 20th century. Within energetics it is a density simulant; inert dummy rounds are used in practice for safe training of future operators. These dummy rounds have representative mass and centre of gravity. The melamine used throughout this study was supplied in the form of a white powder. The particle size distribution has been supplied in Table 5 and plotted in Figure 22. The size distribution was compared to available classes of RDX in Table 6, and most closely match that of Class 6.

*Table 5. Table detailing the percentage mass of melamine, used in this research programme, which passed through the sieve with the specified mesh size*

| **Sieve Size, µm** | **% Mass Through** |
|---|---|
| 212 | 99.5 |
| 125 | 79.6 |
| 106 | 54.4 |
| 90 | 40.4 |
| 63 | 27.7 |
| 53 | 5.0 |

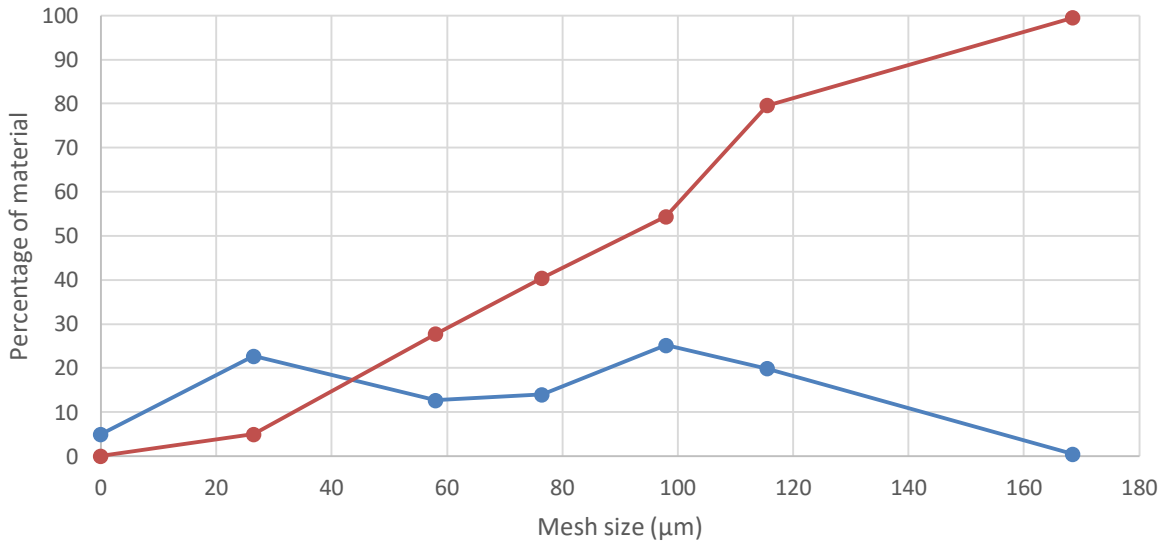


*Figure 22.Graph demonstrating the mass percentage of melamine passing through sieves of specified mesh sizes. It demonstrates the cumulative amount, in red, and the amount at each sieve, blue*

*Table 6. Table detailing the percentage of powder that passes through sieves with a specified mesh size for a range of RDX Classes [chemringnobel.no, 2019(b)]*

| ASTM Sieve no. | Opening [mm] | % through | | | | | | | |
|---|---|---|---|---|---|---|---|---|---|
| | | Class 1 | Class 2 | Class 3 | Class 4 | Class 5 | Class 6 | Class 7 | Class 8 |
| 8 | 2,360 | | | | 100 | | | | |
| 12 | 1.700 | | | 99-100 | 85-100 | | | | |
| 20 | 0.850 | 98-100 | | | | | | 98-100 | |
| 35 | 0.500 | | 98-100 | | 0-40 | | | | 100 |
| 50 | 0.300 | 80-100 | 90-100 | 30-50 | | | | | 98-100 |
| 60 | 0.250 | | | | | | 96-100 | | |
| 80 | 0.180 | | | | | | 91-100 | | |
| 100 | 0.150 | 30-90 | 50-80 | 10-30 | | | | 82-98 | 90-100 |
| 120 | 0.125 | | | | | | 67-93 | | |
| 170 | 0.090 | | | | | | 43-80 | | |
| 200 | 0.075 | 5-45 | 20-46 | 0-20 | | | | 31-61 | 55-80 |
| 230 | 0.063 | | | | | | 22-50 | | |
| 325 | 0.045 | | | | | 97-100 | 8-36 | | 40-60 |

## 3.2 Planetary Mixing

Planetary mixing was conducted on the smallest available mixer, an IKA Planetron HKV-1, which has a 1 L capacity and a 300 g minimum material requirement. For fairness, it was intended to keep the batch size the same, but this was the smallest available mixer. The blade speed ranged from 12 to 18 rpm. Below 12 rpm there is a risk of the mixer motor stalling, and not exceeding 18 rpm ensures that there is not sufficient energy imparted into the

mixture to either cause damage or initiation when explosive materials are mixed. The planetary mixed samples were mixed under vacuum, ranging up to 100 mbar. The melamine was added in two additions and the isocyanate added last. Mixing occurred for 1 hour after each powder addition, and 30 minutes after the cross-linker was added. The mix notes were summarised in Table 7. At the higher solid loadings the sample did not flow without external stimuli and was too viscous to cast easily.

The samples were cast into finger moulds and cured at 50 °C for 1 week. Due to the lack of anti-oxidant, there was a 2 mm yellow oxidised layer on the top surface. Samples with a greater level of HTPB had a richer yellow colour as the surface was binder rich in comparison to the samples with the higher solid loadings.

*Table 7. Formulation table of HTPB-Melamine Planetary Mixed samples with mixing notes*

| | | | | |
|---|---|---|---|---|
| **0.66 Solid Loading** | HTPB | Melamine | Planetary Mixed | Sample had very good flow properties and cast well |
| | 0.34 | 0.66 | | |
| **0.73 Solid Loading** | HTPB | Melamine | Planetary Mixed | Sample had reasonable flow properties and cast with some encouragement from a spatula |
| | 0.27 | 0.73 | | |
| **0.80 Solid Loading** | HTPB | Melamine | Planetary Mixed | Sample had poor flow properties and could not be cast. Had to be smeared into mould |
| | 0.20 | 0.80 | | |

### 3.3 LabRAM Mixing

As the LabRAM is an experimental technique, mix conditions were altered as mixing was occurring. Some methodology was adapted from the conventional planetary mixing to keep the comparison consistent, such as the sequential approach with the addition of material; HTPB and half of the melamine were added prior to the first mix, the remaining melamine was added prior to the second mix with the IPDI cross-linker added prior to the third mix. As this is a novel mixing technique there are alternate methods such as adding all constituent parts, including the cross-linker, and adding the binder system in last. The LabRAM samples were mixed under vacuum in 200 g batches in 8 oz polystyrene pots. An example mix diagram is in Figure 23. This is produced by the Resodyn software during mixing. It includes the resonant frequency of the system, the acceleration that is applied and the power that is input. Acceleration is measured in G and the power is a percentage of the mixers maximum capability. The mix was controlled manually using visual indicators to assess mixing. The mix started at 10% intensity and was sequentially increased until the sample flowed within the

vessel. The corresponding power percentage was within the 40 to 65% bracket which correlated to an acceleration of up to 80 G. Details on understanding the mix diagram can be found in Chapter 8.2.

The lower filler loading levels had reasonable flow properties and cast with ease. As the solid loading increased, the viscosity reduced, and as described in Table 8, the material did not effectively cast without external stimuli. An attempt was made to mix a 0.90 solid loading sample; however, it did not wet effectively and the powder did not integrate within the binder system. As such, it was not a viable composition.

The material was cast and cured for 1 week at 50 °C. Again, samples did not contain antioxidant so the top layer of the cast samples were oxidised and discoloured.

*Table 8. Formulation table of HTPB-Melamine LabRAM samples with mixing notes*

| | | | | |
|---|---|---|---|---|
| **0.66 Solid Loading** | HTPB<br>0.34 | Melamine<br>0.66 | LabRAM | Sample had good flow properties and cast well |
| **0.73 Solid Loading** | HTPB<br>0.27 | Melamine<br>0.73 | LabRAM | Sample had reasonable flow properties and cast with some help |
| **0.80 Solid Loading** | HTPB<br>0.20 | Melamine<br>0.80 | LabRAM | Sample had poor flow properties and was at the very limit of casting |
| **0.90 Solid Loading** | HTPB<br>0.10 | Melamine<br>0.90 | LabRAM | Sample abandoned due to lack of binder. Just powder flow |

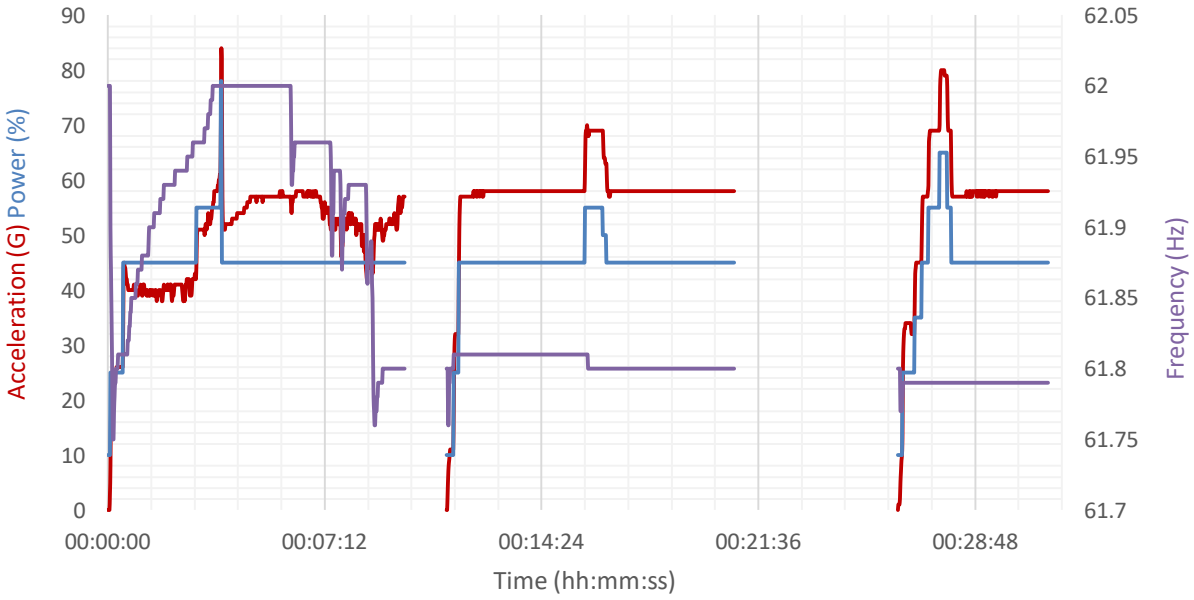


*Figure 23. LabRAM mixing diagram for 0.73 solid loading HTPB-Melamine sample, demonstrating the acceleration and power input and the associated frequency set by the RAM. There are two gaps within the diagram where the mix was stopped and material was added*

## 3.4 Characterisation

Characterisation focused on microscopy and mechanical and thermal analysis. Optical microscopy investigated any visual changes in the material, such as variation in particle size, particle cleavage or fracture, visible dewetting and de-bonding or binder failure. Thermal analysis was conducted via differential scanning calorimetry (DSC) with a temperature sweep determining thermal transition points of the material. Mechanical testing was conducted via dynamic mechanical analysis (DMA) to determine the low strain rate mechanical behaviour. Prior to testing, the oxidised layer on the top surface was removed.

### 3.4.1 Mechanical

Mechanical characterisation was conducted on these compositions via DMA. The sample, with nominal dimensions of 6 mm x 10 mm x 50 mm, was clamped vertically with one clamp connected to an oscillating motor and the other to a torque measuring system, and enclosed in a thermal chamber. DMA measures three key parameters; the elastic/storage modulus, the loss modulus and the tan(delta). The elastic/storage modulus is a measure of the materials elastic behaviour, and can be referred to as the real component or the proportion of energy stored during a loading cycle. The loss modulus is the viscous behaviour and is out of phase to the applied stress wave; it is the materials ability to lose energy through friction and internal

movements and is referred to as the imaginary component. Delta is the phase difference between the two moduli; a 0 ° phase difference indicates a purely elastic material, and a 90 ° phase difference indicates a purely viscous material. The tan(delta) is the ratio between the two moduli and measures the materials dampening capability. A higher tan(delta) indicates a more viscous material and a greater energy loss, whereas a lower value can indicate a more elastic sample [Menard, 2002] [Ehrenstein, 2004].

It is the preferred mechanical technique for energetics. Samples are smaller than JANNAF or PERME tensile testing pieces, which are 25 mm x 125 mm and 30 mm x 75 mm respectively, the DMA samples are a single bar, and require less machining than the dog bone shaped tensile pieces. Machining of energetics can be a high risk and labour intensive task; incidents do occur and it is beneficial to reduce the machining required where possible. Additionally, measuring over a range of temperatures provides the glass transition temperature, where the material transitions from brittle to more rubbery; a low glass transition temperature is required for energetics as they can be used in air loaded weapons which experience a range of temperatures. If the material becomes brittle whilst in use, there is a risk of cracks forming throughout which can be a serious safety and performance issue. DMA tends to be a non-destructive technique as the strain input is minimal, typically less than 1% and is rarely enough to cause damage in the material; this means samples can be retested as opposed to tensile testing which is commonly tested to failure.

Two test samples were taken from each material. The testing was performed on a Rheometrics RDAII dynamic mechanical analyser, testing from -110 °C to +80 °C in 3 °C steps with a nominal strain of 0.1% and a frequency of 1 rad $s^{-1}$ as according to STANAG 4540 STANAGs are a NATO document that standardises the testing methodology for explosive materials. STANAG 4540 specifically focuses on DMA testing and determining the glass transition temperature. Graphs have been produced and plotted in Figure 24 to Figure 26.

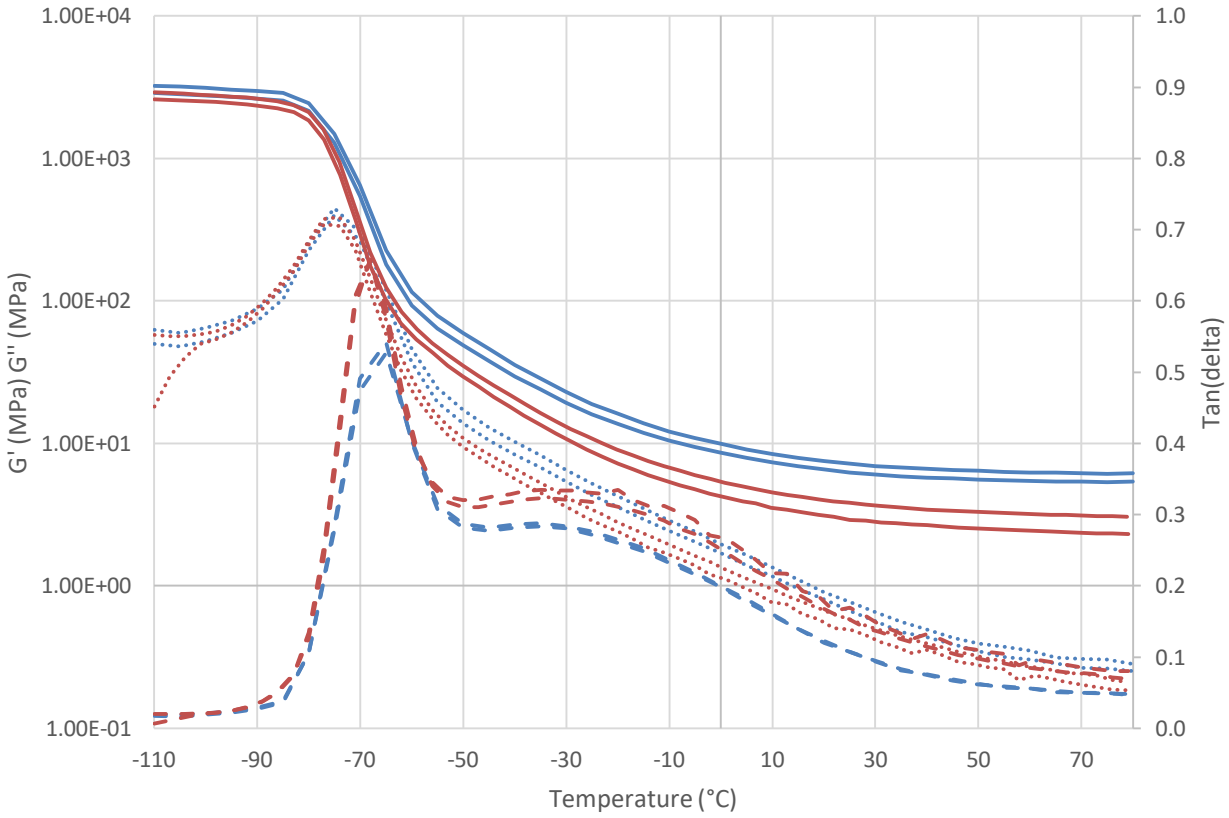


*Figure 24. DMA graph for 0.66 solid loading HTPB-Melamine samples plotting the elastic modulus or G' (solid line), loss modulus or G" (dotted line) and tan(delta) (dashed line), and comparing the LabRAM samples (red) with the planetary mixed samples (blue). The samples show variation beginning at the glass transition temperature, with the planetary mixed samples behaving more elastically*

The 0.66 loading samples showed variation in the graphs, seen in Figure 24. The storage modulus, G' or elastic component, is consistent below the glass transition temperature; variation occurs after this point as the polymeric chains begin to be able to freely move within the material. The LabRAM samples are softer and this is attributed to poor cross-linkage of the binder system which allows greater movement of these chains. Like the G', the G'' and loss modulus demonstrate a variation between the mixing methods after the glass transition point with the planetary mixed samples dissipating a greater amount of energy. The planetary mixed samples show a greater level of consistency in comparison to the LabRAM samples indicating the LabRAM samples are heterogeneous with a variation in the cross-linking throughout the sample. In the LabRAM, the isocyanate was insufficiently mixed throughout the material and this is supported through the softer DMA results.

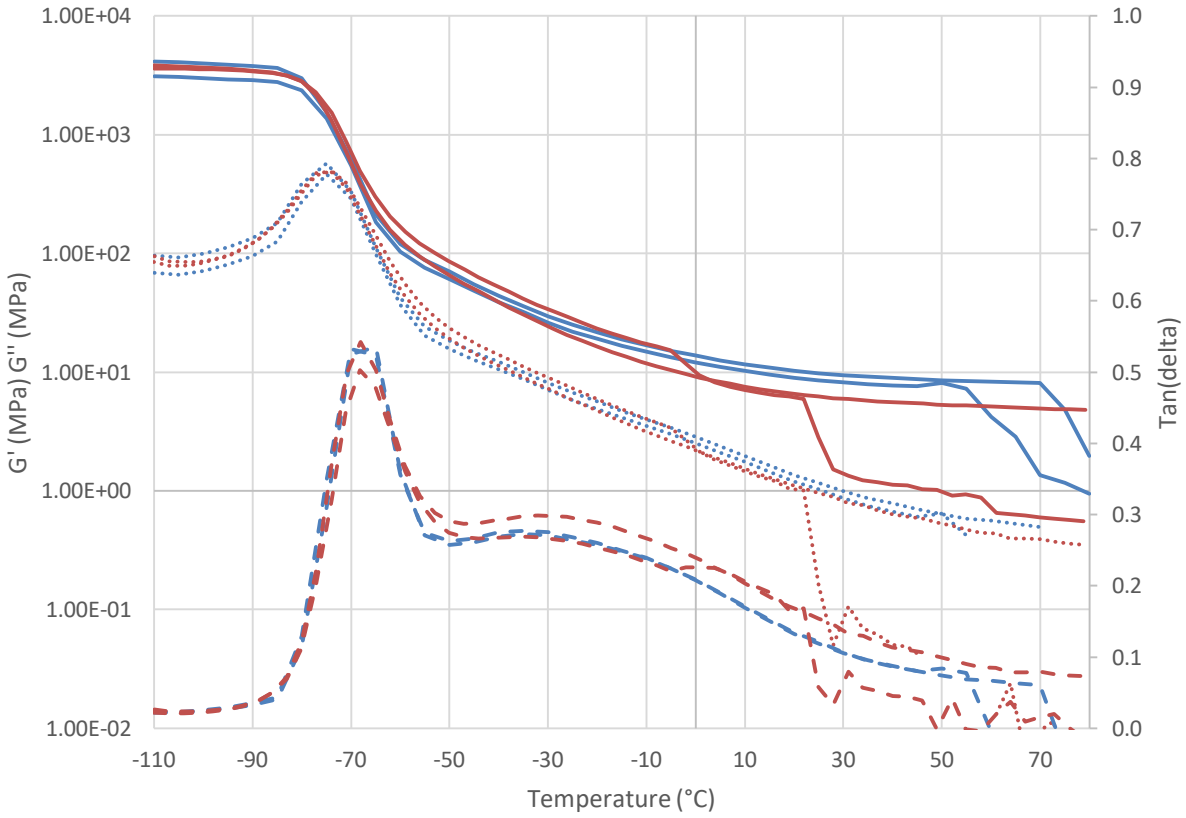


*Figure 25. DMA graph for 0.73 solid loading HTPB-Melamine samples plotting the elastic modulus or G' (solid line), loss modulus or G" (dotted line) and tan(delta) (dashed line), and comparing the LabRAM samples (red) with the planetary mixed samples (blue). The samples show consistency between the samples but demonstrated erratic behaviour at the higher temperatures due to poor sample clamping*

The 0.73 solid loading level samples, Figure 25, suffered from insufficient clamping, which can be seen from the erratic results at 20 °C onwards. Compared to the 0.66 solid loading samples, these samples are more consistent exhibiting less deviation. The planetary mixed samples before the glass transition point are varied; one of the samples is negligibly softer. This is characteristic of changes in the chain length which indicates either poor cross-linking or damage to the polymer chains. Between the glass transition temperature and -10 °C, the planetary mixed samples are softer as the polymeric chains are able to move more. This coincides with the loss modulus, G'', increasing in comparison to the LabRAM samples as there is a greater energy dissipation within the sample. However, after -10 °C, the LabRAM samples are softer demonstrated by the lower G'. The mechanical behaviour does not exhibit significant behaviour change between the LabRAM and planetary mixed samples. Like the 0.66 solid loading samples, the LabRAM samples show weaker behaviour. The exception to this is during the glass transition temperature range, where the LabRAM samples had improved mechanical properties.

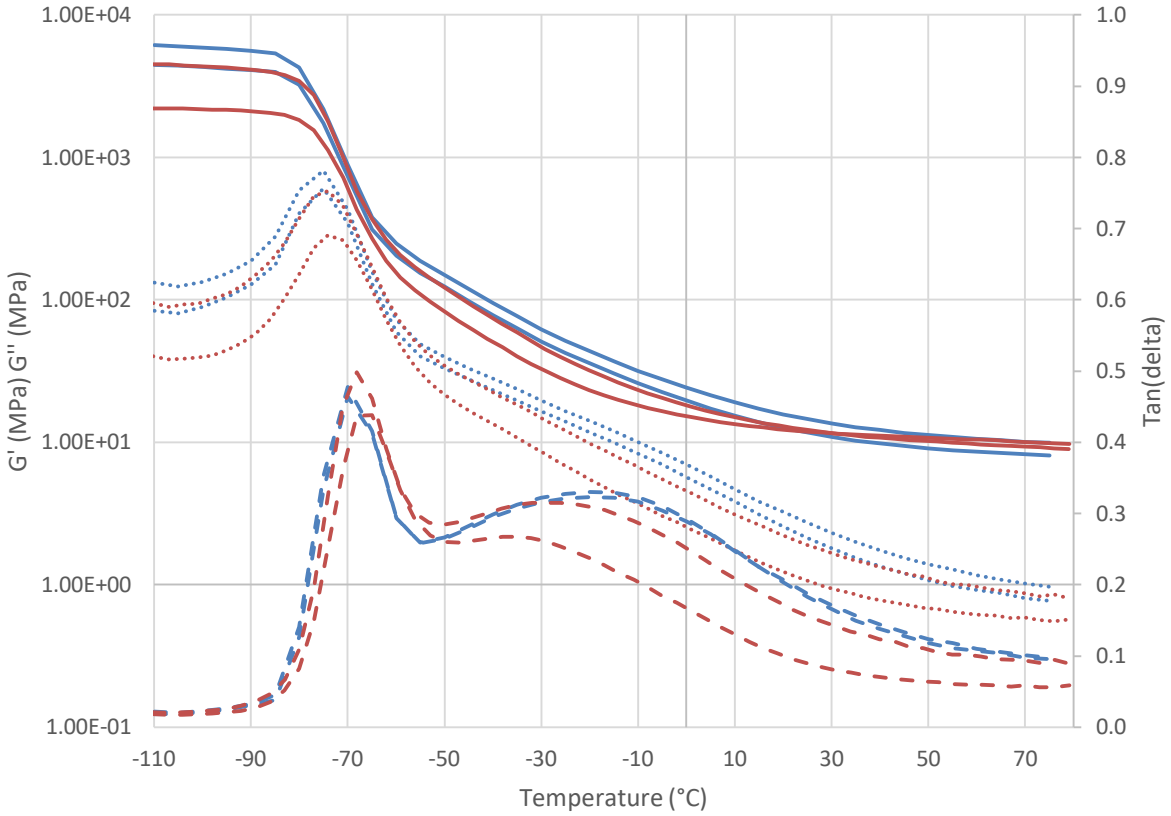


*Figure 26. DMA graph for 0.80 solid loading HTPB-Melamine samples plotting the elastic modulus or G' (solid line), loss modulus or G" (dotted line) and tan(delta) (dashed line), and comparing the LabRAM samples (red) with the planetary mixed samples (blue).. The samples show a shifted glass transition peak on the tan(delta) curve*

The graph for the 0.80 solid loading samples, Figure 26, exhibit inconsistent behaviour for both sample sets; the second LabRAM sample is hidden on the graph by the planetary mixed sample. Both mixing methods struggled to distribute the isocyanate effectively throughout the sample at this high solid loading. However, the LabRAM samples demonstrated greater variation and weaker behaviour indicating that the binder system consisted of a poorer network. This graph had a feature that was not observed on the lower solid loading samples. The second, broader tan(delta) peak is at a maximum at two different temperatures for the LabRAM and planetary mixed samples. This is attributed to the poor isocyanate distribution which caused a rate change in binder curing and change in how the network forms.

To ensure reasonable results, they have been compared with available literature. Table 9 details two papers; one is pure HTPB and the other is PBXs. Although the spread is greater

than that seen in literature, the results are within the expected range for a HTPB-based composite.

*Table 9. Table comparing the HTPB-Melamine DMA results with literature*

| **Source with summary of programme** | High Strain Rate and Shock Properties of Hydroxyl- Terminated Polybutadiene (HTPB) with Varying Amounts of Plasticizer, [Jordan et al, 2016] | Understanding damage in polymer-bonded explosive composites, [Drodge et al, 2016] |
|---|---|---|
| **Material** | Variations of HTPB cured with IPDI using just under a 10:1 ratio. Some samples have additional plasticisers (DOA, IDP and DOS). Focus is on the pure HTPB with the IPDI cross-linker (designated HTPB0). Several samples were tested for each material. | There were four compositions used in this research programme; pure binder, coarse RDX with binder, fine RDX with binder and coarse and fine RDX with binder. The solid loading for the fine composite was 54%, the coarse was 60% and the bimodal was 67%. The binder system consisted of HTPB, DOS, Lecithin (a wetting agent) and Lowinox (an antioxidant). |
| **Test Regime** | TA Instrument Q800, with sample sizes of 30 mm x 8 mm x 2 mm. Testing conducted from 150 K (-123.15 °C) to 300 K (26.85 °C) with frequency of 1, 10 and 100 Hz. No strain rate specified. | TA Instrument Q2000 with a single-cantilever flexure. It operated at a frequency of 1 Hz. |
| **Results** | The graphs below contain the storage modulus and the tan(delta) over the temperature range. The storage modulus demonstrated variation between like samples and a Tg range of -63 °C to 30 °C. The storage modulus before the glass transition point was ~1.1 GPa; after the Tg it is 1 – 1.1 MPa. The tan(delta) graph, although not explicitly stated, is assumed to be for the 1 Hz testing and the average of the samples and had a value of just over 1, which is expected for a viscoelastic polymer. | The graph below demonstrates the behaviour of the binder and the coarse RDX composite. The sample exhibited a storage modulus ranging from between $10^{10}$ Pa down to $10^{6}$ Pa and a Tg of approximately -80 °C. The particle size of the filler did not impact the storage modulus, but the coarser particles did have cause a shift in the tan(delta) peak. |

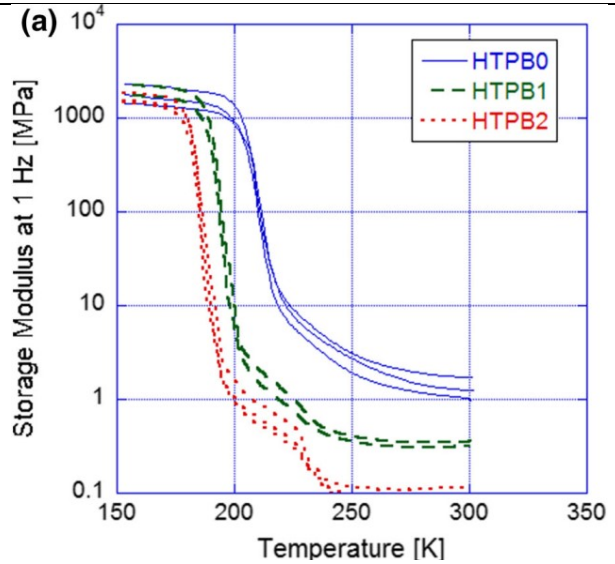
(a)
Storage Modulus at 1 Hz [MPa]
Temperature [K]
HTPB0
HTPB1
HTPB2

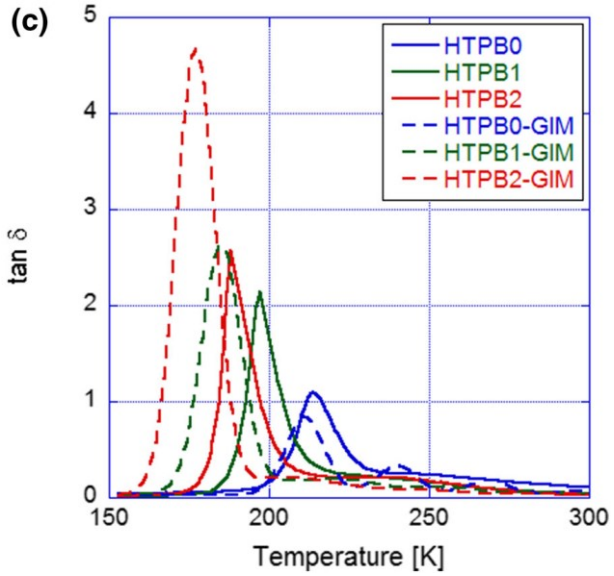
(c)
tan δ
Temperature [K]
HTPB0
HTPB1
HTPB2
HTPB0-GIM
HTPB1-GIM
HTPB2-GIM

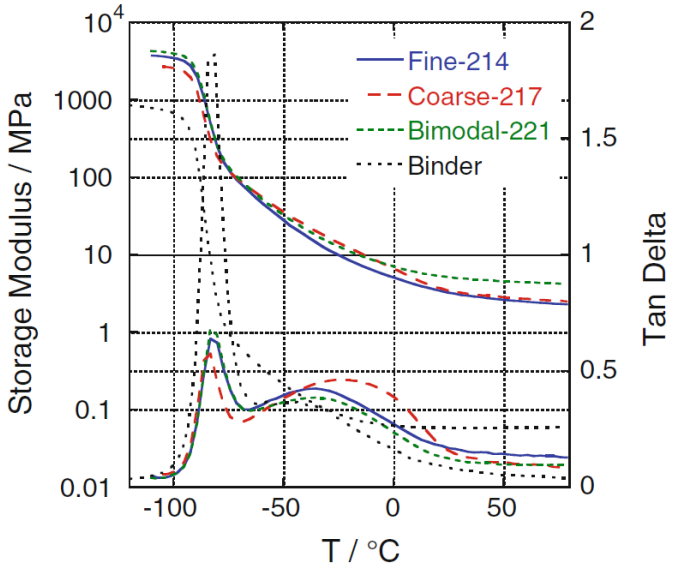
Storage Modulus / MPa
Tan Delta
T / °C
Fine-214
Coarse-217
Bimodal-221
Binder

| | | |
|---|---|---|
| **Comparison with this research programme** | The samples in this literature did have a level of variation between like samples, indicating that some level of variation is to be expected and is normal. The storage modulus was smaller in the literature, indicating that in this programme the samples have less elastic movement. This is expected with the addition of filler particles, as they will hinder the movement of the polymer chains. This study illustrates that the behaviours seen with these compositions is as expected for an HTPB-based composite but the spread was greater due to non-optimised mix conditions. | This literature is consistent with the research in this programme. The samples are within the same ranges for the storage modulus, although in this programme they do have a greater discrepancy between like samples as a result of the poor isocyanate distribution. The shifted tan(delta) peak in the coarse composite in the literature does not pass comment on the shifted tan(delta) peak at the higher solid loadings in this research. In this research programme, the samples have the same filler system and it is an impact of an insufficiently cured binder system. Although the samples in this research programme have greater variation, the range is within that expected for an HTPB-based composite indicating that the results are accurate. |

### 3.4.2 Thermal

Differential scanning calorimetry (DSC) is a thermal analysis technique investigating change in materials heat capacity over temperature range. Heat capacity is the amount of energy a material requires to increase its temperature by 1 °C. This technique can determine material transitions, such as melting, curing, glass transition or phase changes [Perkin Elmer Inc, 2014]. It compares the input required to heat an empty reference pan and a pan containing sample at the same rate [PSLC, 2017]. There are two DSC modes; heat flow or heat flux. Heat flow is preferable as the instruments two furnaces have a great sensitivity to smaller transitions and provide higher accuracy for heat capacity and enthalpy [Perkin Elmer Inc, 2014]. As pure materials have well defined thermal transitional points, DSC can help identify any impurities or variation within the composition. It requires quantities less than 10 mg of material. An example DSC themogram can be found in Figure 27.

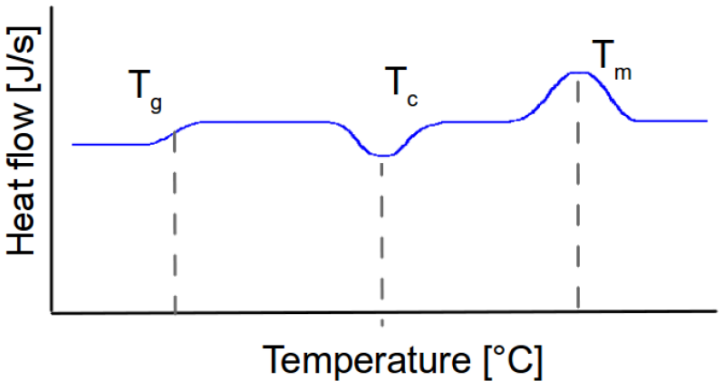


*Figure 27. Example DSC plot indicating glass transition ($T_g$), crystallization ($T_c$) and melting points ($T_m$) [Humboldt Universitat zu Berlin, 2017]*

A temperature sweep was conducted from 30 °C to 600 °C, with a ramp rate of 10 °C $min^{-1}$ under a nitrogen atmosphere. Three samples were tested at each loading level and mixing technique; only one thermogram has been included as they are consistent. The thermograms, in Figure 28 to Figure 33 exhibits a linear slope until 330 °C indicating a steady specific heat capacity, until two endothermic peaks occurs. Melamine begins to decompose at nominally 280 °C and then sublimes at 340 °C [UNEP Publications, 2019] [PubChem Open Chemistry Database, 2019]. Research [Sinha et al, 2014] conducted on an HTPB based composite was found to be dominated by HTPB. The sample exhibited two thermal peaks, one exothermic peak at around 370 °C and an endothermic at 460 °C. The first peak was attributed to the release of entrapped gaseous products, depolymerisation and further cross-linking of the urethane linkage. The second was the depolymerisation of any residue.

With the samples in this study, the two endothermic peaks indicate melting. The first peak is the melting or sublimation of the melamine. The melamine in literature was a pure material; by combining it with the HTPB to form a binary mixture there is an increase in the systems energy as the amine groups in the melamine react with the hydroxyl groups in the HTPB. As such, there is an associated increase in melting or sublimation temperature. The second peak is the degradation of the HTPB binder system. The samples found in literature were cross-linked with a different isocyanate, TDI instead of IPDI, which would have an impact on the melting temperature. This combined with the already transitioned melamine causes a downward shift in the melting point. These curves were not integrated due to their overlap. After the two melting points the thermograms exhibit decomposition which is inconsistent between like samples.

There was insignificant difference in the thermograms for LabRAM and planetary mixed samples. The onsets for the two thermal transitions are 340 °C and 375 °C. Both the 0.66 and the 0.80 solid loading samples had consistent thermal onsets and visually similar peaks; there is no significant variation between the mixing methods. For the 0.66 solid loading samples, there is a minor exothermic peak at 260 °C observed in the planetary mixed samples that is not seen in the LabRAM samples which is attributed to sample impurity and potential solvent entrapment. The 0.73 solid loading samples showed the greatest variation; it should be noted that the scale for the LabRAM sample is half that of the planetary mixed sample due to sample mass. Table 10 contains the sample masses; the 0.73 LabRAM sample has a 32% smaller mass than the average of the remaining samples. The other inconsistency in the 0.73 LabRAM samples is the different shaped double peaks. Whereas the other samples have a distinct split between the two thermal transitions, the 0.73 LabRAM sample has a larger overlap. This is due to a larger than average melamine peak, indicating that the sample has a higher degree of impurity. This is not consistent between all of the LabRAM samples and is exclusive to the 0.73 solid loading. As such, it is not a mixing flaw.

*Table 10. DSC sample masses for the HTPB-Melamine samples*

| Sample Type | Planetary Mixed | LabRAM |
|---|---|---|
| 0.66 Solid Loading | 9.9 mg | 9.5 mg |
| 0.73 Solid Loading | 8.2 mg | 5.9 mg |
| 0.80 Solid Loading | 8.4 mg | 7.6 mg |

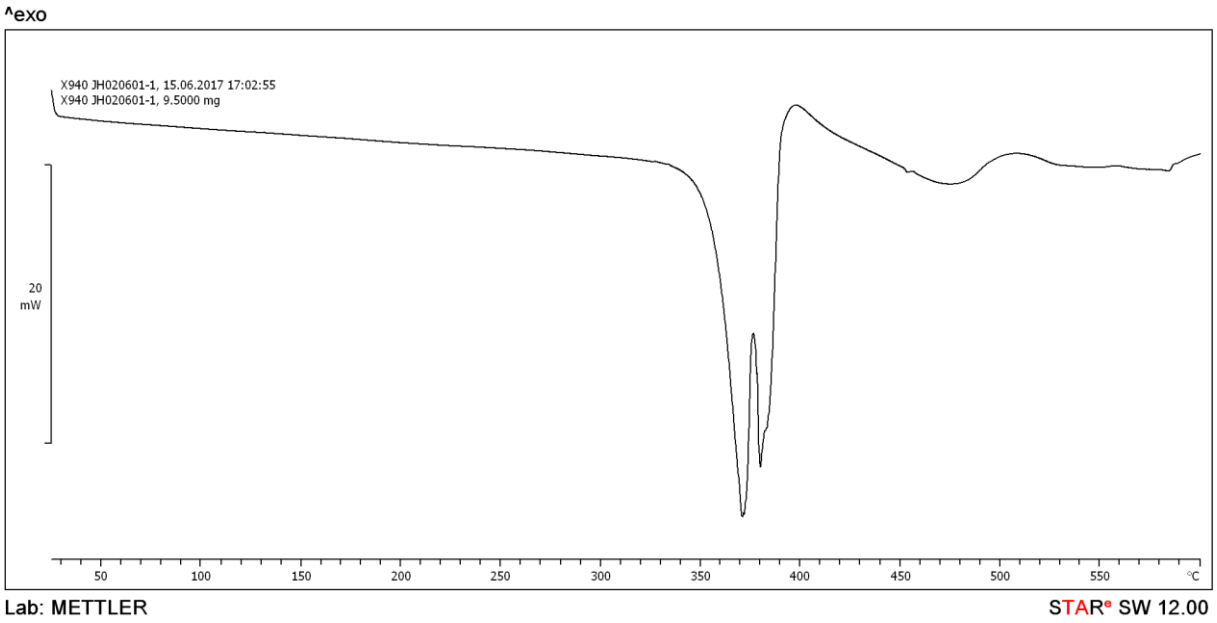


*Figure 28. DSC thermogram of 0.66 solid loading LabRAM sample demonstrating two endothermic peaks due to melamine sublimation, at 370 °C, and HTPB decomposition, at 385 °C*

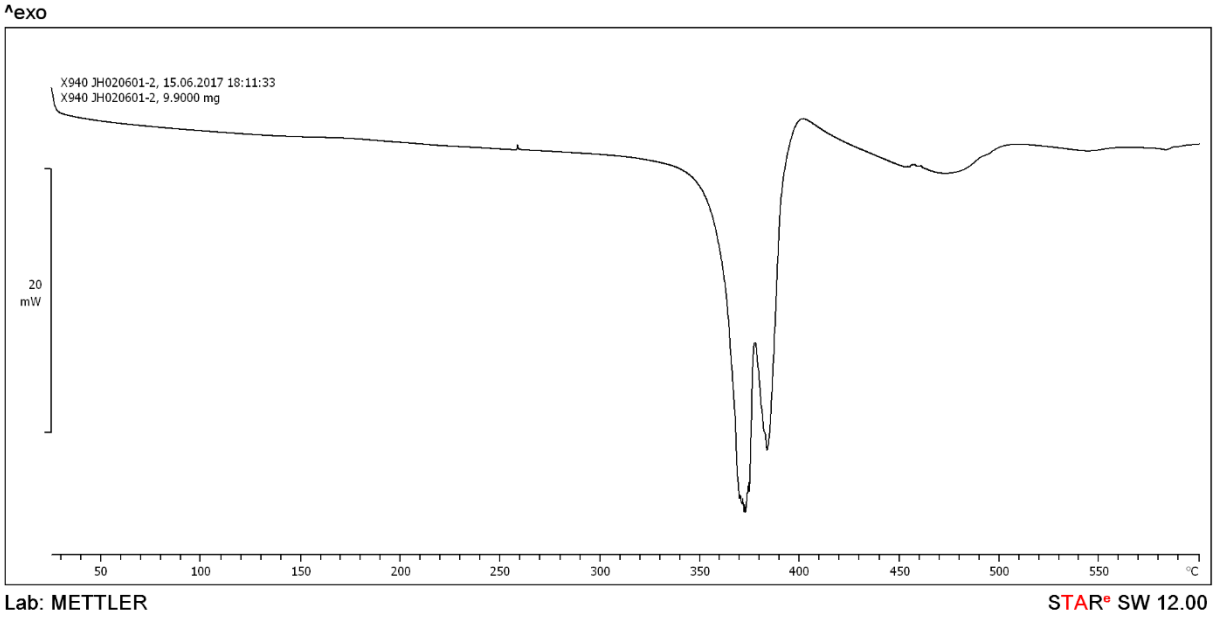


*Figure 29. DSC thermogram of 0.66 solid loading planetary mixed sample demonstrating two endothermic peaks due to melamine sublimation at 370 °C, and HTPB decomposition, at 385 °C*

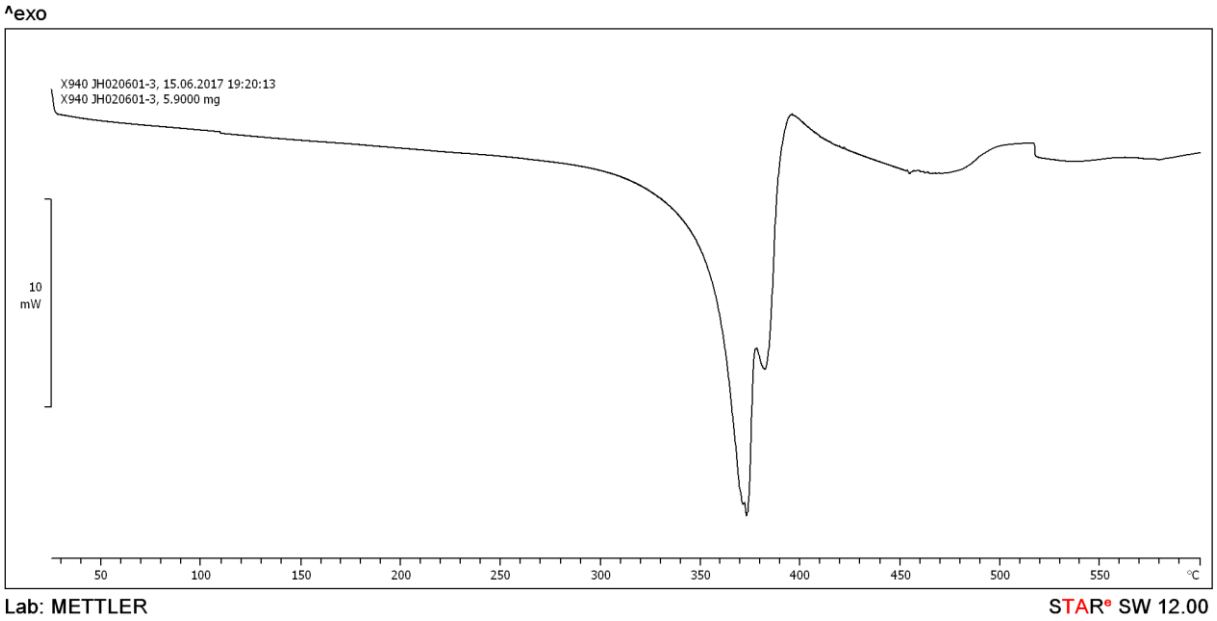


*Figure 30. DSC thermogram of 0.73 solid loading LabRAM sample demonstrating an overlap of the two endothermic peaks. The peaks are associated with melamine sublimation and HTPB decomposition; the broadness of the melamine sublimation peaks indicates impurity within the melamine.*

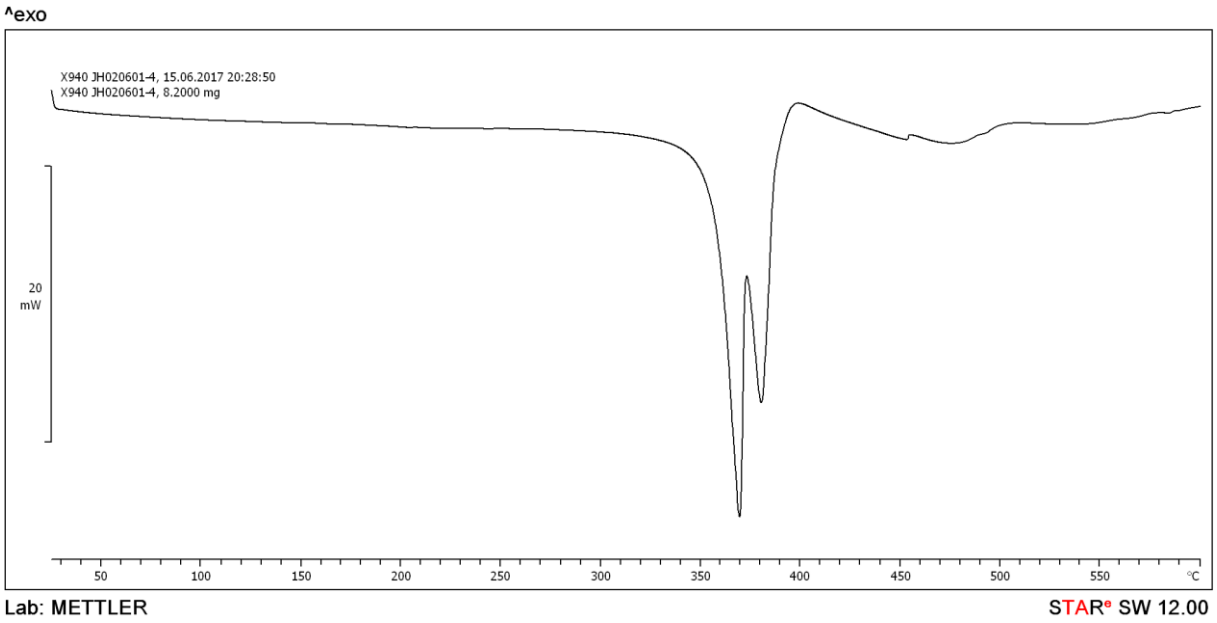


*Figure 31. DSC thermogram of 0.73 solid loading planetary mixed sample demonstrating two endothermic peaks due to melamine sublimation at 370 °C, and HTPB decomposition, at 385 °C*

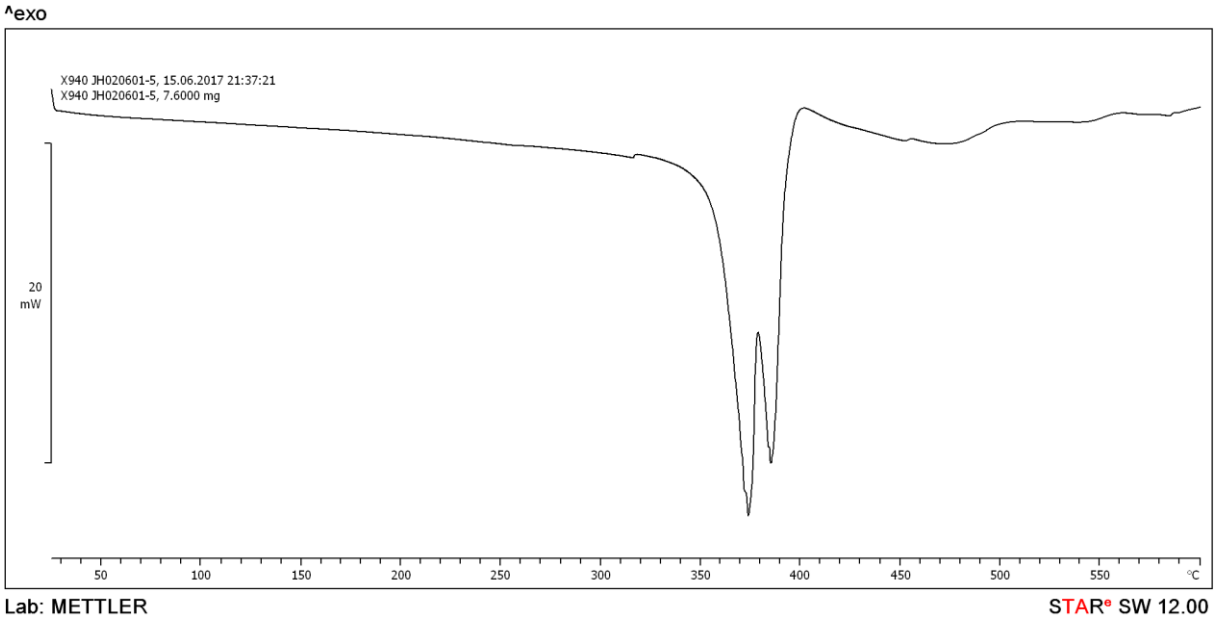


*Figure 32. DSC thermogram of 0.80 solid loading LabRAM sample demonstrating two endothermic peaks due to melamine sublimation at 375 °C, and HTPB decomposition, at 390 °C*

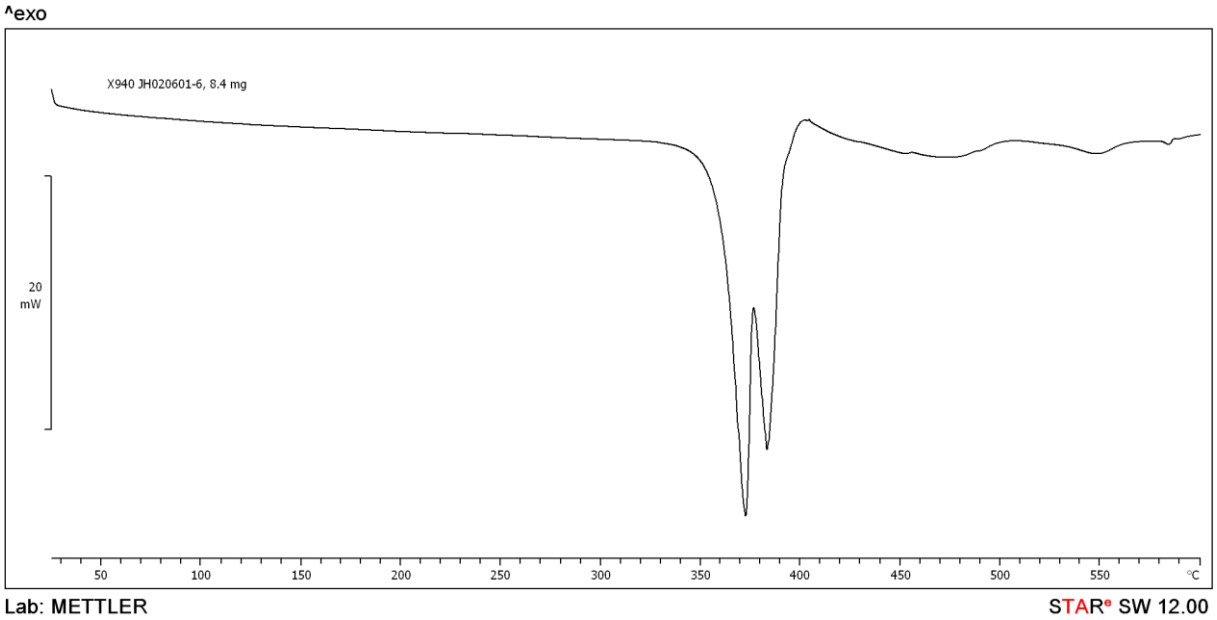


*Figure 33. DSC thermogram of 0.80 solid loading planetary mixed sample demonstrating two endothermic peaks due to melamine sublimation at 375 °C, and HTPB decomposition, at 390 °C*

### 3.4.3 Chemical

Due to the mechanical results and the shifted tan delta peak for the highly loaded LabRAM samples, nuclear magnetic resonance (NMR) was undertaken to determine the homogeneity. NMR is based on the spin of some atoms like carbon-13 and hydrogen. That spin has a magnetic moment which can interact with an applied magnetic field, generating two energy levels. By applying electromagnetic pulses of specific frequencies and energies, nuclei at the lower energy level can be excited to the higher one. Once the electromagnetic radiation is released these excited nuclei can drop or relax back down to the lower energy level and release an emission signal. This is called a free induction decay (FID). It undergoes a fourier transform to produce a spectrum [Keeler, 2002]. NMR, as a technique, is effective at identifying unknown components within samples and quantifying concentration.

The 0.80 solid loading LabRAM samples, shown in Figure 34, showed discolouration as they aged due to the polymer oxidising, which was expected due to the lack of antioxidant; however, the discolouration was irregular and appeared in a marbled pattern. Polymer oxidation damages the material, fracturing the polymer chains, which has a negative impact on the materials mechanical behaviour, reducing its elasticity [Callister Jr, 2007]. The image was edited to fully demonstrate this; it was sharpened by 24%, brightened by 40% and the contrast was increased to 34%. This marbling effect suggests inhomogeneity with binder rich and poor areas. As such, a protonquant NMR was conducted. Protonquant NMR measures the $^{1}H$ and uses a known standard to quantify the available and extractable HTPB concentration; extractable HTPB has not been crosslinked to form the larger polyurethane network. The two DMA samples were used, and 0.5 g mass of material was taken from both ends and the middle. A deuterated chloroform, $CDCL_3$, and tris(trimethylsilyl)silane, TTMS, standard was used. The samples were extracted for a day.

*Figure 34. Modified image of LabRAM 0.80 solid loading DMA samples demonstrating colour variation. The yellowing colour is due to the oxidation of HTPB, and the inconsistent colour demonstrates an inhomogeneous sample*

*Table 11. NMR results showing the extractable and available HTPB concentration of the 0.80 solid loading HTPB-Melamine samples mixed by RAM. The samples demonstrate significant variation between the like samples indicating variation in either the distribution of the HTPB or the cross-linking*

| **Sample** | | **Extractable HTPB Concentration (%)** | **Average (%)** | **Standard Deviation** |
|---|---|---|---|---|
| LabRAM 0.80 Sample 1 | 1 | 2.731 | 2.510 | 1.350 |
| | 2 | 3.736 | | |
| | 3 | 1.064 | | |
| LabRAM 0.80 Sample 2 | 1 | 1.252 | 1.250 | 0.018 |
| | 2 | 1.232 | | |
| | 3 | 1.267 | | |

The results, tabulated in Table 11, demonstrate variations in available HTPB concentrations. Sample 2 has a reasonable consistency but sample 1 is erratic with significant deviation. The samples were taken from the same batch of material highlighting an overlying issue with the total sample/batch. This variation in available/extractable HTPB also explains the tan delta peak shift and the lack of consistency between the two LabRAM samples.

### 3.4.4 Optical Microscopy

Optical microscopy was conducted on an Axio Zeiss M1M. Microscopy images were taken to provide visual evidence about the structure of the material and determine whether there was any difference in any of the components. For the filler, there was concern that the microscopy images would demonstrate changes in either the particle size or shape, as the particles either fracture or smooth off. This could be due to either the mechanical input of the blades or the flow from the material during RAM mixing. The binder system was is less clear in the microscopy images, but can be seen as long strands of material. There was concern that these strands would be shorter, indicating either poor cross-linking or damage to the chains, known as chain scissoring [Callister Jr, 2007]. As the polymeric matrix is the structural component of the composite, damage to the chains has a direct negative impact on the mechanical behaviour.

The samples were prepared at room temperature using a laboratory scalpel which caused a ductile failure. This causes variation in sample height and areas on the image being out of focus. Although a brittle failure would be more representative of the bulk material and would reduce the deformation in the sample, the materials have a low glass transition temperature which could not be reached during preparation. Whilst preparing the samples, melamine did crumble out of the bulk material. The filler particles are not chemically bonded into the binder system and instead encased within the polymeric chains. When cutting the bulk sample these polymeric chains are broken allowing the trapped melamine to escape. There was no noticeable difference in the ease at which the melamine freed itself from the bulk material.

The images, Figure 35 to Figure 37, demonstrated no differences between the LabRAM and planetary mixed samples. The melamine crystals and the HTPB chains can be observed; the melamine crystals have been circled. The filler is consistent in shape and size and there is no shearing or fracturing. The polymer chains do not appear to be shorter or damaged either. The distribution of the melamine within the binder system is visually consistent.

In the 0.80 LabRAM samples there is greater binder network visible within the image compared to the planetary mixed sample, Figure 37. This provides additional evidence that there is variation in extractable HTPB concentration between the planetary mixed samples and the RAM samples.

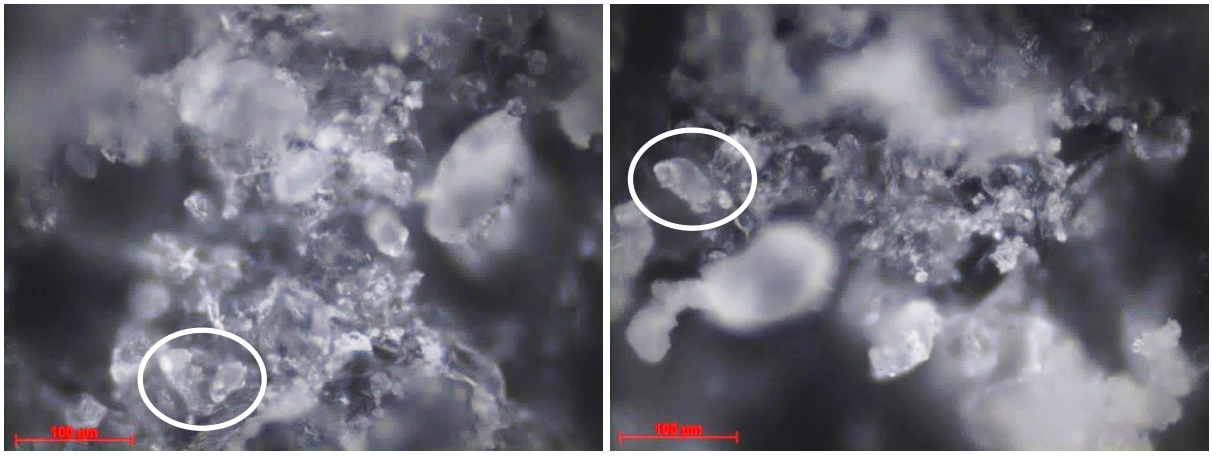

*Figure 35. Microscopy images of the 0.66 solid loading HTPB-Melamine samples mixed by LabRAM (left) and planetary mixing (right). A melamine crystal has been circled in each image. The HTPB can be observed as long strands throughout the image; however, due to the concentration they are not as prevalent. The melamine crystals do not appear to differ in either shape or size and the HTPB strands do not appear to be damaged or shorter when comparing the two mixing methods.*

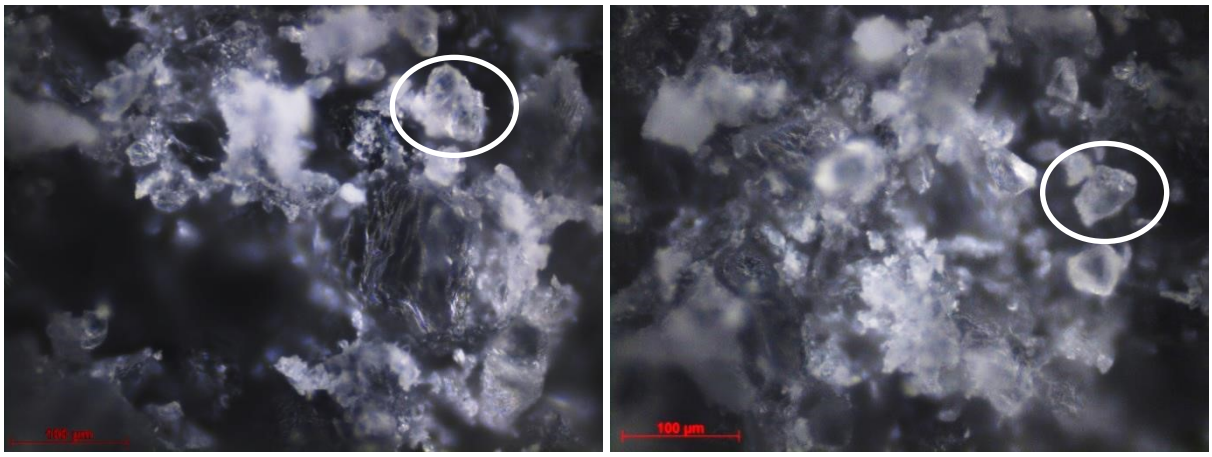

*Figure 36. Microscopy images of the 0.73 solid loading HTPB-Melamine samples mixed by LabRAM (left) and planetary mixing (right). A melamine crystal has been circled in each image. Small amounts of the HTPB can be observed as long strands throughout the image; however, due to the concentration they are not as prevalent. The melamine crystals do not appear to differ in either shape or size and the HTPB strands do not appear to be damaged or shorter when comparing the two mixing methods.*

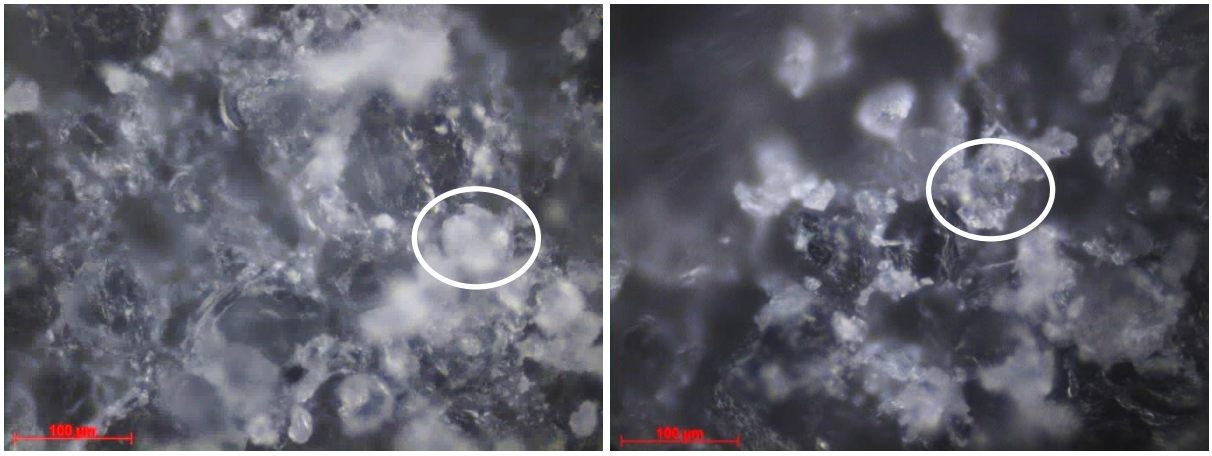

*Figure 37. Microscopy images of the 0.66 solid loading HTPB-Melamine samples mixed by LabRAM (left) and planetary mixing (right). A melamine crystal has been circled in each image. The HTPB can be observed as long strands throughout the image; however, due to the concentration they are not as prevalent. The melamine crystals do not appear to differ in either shape or size and the HTPB strands do not appear to be damaged or shorter when comparing the two mixing methods. However, there does appear to be significantly more HTPB visible in the RAM sample compared to the planetary mixed sample.*

## 3.5 Discussion and Conclusions

The HTPB-Melamine samples highlighted initial limitations and considerations. Planetary mixing has a physical input within the sample forcing flow, whereas LabRAM is significantly more dependent on the mix parameters. The DMA results demonstrated that the mixing regime that was appropriate for the lower solid loading samples did not sufficiently distribute the isocyanate through the 0.80 solid loading samples. However, with the appropriate parameters three LabRAM mixes were completed in a day instead of one. Material characterisation was limited in this chapter to DMA, DSC, optical microscopy and NMR, for selected samples, to get an indication of where focus should be. The mechanical behaviour was driven by the binder system and the cross-linking, whereas the thermal behaviour was dominated by the components individual transition points. As such, a greater emphasis will be given on mechanical behaviour for future compositions.

The mechanical behaviour did demonstrate variation between mixing methods. The moduli for the 0.73 solid loading samples had minor variation between the LabRAM and the planetary mixed samples whereas the 0.66 solid loading LabRAM samples were significantly weaker past the glass transition point. The 0.80 solid loading sample had discrepancy between the LabRAM samples, with only one sample resembling the planetary mixed samples. This behaviour was due to variation in extractable HTPB concentration and confirmed by a

protonquant NMR demonstrating poor distribution of the isocyanate. The optical microscopy images do not highlight any differences in the sample in terms of the crystal size or shape, although does indicate inconsistent distribution of the HTPB in the RAM samples. There was no evidence to suggest variation in the interactions between the filler particles and the binder. There is no chemical bonding between the two phases, and the filler is entrapped in the polymer network.

This chapter and these samples highlighted the importance of ensuring that the appropriate parameters are applied to whatever mixing method is used. Conventional planetary mixing has the advantage of being an established, well understood technique with a physical intrusive blade that forces material to flow. RAM requires a greater level of optimisation that is not easily identified. However, it has demonstrated, primarily with the 0.73 solid loading sample, that when mix parameters are optimised it is a quicker technique that has not significantly impacted the material.

# 4 HTPB-Melamine-Barium Sulphate

The 0.73 solid loading HTPB-Melamine samples exhibited consistent behaviour and provided no evidence that RAM mixing had any significant impact on the samples. The 0.66 and 0.80 solid loading samples exhibited deviation due to poor distribution of isocyanate. As stated in Chapter 3, any variation in the results are defined as significant or insignificant. Significant variation is greater than 10% and is based on material specifications.

The next stage increased complexity of the composition by using a bimodal filler system, allowing a greater packing density and higher filler loading. Figure 38 illustrates this concept; microscopy images were taken of diamond composites with a magnesium matrix [Molina-Jorda, 2015]. The images on the left are scanning electron microscopy (SEM) images and the images on the right are of the diamond surface. The top set has 100% D1 particles, with an average diameter of 400 μm, whereas the bottom images have 70% D1 and 30% D8, which have an average particle size of 58 μm. By using the D8 particles, there is an increase of 15% in volume fraction which would otherwise be unfeasible. In energetics, PBXs and composite propellants use a bimodal filler system. High explosive fillers such as RDX and HMX, like the diamond particles, are available in multiple classes. RDX classes are summarised in Table 6. Although a large range of particle sizes give an improved packing density and greater solid loading with the same rheological properties, cost and batch to batch variability make this an unpopular option. Some classes allow a large variation and wide spread of properties, which increases batch-to-batch variation.

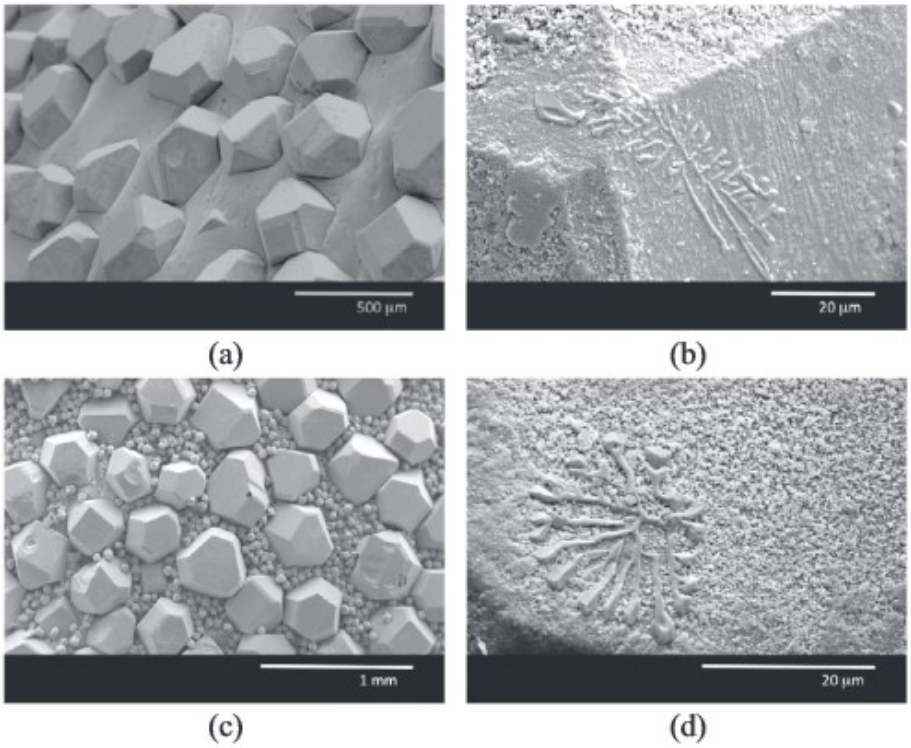


*Figure 38. SEM images comparing a monomodal filler system (a and b) with a bimodal filler system (c and d) and demonstrating the higher solid loadings achieved through the bimodal system. In the bimodal system the second filler size distributes around the larger particles, filling the blank space which would require additional matrix [Molina-Jorda, 2015]*

## 4.1 Materials

Like melamine, barium sulphate is used as a density simulant for HE crystals and does not represent the mechanical properties of the HE or the energetic composite. It is an inorganic, white, odourless powder. When comparing a typical HE filler with barium sulphate it is not a good density mimic; however, the finer filler is a minor component so results are dominated by the coarser filler. A summary of material densities can be found in Table 12. Like with the melamine, the barium sulphate was put in an oven overnight at 70 °C prior to use. A ratio of coarse: fine filler of 73:27 was used based on operator experience.

*Table 12. Table comparing the densities of commonly used fillers for explosive composites and mimics*

| **Material** | RDX | HMX | Ammonium Perchlorate | Melamine | Barium Sulphate |
|---|---|---|---|---|---|
| **Density/ g cm$^{-3}$** | 1.8 [chemringnobel.no, 2019] | 1.9 [chemringnobel.no, 2019(b)] | 1.95 [www.chemicalbook.com, 2019] | 1.57 [Inchem.org, 2019] | 4.25 [PubChem, 2019(b)] |

## 4.2 Planetary Mixing

An IKA Planetron HKV-1, with a minimum mixing capacity of 300 g, was used and a 0.1 bar to 0.2 bar vacuum was applied. Blade speed varied between 11 and 18 rpm. Planetary mixing remains consistent in its processing parameters when mixing like materials. There was no temperature monitoring available on the mixer and although there was a water jacket built into the mix bowl it was not used. Temperature controls are applied to reduce binder viscosity. The LabRAM vessel used does not have this feature. Like with the HTPB-Melamine samples the 0.80 solid loading samples were highly viscous and required an external stimuli, like a spatula, for the material to move. It would not flow under its own impetus, and instead required the operator to scoop material out. Details on the materials can be found in Table 13.

*Table 13. Formulation table of HTPB-Melamine-Barium Sulphate Planetary mixed samples*

| | | | | | |
|---|---|---|---|---|---|
| **0.66 solid loading** | HTPB | Melamine | Barium Sulphate | Planetary Mixed | Sample had very good flow properties and cast well |
| | 34 | 47.52 | 18.48 | | |
| **0.73 solid loading** | HTPB | Melamine | Barium Sulphate | Planetary Mixed | Sample had good flow properties and cast without external stimuli |
| | 27 | 52.56 | 20.44 | | |
| **0.80 solid loading** | HTPB | Melamine | Barium Sulphate | Planetary Mixed | Sample had poor flow properties and required external stimulus to cast |
| | 20 | 57.6 | 22.4 | | |

The 0.80 solid loading sample contained minor voidage of no more than 2 mm diameter throughout due to the samples high viscosity. Samples with the least voidage was chosen for testing. Figure 39 is the 0.80 solid loading planetary mixed dynamic mechanical analysis (DMA) sample which was worst case.

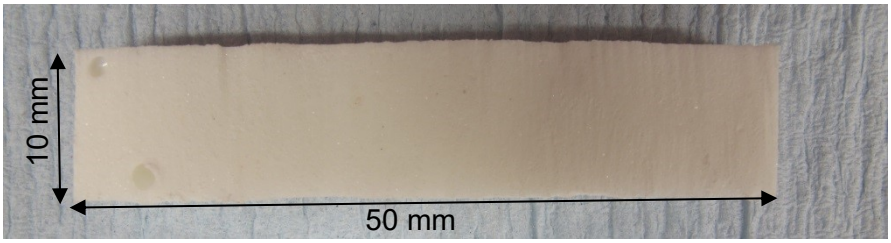


*Figure 39. 0.80 solid loading planetary mixed DMA samples with visible voids at the left hand side of the sample approximately 2 mm diameter*

## 4.3 LabRAM Mixing

Mixing parameters for the HTPB-Melamine samples were used as a baseline for these compositions; the regime was still directed by operator observations, which are detailed in Chapter 8.2. The input applied by the LabRAM was increased systematically until flow was visible within the sample; there is a small boundary between the material remaining stationary with no mixing occurring and the sample debonding from the vessel. This is demonstrated in Figure 40.

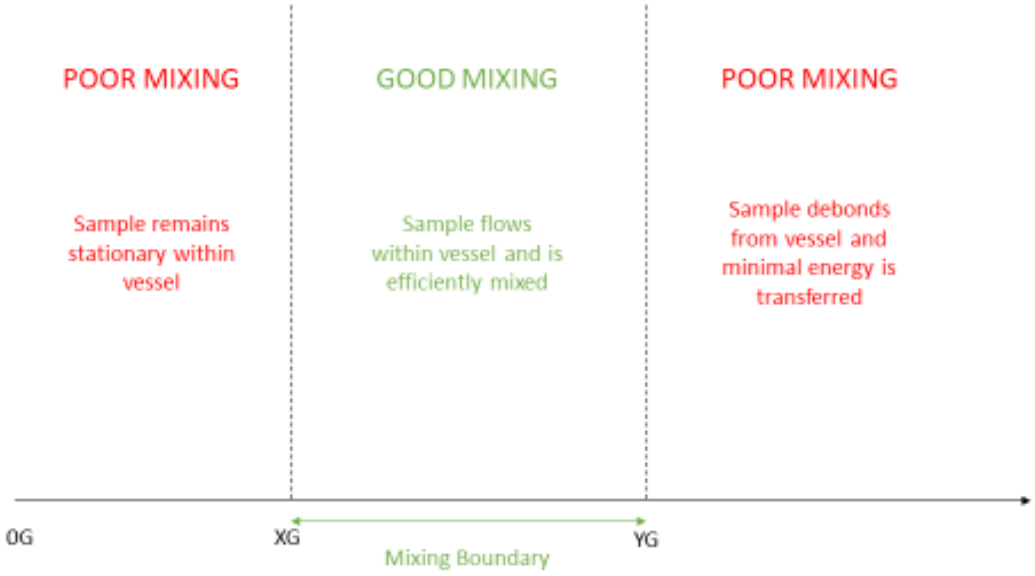


*Figure 40. Diagram indicating the impact of acceleration on whether a sample will mix by RAM*

As there were issues with the isocyanate being properly distributed throughout the sample in the HTPB-Melamine samples in Chapter 3, the time when the material was flowing within the vessel was increased. For this composition, the temperature was monitored throughout the mix. Higher temperature reduces the binder and aids mixing but can reduce the pot-life and

when processing with energetics have an associated safety risk. As these are inert materials it was used to monitor and provide information for later phases of this study.

Compositions were mixed in 8 oz polystyrene pots in 200 g batches under a vacuum of 5 mbar. The samples and their mixing notes are detailed in Table 14. The power percentage was manually set and modified based on visual observations and real-time frequency. The processing ability of the bimodal composites was greatly improved in comparison to the monomodal system; this was seen primarily in the flow capability of the highly loaded sample which cast with ease. After mixing, the material was poured from the vessel into the mould; vacuum casting was not deemed suitable due to the mould type and the small amount of material. The coarse melamine and fine barium sulphate were added in two equal proportions throughout the mixing process. The mixing with the temperature change is plotted in Figure 41. The power input was set up to 75%, which correlated to an acceleration of between 40 and 50 G. During mixing there was a temperature increase of 50 °C as a result of internal friction due to sample flow.

*Table 14. Formulation table of HTPB-Melamine-Barium Sulphate LabRAM samples*

| | | | | | |
|---|---|---|---|---|---|
| **0.66 solid loading** | HTPB | Melamine | Barium Sulphate | LabRAM | Sample had very good flow properties and cast well |
| | 34 | 47.52 | 18.48 | | |
| **0.73 solid loading** | HTPB | Melamine | Barium Sulphate | LabRAM | Sample had very good flow properties and cast well |
| | 20 | 57.6 | 22.4 | | |
| **0.80 solid loading** | HTPB | Melamine | Barium Sulphate | LabRAM | Sample had very good flow properties and cast well |
| | 27 | 52.56 | 20.44 | | |

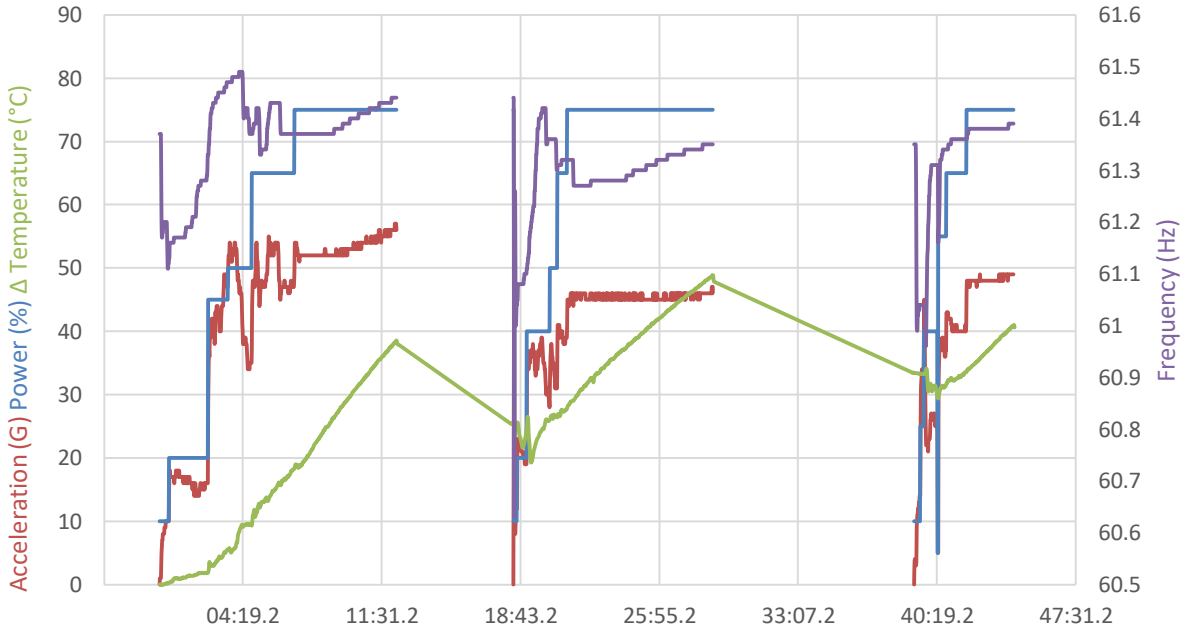


*Figure 41. Mixing graph for the 0.80 solid loading HTPB-Melamine-Barium Sulphate sample showing the acceleration in G (red), power input (blue), temperature change in Celsius (green) and the LabRAM frequency in Hz (purple). The mix is stopped twice for material to be added to the sample*

Unlike the higher loaded and more viscous samples, the 0.66 solid loading samples struggled to break down the agglomerates of barium sulphate which could be up to several centimetres in diameter. The first 0.66 solid loading sample was unsuccessful as these agglomerates were closely packed throughout the cast sample, causing the remainder of the material to be binder rich and highly rubbery. Remixing the sample used a higher power input, and a spatula was used to break some of these larger agglomerates.

## 4.4 Characterisation

Characterisation conducted had a large emphasis on mechanical testing; DMA testing for the previous samples showed little variation when a consistent mix was achieved and was expected to behave the same with these materials. Hardness testing was conducted on the bulk material. Density measurements were taken and thermal expansion tests were also conducted. Optical microscopy was used to assess the wetting of the filler particles.

### 4.4.1 DMA Testing

DMA testing was conducted with the same conditions as the HTPB-Melamine samples which can be found in Chapter 3.4.1. As with the HTPB-Melamine composition, there was no anti-oxidant and the oxidised layer was removed. Testing was performed on a Rheometrics RDAII dynamic mechanical analyser, from -110 °C to +80 °C in 3 °C increments with a nominal strain of 0.1%.

Graphs were plotted for each solid loading level, comparing the LabRAM, plotted in red, and the planetary mixed samples, plotted in blue. The storage modulus, G', and loss modulus, G'', were plotted on the primary y-axis, with solid lines and dotted lines respectively. The tan(delta) was plotted on the secondary y-axis with dashed lines.

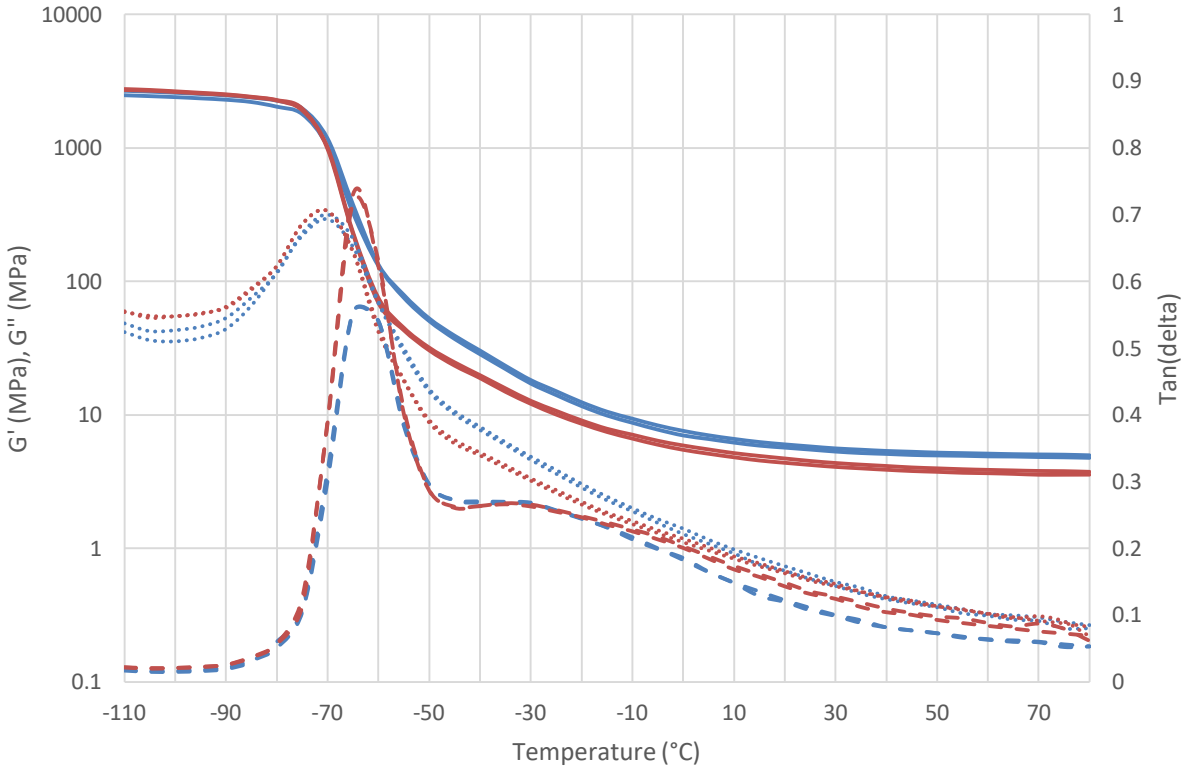


*Figure 42. DMA graph for 0.66 solid loading HTPB-Melamine-Barium Sulphate samples plotting the elastic modulus or G' (solid line), loss modulus or G'' (dotted line) and tan(delta) (dashed line), and comparing the LabRAM samples (red) with the planetary mixed samples (blue). The samples showed good consistency with the planetary mixed samples behaving more elastic after the glass transition temperature.*

The 0.66 solid loading samples are plotted in Figure 42; like samples are consistent and overlay. The LabRAM samples exhibited less elastic behaviour and greater loss modulus

after the glass transition temperature, indicating greater movement of the polymeric chains and a softer material. This could be a result of poor cross-linkage, chain scission or less polymer entanglements. The loss modulus, G'', indicated that prior to the glass transition the LabRAM samples had greater energy dissipation, either as heat or friction, but after the planetary mixed samples had greater energy dissipation. The tan(delta) has an increased glass transition peak for the LabRAM samples, which confirms the large energy loss within the sample and the greater non-elastic component at this temperature.

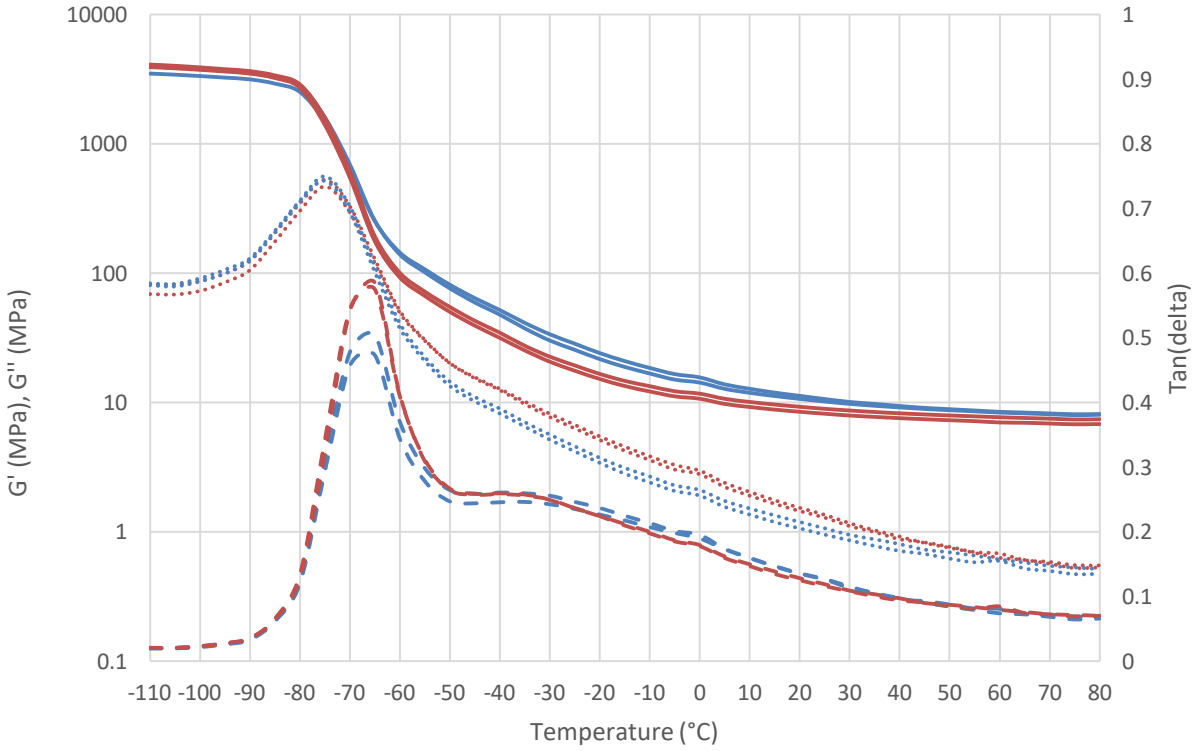


*Figure 43. DMA graph for 0.73 solid loading HTPB-Melamine-Barium Sulphate samples plotting the elastic modulus or G' (solid line), loss modulus or G" (dotted line) and tan(delta) (dashed line), and comparing the LabRAM samples (red) with the planetary mixed samples (blue). The samples showed good consistency with the planetary mixed samples behaving more elastic after the glass transition temperature.*

The 0.73 solid loading compositions, plotted in Figure 43, showed consistency through both mixing methods. The moduli overlay at both the high and low temperatures; however, there is a minor deviation between -70 °C and 30 °C. Between these temperatures the LabRAM samples exhibit less elastic behaviour and are softer than the planetary mixed counterparts. As with the 0.66 solid loading sample, this is due to additional movement of the polymeric chains. There is also minor variation in the loss modulus, G'', which indicates that the

samples are dissipating energy at different rates; the planetary mixed samples lost more energy below the glass transition temperatures whereas the LabRAM samples dissipated the energy after this point. There was an increase in the tan(delta) peak indicating that the LabRAM samples are more viscoelastic and have greater energy loss due to either friction or heat. Both of these are a consequence of the sample being able to move when stimuli is applied.

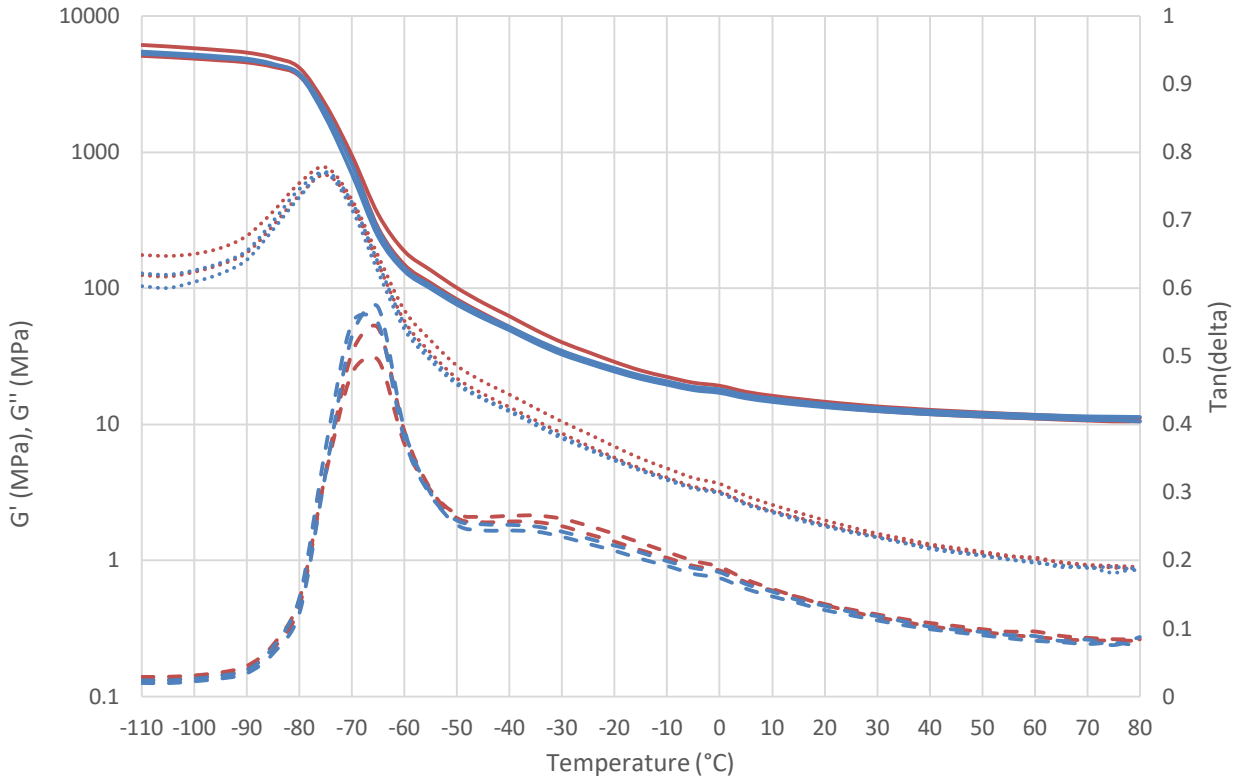


*Figure 44. DMA graph for 0.80 solid loading HTPB-Melamine-Barium Sulphate samples plotting the elastic modulus or G' (solid line), loss modulus or G" (dotted line) and tan(delta) (dashed line), and comparing the LabRAM samples (red) with the planetary mixed samples (blue). The samples showed high levels of consistency.*

The 0.80 solid loading samples, in Figure 44, were consistent. The storage modulus overlays over the temperature range; the deviation seen in Figure 43 from -60 °C to 0 °C is reduced. The loss moduli are consistent across the mixing methods; at the lower end of the temperature range, there is minor variation which does have a relationship with the mixing method. The tan(delta) curve shows minor deviation; however, it is not significant. As opposed to the 0.66 and 0.73 solid loading samples, the 0.80 LabRAM samples were slightly stronger when compared to the planetary mixed samples; it was thought that this could be a

result of the voids that were more prominent in the planetary mixed samples. However, due to the consistency between the planetary mixed samples this has been disregarded.

The results, as with the HTPB-Melamine composition, have been compared with a result in literature and the results from the previous chapter and summarised in Table 15. This provides confidence and context for the data generated in this study. The paper chosen investigates a composite propellant. The previous chapter, 3.4.1, has a similar composition and has been compared with other literature to provide confidence in the results.

*Table 15. Table comparing the HTPB-Melamine-Barium Sulphate DMA results with literature*

| **Source with summary of programme** | HTPB-Melamine, Chapter 3.4.1 | Ageing behaviour of composite rocket propellant formulations investigated by DMA, SGA and GPC [Bohn et al, 2010] |
|---|---|---|
| **Material** | HTPB and melamine composite manufactured by LabRAM and planetary mixing with solid loadings of 0.66, 0.73 and 0.80. There were two tests per sample, and the sample size was 6 mm x 10 mm x 50 mm | HTPB based composite propellant with ammonium perchlorate and aluminium totalling to 0.84 solid loading. The HTPB binder is 0.67 HTPB and 0.25 plasticiser (DOS). One sample tested for each composition due to high reproducibility. Sample size of 10 mm x 4 mm x 50 mm. |
| **Test Regime** | Rheometrics RDAII dynamic mechanical analyser, with a temperature range of -110 °C to +80 °C in 3 °C steps. The nominal strain was 0.1%. | Rheometric Scientific ARES with a temperature range of -100 °C to +70 °C with a heating rate of 1 °C $min^{-1}$ and a soak time of 28 seconds. Tested at multiple frequencies: 0.1, 1.0. 10.0, 56.0 Hz. |
| **Results** | The moduli for all three solid loadings ranged from $10^{10}$ to $10^{5}$ Pa across the whole temperature range. The results had a large spread attributed to poor isocyanate distribution throughout the sample. The tan(delta) has two peaks, one sharp one at nominally -65 °C, and one broader one at nominally -20 °C. The highest solid loading sample, in the graph below, had a shifted tan(delta) peak for the LabRAM sample, indicating a poor cure. | The graph below demonstrates the effect of ageing with the tan(delta) curve. The unaged sample had two tan(delta) peaks; the first is a sharp peak around -70 °C and is around 0.7. This is driven by the binder system. The second is a much broader peak starting at -40 °C resulting from the filler system. The unaged sample peaks at ~ 0.4 and -10 °C. |

| | | |
|---|---|---|
| | 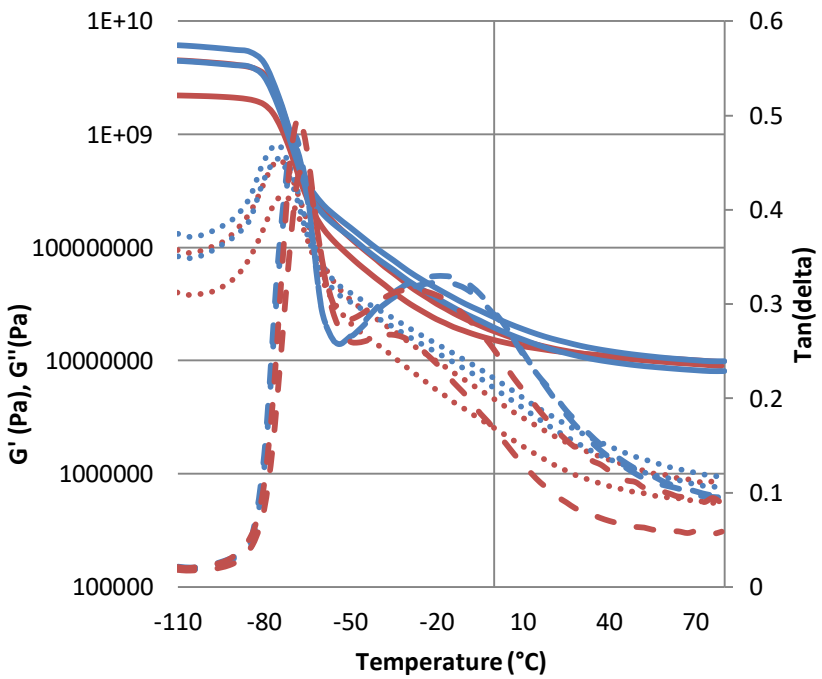 | 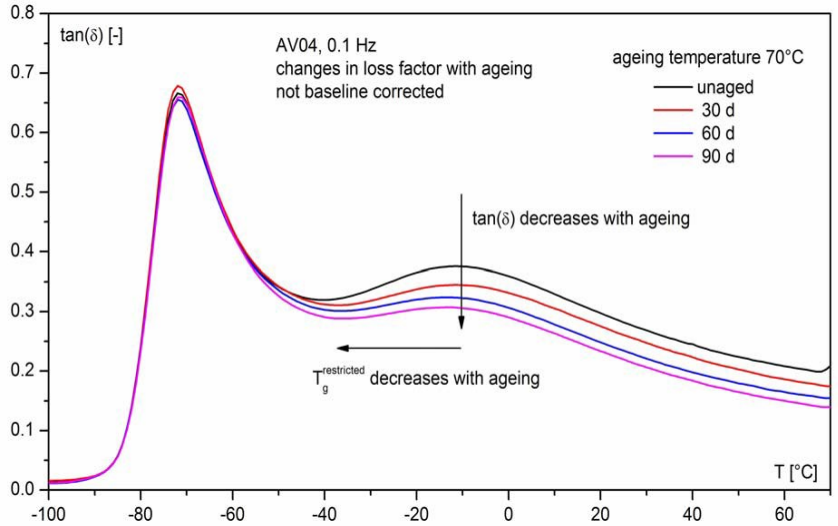 |
| **Comparison with this research programme** | The materials in this chapter were more consistent indicating more efficient mixing. The moduli and the tan(delta) remain within the same range, and there is no shifted tan(delta) peak in any of the results. This indicates that not only are these results reasonable and expected, but that the mixing was improved compared to previous chapters. | The materials exhibit the same double tan(delta) peak that is observed in this research programme, due to the addition of filler particles. Both peaks in this chapter are smaller, within 50% of the literature, but occur at the same temperature. The samples in the literature contained plasticiser which is responsible for the greater plasticity. |

### 4.4.2 **Hardness**

Hardness is a materials ability to resist permanent indentation and deformation when a fixed load is applied. Testing is quick and labour light. Measurements are taken of either the depth or area of indentation produced. There are several variations of this test; Rockwell, Brinell, Vickers and Knoop are for metallic materials [hardnesstesters.com, 2017] [www.gordonengland.co.uk, 2017] [web.calce.umd.edu, 2018]. Shore A hardness is a more appropriate technique for polymer based composites and is commonly used for elastomers. A calibrated spring indents a rod into the sample and measures the indentation. As polymers can relax, a dwell time is included with the results. The measurement is taken at the end of this dwell time and will influence the results [Barnwell.co.uk, 2019] [Matweb.com, 2019]. It is recommended that the sample thickness is at least 10x the depth of the indent. There can be large variation in results due to local surface effects, polymer relaxation and potential piercing of the material which could produce false results. Achieving consistent results can be hard and results can be a poor representation of the behaviour. However, hardness testing can be used in material specifications to ensure samples are not undercured; a material that is undercured will be softer, more malleable and more likely to slump. During use, undercured material may not retain its structural integrity and move within the casing, potentially experiencing sufficient shock and friction for initiation.

Hardness testing in this study was conducted with a PosiTector Standard portable hardness tester using the Shore A Hardness methodology and having a test time of 15 seconds. Testing was conducted on a cut bulk surface; the exposed surfaces had minor discolouration due to oxidation of the binder system. Samples were 5 mm thick and were placed on the calibration block during testing. The results were tabulated in Table 16 and summarised in Table 17 with the percentage change from the LabRAM average to the planetary mixed average and the T-test probability. More information on T-tests can be found in Chapter 2.4.

The samples demonstrated variation between mixing methods with a hardness percentage change up to 5.2%. There was no relationship between mixing method and this change; the highest solid loading samples had an increase of 2.76% whereas the other samples had a decrease in hardness. All the samples lie below the accepted boundary for significant change. Using the 0.05 alpha level, the statistical analysis did not provide any evidence to reject the null hypothesis. The 0.73 solid loading sample, which had the greatest change, had the lowest probability and was closest to indicating statistical difference between the mixing methods.

*Table 16. Table detailing the results from the hardness test conducted on the HTPB-Melamine-Barium Sulphate samples. The samples had a hardness between 70 and 90 Shore A*

| Sample | | Hardness Result 1 | Hardness Result 2 | Hardness Result 3 |
|---|---|---|---|---|
| 0.66 | Planetary Mixed | 78.8 Shore A | 75.2 Shore A | 83.2 Shore A |
| | LabRAM | 79.2 Shore A | 76.7 Shore A | 75.0 Shore A |
| 0.73 | Planetary Mixed | 73.9 Shore A | 78.5 Shore A | 75.0 Shore A |
| | LabRAM | 72.3 Shore A | 72.8 Shore A | 70.5 Shore A |
| 0.80 | Planetary Mixed | 79.7 Shore A | 84.0 Shore A | 85.9 Shore A |
| | LabRAM | 85.6 Shore A | 81.1 Shore A | 89.8 Shore A |

*Table 17. Table detailing the average hardness result for each HTPB-Melamine-Barium Sulphate sample set, the percentage change of the LabRAM results from the planetary mixed results and the calculated T-Test probability. The variation between the RAM and the planetary mixed samples was not significant*

| Sample | Planetary | LabRAM | % Change | T-Test Probability |
|---|---|---|---|---|
| 0.66 | 79.1 Shore A | 77.0 Shore A | -2.66% | 0.470 |
| 0.73 | 75.8 Shore A | 71.9 Shore A | -5.19% | 0.064 |
| 0.80 | 83.2 Shore A | 85.5 Shore A | +2.76% | 0.501 |

Table 18 is a comparison with specifications and papers to prove these results are reasonable and within the expected range. It also demonstrates the large allowed variation in material specifications. The oxidation of the binder system caused an increase in hardness, which is reflected in the table below.

*Table 18. Table comparing the hardness results of the HTPB-Melamine- Barium Sulphate samples with literature*

| | | | |
|---|---|---|---|
| **Source with summary of programme** | Explosive, Plastic-Bonded, Cast PBXN-110, MIL-DTL-82901A [Naval Sea Systems Command, 2002] | Explosive, Plastic-Bonded, Cast PBXN-109, MIL-DTL-82886 [Naval Sea Systems Command, 1993] | Formulation and Performance Studies of Polymer Bonded (PBX) Containing Energetic Binder Systems [Provatas, 2003] |
| **Material** | PBXN-110 (HTPB based with a solid loading of HMX between 86 – 89%) | PBXN-109 (HTPB based with a solid loading of RDX between 62 – 66% and aluminium between 18 - 22%) | PBXs with a RDX loading ranging from 77 – 79% with a PolyGLYN binder system |
| **Test Regime** | Shore A hardness testing with a 15 second delay. Tested at 25 °C using a Type A-2 durometer. | Shore A hardness testing with a 30 second delay. Tested at 25 °C using a Type A-2 durometer. | Shore A hardness with a Shore A-2 Durometer with a Shore Conveloader test stand |
| **Results** | Minimum 15 | Minimum 30 | 51 - 59 |
| **Comparison with this research programme** | Specifications have a large variation, particularly with hardness testing. The PBXN-110 specification states a minimum of 15 without a maximum limit. These samples fall within that limit. | The PBXN-109 specification has a minimum hardness that is twice that of the PBXN-110. The samples within this research programme are within range. | The samples in this chapter had no antioxidant so during curing the binder is expected to oxidise which causes an increase in hardness. The range for these samples was greater in comparison to the literature, but the results were within the expected range. |

### 4.4.3 **Density**

Density is the mass of material in a given volume. For highly loaded composites density changes are primarily due to change in the filler packing; the greater the density the more filler particle volume. For energetic materials not only does it tend to have a greater explosive content as explosive crystals have a higher density than the binder, the higher density is also usually linked to a higher velocity of detonation (VoD) for a given explosive. A higher VoD results in a higher shock output and a higher destructive capability.

The two methods for density measurements of solid materials are the Archimedean immersion method and pycnometry. The immersion method submerses an object in a liquid and measures the perceived change in object mass. It is a simplistic, quick method, and does not require advanced machinery [www.labdepotinc.com, 2019]. Pycnometry uses an evacuated glass container with a defined volume; sample is put in the container and gas is introduced to a certain pressure. The mass is measured before and after and density is determined from that. It is a slow process, but is automated [Pycnometry, 2019].

Density measurements were conducted by helium pycnometry, using a Quantachrome Ultrapyc 1200e, with a cell volume of 19.1586 cc. It was suspected that the mixing method could alter the packing within the material, and therefore change the density. Helium was used with an automatic equilibrium time, to reach a target pressure of 19.0 psig; the flow purge was 1.0 minute. The material was tested 3 times, and the average was taken and summarised in Table 19, alongside the percentage change of density from the planetary mixed to the LabRAM samples. The test equipment has an accuracy of ±0.003%. The standard deviation was below 0.0001 g $cc^{-1}$ for all materials and mixing methods.

*Table 19. Table detailing the average density measurements of each of the HTPB-Melamine-Barium Sulphate sample sets, the percentage change of the RAM sample from the planetary mixed samples and the calculated T-Test probability. The 0.66 and 0.73 solid loading samples were statistically different materials, but the variation was not significant.*

| Sample | Planetary Mixing | LabRAM | % Change | T-Test Probability |
|---|---|---|---|---|
| 0.66 solid loading | 1.3772 g $cc^{-1}$ | 1.3755 g $cc^{-1}$ | -0.12% | 2.27 x $10^{-5}$ |
| 0.73 solid loading | 1.4670 g $cc^{-1}$ | 1.4785 g $cc^{-1}$ | +0.79% | 1.59 x $10^{-14}$ |
| 0.80 solid loading | 1.5513 g $cc^{-1}$ | 1.5498 g $cc^{-1}$ | -0.10% | 0.58 |

The overall results indicate that the mixing method does not make a significant change to the density of the material. In Table 19 the density was tabulated for both the planetary mixed and LabRAM samples, with a percentage change from the planetary mixed sample and t-test probability. All the samples exhibit a less than 0.8% density change indicating an insignificant density change; standard for PBXs have an acceptable range of up to ±2.5%. There is no consistency with regards to whether samples are more or less dense. Both the 0.66 and the 0.80 solid loading sample had a negative density change as the planetary mixed samples were denser, indicating the LabRAM samples had a less effective packing density. The 0.73 solid loading sample had a positive density change and LabRAM sample was denser.

The 0.80 solid loading sample had a t-test probability of 0.58, which does not provide any evidence to reject the null hypothesis. However, the probability for the 0.73 and 0.80 solid loading samples is below the alpha level so the null hypothesis, that there is no variation between the RAM and planetary mixed samples, can be rejected due to the statistical variation between samples.

When comparing the results found in this research programme to that found in literature, see Table 20, the samples had lower densities compared to the higher loaded PBXs. This was expected, due to the lower quantity of filler. The PBXs found in literature typically had loadings of above 80%, which was the maximum used in this chapter. However, composite propellants typically have a lower solid loading and this is reflected in the density results. The samples in this research programme lie within the values stated in the composite propellant literature, and the 0.80 solid loading samples are less than 10% smaller than the PBX literature.

*Table 20. Table comparing the density results of the HTPB-Melamine-Barium Sulphate samples with literature*

| | | |
|---|---|---|
| **Source with summary of programme** | Explosive, Plastic-Bonded, Cast PBXN-110, MIL-DTL-82901A [Naval Sea Systems Command, 2002] | Explosive, Plastic-Bonded, Cast PBXN-109, MIL-DTL-82886 [Naval Sea Systems Command, 1993] |
| **Material** | PBXN-110 (HTPB based with a solid loading between 86 – 89%) | PBXN-109 (HTPB based with a solid loading of RDX between 62 – 66% and aluminium between 18 - 22%) |
| **Test Regime** | Two samples weighing between 10g - 20g tested on an analytical balance equipped for underwater weighing with an accuracy of 0.1mg. Testing shall occur at 25°C. | Two samples weighing between 10g - 20g tested on an analytical balance equipped for underwater weighing with an accuracy of 0.1mg. Testing shall occur at 25°C. |
| **Results** | 1.62 – 1.70 g $cc^{-1}$ | 1.60 – 1.70 g $cc^{-1}$ |
| **Comparison with this research programme** | The samples in this literature are denser than the samples in this programme of research; this is expected due to the higher solid loading in the literature. | The samples in this literature have a higher solid loading and the associated higher density, when compared to this research programme. |

### 4.4.4 Thermomechanical Analysis (TMA)

DSC was driven by the melting temperatures of the components with no impact from the mixing method. It was believed that the addition of the Barium Sulphate would not change this and as such an alternative thermal technique was used. Thermomechanical analysis (TMA) determines the thermal expansion which is an issue for munitions. There are two main causes of thermal expansion. During storage, munitions see an environmental cycle that relates to the local temperature; typically this daily cycle, or diurnal cycle, will induce a degree of stressing within the material. This is due to the differential in the thermal expansion of the energetic material and the casing. For typical systems this factor is about 10. Repeated stressing, even at low levels, can cause cracking. More extreme thermal gradients occur when munitions are air carried. Air friction on the outer skin causes high temperatures, whereas the interior of the munition remains at a much cooler temperature. These thermal expansions can induce stress and cracking within materials which impact safety or performance [Ministry of Defence, 2006] [Kimura et al, 2017] [Devenas, 1993].

Samples were prepared using an 8 mm biopsy punch, and sliced to a nominal 5 mm length. Testing were conducted on a Mettler TMA/STD84e\241 using a 3 mm diameter ball end probe which applied a force of 0.02 N via a 6 mm diameter silica disc spreader with a thickness of 0.5 mm. A temperature sweep was conducted from -40 °C to +60 °C with a 2 °C $min^{-1}$ rate. Samples were measured at 20 °C in situ, cooled to -50 °C and left to dwell for 20 minutes. Two samples were tested for each composition, and samples were run twice to determine any irreversible changes. The thermal expansion, measured over the temperature sweep, has units of ppm $K^{-1}$. Results were tabulated in Table 23 and summarised in Table 21 and Table 22; they detail the average result and the percentage change from planetary mixed to LabRAM for the first and second runs.

*Table 21. Table containing the averages of the first TMA run for each HTPB-Melamine-Barium Sulphate sample set, the percentage change from the planetary mixed samples to the LabRAM samples and the calculated T-Test probability. The results did not demonstrate any significant variation*

| Sample | Planetary Mixing | LabRAM | % Change | T-Test Probability |
|---|---|---|---|---|
| 0.66 solid loading | 141.35 ppm $K^{-1}$ | 138.25 ppm $K^{-1}$ | -2.19% | 0.311 |
| 0.73 solid loading | 118.01 ppm $K^{-1}$ | 116.24 ppm $K^{-1}$ | -1.50% | 0.188 |
| 0.80 solid loading | 101.09 ppm $K^{-1}$ | 98.43 ppm $K^{-1}$ | -2.63% | 0.260 |

*Table 22. Table containing the averages of the second TMA run for each HTPB-Melamine-Barium Sulphate sample set, the percentage change from the planetary mixed samples to the LabRAM samples and the calculated T-Test probability. The results did not demonstrate any significant variation*

| Sample | Planetary Mixing | LabRAM | % Change | T-Test Probability |
|---|---|---|---|---|
| 0.66 solid loading | 146.26 ppm $K^{-1}$ | 141.82 ppm $K^{-1}$ | -3.04% | 0.055 |
| 0.73 solid loading | 119.60 ppm $K^{-1}$ | 119.55 ppm $K^{-1}$ | -0.04% | 0.953 |
| 0.80 solid loading | 103.46 ppm $K^{-1}$ | 100.68 ppm $K^{-1}$ | -2.69% | 0.407 |

*Table 23. Table comparing the thermal expansion results for each run for the HTPB-Melamine-Barium Sulphate sample sets*

| Sample | | TMA Run 1 | TMA Run 2 |
|---|---|---|---|
| 0.66 | LabRAM | 137.94 ppm $K^{-1}$ | 141.09 ppm $K^{-1}$ |
| | | 138.55 ppm $K^{-1}$ | 142.55 ppm $K^{-1}$ |
| | Planetary Mixed | 143.63 ppm $K^{-1}$ | 147.06 ppm $K^{-1}$ |
| | | 139.06 ppm $K^{-1}$ | 145.45 ppm $K^{-1}$ |
| 0.73 | LabRAM | 116.54 ppm $K^{-1}$ | 118.87 ppm $K^{-1}$ |
| | | 115.93 ppm $K^{-1}$ | 120.23 ppm $K^{-1}$ |
| | Planetary Mixed | 118.86 ppm $K^{-1}$ | 119.63 ppm $K^{-1}$ |
| | | 117.16 ppm $K^{-1}$ | 119.56 ppm $K^{-1}$ |
| 0.80 | LabRAM | 97.24 ppm $K^{-1}$ | 99.84 ppm $K^{-1}$ |
| | | 99.61 ppm $K^{-1}$ | 101.51 ppm $K^{-1}$ |
| | Planetary Mixed | 102.33 ppm $K^{-1}$ | 106.00 ppm $K^{-1}$ |
| | | 99.85 ppm $K^{-1}$ | 100.92 ppm $K^{-1}$ |

The thermal testing did not demonstrate significant discrepancies between the planetary mixed and the LabRAM samples. The thermal expansion does change between each of the samples and the LabRAM samples have consistently smaller expansion of up to 3.05% change. Thermal expansion is caused by the increased vibrations of the molecules as thermal energy is applied to a material. The increased molecular vibrations cause the molecules to move into free space within the material, causing the material to expand [Liu et al, 2017]. As the LabRAM samples have consistently smaller thermal expansion it indicates that there is less free space within the sample. Using the alpha value of 0.05, the null hypothesis cannot be rejected for any of these samples.

When comparing these results to that in literature, see Table 24, the thermal expansions are within similar ranges. The results found in literature are assumed to have modifiers within the binder system, which affects the results and provide greater free space within the binder system. Both sets of literature have thermal expansion from within the 90 to 120 ppm $K^{-1}$ range which is within the set from this study.

*Table 24. Table comparing the thermal expansion results of the HTBP-Melamine-Barium Sulphate samples with literature*

<table>
<tr><td>Source with summary of programme</td><td>Thermal and fracture behaviour of rocket motor materials [Ide, 1997]</td><td>Micromechanics-Based Prediction of Thermoelastic Properties of High Energy Materials [Banerjee et al, 2002]</td></tr>
<tr><td>Material</td><td>Composite propellant with an HTPB binder and 80% ammonium perchlorate</td><td>PBX 9501- Estane based, highly loaded pressed PBX (95% solid loading)</td></tr>
<tr><td>Test Regime</td><td>Mettler TA400 Thermal Mechanical Analyser testing from -100 °C to +300 °C with a heating and cooling rate of 2 °C $min^{-1}$.</td><td>Testing conducted at 23 °C - no further details provided</td></tr>
<tr><td>Results</td><td>The results were presented in a graph, illustrating the thermal expansion over a range of termperatures. There is fluctuation over the termperature ranges following the same pattern as the AP filler system. The behaviour is dominated by the filler due to the small quantity of binder<br> 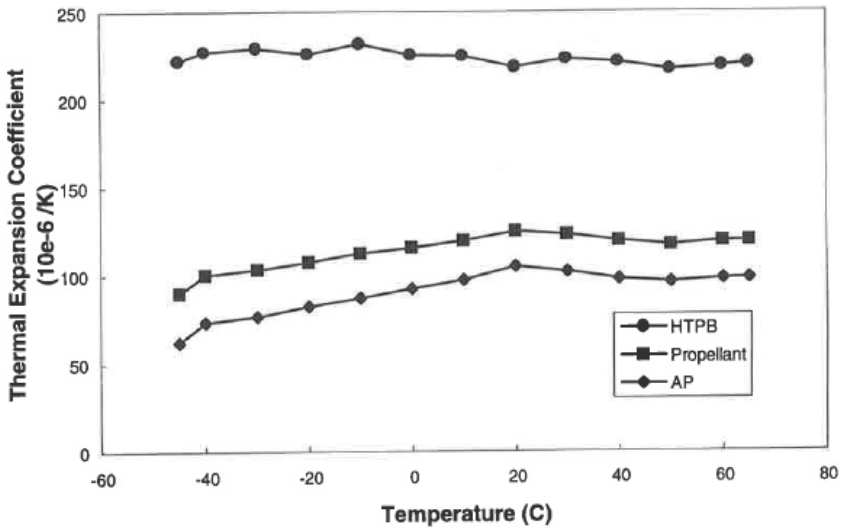
</td><td>The results were presented in a table detailing the overall composite and the varying components. The binder, as expected, had the greatest thermal expansion, but the overall composite is dominated by the high solid loading.
<table>
<tr><td>Material</td><td>Thermal Expansion</td></tr>
<tr><td>PBX 9501</td><td>120 ppm $K^{-1}$</td></tr>
<tr><td>HMX</td><td>116 ppm $K^{-1}$</td></tr>
<tr><td>Binder</td><td>200 ppm $K^{-1}$</td></tr>
</table></td></tr>
</table>

| | | |
|---|---|---|
| **Comparison with this research programme** | The samples have the same solid loading as the highest solid loading samples in this research programme. It is assumed that the binder has modifiers such as plasticisers and stabilisers in it in this literature. The highest solid loading had a smaller thermal expansion than the samples in literature; however, they were within the same range. | The samples in the literature differ from this research programme; these highly loaded samples require pressing as they will not cast and the binder is a very small constituent in the composite. The samples in this stage of this research programme are limited to 80% solid loading and were at the upper limit of their casting capability. |

### 4.4.5 Optical Microscopy

Visual examination can provide beneficial understanding of the internal structure of material. Samples were prepared by cutting at room temperature, inducing a ductile failure, then examined with an Axio Zeiss M1M. A spotlight was applied to illuminate the sample causing the bright central circle and dark external edges observed in the images.

Whilst preparing samples, there was separation between filler and binder. Like with the HTPB-Melamine samples, the HTPB produces a binder cage around the particles as opposed to a primary chemical bond. When the samples were cut some of those cages were damaged and powder detached from the bulk causing crumbling at the surface. There was no noticeable difference between the LabRAM and the planetary mixed samples, such as large quantities of powder separating from the bulk material or surfaces with a lower than average filler concentration, indicating that both mixing methods experience the same mechanism and degree (or lack of) of bonding between the filler and binder.

The microscopy images are displayed in Figure 45, Figure 46 and Figure 47 and show the crystals encased in the binder system in the cage format. There is a greater concentration of binder at the surface due to debonding of the filler and deformation of the binder during cutting. In the sample bulk, the filler appears well distributed with no areas of significantly higher or lower concentrations of powder. The images do not highlight any issues with regards to distribution or damage to the binder system.

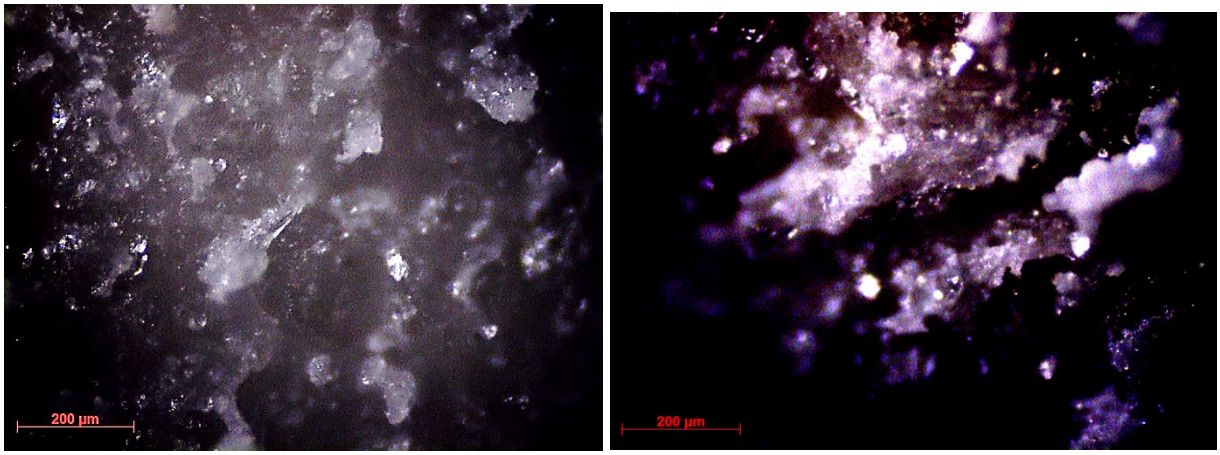


*Figure 45. Microscopy images of the 0.66 solid loading HTPB-Melamine-Barium Sulphate samples mixed by LabRAM (left) and planetary mixing (right). The melamine and barium sulphate can be observed within the HTPB strands. The filler crystals do not appear to differ in either shape or size and the HTPB strands do not appear to be damaged or shorter when comparing the two mixing methods.*

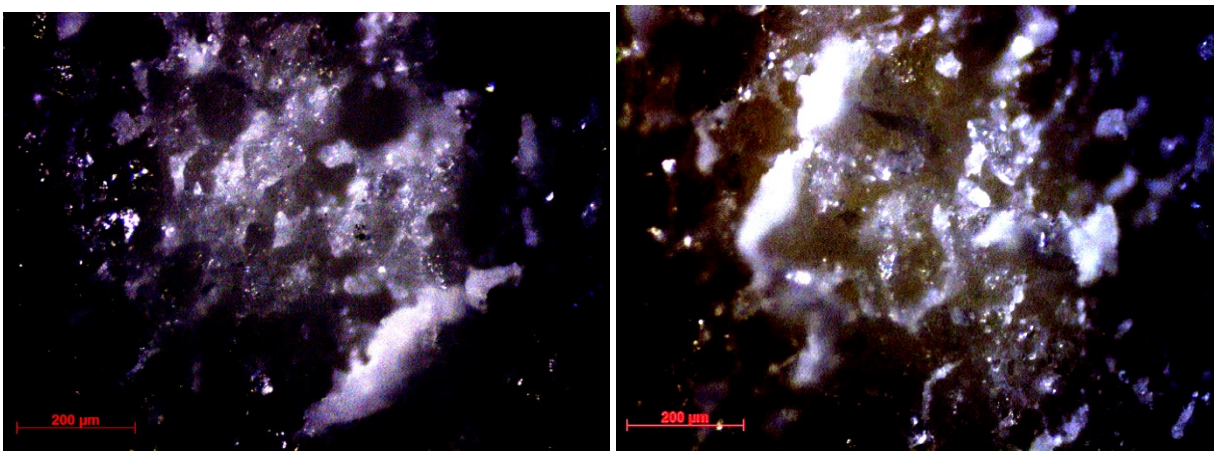


*Figure 46. Microscopy images of the 0.73 solid loading HTPB-Melamine-Barium Sulphate samples mixed by LabRAM (left) and planetary mixing (right). The melamine and barium sulphate can be observed within the HTPB strands. The filler crystals do not appear to differ in either shape or size and the HTPB strands do not appear to be damaged or shorter when comparing the two mixing methods.*

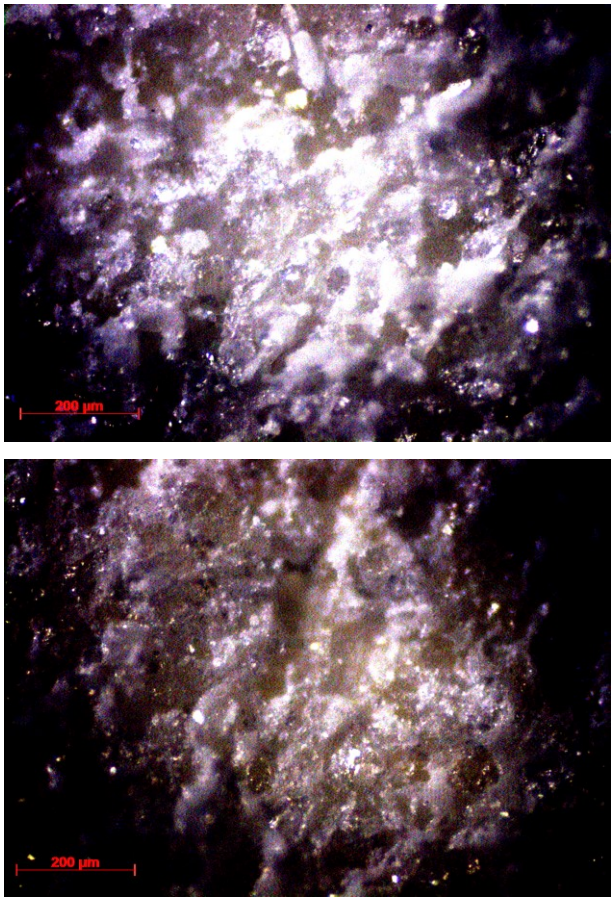


*Figure 47. Microscopy images of the 0.80 solid loading HTPB-Melamine-Barium Sulphate samples mixed by LabRAM (left) and planetary mixing (right). The melamine and barium sulphate can be observed within the HTPB strands. The filler crystals do not appear to differ in either shape or size and the HTPB strands do not appear to be damaged or shorter when comparing the two mixing methods.*

## 4.5 Discussion and Conclusions

The mechanical behaviour of the compositions showed high consistency between mixing method. DMA samples had variation in the -70 °C to the +30 °C region, but were mostly consistent. The 0.66 and 0.73 solid loading samples had poorer properties when mixed by LabRAM but the 0.80 solid loading sample were stiffer. The hardness testing results had greater variation within mixing method, particularly when compared to the DMA samples. It was inconsistent in both mixing methods, which is an artefact of test as opposed to material. Density measurements are highly consistent within the 0.66 and 0.80 solid loading samples; the 0.73 solid loading samples had the highest variation with a percentage change of 0.79% from planetary mixed to LabRAM. There is no consistency in whether the LabRAM samples are more or less dense. The 0.73 and 0.80 solid loading samples provided statistical evidence

that the null hypothesis could be rejected and that the samples were different. The thermal expansion was consistently smaller when mixed via LabRAM.

There is an interest to determine any patterns in the behaviour of the LabRAM samples compared to the conventional planetary mixed samples. In Table 25 the results have been summarised and colour coded to demonstrate which had the higher results; this follows the same scheme used throughout with red as LabRAM and blue as the planetary mixed samples. Samples in bold indicate that there is evidence that the null hypothesis can be rejected. Each of the individual results have shown variations in behaviour between the LabRAM and planetary mixed HTPB-Melamine-Barium Sulphate samples; however, this has been negligible and insignificant.

*Table 25. Table summarising the results of HTPB-Melamine-Barium Sulphate characterisation. The DMA column indicates the temperature range in which the results vary. The remaining results are percentage changes of the RAM samples from the planetary mixed samples. The colour coding indicates which sample had the higher results, with the planetary mixed samples being blue and the RAM samples being red. The results did not demonstrate any significant difference in the samples behaviour.*

| | DMA | Hardness | Density | TMA Run 1 | TMA Run 2 |
|---|---|---|---|---|---|
| 0.66 solid loading | -70 °C onwards | 2.66% | **0.12%** | 2.19% | 3.04% |
| 0.73 solid loading | -70 °C to +30 °C | 5.19% | **0.79%** | 1.50% | 0.04% |
| 0.80 solid loading | -65 °C to 0 °C | 2.76% | 0.10% | 2.63% | 2.69% |

Using Table 25, there is no pattern between the behaviour. It would be expected that an increase in density would cause an increase in the mechanical properties and a decrease in the thermal expansion as the available empty space within the material would reduce, limiting the ability of the material to move freely. It also has the added benefit of increasing the amount of tougher filler particles within a given volume.

The 0.66 solid loading samples had a lower density and poorer mechanical properties when mixed via LabRAM which could indicate that the filler packing is less efficient or that the binder network is less cross-linked, allowing greater movement within the sample. The density results were statistically different, with enough evidence to reject the null hypothesis. The TMA results were greater for the planetary mixed samples indicating greater free space, which is consistent over all the solid loadings in this chapter. This behaviour is not consistent

with the expected behaviour and mechanisms but as the variation is insignificant material behaviour could be dominated by natural variation in test or within the sample.

The 0.73 solid loading samples have higher density and less free space when mixed by LabRAM, indicating that a more efficient filler packing for LabRAM samples. The density results provide sufficient evidence to reject the null hypothesis and be statistically different between mixing methods. This sample had the highest density variation. The mechanical behaviour is poorer for the LabRAM samples, which indicates that the binder system is weaker. This sample had the highest hardness variation out of the solid loadings. This is attributed to poor isocyanate distribution and curing. As with the 0.66 solid loading samples, the variation is insignificant and there was no evidence that mixing via LabRAM affected the materials properties.

The 0.80 solid loading samples, like the 0.66 solid loading samples, did not follow an expected behaviour and the variation between the mixing methods is negligible. None of the results provided evidence to reject the null hypothesis and consider the samples as statistically different. Like with the 0.66 solid loading samples, the planetary mixed samples were denser but had greater free space and a greater thermal expansion; as these results were not statistically different, this is likely to be due to variation in local sample or in test. The LabRAM samples had greater mechanical results, with higher hardness and greater stiffness, indicating that the binder system is superior when mixed by RAM. However, as stated, the results are insignificant and any impact the mixing method has on the material properties is negligible.

These compositions did not demonstrate that the LabRAM had any significant impact on the results of the characterisation conducted. The variation for all the techniques was minor, and there was no relationship within the changes in material properties. The samples in this chapter were effectively mixed via LabRAM.

# 5 HTPB-DOS-Melamine-Barium Sulphate

The two part compositions had consistent thermal behaviour but at the higher loadings had poor distribution of isocyanate which affected the mechanical properties. The HTPB-Melamine-Barium Sulphate samples had greater consistency and the behaviour was not significantly affected by mixing via LabRAM. The thermal expansion was consistently smaller for the LabRAM samples but there was no consistency or pattern with the mechanical behaviour and the density. Previous research was limited by filler loadings due to the samples high viscosity. The addition of plasticiser improved this and allowed an increase in filler loading from 80% to 85%. Additional processing was required to mix the binder system prior to the addition of filler.

## 5.1 Materials

Dioctyl Sebacate (DOS), or Bis(2-ethylhexyl) sebacate, seen in Figure 48, is a plasticiser used to improve the mechanical properties of material and reduce the glass transition temperature. It slots between the chains of the polymer spacing them out providing greater opportunity and space to move. Experience shows that the optimum mass percentage for DOS with energetic materials is around 30% of the binder; however, higher loadings may require more plasticiser to flow. Too much plasticiser should be avoided as it can cause the material to exhibit tacky properties. The addition of plasticiser also reduces the glass transition temperature, providing those necessary mechanical properties at much lower temperatures.

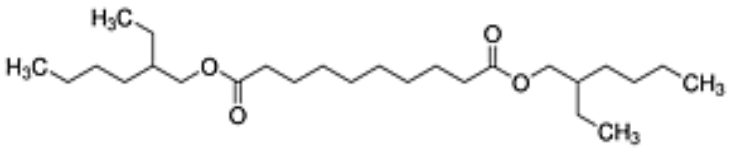


*Figure 48. The chemical structure of DOS [Sigmaaldrich.com, 2016]*

Plasticiser migration is a contributor to ageing particularly with rocket motors; plasticiser migrates from the binder rich surface into the liner, causing the liner to become more ductile reducing its effectiveness. Plasticiser in the central core then migrates to the outer edges of the sample where there is low plasticiser concentration, leaving a brittle core in the material. This increases the cracking potential creating additional burning surfaces and causing failure. Plasticiser migration is monitored as a safety concern during a systems lifespan.

## 5.2 Planetary Mixing

Samples were mixed using an IKA Planetron HKV-1 as in Chapter 3.2. A 0.1 bar to 0.2 bar vacuum was applied and blade speed varied between 11 and 18 rpm. The barium sulphate was sieved prior to mixing; however, the planetary mixer has successfully broken these agglomerates previously. The formulations are in Table 26.

*Table 26. Formulation table of HTPB-Melamine-Barium Sulphate- DOS Planetary mixed samples*

| | | | | | | |
|---|---|---|---|---|---|---|
| **0.66 Solid Loading** | HTPB | DOS | Melamine | Barium Sulphate | Planetary Mixed | Very good flow properties |
| | 22.78 | 11.22 | 48.18 | 17.82 | | |
| **0.73 Solid Loading** | HTPB | DOS | Melamine | Barium Sulphate | Planetary Mixed | Good flow properties |
| | 18.09 | 8.91 | 53.29 | 19.71 | | |
| **0.85 Solid Loading** | HTPB | DOS | Melamine | Barium Sulphate | Planetary Mixed | Very viscous and did not flow |
| | 10.05 | 4.95 | 62.05 | 22.95 | | |

## 5.3 LabRAM Mixing

LabRAM samples were mixed in 200 g batches and filler was added in two intervals. Mix observations were comparable to previous compositions; during the binder mixing phase the material bubbled despite having dried the HTPB prior to mixing. The DOS had not been dried but was taken from a new bottle. Vacuum was applied at each stage, ranging below 0.01 bar. As previously stated, the highest solid loading was increased due to the addition of the DOS to the previous composition of HTPB-Melamine-Barium Sulphate. The mixture was at the maximum limit of the flow capability; however, it was still castable. Compositions with solid loadings higher than these would be pressed instead of being cast.

The formulation table, included in Table 27, details mass percentage of each component and the casting comments. This is supported by a mixing diagram in Figure 49; mixing occurred within the 30 to 45% power range and the 30 to 50 G range. The intervals where additions were made can be observed on the diagram, coinciding with cooling periods.

*Table 27. Formulation table of HTPB-DOS-Melamine-Barium Sulphate LabRAM samples*

| | | | | | | |
|---|---|---|---|---|---|---|
| **0.66 Solid Loading** | HTPB | DOS | Melamine | Barium Sulphate | LabRAM | Very good flow properties |
| | 22.78 | 11.22 | 48.18 | 17.82 | | |
| **0.73 Solid Loading** | HTPB | DOS | Melamine | Barium Sulphate | LabRAM | Good flow properties |
| | 18.09 | 8.91 | 53.29 | 19.71 | | |
| **0.85 Solid Loading** | HTPB | DOS | Melamine | Barium Sulphate | LabRAM | Very viscous, required external stimuli to cast |
| | 10.05 | 4.95 | 62.05 | 22.95 | | |

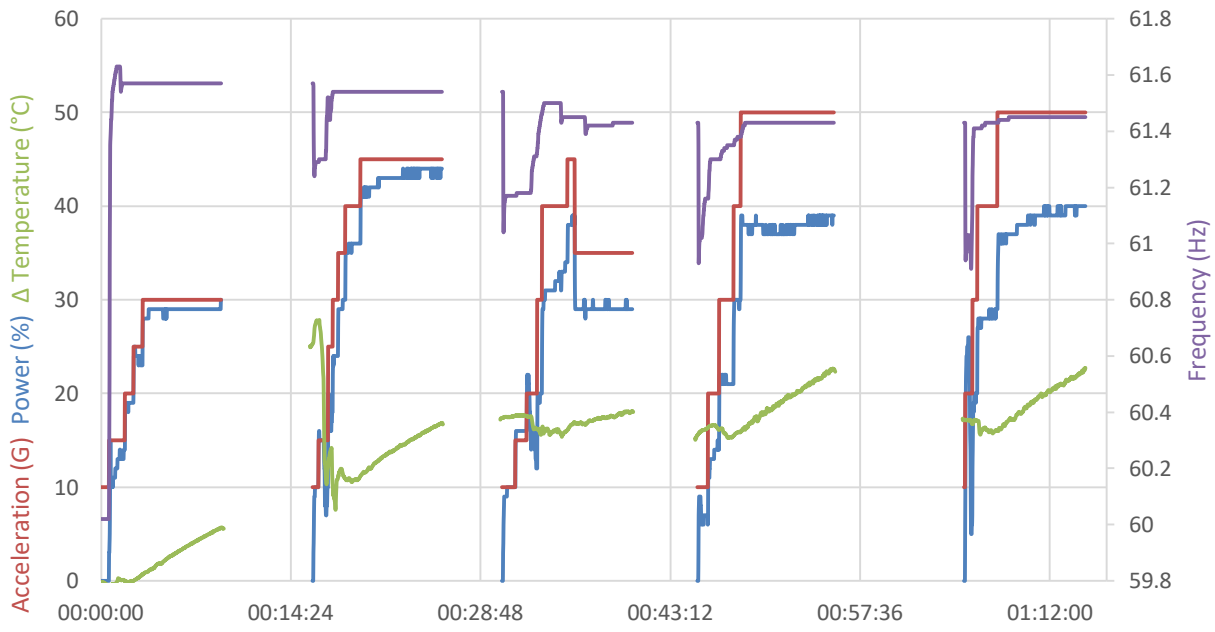


*Figure 49. Mixing graph for the 0.66 solid loading HTPB-DOS-Melamine-Barium Sulphate sample showing the acceleration in G (red), power input (blue), temperature change in Celsius (green) and the LabRAM frequency in Hz (purple). The mix is stopped twice for material to be added to the sample*

### 5.3.1 Powder agglomerations

The first set of samples, similarly to the HTPB-Melamine-Barium Sulphate samples, exhibited agglomeration of barium sulphate. The 0.66 solid loading cast and cured sample is pictured in Figure 50 and identify these agglomerates. Regions of excess powder, and binder make the sample highly inhomogeneous and detrimentally affect the mechanical properties. Multiple powder agglomerations could be seen at the bottom of the sample. These were discarded and manufacture was repeated. The LabRAM was unable to break these large particle agglomerates. In order to prevent this, the barium sulphate was sieved through a 1mm aperture sieve, seen in Figure 51. The large agglomerations were excluded from the sample, and further mixes were more consistent.


*Figure 50. The 0.66 solid loading HTPB-DOS-Melamine-Barium Sulphate sample with visible indicators of inhomogeneity. Feature A is a pocket of uncured binder and feature B is a collection of powder agglomerations between the fingers of the sample*

*Figure 51. Pictured is the barium sulphate in a sieve with 1mm mesh size, comparing the powder that was used in the initial experiments and the powder that was used in the remaining experiments.*

## 5.4 Characterisation

Characterisation focused on mechanical properties and moisture diffusion of the materials. Both low strain rate and high strain rate mechanical testing was chosen; DMA provides a useful overview of mechanical properties over a range of temperatures, and Split Hopkinson Bar indicates the behaviour at high strain rates.

### 5.4.1 DMA

DMA testing was conducted under the same conditions as Chapter 3.4.1. Due to the lack of antioxidant the samples had an oxidised surface that was removed to ensure that the recorded behaviour was representative of the bulk material.

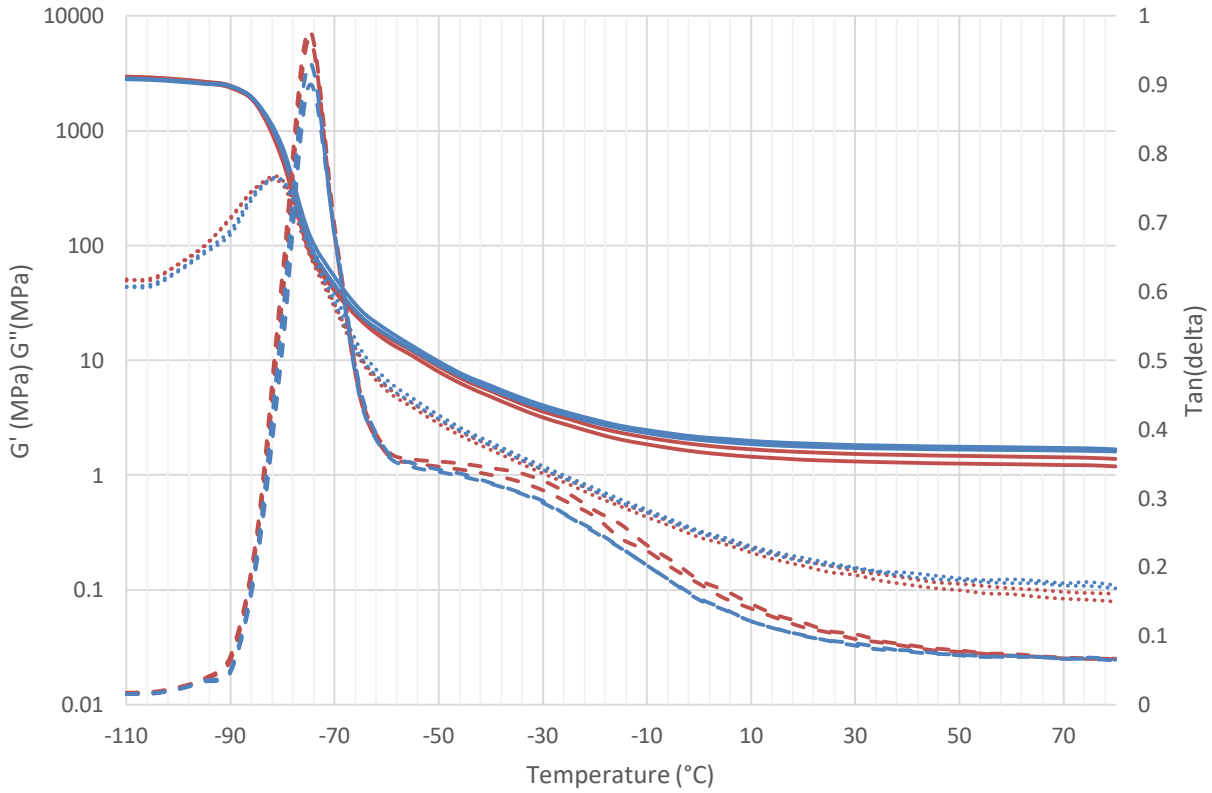


*Figure 52. DMA graph for 0.66 solid loading HTPB-DOS-Melamine-Barium Sulphate samples plotting the elastic modulus or G' (solid line), loss modulus or G'' (dotted line) and tan(delta) (dashed line), and comparing the LabRAM samples (red) with the planetary mixed samples (blue). The samples demonstrate high consistency in the mechanical behaviour*

Figure 52 shows consistency between the planetary mixed and LabRAM 0.66 solid loading samples. The storage modulus, G', and the loss modulus, G'', show a slight decrease at the higher temperatures for the LabRAM samples indicating the LabRAM samples are softer and the polymer chains are able to more freely move; however, this is negligible. The tan(delta) indicates a consistent behaviour; a minor variation is observed on both the first and the second, broader peak indicating a greater energy loss through either heat or friction in the LabRAM samples. With this composition the material has been unaffected by the novel mixing method.

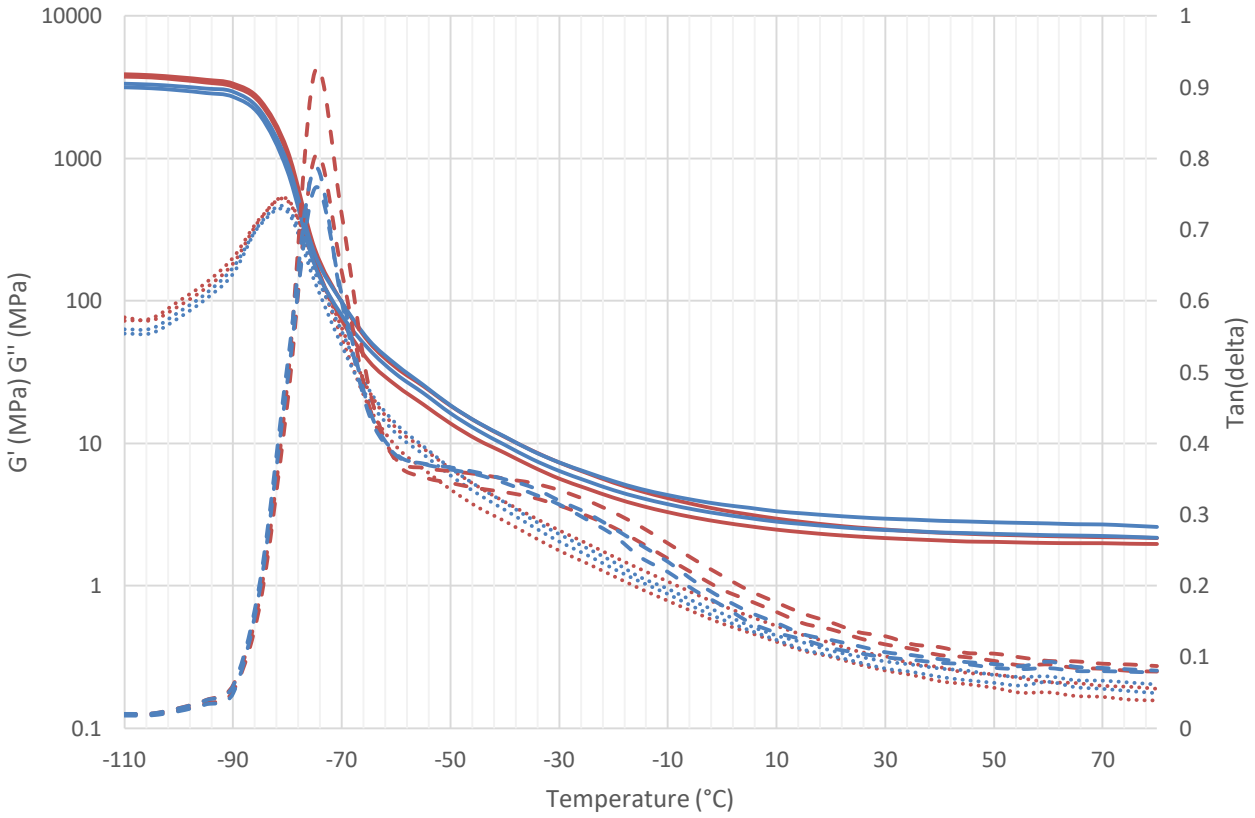


*Figure 53. DMA graph for 0.73 solid loading HTPB-DOS-Melamine-Barium Sulphate samples plotting the elastic modulus or G' (solid line), loss modulus or G'' (dotted line) and tan(delta) (dashed line), and comparing the LabRAM samples (red) with the planetary mixed samples (blue). The samples demonstrate high consistency in the mechanical behaviour*

The 0.73 solid loading samples, plotted in Figure 53, demonstrate minor variation between samples. Prior to the glass transition temperature the planetary mixed samples are softer attributed to greater free space within the binder system; the chains have greater freedom of movement. However, after the glass transition point the LabRAM samples have greater movement of the polymeric chains and greater energy loss causing the sample to be softer. This is negligible when compared the planetary mixed samples. There is variation at the higher temperatures between the planetary mixed samples which is attributed to damage when preparing the sample and removing the oxidised layer. This variation is not consistent throughout the test so is not related to the material. The mechanical behaviour of these materials is not significantly affected by the mixing method.

The 0.85 solid loading samples are plotted in Figure 54 and indicate no significant difference in the low strain rate mechanical behaviour of the LabRAM and planetary mixed samples. There is variation throughout the temperature range with the planetary mixed samples having

poorer moduli indicating that the LabRAM samples have less movement within the polymer chains. This is attributed to the LabRAM samples having a greater cross-linked network; it is plausible for the metal blades in the planetary mixer to cause minor damage and limit the polymeric network. The tan(delta) curves exhibit minor discrepancies with the first peak as the planetary mixed samples dissipate more energy through friction generated by the moving polymeric chains.

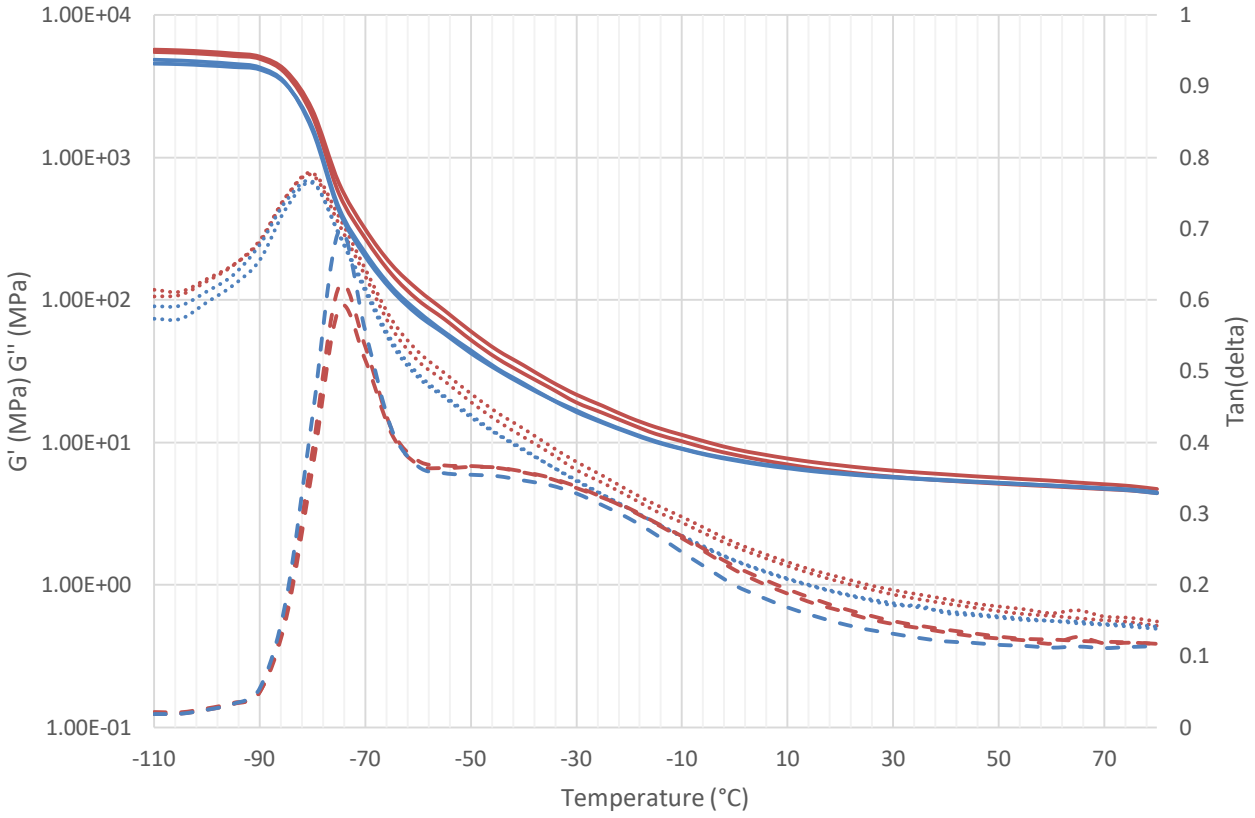


*Figure 54. DMA graph for 0.85 solid loading HTPB-DOS-Melamine-Barium Sulphate samples plotting the elastic modulus or G' (solid line), loss modulus or G'' (dotted line) and tan(delta) (dashed line), and comparing the LabRAM samples (red) with the planetary mixed samples (blue). The samples demonstrate high consistency in the mechanical behaviour*

For each of the formulations there was no significant difference in the small scale mechanical behaviour when comparing the mix type. The research in this chapter was compared with available literature, in Table 28, to ensure that results are reasonable and within expected range. The addition of plasticiser to this composition increases the malleability of the sample and reduces the glass transition temperature. The report found in literature, [Ripani et al, 2017], has limited information but does demonstrate the same transitions in the DMA graph.

*Table 28. Table comparing the DMA result of the HTPB-DOS-Melamine-Barium Sulphate samples with literature*

| | | |
|---|---|---|
| **Source with summary of programme** | HTPB-Melamine- Barium Sulphate ,Chapter 4.4.1 | Dynamical Characterization of Propellant using the DMA, [Ripani et al, 2017] |
| **Material** | HTPB-Melamine-Barium Sulphate composites, with 0.66, 0.73 and 0.80 solid loading. Mixed by either LabRAM or planetary mixing. | HTPB based composite propellant with ammonium perchlorate. The solid loading was not specified. Specimen thickness of between 3 and 4 mm with a dog bone shape. |
| **Test Regime** | Rheometrics RDAII dynamic mechanical analyser, testing from -110 °C to +80 °C in 3 °C steps with a nominal strain of 0.1% as according to STANAG 4540 | TA Q800 DMA instrument with a single cantilever clamp. The experiment was run from -100 °C to 0 °C with a 1 °C $min^{-1}$ increase and a 1 Hz frequency. |
| **Results** | The results have a high level of consistency between like samples. There is minor variation between the LabRAM and planetary mixed samples but there is pattern in the results. The 0.66 and 0.73 solid loading LabRAM samples had poorer mechanical properties when compared to the planetary mixed samples; the graph below is the 0.73 solid loading sample with the same colour coding as the graphs in this chapter. The 0.80 solid loading LabRAM sample had improved mechanical properties when compared to the planetary mixed sample. | The sample was run from -100°C to 0°C and no values have been added to the plot making it hard to quantitatively compare. However, the .plot, seen below, does demonstrate the expected transitions in this temperature range. The sample has the steep decrease in the storage modulus at the glass transition temperature with the associated loss modulus peak and tan(delta) peak. The tan(delta) has the sharp peak at this lower temperature and then a broader peak at higher temperatures. The temperature range stops before the broader peak is complete. |

| | | |
|---|---|---|
| | 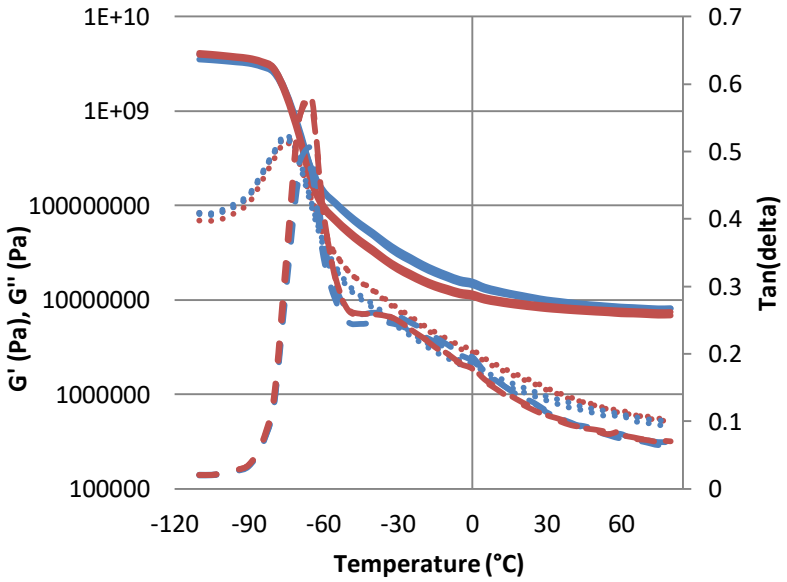 | 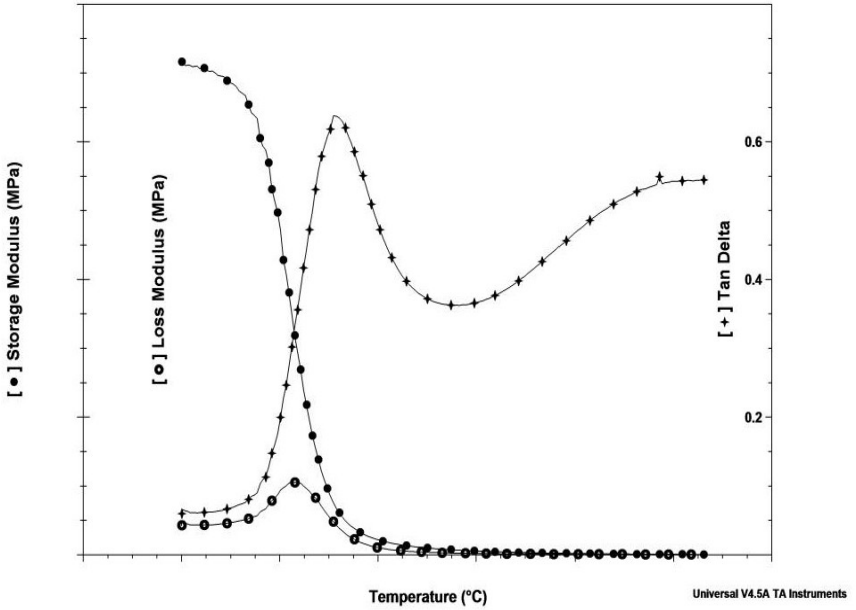 |
| **Comparison with this research programme** | The samples in this research programme, like the samples from the previous chapter, are very consistent between like samples. The variation between the LabRAM and the planetary mixed samples is insignificant in both this study and the previous chapter. There is an expected increase in the tan(delta) and decrease in the glass transition temperature with the addition of the plasticiser; the moduli remains consistent. | Limited information is given about the reported composition and limited information is on the graph. The plot in this literature contains the same transitions as the compositions in this chapter; they exhibit the same drop in storage modulus and peak in loss modulus at the glass transition temperature and the same double tan(delta) peaks. |

### 5.4.2 Split Hopkinson Pressure Bar (SHPB)

The Split Hopkinson Pressure Bar (SHPB) was developed in 1949 and investigates the compressive dynamic response of material. An elastic wave pulse is produced by a projectile striking the incident bar. This wave travels through the incident bar; partly reflecting at the end of the incident bar and partly travelling through the sample and into the transmission bar on the other side. Strain gauges are placed on the transmission and incident bar to measure the deformation in the transmitted and reflected waves. The stress-strain of the sample can then be calculated from the measured strains [HBM, 2017]. High strain rate testing is of great interest within the industry as munitions will experience high strain rates whilst in service. The SHPB is a high strain rate test, in comparison to 0.1% strain rate DMA testing. As with most tests, there is a high level of dependency on the testing regime.

High strain rate compressive testing was conducted by SHPB at Imperial College London, using 7068 aluminium alloy input and output bars and striker, with respective lengths of 1500 mm, 1000 mm and 560 mm. Semi-conductor strain gauges, AFP-500-090 with resistances of 500 ±10% Ω, were used to measure the strains and mounted on the input and output bars at a distance of 750 mm and 1400 mm from the bar interfaces respectively. The pulses were recorded on a Tektronix oscilloscope at a sampling rate of 2.5 megasamples per second (MS $s^{-1}$). These were converted to classic engineering stress-strain curves and plotted in Figure 55 to Figure 57. Samples were prepared by 8 mm biopsy punches and cut to a nominal 2.7 mm length producing a strain rate of 3350 $s^{-1}$.

Due to sample preparation, there was variation in surface properties which could result in minor variation between samples from the same batch. The sample averages and standard deviation for the three main parameters have been tabulated in Table 29. The sample length had a large amount of variation although there was small deviation within like samples. This is taken into consideration when the results are analysed. The firing pressure is the controlled variable for the strain rate. Between the planetary mixed and the LabRAM samples there is little variation between the LabRAM and planetary mixed compositions. The strain rate has a greater variation but with the exception of the 0.73 solid loading samples the strain rates are comparable.

*Table 29. A table detailing the average experimental variables and the associated standard deviation for HTPB-DOS-Melamine-Barium Sulphate high strain rate samples.*

| Sample | Average Length/ mm | Standard Deviation | Average Strain Rate/ $s^{-1}$ | Standard Deviation | Average Firing Pressure/ bar | Standard Deviation |
|---|---|---|---|---|---|---|
| 0.66 LabRAM | 2.73 | 0.037 | 3397.2 | 45.83 | 1.37 | 0.005 |
| 0.66 Planetary Mixing | 2.65 | 0.127 | 3381.8 | 97.86 | 1.37 | 0.005 |
| 0.73 LabRAM | 2.73 | 0.010 | 3382.8 | 105.37 | 1.47 | 0.007 |
| 0.73 Planetary Mixing | 2.66 | 0.054 | 3443.8 | 131.44 | 1.48 | 0.006 |
| 0.85 LabRAM | 2.66 | 0.034 | 3505.8 | 103.63 | 1.58 | 0.007 |
| 0.85 Planetary Mixing | 2.69 | 0.095 | 3542.8 | 171.11 | 1.58 | 0.005 |

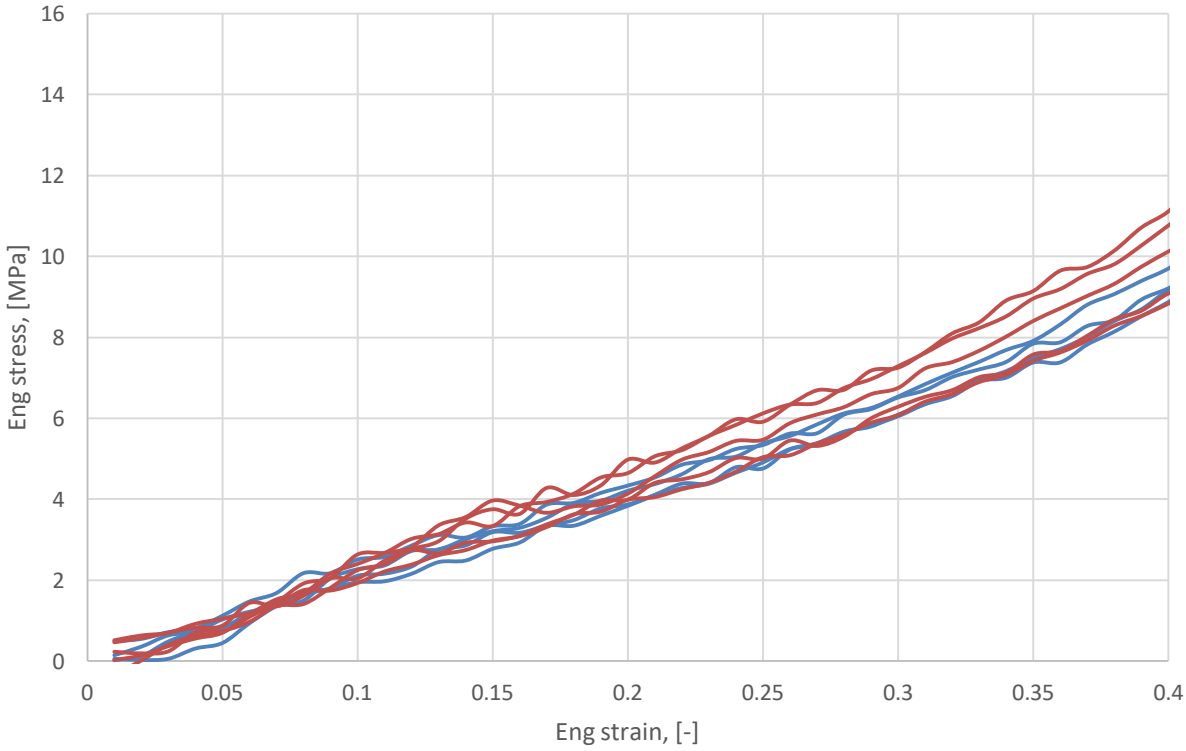


*Figure 55. The engineering stress-strain graph for the high strain rate testing of the 0.66 solid loading HTPB-DOS-Melamine-Barium Sulphate samples. The LabRAM samples are in red and the planetary mixed samples are in blue. The RAM samples demonstrate larger variation than the planetary mixed samples.*

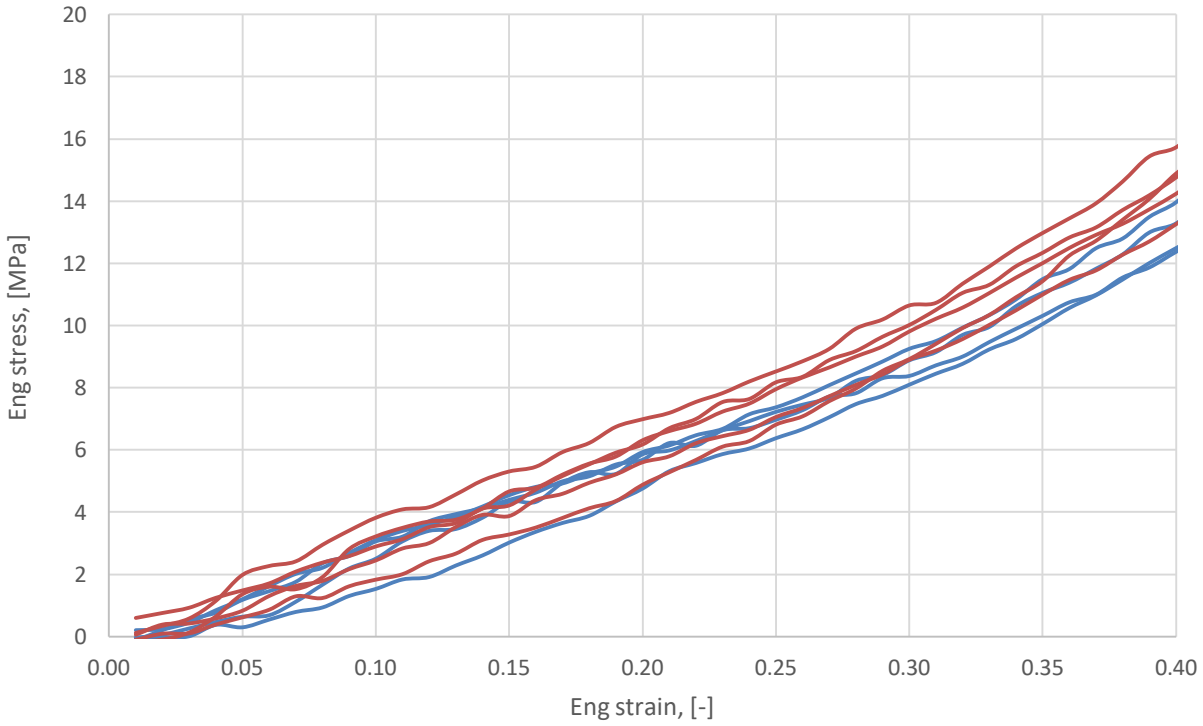


*Figure 56. The engineering stress-strain graph for the high strain rate testing of the 0.73 solid loading HTPB-DOS-Melamine-Barium Sulphate samples. The LabRAM samples are in red and the planetary mixed samples are in blue. The RAM samples demonstrate a minor increase in stress compared to the planetary mixed samples*

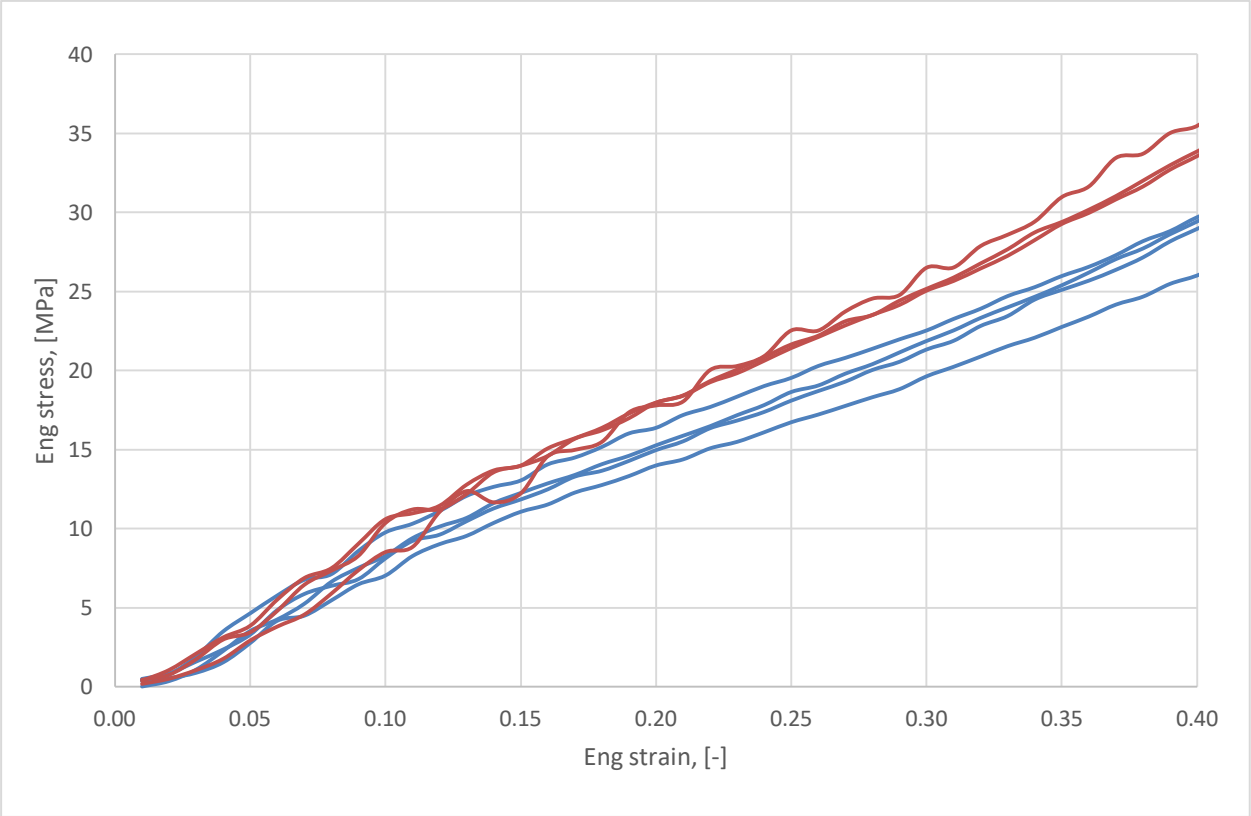


*Figure 57. The engineering stress-strain graph for the high strain rate testing of the 0.85 solid loading HTPB-DOS-Melamine-Barium Sulphate samples. The LabRAM samples are in red and the planetary mixed samples are in blue. The RAM samples demonstrate a clear increase in stress compared to the planetary mixed samples*

In comparison to the DMA results, the high strain rate testing samples have a much greater variability. Figure 55 and Figure 58, for the 0.66 solid loading sample, demonstrate a linear positive relationship between the stress and the strain. The 0.66 solid loading samples have minor variability between samples of the same and different mixing methods. The graphs diverge at 0.3 strain as the planetary mixed samples remain more consistent when compared to the increasingly spread LabRAM samples. The LabRAM samples have higher stress to strain behaviour as greater force is required to cause further strain of the materials making the materials stronger and implying the samples have a greater density. The t-test data shows that there is no evidence to reject the null hypothesis.

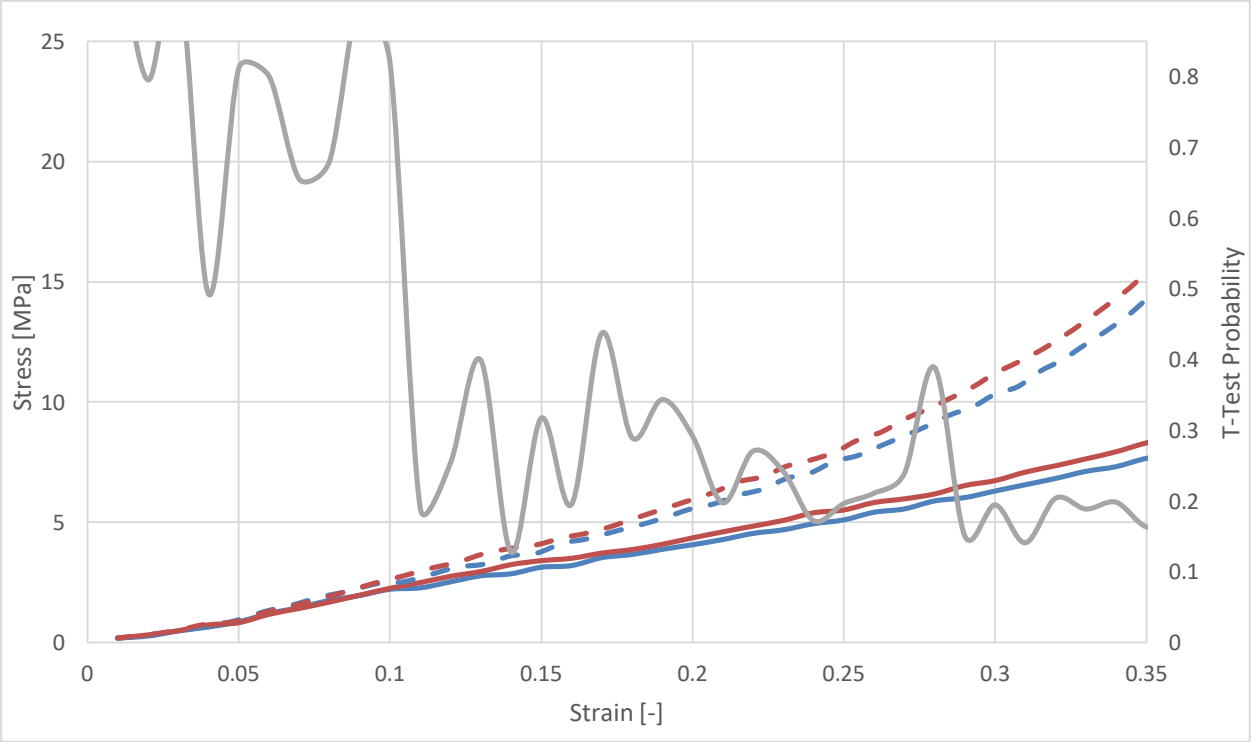


*Figure 58. The stress-strain graph for the high strain rate testing of the 0.66 solid loading HTPB-DOS-Melamine-Barium Sulphate samples, plotting both the engineering stress-strain curve (solid line) and the true stress-strain curve (dashed line). The LabRAM samples are in red and the planetary mixed samples are in blue. The T-Test probability is the grey line. The RAM samples show a minor increase in stress compared to the planetary mixed samples, which is neither statistically different nor significant.*

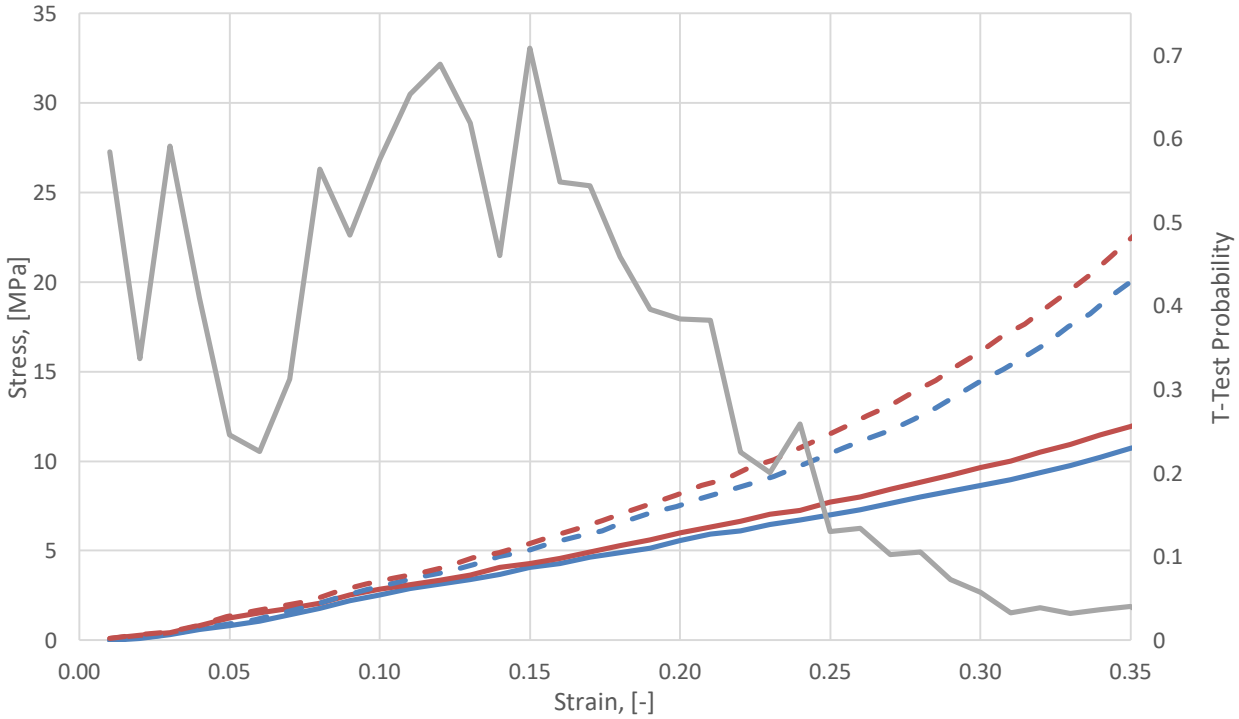


*Figure 59. The stress-strain graph for the high strain rate testing of the 0.73 solid loading HTPB-DOS-Melamine-Barium Sulphate samples, plotting both the engineering stress-strain curve (solid line) and the true stress-strain curve (dashed line). The LabRAM samples are in red and the planetary mixed samples are in blue. The T-Test probability is the grey line. The RAM samples show a minor increase in stress compared to the planetary mixed samples, which is not significant but begins to be statistically different at the higher strains.*

Like the 0.66 solid loading samples, the 0.73 LabRAM samples have improved high strain rate behaviour. The graphs are plotted in Figure 56 and Figure 59. This indicates a denser material and better filler packing density as the material is unable to deform as easily. There is greater variation in the LabRAM samples when compared to the planetary mixed samples; as seen throughout this programme it is hard to ensure consistency when mixing with LabRAM. From 0.3 strain the t-test probability is below the 0.05 level providing evidence that the null hypothesis can be rejected; at the higher strains the samples are statistically not the same.

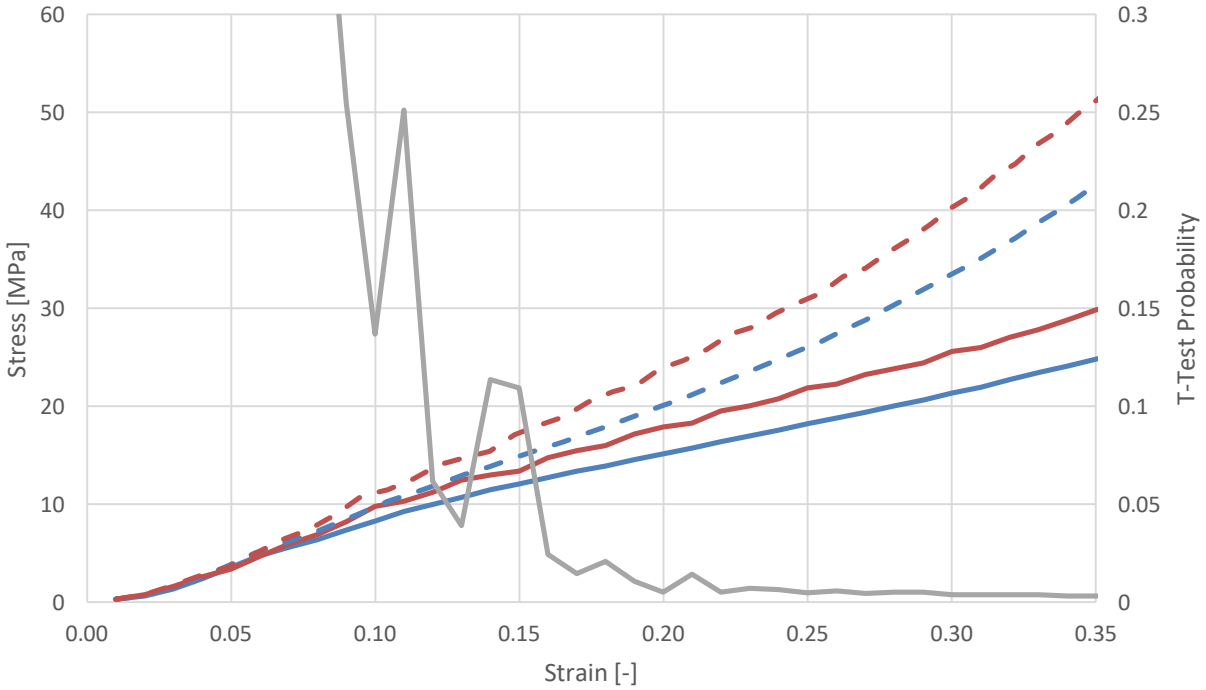


*Figure 60. The stress-strain graph for the high strain rate testing of the 0.85 solid loading HTPB-DOS-Melamine-Barium Sulphate samples, plotting both the engineering stress-strain curve (solid line) and the true stress-strain curve (dashed line). The LabRAM samples are in red and the planetary mixed samples are in blue. The T-Test probability is the grey line. The RAM samples show an increase in stress compared to the planetary mixed samples, which is statistically different at approximately 0.17 strain.*

The 0.85 solid loading results are plotted in Figure 57 and Figure 60. Whereas the 0.66 solid loading sample and the 0.73 solid loading sample are comparable across most of the strain, the 0.85 are not consistent with the t-test giving sufficient evidence to reject the null hypothesis. Both the LabRAM and the planetary mixed samples have a narrow spread. As with the lower solid loading compositions the LabRAM samples have superior mechanical properties, with a higher stress for each strain.

Some of the samples did exhibit damage and failure within the results. There was no correlation between the mixing method and the likelihood of failure. The failures could be categorised into two groups; either the samples exhibited a clean hole in the centre or the sample cracked and fractured around the edges. Both of these can be seen in Figure 61. These failures are expected, due to the nature of the test.

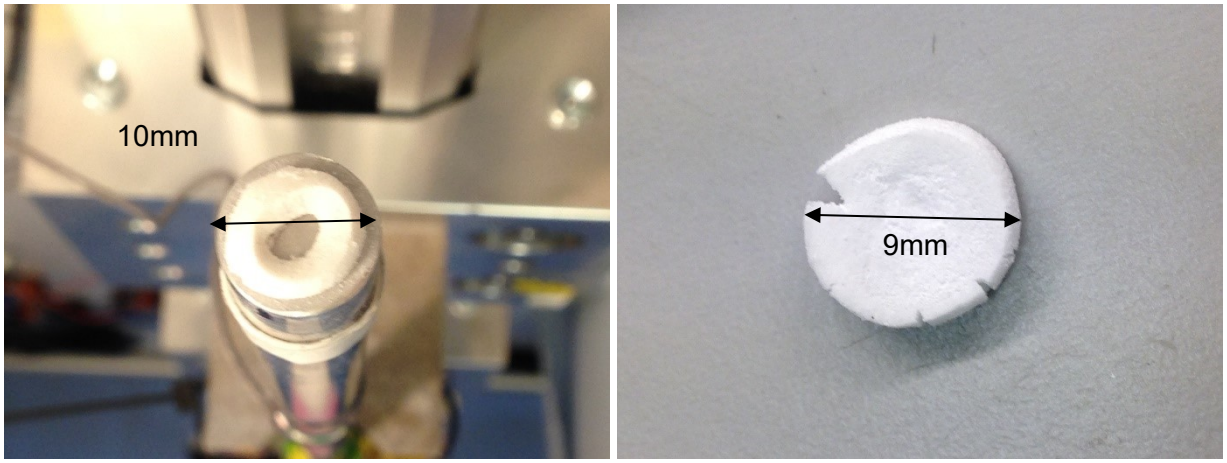


*Figure 61. Pictures illustrating the two types of failures seen by these samples due to the SPHB test. The sample on the left has been punctured in the middle and the sample on the right has cracked around the edges of the diameter.*

The stress-strain curves have been compared with literature to provide context to the results in Table 30. The first paper investigated the high strain rate testing of energetic materials, which used significantly different testing parameters. This gentler test regime, with smaller strain rates, strains and shock, was seen throughout a range of high strain rate testing of energetic materials. Inert materials are able to increase the intensity and harshness of the testing regime without the same safety concerns, and this is reflected in the second paper. The second paper tested an inert highly loaded polymer composite and used comparable testing regimes. The mechanical properties supported the behaviour exhibited by these composites.

*Table 30. A table comparing the SPHB results of the HTPB-DOS-Melamine-Barium Sulphate samples with literature*

| **Source with summary of programme** | Uniaxial Dynamic Compressive Properties of HTPB Casting Explosives, [Xiao et al, 2017] | Dynamic Compressive Mechanical Response of a Soft Polymer Material, [Fan et al, 2015] |
|---|---|---|
| **Material** | The material was a 60% RDX PBX, with a binder system consisting of a plasticiser, curing catalyst, curative and nanometric aluminium. Samples were 16mm diameter discs with a thickness of either 4mm, 3mm or 2mm. | Polymer composite consisting of a Clear Flex 75 binder system and an unknown quantity of solid particles. Sample size of 10mm diameter with 5mm length. |
| **Test Regime** | Aluminium striker, incident and transmission bars with a diameter of 20mm. The incident bar and the transmission bar had a length of 1500mm each. Strains rates of nominally $891s^{-1}$, $1290s^{-1}$ and $2000s^{-1}$. | Aluminium striker, incident and transmission bars with a diameter of 20mm with respective lengths of 400mm, 2000mm and 2000mm. Strain rate of 4000 $s^{-1}$. |
| **Results** | The results were processed and plotted into stress-strain curves with details on whether the samples failed or not. The graph, which can be seen below, indicates that at the lower strain rates the samples did not fail. At the highest strain rate, $2000s^{-1}$ the samples did exhibit failure and cracking. The results range up to just over 0.20 strain; initially the samples require a greater stress to cause deformation and strain within the sample, but then exhibited greater strain for stress behaviour. | The recorded strain ranged up to 60% with stresses up to 244MPa, seen in the graph below. There was a large stress required to cause any strain within the sample; after this initial stress the sample exhibited a consistent increase until a peak at 50% strain. The sample did not fail during this testing; however, after testing there was a macro crack observed with a 320μm region of crazing and microcracks ahead of it. |

| | | |
|---|---|---|
| | 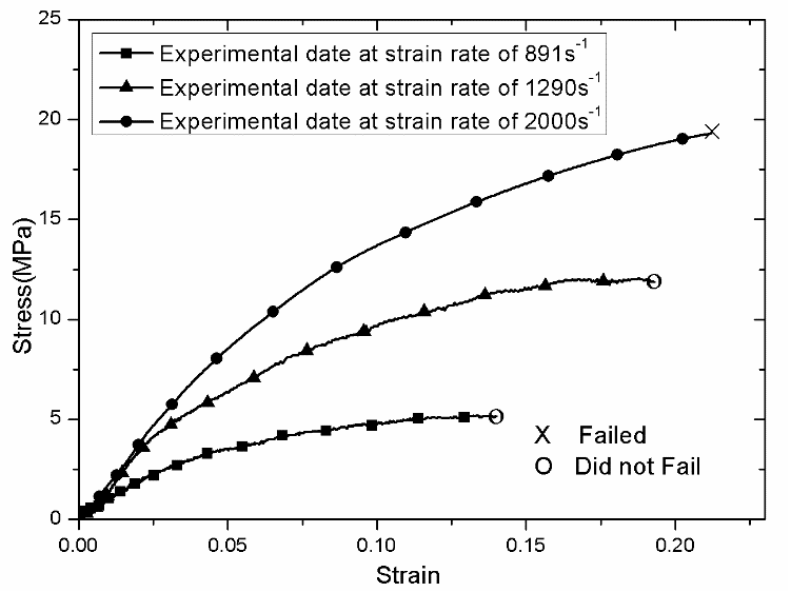 | 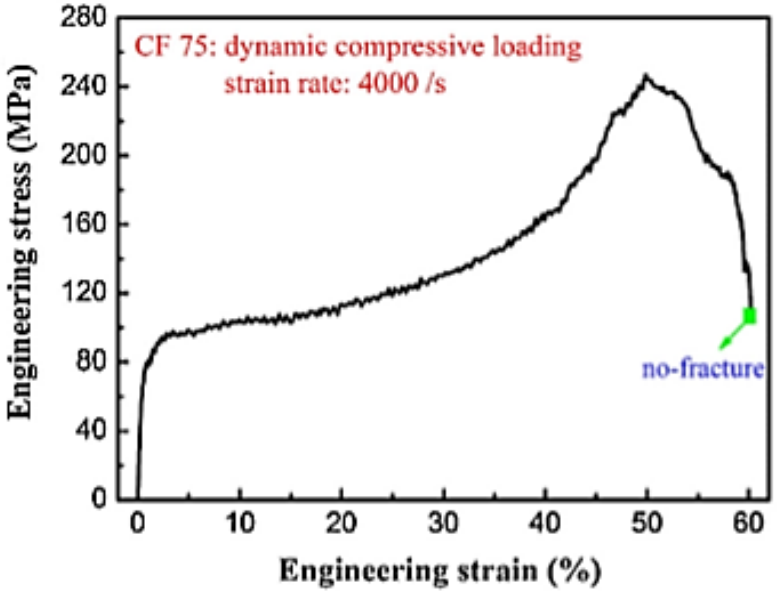 |
| **Comparison with this research programme** | The testing that occurred in this literature paper differed substantially from that conducted in this chapter. This literature followed a wider trend for high strain rate testing for explosives; the strain rates were smaller than what were used for these inert samples. The stresses reported in the literature was 20MPa, which is within the same region as the samples in this chapter. | The testing that occurred in this literature demonstrates a similar behaviour as the samples in this chapter. The graphs in this chapter start at 0.1 strain so do not demonstrate the initial increase in stress. The literature exhibited a linear relationship until 0.3 strain comparable to the samples in this chapter. The stress was much greater than the stress seen in this chapter, which is due to the different binder system. |

### 5.4.3 Moisture Diffusion

Munitions are expensive, and as such it is important that they have a sufficient shelf life. It is not uncommon for munitions to undergo life extensions and surveillance. The assets are visually inspected and the explosives are chemically and physically characterised to determine whether they are safe and suitable for use. As part of this process, materials are artificially aged to help predict the behaviour in the future. The various types of explosives, such as PBXs and propellants, have different aging mechanisms and routes and require alternative characterisation and artificial ageing regimes. It is important to understand these mechanisms and how they best fit the materials used in this research programme.

Propellant ageing is of greatest concern; there are two main mechanisms that can cause degradation and ageing to occur. Chemical ageing results from changing the chemical components; cross-linking, chain scission, oxidation and chemical degradation are the primary mechanisms and all can be accelerated by temperature. Oxidation is initiated throughout the processing and production phase of the process. Additionally, the migration or depletion of components such as stabilisers and plasticisers or the introduction of moisture or other potentially damaging constituents can age the material. Finally external mechanical stimuli can also cause degradation and ageing, as samples experience vibration, shock or thermal shock which could introduce stress within the material. As nitrocellulose undergoes chemical degradation even at room temperature, one of the primary concerns with nitrocellulose based propellants is the stabiliser concentration; nitrocellulose degradation products act as a catalyst for further exponential ageing and degradation [Matecic, 2013]. As such, the most common method of testing is to NATO Standard AOP48 [NATO Standardization Agency, 2008], which is designed to predict the stabiliser content of a nitrocellulose based propellants after 10 years at ambient conditions (25° C) in storage. There are several temperature-time variations and ageing is assessed by stabiliser depletion; it is measured against an unaged baseline. As already stated, the degradation and ageing is an exponential process, due to the catalytic nature of the majority of the degradation products in nitrate ester propellants; it should be noted that some stabiliser degradation products are taken into consideration during this testing as not all stabilisers products behave this way.

With conventional PBXs and composite propellants ageing is not as concerning; RDX, HMX and AP are typically very stable crystals. Oxidation is the biggest risk, as further cross-linking could occur, causing hardening and brittleness within the sample [Daniel, 2006]; however, with the addition of anti-oxidant this can occur over a much longer period of time and can be much less noticeable when trying to characterise this. PBXs can crack due to plasticiser

migration but this is a slower process, and the nature of the materials use allows a greater leniency on this. There is not a comparable standard as AOP48 and ageing results tend to have less impact on the behaviour of the component. However, it is still important to quantify the ageing behaviour so testing is undertaken.

As these samples are based on PBXs and composite propellants, measuring the oxidation of the binder system is the most appropriate ageing test. As the greater risk of oxidation is from moisture absorption a permeation and diffusion experiment was conducted to determine the rate of moisture diffusion throughout the sample. Surface diffusion was undertaken; samples were cut so they were the same length, 3 cm, with a top cross-sectional area of 3 cm by 1 cm, then covered in aluminium tape leaving only this top cross-section exposed. These samples were placed in a desiccator with a salt solution consisting of NaCl and water at 70°C, giving a nominal relative humidity of 75% [www.omega.com, 2018] [Quincot, 2008]. Moisture ingress is conducted through the binder system. Once cured HTPB forms a polyurethane which is an amorphous polymer; amorphous polymers have a greater rate of diffusion as there is typically more free space within the material for the water to diffuse through. It should be noted that there does not need to be much free space for the moisture to diffuse.

The data presented is the result of the long term permeation experiment; shorter experiments were conducted over a period of 4 and 24 hours. The short term experiments did not exhibit any relationship between mixing method and diffusion characteristics. The initial permeation of these materials does not appear to be influenced by the mixing method. Initially the samples were due to be aged for a month; however, by day 12 the samples had shown too much damage and the aluminium tape had become eroded so the test was stopped and the samples were abandoned.

The 0.66 solid loading sample results, detailed in Table 31, Table 32 and Figure 62, show a steady increase in mass up to day 8. The samples have a greater absorption over the first day and then demonstrate a slow gradual increase. The initial mass increase over the first day was expected as the surface is binder rich; sedimentation occurs as curing takes up to a week. The initial mass increase is related to the depth and the density of the binder rich layer as they are the dominating factors on how quickly and how deeply moisture can diffuse. Both the planetary mixed samples and one of the LabRAM samples have consistent behaviour over the first day. The other LabRAM sample exhibits greater absorption with an increase in the rate of mass change indicating that there is greater free space in the binder rich surface for the moisture to diffuse through. After the first day, the mass increase slows as the moisture reaches the bulk of the material. The LabRAM samples have a greater mass

increase and a greater variation per sample indicating that there is either more free space within the binder system or less filler in a given volume when mixed via LabRAM but less consistency.

*Table 31. Mass increase, in grams, over the duration of the diffusion experiments on the 0.66 solid loading HTPB-DOS-Melamine-Barium Sulphate samples*

| Time/days | Planetary Sample 1 | Planetary Sample 2 | LabRAM Sample 1 | LabRAM Sample 2 |
|---|---|---|---|---|
| 0 | 0.0000 | 0.0000 | 0.0000 | 0.0000 |
| 1 | 0.0041 | 0.0032 | 0.0060 | 0.0045 |
| 2 | 0.0048 | 0.0041 | 0.0068 | 0.0057 |
| 7 | 0.0072 | 0.0070 | 0.0136 | 0.0089 |
| 8 | 0.0135 | 0.3145 | 0.0150 | 0.0098 |
| 9 | 0.0252 | 0.0514 | 0.0303 | 0.0119 |
| 10 | 0.0315 | 0.0665 | 0.0412 | 0.0329 |

*Table 32. Mass increase in grams for phase 1, the initial absorption, and phase 2, the bulk absorption, of the diffusion experiment for the 0.66 solid loading HTPB-DOS-Melamine-Barium Sulphate samples*

| Duration | Planetary Sample 1 | Planetary Sample 2 | LabRAM Sample 1 | LabRAM Sample 2 |
|---|---|---|---|---|
| 0-1 days | 0.0041 | 0.0032 | 0.0060 | 0.0045 |
| 2-7 days | 0.0005 | 0.0006 | 0.0014 | 0.0006 |

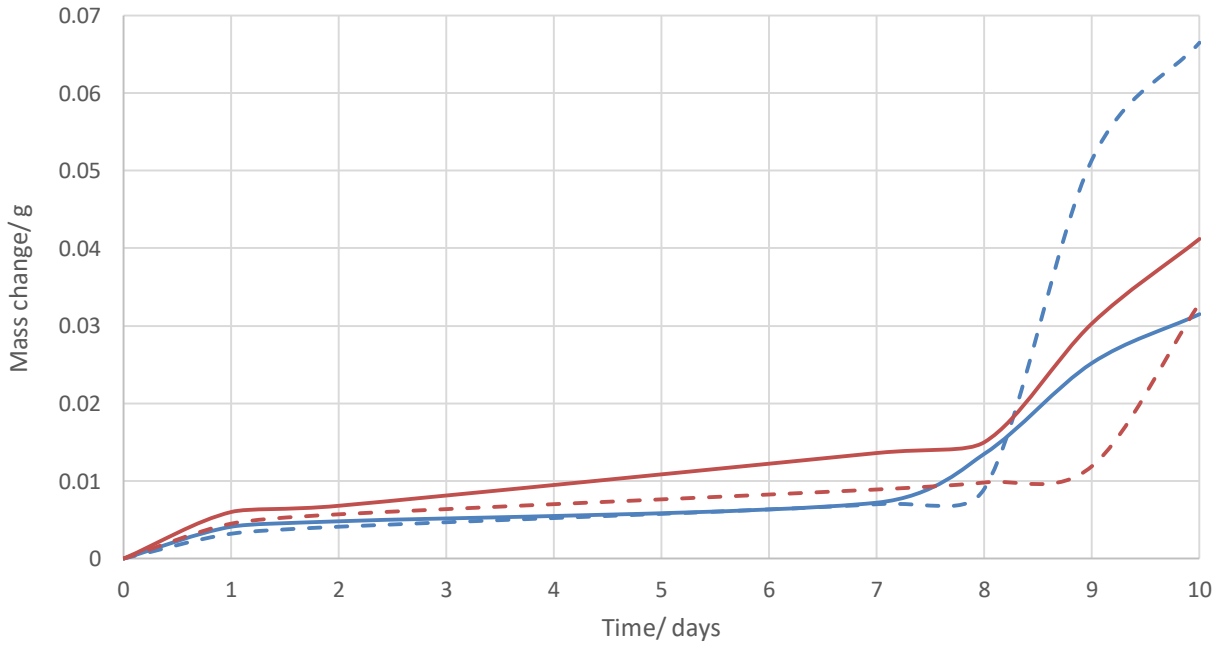


*Figure 62. Graph depicting the mass change during the diffusion experiments the for 0.66 solid loading HTPB-DOS-Melamine-Barium Sulphate samples with the LabRAM samples in red and the planetary mixed samples in blue. The solid line is sample 1 and the dashed line is sample 2. The samples exhibit a larger increase over the first day, which plateaus out until day 8. After day 8 the samples exhibit an erratic mass increase attributed to corrosion of the aluminium tape. The RAM samples demonstrates increased moisture absorption.*

The results of the 0.73 solid loading samples are summarised in Table 33, Table 34 Table 33and Figure 63. The planetary mixed samples have an overall lower absorption of moisture throughout the experiment indicating less available free space in the sample. Over the first day the LabRAM samples have a greater mass increase when compared to the planetary mixed samples indicating that the binder rich surface is less densely packed and has more free space for the moisture to diffuse through. The LabRAM samples also have greater variation. After the first day and until day 7 samples mixed by both mixing methods had large variation as the moisture diffused through the samples at varying rates. The LabRAM samples on average had a larger mass increase and the moisture diffused through the bulk of the material with greater ease. After day 7 there was a dramatic increase in moisture uptake with all bar one LabRAM sample. However, at this point the masses are erratic, which is attributed to erosion of the aluminium tape, and the test is no longer valid.

*Table 33. Mass increase, in grams, over the duration of the diffusion experiments on the 0.73 solid loading HTPB-DOS-Melamine-Barium Sulphate samples*

| Time/days | Planetary Sample 1 | Planetary Sample 2 | LabRAM Sample 1 | LabRAM Sample 2 |
|---|---|---|---|---|
| 0 | 0.0000 | 0.0000 | 0.0000 | 0.0000 |
| 1 | 0.0025 | 0.0036 | 0.0036 | 0.0047 |
| 2 | 0.0038 | 0.0042 | 0.0047 | 0.0070 |
| 7 | 0.0056 | 0.0121 | 0.0084 | 0.0156 |
| 8 | 0.0295 | 0.0223 | 0.0088 | 0.0262 |
| 9 | 0.0454 | 0.0455 | 0.0149 | 0.0574 |
| 10 | 0.0271 | 0.0554 | 0.0482 | 0.0507 |

*Table 34. Mass increase in grams for phase 1, the initial absorption, and phase 2, the bulk absorption, of the diffusion experiment for the 0.73 solid loading HTPB-DOS-Melamine-Barium Sulphate samples*

| Duration | Planetary Sample 1 | Planetary Sample 2 | LabRAM Sample 1 | LabRAM Sample 2 |
|---|---|---|---|---|
| 0-1 days | 0.0025 | 0.0036 | 0.0036 | 0.0047 |
| 2-7 days | 0.0004 | 0.0016 | 0.0007 | 0.0017 |

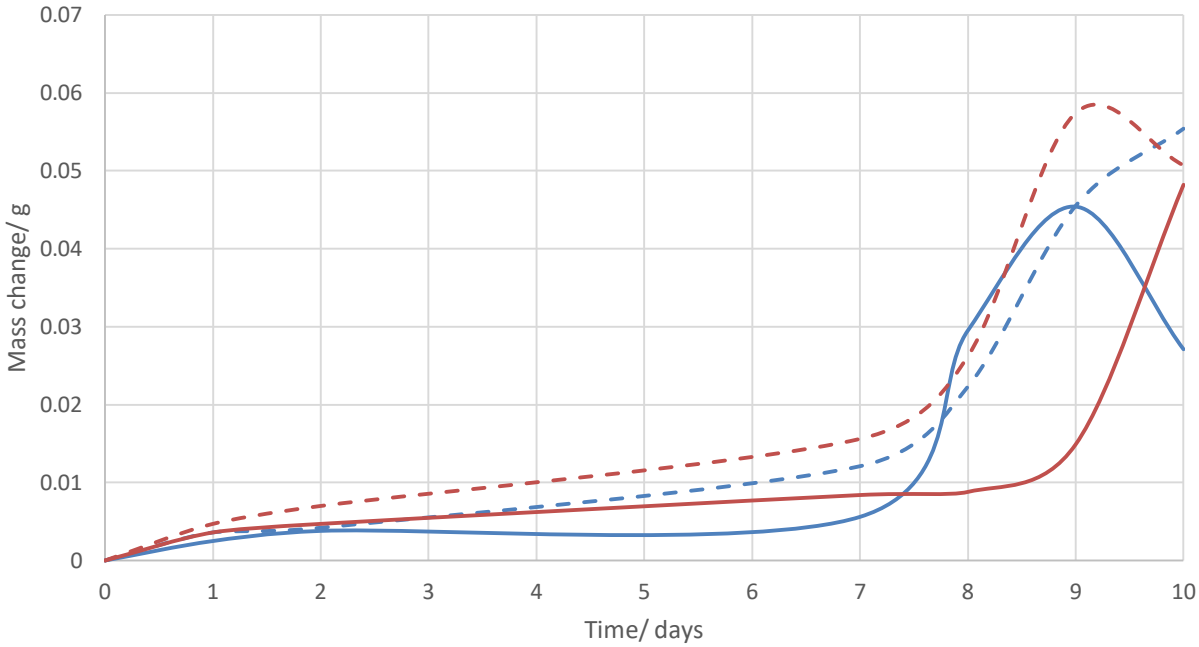


*Figure 63. Graph depicting the mass change during the diffusion experiments the for 0.73 solid loading HTPB-DOS-Melamine-Barium Sulphate samples with the LabRAM samples in red and the planetary mixed samples in blue. The solid line is sample 1 and the dashed line is sample 2. The samples exhibit a larger increase over the first day, which plateaus out until day 8. After day 8 the samples exhibit an erratic mass increase attributed to corrosion of the aluminium tape. The mass increase for the RAM and planetary mixed samples overlap.*

The 0.85 solid loading samples, in Table 35, Table 36 and Figure 64, have a consistent behaviour across all mixing methods over the duration of the first day, indicating that the binder rich surface layer is comparable in all samples in terms of density. The planetary mixed samples continue the rate of mass increase over the next day which indicates that the LabRAM samples have a shallower binder rich surface layer. After the first day, the mixing methods deviate as the planetary mixed samples have a greater mass increase and a larger variation. The LabRAM samples are both consistent and have low moisture ingress demonstrating that the sample has a consistent highly packed filler system. After day 7 the samples exhibit the same erratic behaviour seen in the alternative samples that is not linked to the material behaviour.

*Table 35. Mass increase, in grams, over the duration of the diffusion experiments on the 0.85 solid loading HTPB-DOS-Melamine-Barium Sulphate samples*

| Time/days | Planetary Sample 1 | Planetary Sample 2 | LabRAM Sample 1 | LabRAM Sample 2 |
|---|---|---|---|---|
| 0 | 0.0000 | 0.0000 | 0.0000 | 0.0000 |
| 1 | 0.0045 | 0.0039 | 0.0034 | 0.0041 |
| 2 | 0.0084 | 0.0063 | 0.0035 | 0.0039 |
| 7 | 0.0141 | 0.0085 | 0.0055 | 0.0064 |
| 8 | 0.0201 | 0.0183 | 0.0163 | 0.0134 |
| 9 | 0.0244 | 0.0684 | 0.0330 | 0.0149 |
| 10 | 0.0404 | 0.0542 | 0.0606 | 0.0908 |

*Table 36. Mass increase in grams for phase 1, the initial absorption, and phase 2, the bulk absorption, of the diffusion experiment for the 0.85 solid loading HTPB-DOS-Melamine-Barium Sulphate samples*

| Duration | Planetary Sample 1 | Planetary Sample 2 | LabRAM Sample 1 | LabRAM Sample 2 |
|---|---|---|---|---|
| 0-1 days | 0.0045 | 0.0039 | 0.0034 | 0.0041 |
| 2-7 days | 0.0011 | 0.0004 | 0.0004 | 0.0005 |

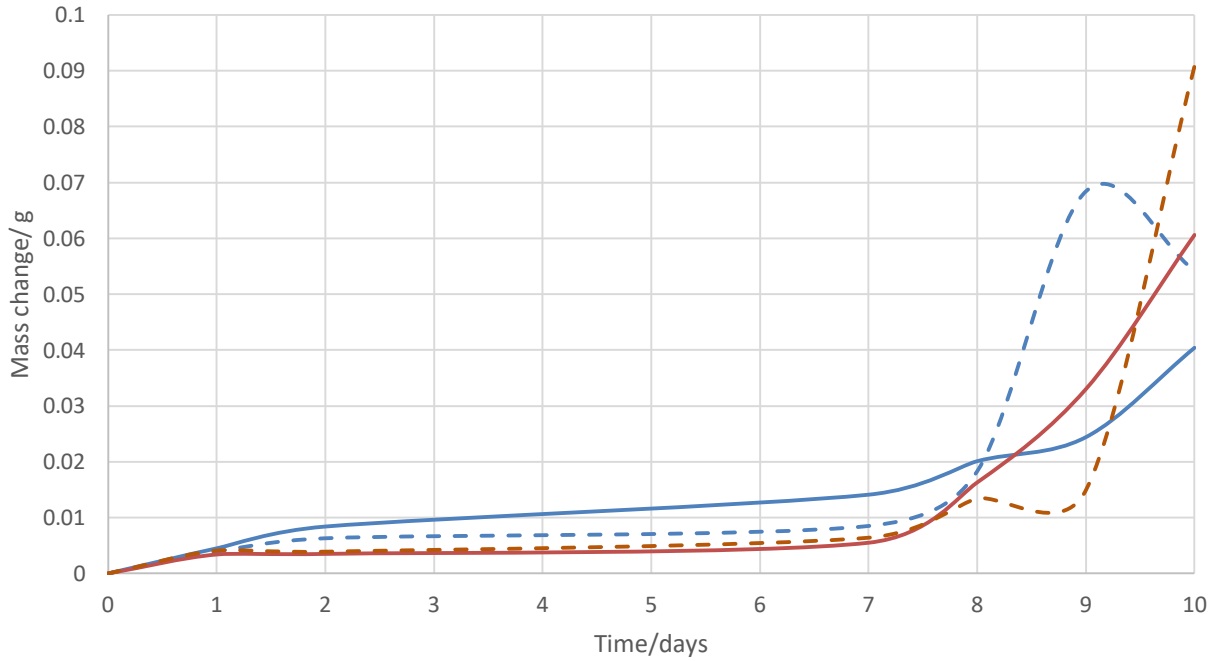


*Figure 64. Graph depicting the mass change during the diffusion experiments the for 0.66 solid loading HTPB-DOS-Melamine-Barium Sulphate samples with the LabRAM samples in red and the planetary mixed samples in blue. The solid line is sample 1 and the dashed line is sample 2. The samples exhibit a larger increase over the first day, which plateaus out until day 8. After day 8 the samples exhibit an erratic mass increase attributed to corrosion of the aluminium tape. The planetary mixed samples demonstrate an increased moisture absorption compared to the RAM samples*

### 5.4.4 Optical Microscopy

Optical microscopy was undertaken on samples using an Axio Zeiss M1M with a light probe casting a spotlight on the samples. The samples were prepared through cutting at room temperature to expose the bulk of the material; like previous materials there might be deformation at the cut surface. The images are seen in Figure 65, Figure 66, and Figure 67. There is no visual indication of the mixing method having any significant effect on the material; the filler crystals appear to be consistent in size between mixing methods, and equally dispersed within the binder system. The filler crystals exhibit some agglomeration that appears to be more prominent in the lower solid loading levels, but with no dependence on mixing method.

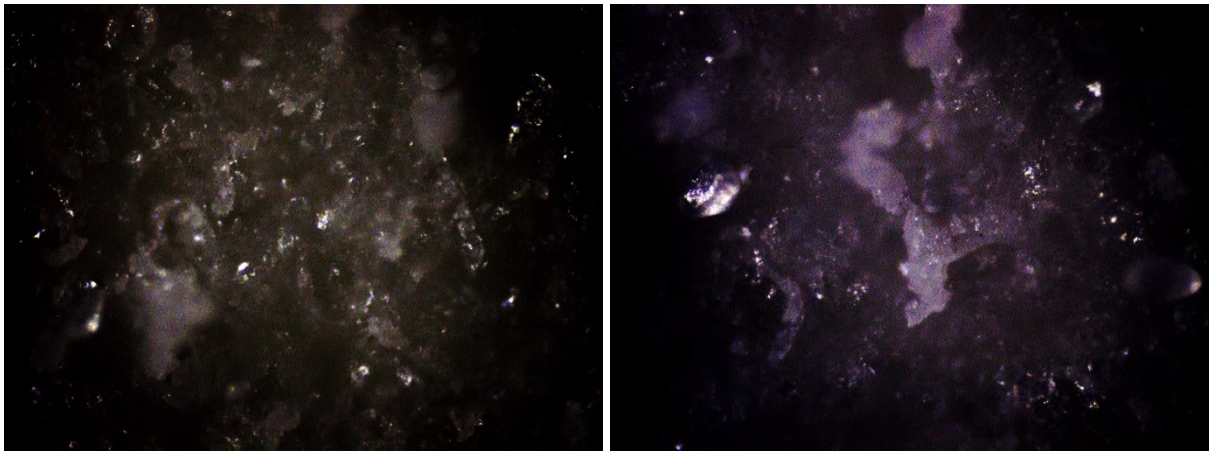

*Figure 65. Microscopy images of the 0.66 solid loading HTPB-DOS-Melamine-Barium Sulphate samples mixed by LabRAM (left) and planetary mixing (right). The melamine and barium sulphate can be observed within the HTPB strands. The filler crystals do not appear to differ in either shape or size and the HTPB strands do not appear to be damaged or shorter when comparing the two mixing methods.*

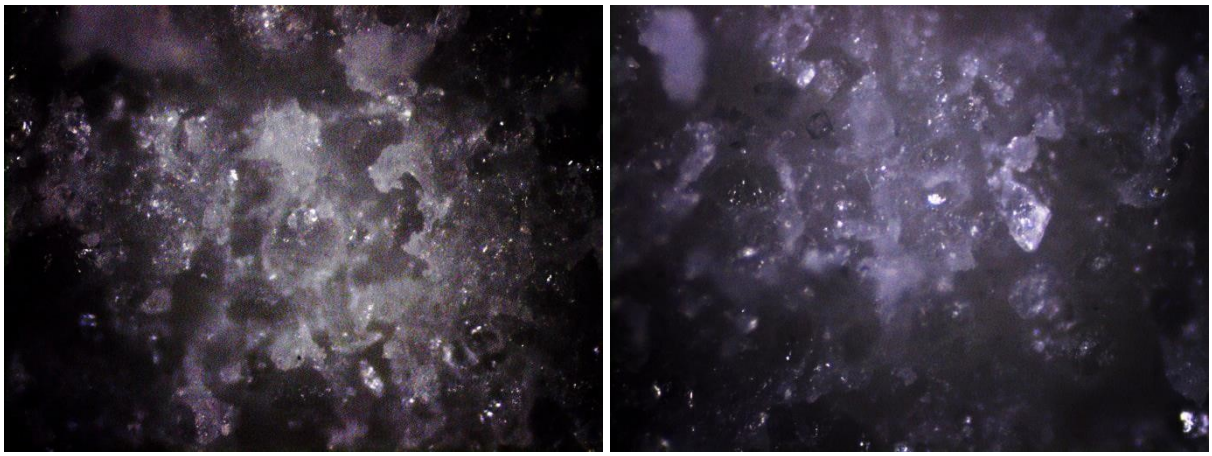

*Figure 66. Microscopy images of the 0.73 solid loading HTPB-DOS-Melamine-Barium Sulphate samples mixed by LabRAM (left) and planetary mixing (right). The melamine and barium sulphate can be observed within the HTPB strands. The filler crystals do not appear to differ in either shape or size and the HTPB strands do not appear to be damaged or shorter when comparing the two mixing methods.*

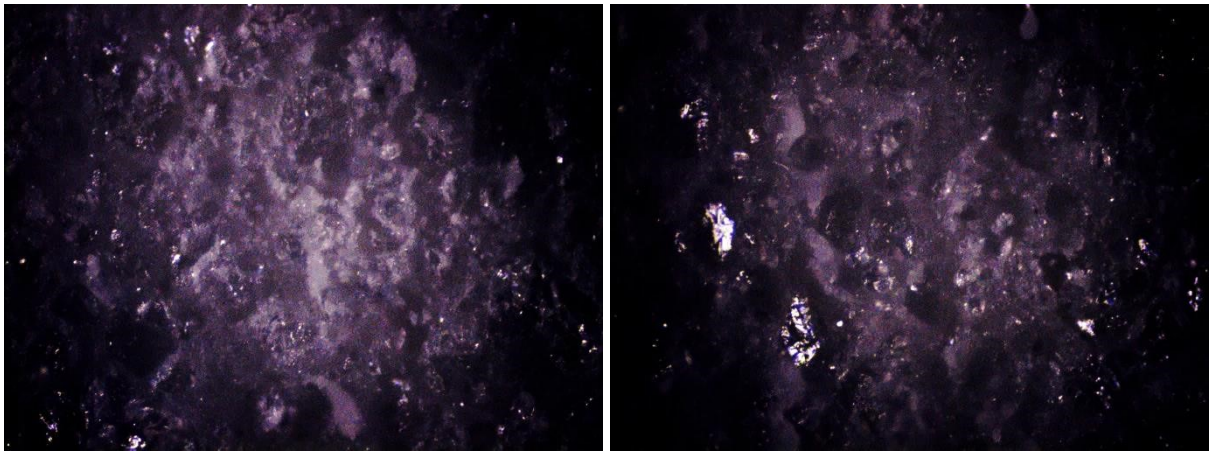

*Figure 67. Microscopy images of the 0.85 solid loading HTPB-DOS-Melamine-Barium Sulphate samples mixed by LabRAM (left) and planetary mixing (right). The melamine and barium sulphate can be observed within the HTPB strands. The filler crystals do not appear to differ in either shape or size and the HTPB strands do not appear to be damaged or shorter when comparing the two mixing methods.*

## 5.5 Discussion and Conclusions

The HTPB-DOS-Melamine-Barium Sulphate samples were mixed and tested by a number of different techniques and have shown to have no significant difference due to mixing method. The initial compositions illustrated a potential issue with the LabRAM; the fine filler component, barium sulphate, agglomerated and mixing was not sufficient to break down these agglomerates. However, sieving the barium sulphate material through a 1mm sized sieve reduced these agglomerations and the material was then homogeneous. The DMA results showed little variation across all of the solid loading levels; the storage and loss moduli overlapped for the majority of the strain. The tan(delta) exhibited minor variation at the peaks; however, these are negligible. The high strain rate behaviour was improved by mixing via LabRAM, and all bar the 0.66 solid loading sample had statistical evidence to reject the null hypothesis. The 0.66 and 0.73 solid loading LabRAM samples did however have greater deviation when compared to the planetary mixed samples. The diffusion experiments had a high level of variation both within like samples and throughout the solid loading levels. This behaviour is dominated by the surface properties which was linked more with post-mixing processing as opposed to the mixing method. The microscopy images indicated that the samples were well distributed. The results are summarised in Table 37. The table is colour coded to demonstrate which had the higher results using the same colour scheme used throughout; red is LabRAM and blue is the planetary mixed samples. Samples in bold indicate sufficient evidence to reject the null hypothesis.

*Table 37. Table summarising the results of HTPB-DOS-Melamine-Barium Sulphate characterisation. The DMA column indicates the temperature range in which the results vary. The remaining results are percentage changes of the RAM samples from the planetary mixed samples. The colour coding indicates which sample had the higher results, with the planetary mixed samples being blue and the RAM samples being red. The results did not demonstrate any significant difference in the samples behaviour, although there was a statistical difference in the 0.73 and 0.85 solid loading samples.*

| | DMA | SHPB | Moisture Diffusion |
|---|---|---|---|
| 0.66 solid loading | -70°C onwards | 0.2 onwards | Day 1 onwards |
| 0.73 solid loading | -70°C onwards | **0.3 onwards** | Day 1 onwards |
| 0.85 solid loading | -70°C to +30°C | **Across range** | Day 1 onwards |

As with previous compositions, it is beneficial to compare the data together. Whereas the tested properties for the HTPB-Melamine-Barium Sulphate compositions had overlapping mechanisms the testing in this chapter does not have the same level. The DMA results are primarily driven by the binder and the ability of the polymeric chains to move. The high strain rate is controlled by the free space within the sample and the packing of the filler particles. The moisture diffusion is driven by the available binder and the surface properties to allow moisture ingress through the material.

Although the 0.66 solid loading LabRAM sample has marginally weaker low strain rate results, as the polymer chains are able to move slightly due to minor poor cross-linking, it should be noted that the variation between samples from the two mixing methods is insignificant. As such, it is much more appropriate to state that the low strain rate mechanical behaviour is comparable and the samples have equal stiffness and therefore equal binder properties. Likewise, the high strain rate testing has no evidence to reject the null hypothesis. The LabRAM samples are stronger when tested under compression noticeably indicating that the filler packing density is superior for the materials mixed via LabRAM. The moisture diffusion indicates there is greater free space within the binder material; as the moisture only requires a small amount free space to diffuse through this supports the DMA results and the implication that the cross-linked network is slightly hindered. The overall results indicate that by mixing via LabRAM, the filler particles have a greater packing density but marginally poorer binder properties. However, the variation is insignificant and the mixing method has not affected the material properties.

The 0.73 LabRAM solid loading samples follow the same pattern with weaker low strain rate mechanical behaviour, greater moisture ingress into and through the sample and higher high strain rate compression behaviour. Like the 0.66 solid loading samples, the 0.73 solid loading

samples are comparable with minor variation between the mixing methods. As before, the overall behaviour indicates that the binder system has an inferior cross-linking and greater filler packing density. Unlike the 0.66 solid loading sample, the 0.73 solid loading SHPB samples provided evidence to reject the null hypothesis, and the moisture diffusion demonstrated greater variation; however, like samples also demonstrated large variation. Although LabRAM mixing had a greater impact at this solid loading the impact was insignificant.

The 0.85 solid loading sample did not follow the same pattern as the two lower solid loading samples. The LabRAM samples had the same improved high strain rate testing results, indicating a greater packing density of the filler particles, and also had superior low strain rate mechanical behaviour which indicated that the samples had either superior cross-linking or a denser binder system. This was supported by the ageing behaviour which demonstrated that the moisture ingress was more prominent in the planetary mixed samples. The large variation in the high strain rate testing and the distinctly different moisture diffusion curves demonstrates that LabRAM mixing did have a beneficial impact on these samples.

The samples, like previous compositions, did not demonstrate a consistent behaviour change when comparing the LabRAM samples to the conventional planetary mixed samples. The lowest solid loading demonstrated no significant change in material properties although the samples did vary as the solid loading increased. Both the 0.66 and the 0.73 solid loading samples exhibited the same weaker cross-linking and superior packing density which limited the low strain rate mechanical behaviour. The highly loaded samples, the 0.85, demonstrated superior properties over all testing methods when mixed via LabRAM. With this composition and the three solid loading levels, the materials have been affected; however, the materials mixed via LabRAM have either exhibited superior properties or insignificant change when compared to the planetary mixed samples.

# 6 Full Inert Composition

Addition of anti-oxidant, Calco, Lowinox or Anti-Oxidant 2246, brings the composition to its final inert state. Further processing has been required due to ageing and discolouration of samples. Anti-oxidant stops this and increases the shelf-life of the product. However, there was an increase in viscosity and at the highest loadings the samples had a number of voids at the bottom of the sample; several attempts were made but it was decided to reduce the solid loading to 0.80. As with the HTPB-DOS-Melamine-Barium Sulphate compositions, the Barium Sulphate was sieved prior to mixing to reduce agglomerates.

## 6.1 Materials

As discussed in Chapter 5.4.3 due to munition cost energetic materials need t have a long (10 years minimum) service life. As demonstrated with the previous compositions the binder system oxidises during curing and over time. Adding antioxidant (AO) prevent this. Oxidation occurs when polymeric chains have free radicals that interact with an oxygen molecule. This forms two new radicals which interact with further oxygen molecules causing a perpetually accelerating ageing process. This oxidation negatively affects the mechanical properties making the material more brittle. The AO used in this research programme is a phenolic antioxidant called AO2246. The chemical structure can be found in Figure 68. Phenolic groups are good hydrogen donors that cause a termination reaction, stopping the autocatalytic oxidation. Only a small quantity of AO is required.

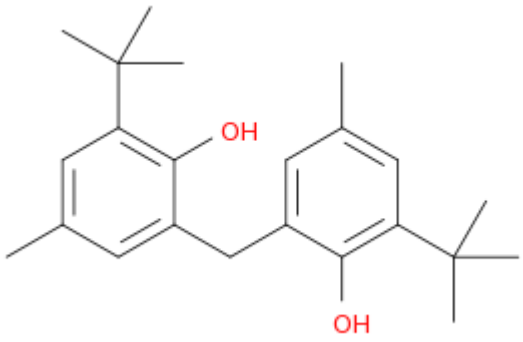


*Figure 68. The chemical structure of the antioxidant used in this formulation, AO2246 [Mol-Instincts, 2017]*

## 6.2 Planetary Mixing

Planetary mixing was conducted using the same parameters as the previous chapters. Further information can be found in Chapter 3.2. The samples had a highly tacky surface,

where the binder rich layer was under cured. The IPDI concentration was not modified to reflect the addition of the plasticiser and the AO; however, this is common with other compositions such as PBXN-110 and was done intentionally. The formulations and mix notes can be found in Table 38.

*Table 38. Formulation table of full inert planetary mixed samples with the mixing comments*

| | | | | | | | |
|---|---|---|---|---|---|---|---|
| **0.66 solid loading** | HTPB | AO | DOS | Melamine | Barium Sulphate | Planetary Mixed | Very good flow properties, cast easily |
| | 22.61 | 0.34 | 11.05 | 48.18 | 17.82 | | |
| **0.73 solid loading** | HTPB | AO | DOS | Melamine | Barium Sulphate | Planetary Mixed | Good flow properties, cast well |
| | 17.955 | 0.27 | 8.775 | 53.29 | 19.71 | | |
| **0.80 solid loading** | HTPB | AO | DOS | Melamine | Barium Sulphate | Planetary Mixed | Acceptable flow properties; flowed once in mould but was stiff when using a spatula |
| | 13.3 | 0.2 | 6.5 | 58.4 | 21.6 | | |

The 0.66 solid loading sample exhibited separation of binder and bulk material; samples have a binder rich surface but this was outside of the acceptable range. Samples were remixed and had a reduced binder layer. Testing was conducted on the new samples.

Several attempts were made to mix and cast the 0.85 solid loading sample; however, they had multiple voids along the bottom of the sample and no test samples were recovered from the bulk. As such, the solid loadings were lowered. This loading level has not been included in the table.

## 6.3 LabRAM Mixing

The LabRAM samples all cast easily and had good flow properties. A few small agglomerates where present at the end of the mix, despite sieving the Barium Sulphate; however, there was only a limited amount noted and were deemed to be negligible. The formulations and mixing notes are found in Table 39.

The 0.80 solid loading sample cast very well and had good flow properties. It was believed that the solid loading could be increased, and that the 0.85 sample would have been achievable. This is an example of the LabRAM having superior mixing capability; however, this could also be attributed to the increased temperature. The LabRAM samples exhibited 20 °C temperature increase which would improve the rheological properties and this improvement in processing ability has been observed for previous compositions.

*Table 39. Formulation table of full inert LabRAM samples with mixing notes*

| | | | | | | | |
|---|---|---|---|---|---|---|---|
| **0.66 solid loading** | HTPB | AO | DOS | Melamine | Barium Sulphate | LabRAM | Very good flow properties, cast easily |
| | 22.61 | 0.34 | 11.05 | 48.18 | 17.82 | | |
| **0.73 solid loading** | HTPB | AO | DOS | Melamine | Barium Sulphate | LabRAM | Good flow properties, cast well |
| | 17.955 | 0.27 | 8.775 | 53.29 | 19.71 | | |
| **0.80 solid loading** | HTPB | AO | DOS | Melamine | Barium Sulphate | LabRAM | Good flow properties, could have potentially increased the solid loading |
| | 13.3 | 0.2 | 6.5 | 58.4 | 21.6 | | |

## 6.4 Characterisation of samples

The full inert compositions had the most detailed and comprehensive set of characterisation. Mechanical investigated the low and high strain rates; DMA was conducted to STANAG 4540, with a temperature sweep of -110 °C to +80 °C in 3 °C increments and 0.1% strain. Split Hopkinson Pressure Bar was conducted at Imperial College London, using 7068 aluminium

alloy bars, aiming for a nominal 3350 $s^{-1}$ strain rate. DSC/TGA was used to investigate thermal transitions and the mass change of the materials. NMR was used to investigate the potential presence of decomposition products and variations in the HTPB, using a $CDCL_3$ and TTMS standard. Microscopy images were taken on the samples prepared by cutting the bulk material at room temperature. The samples were also tested for density using hydrogen pycnometry. Ageing studies were conducted with the antioxidant using single surface moisture diffusion and mass change.

### 6.4.1 DMA

DMA testing was conducted using the same parameters as previous compositions; this can be found in Chapter 3.4.1. As the samples contained antioxidant the surface did not oxidise. Graphs were plotted for each solid loading level, comparing storage modulus, G', loss modulus, G'', and tan(delta). The red samples are LabRAM and blue are planetary mixing; the solid lines are G', dotted line G'' and dashed lines are tan(delta).

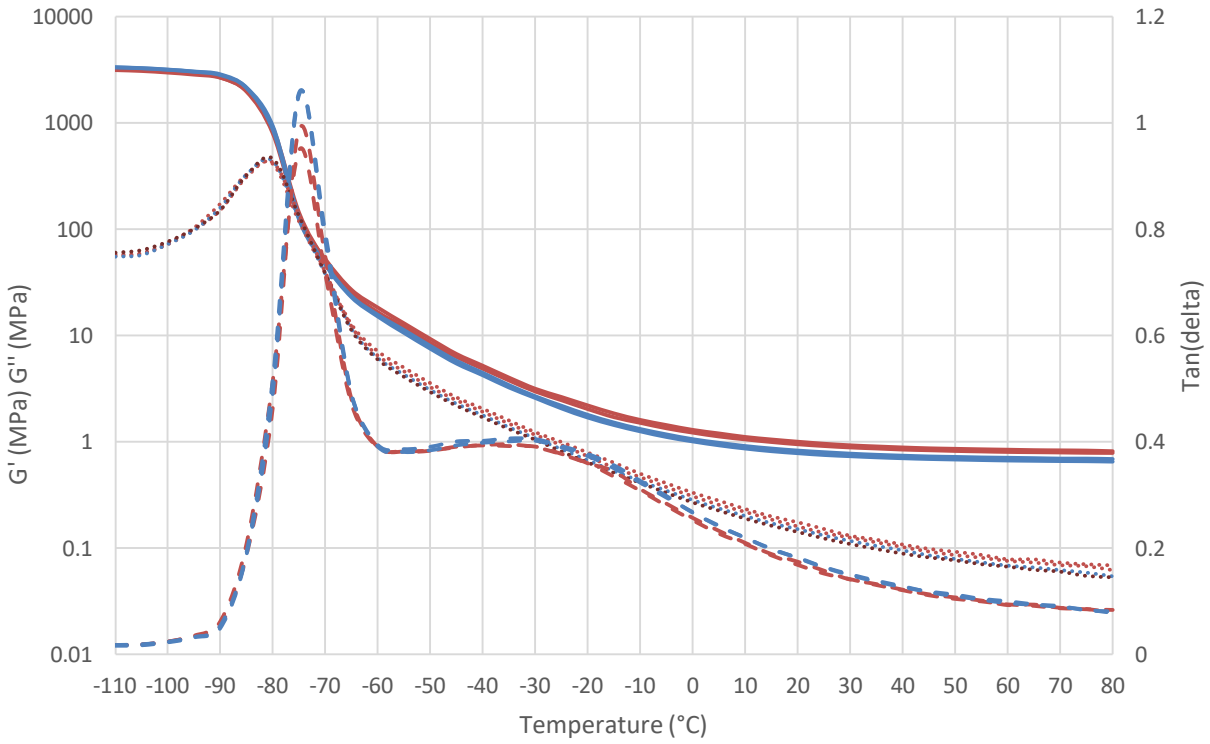


*Figure 69. DMA graph for 0.66 solid loading full inert samples plotting the elastic modulus or G' (solid line), loss modulus or G'' (dotted line) and tan(delta) (dashed line), and comparing the LabRAM samples (red) with the planetary mixed samples (blue). The samples demonstrate high consistency in the mechanical behaviour*

The 0.66 solid loading samples, in Figure 69, demonstrate consistency between mixing methods. Both moduli and the tan(delta) overlap demonstrating the samples have not been affected by the mixing method. At the glass transition temperature, the planetary mixed samples have a marginally increased tan(delta) peak, indicating more energy lost but it is insignificant. After the glass transition temperature the planetary samples exhibit slightly softer behaviour. Any variation is insignificant and the mixing method has not affected the mechanical properties.

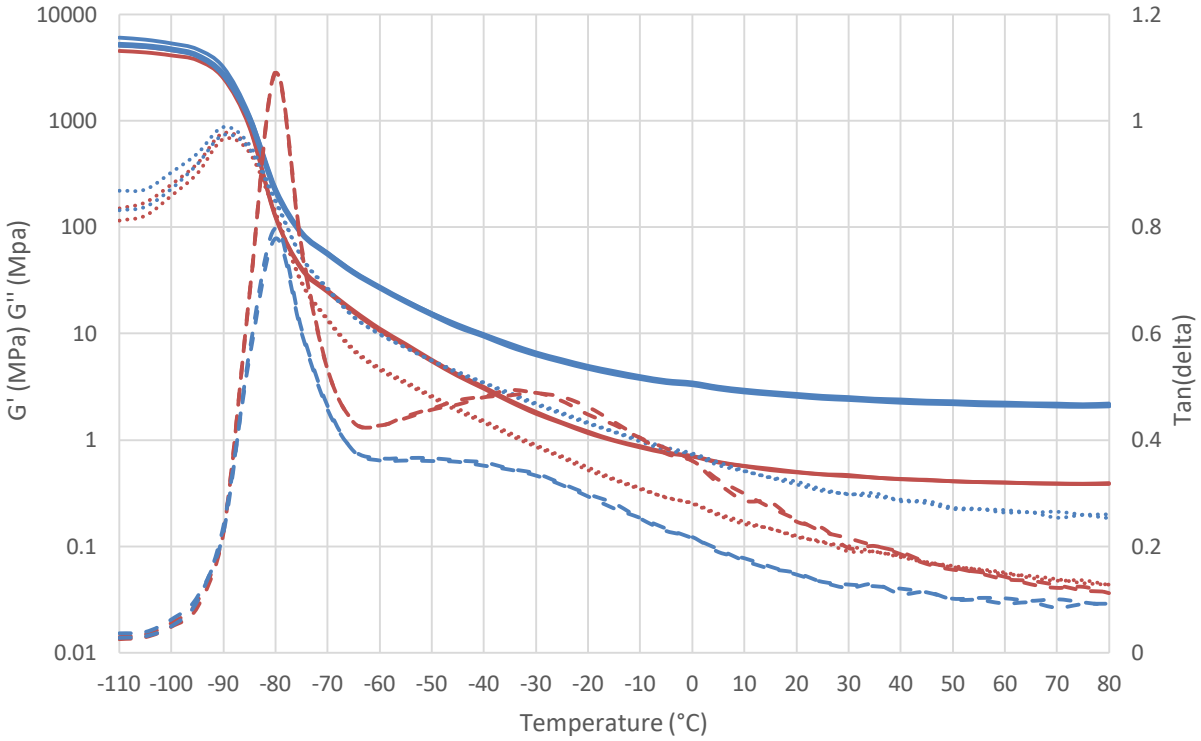


*Figure 70. DMA graph for 0.73 solid loading full inert samples plotting the elastic modulus or G' (solid line), loss modulus or G'' (dotted line) and tan(delta) (dashed line), and comparing the LabRAM samples (red) with the planetary mixed samples (blue). The samples demonstrate significant variation with the planetary mixed samples exhibiting more elastic behaviour after the glass transition temperature*

The 0.73 solid loading samples in Figure 70 shows significant variation between the two mixing methods. The LabRAM sample is significantly softer as the polymer chains are able to move freely due to poor cross-linking in the LabRAM sample; the isocyanate curative is not effectively distributed throughout the sample. This demonstrates an issue with LabRAM mixing; unlike the intrusive planetary mixing, the optimisation of mixing parameters is required to ensure that mixing occurs on a global level not just in the micro-mixed cells. Planetary

mixing has the benefit of experience and accepted practices to ensure that mixing is complete prior to removing the material from the mixer and the intrusive blades force flow within the sample. The poor distribution of isocyanate means the LabRAM samples have significantly lower moduli after the glass transitional peak. This is also seen in the significantly higher tan(delta) peaks as a lot of energy is lost through friction or heat from these free moving polymeric chains.

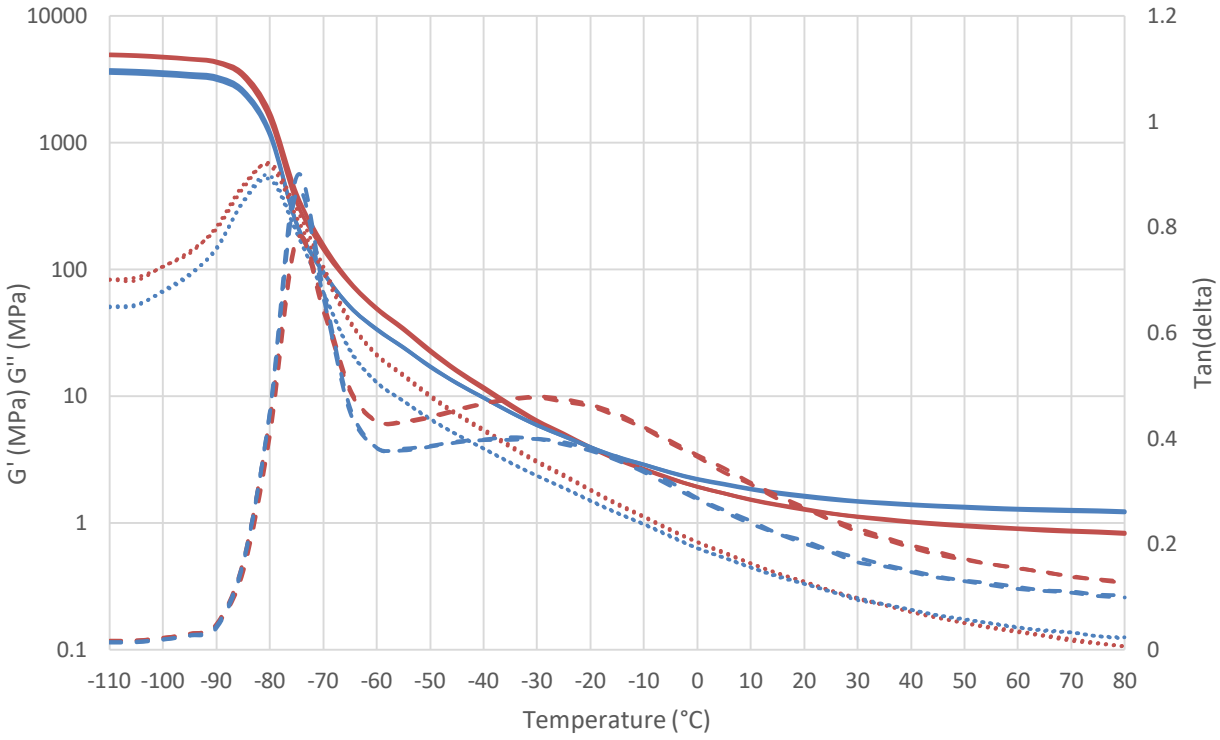


*Figure 71. DMA graph for 0.80 solid loading HTPB-DOS-Melamine-Barium Sulphate samples plotting the elastic modulus or G' (solid line), loss modulus or G" (dotted line) and tan(delta) (dashed line), and comparing the LabRAM samples (red) with the planetary mixed samples (blue). The samples demonstrate consistency in the mechanical behaviour*

For the 0.80 solid loading samples, in Figure 71, there is a variation in the moduli as the LabRAM samples are softer. At temperatures lower than -20 °C the LabRAM samples had superior mechanical properties as the polymeric chains could not move which indicates that there is less free space particularly within the binder system. This has been observed in previous materials. The tan(delta) curve demonstrated that at -20 °C there is a large amount of energy lost in the LabRAM samples which coincides with the comparative decrease in the elastic moduli.

Table 40 compares the research in this programme with data found in literature to provide context that the results are reasonable and within the expected range. Comparing with the previous chapter and a paper demonstrates that the samples are as expected.

*Table 40. A table comparing the DMA result of the full inert samples with literature*

| **Source with summary of programme** | Chapter 5 | Thermo-Mechanical Analysis of Heterogeneous Solid Rocket Propellant, [Cegla et al, 2018] |
|---|---|---|
| **Material** | HTPB – DOS – Melamine - Barium Sulphate with solid loading levels of 0.66, 0.73 and 0.80 | Rocket propellant H2 consisting of 70% ammonium perchlorate, 15% aluminium powder and 15% PBAN rubber. |
| **Test Regime** | Testing conducted on a Rheometrics RDAIIII with a 0.1% strain, and a temperature range of -110 °C to +80 °C. The temperature was incremented at 3 °C $min^{-1}$. | Testing was conducted on a Netzsch DMA 242C analyser with a temperature range of -120 °C to +80 °C and a 2 °C $min^{-1}$ incremental temperature rise. |
| **Results** | Both the LabRAM and the planetary mixed samples had high level of consistency across all the solid loading levels with the plots overlapping between the mix methods. The 0.66 solid loading is plotted and included below. The glass transition peak is at -75 °C with a secondary tan(delta) peak at approximately -35 °C. The G' is 3.3 GPa prior to Tg and 2.2 MPa after. | The DMA plot is included below and highlights the behaviour of the sample. The onset of the glass transition is at -77 °C, and exhibits the decrease in the elastic modulus. The loss modulus also exhibits the same change with a peak at -57 °C. The tan(delta) peaks at 22 °C which is attributed to the softening temperature of the sample. There is no explanation for the lack of a tan(delta) peak at the glass transition temperature. |

| | | |
|---|---|---|
| | 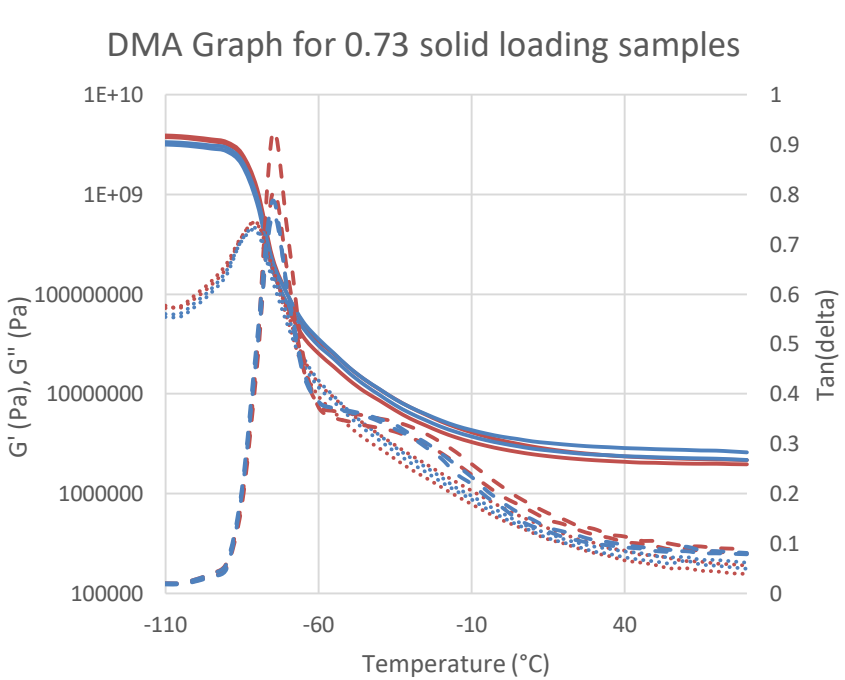 | 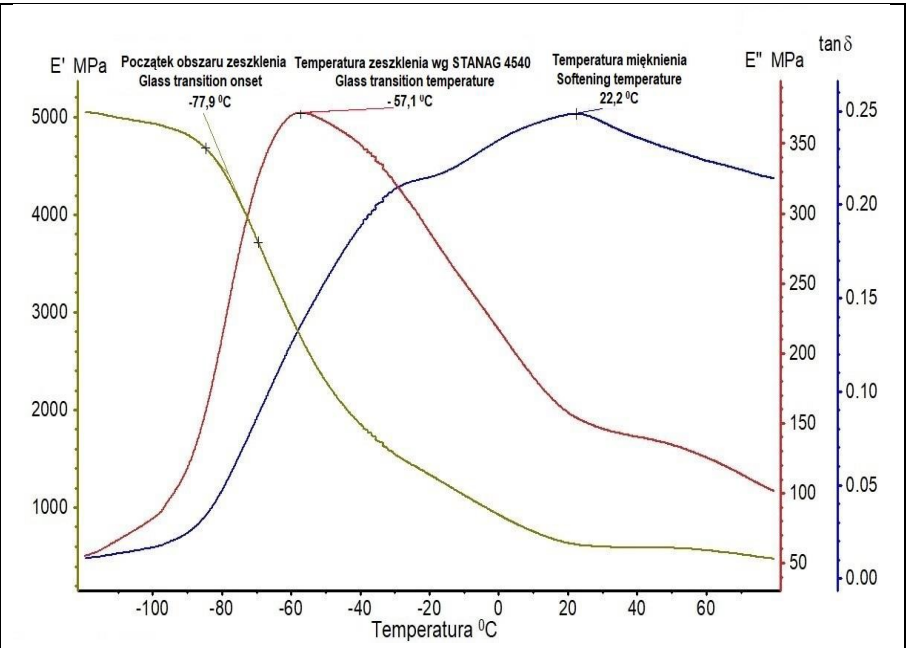 |
| **Comparison with this research programme** | The samples in the previous chapter exhibited highly consistent results, which was not achieved in this research phase. The 0.66 and 0.80 solid loading samples showed a similar level of consistency; however, the 0.73 solid loading sample exhibited the same poor cross-linking as noted in previous chapters. As this composition only had the addition of AO, it was not expected that the mechanical properties would change. This was true for the G' before the Tg, but after the Tg these materials had an increased stiffness. | The moduli curves, both storage and loss, exhibit the same behaviour as seen in this research programme; G' reduces in stiffness as the temperature increases and the G'' exhibits a low temperature peak. The glass transition temperature is within the same range as that in this research programme and the moduli is within the same level of magnitude. The tan(delta) differs substantially as the peak is not at the glass transition temperature and this is not explained within the literature. However, the other data supports the results in this research programme. |

### 6.4.2 Split Hopkinson Pressure Bar

High strain rate compressive testing was conducted by Split Hopkinson Pressure Bar (SHPB). The SHPB, at Imperial College London, used 7068 aluminium alloy input and output bars and striker, with respective lengths of 1500 mm, 1000 mm and 560 mm. Semi-conductor strain gauges, AFP-500-090 with resistances of 500 ±10% Ω, were used to measure the strains and mounted on the input and output bars at a distance of 750 mm and 1400 mm from the bar interfaces respectively. The pulses were recorded on a Tektronix oscilloscope at a sampling rate of 2.5 MS/s. These were then converted to classic engineering stress-strain curves and plotted in Figure 6 to Figure 8. Samples were prepared by 8mm biopsy punches and cut to a nominal 2.7 mm length producing a strain rate of 3350 $s^{-1}$. More details on the technique are covered in Chapter 5.4.2.

On each graph, the average stress-strain curve of the shots of each composition and mixing method was plotted with the t-test probability. Due to sample preparation, there was variation in surface properties which could result in minor variation between samples from the same batch. As stated in earlier chapters, keeping parameters consistent is important in experimental design but is not always possible. Table 41 details the various parameters and the standard deviation. The length was nominally 2.7 mm and was within 0.02 mm between the mixing methods.

*Table 41. A table detailing the average experimental variables and the associated standard deviation for HTPB-DOS-Melamine-Barium Sulphate high strain rate samples*

| Sample | Average Length/ mm | Standard Deviation | Average Strain Rate/ $s^{-1}$ | Standard Deviation | Average Firing Pressure/ bar | Standard Deviation |
|---|---|---|---|---|---|---|
| 0.66 LR | 2.74 | 0.039 | 3303.6 | 79.98 | 1.37 | 0.009 |
| 0.66 PM | 2.73 | 0.041 | 3381.8 | 97.86 | 1.37 | 0.007 |
| 0.73 LR | 2.72 | 0.043 | 3411.3 | 46.98 | 1.47 | 0.009 |
| 0.73 PM | 2.72 | 0.028 | 3357.8 | 60.31 | 1.48 | 0.013 |
| 0.80 LR | 2.70 | 0.094 | 3346.75 | 77.34 | 1.57 | 0.010 |
| 0.80 PM | 2.72 | 0.0676 | 3420.6 | 159.30 | 1.58 | 0.012 |

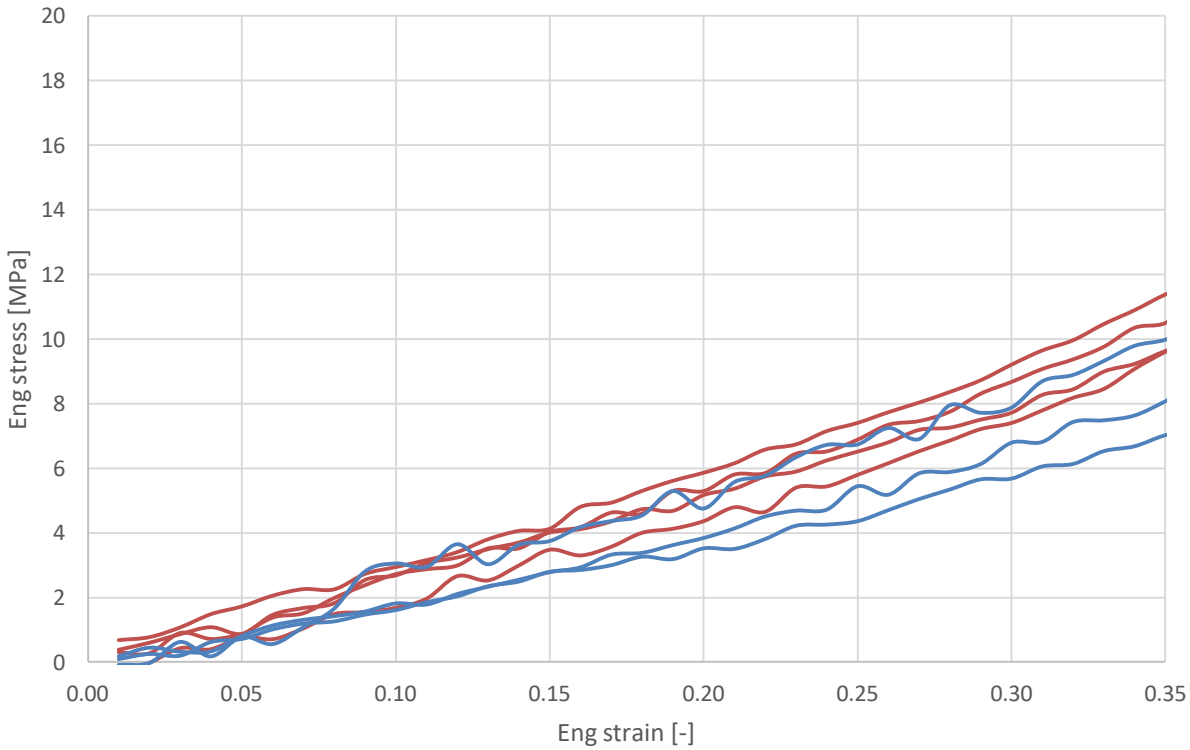


*Figure 72. The engineering stress-strain graph for the high strain rate testing of the 0.66 solid loading full inert samples. The LabRAM samples are in red and the planetary mixed samples are in blue. The RAM samples demonstrate slightly higher stress than the planetary mixed samples*

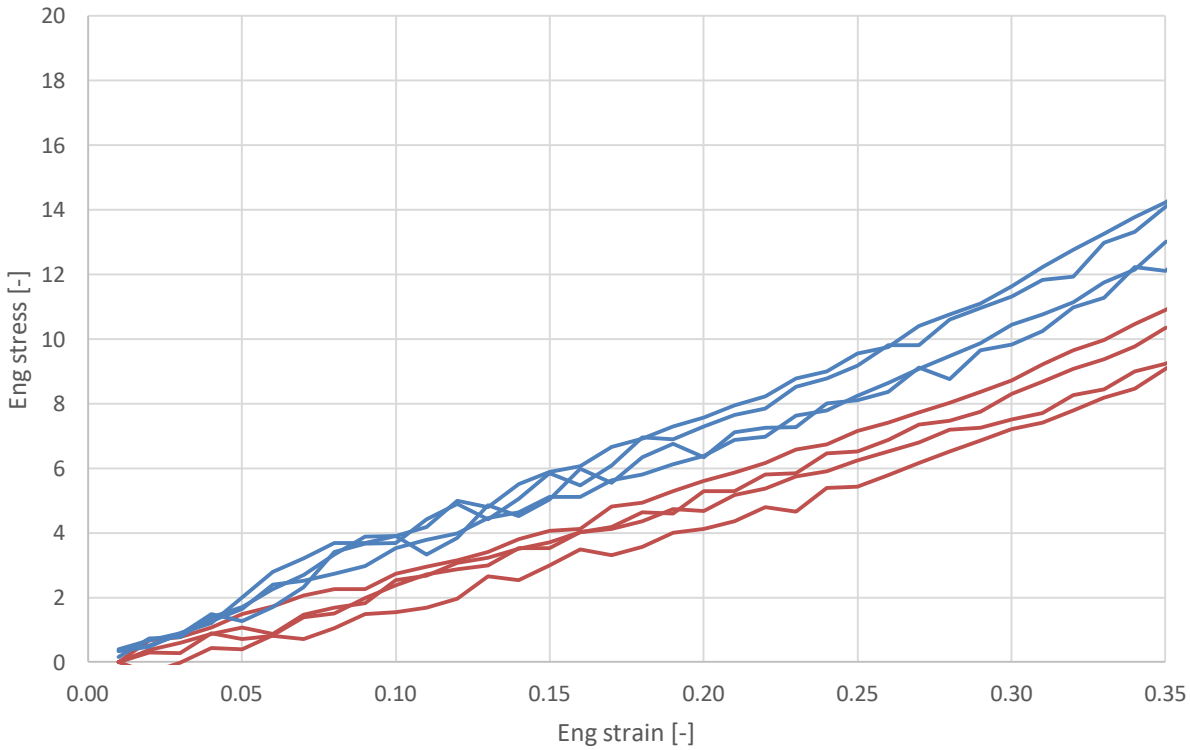


*Figure 73. The engineering stress-strain graph for the high strain rate testing of the 0.77 solid loading full inert samples. The LabRAM samples are in red and the planetary mixed samples are in blue. The planetary mixed samples demonstrate higher stress than the RAM samples*

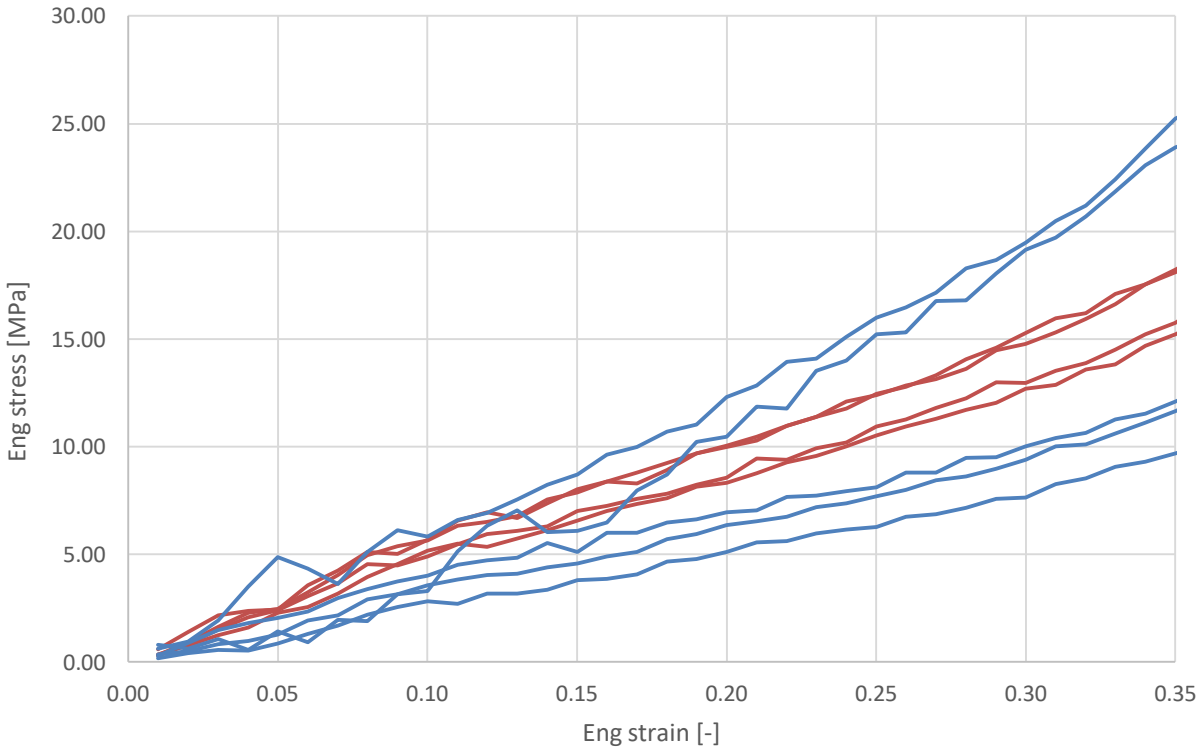


*Figure 74. The engineering stress-strain graph for the high strain rate testing of the 0.80 solid loading full inert samples. The LabRAM samples are in red and the planetary mixed samples are in blue. The planetary mixed samples demonstrate significantly larger spread than the RAM samples*

The 0.66 solid loading samples, in Figure 72 and Figure 75, had minor variation, with the planetary mixed samples having a greater spread of results. The LabRAM samples exhibited stiffer mechanical behaviour with greater force required to deform the sample across the entire strain range. The variation between mix methods increased as the strain increased. Statistical analysis did not provide any evidence to reject the null hypothesis; these samples are statistically similar.

The 0.73 solid loading samples, in Figure 73 and Figure 76, had distinct curves for each mixing methods; both mixing methods had equal spread demonstrating equal variability within batch. The planetary mixed samples were stiffer under compression over the entire range of strain with a maximum difference of either 3 MPa for the engineering stress or 8 MPa for the true stress. This indicates that the planetary mixed samples allow less movement under compression; likely due to a higher filler packing density. Using the 10% significance level, mixing via LabRAM had a significant impact with the samples being weaker than their planetary mixed counterpart. The t-test also provided sufficient evidence to reject the null hypothesis, demonstrating that the samples are statistically different.

Like with the 0.66 solid loading samples, the 0.80 solid loading samples, in Figure 74 and Figure 77, had greater spread for the planetary mixed results; the LabRAM samples are highly consistency. The planetary mixed samples have a significant spread indicating a high level of inconsistency within the results. The average samples are consistent, and although the planetary mixed samples are stiffer the variation is negligible indicating comparable filler density. The t-test probability is high demonstrating that there is insufficient evidence to reject the null hypothesis. Mixing via RAM has not impacted the average mechanical behaviour at this high strain rate, although it has improved the consistency in the sample batch.

Table 42 provides context for these results. Referencing Chapter 5.4.2 and a paper investigating ammonium perchlorate (AP) based propellants [Balzer et al, 2004]. Both papers demonstrated comparable results with the results in this chapter, proving that they are reasonable and expected.

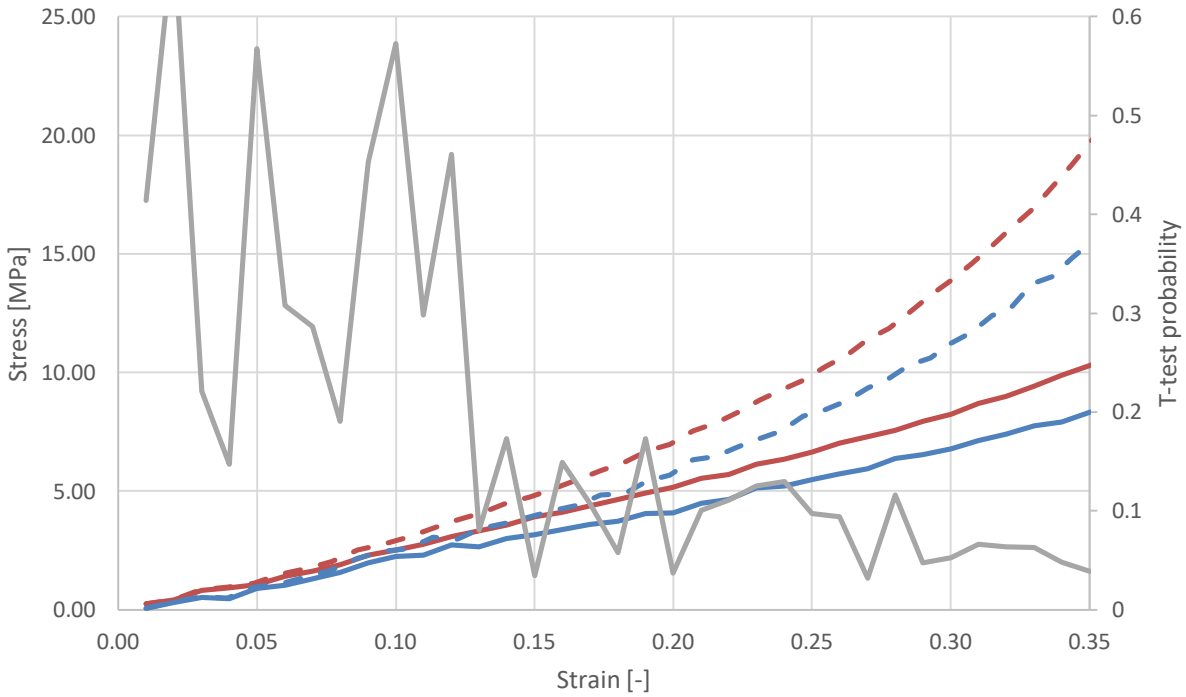


*Figure 75. The stress-strain graph for the high strain rate testing of the 0.66 solid loading full inert samples, plotting both the engineering stress-strain curve (solid line) and the true stress-strain curve (dashed line). The LabRAM samples are in red and the planetary mixed samples are in blue. The T-Test probability is the grey line. The RAM samples show a minor increase in stress compared to the planetary mixed samples, which is not significant but begins to be statistically different at the higher strains.*

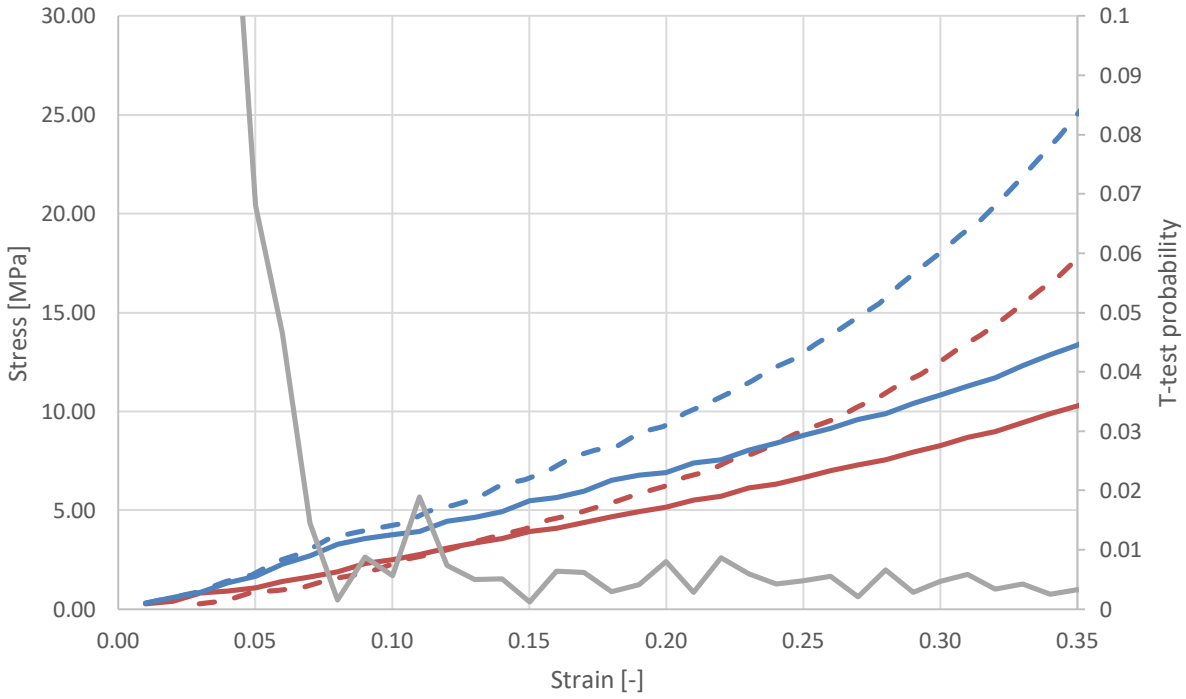


*Figure 76. The stress-strain graph for the high strain rate testing of the 0.73 solid loading full inert samples, plotting both the engineering stress-strain curve (solid line) and the true stress-strain curve (dashed line). The LabRAM samples are in red and the planetary mixed samples are in blue. The T-Test probability is the grey line. The RAM samples show a significant and statistical decrease in stress compared to the planetary mixed samples across the entire strain range*

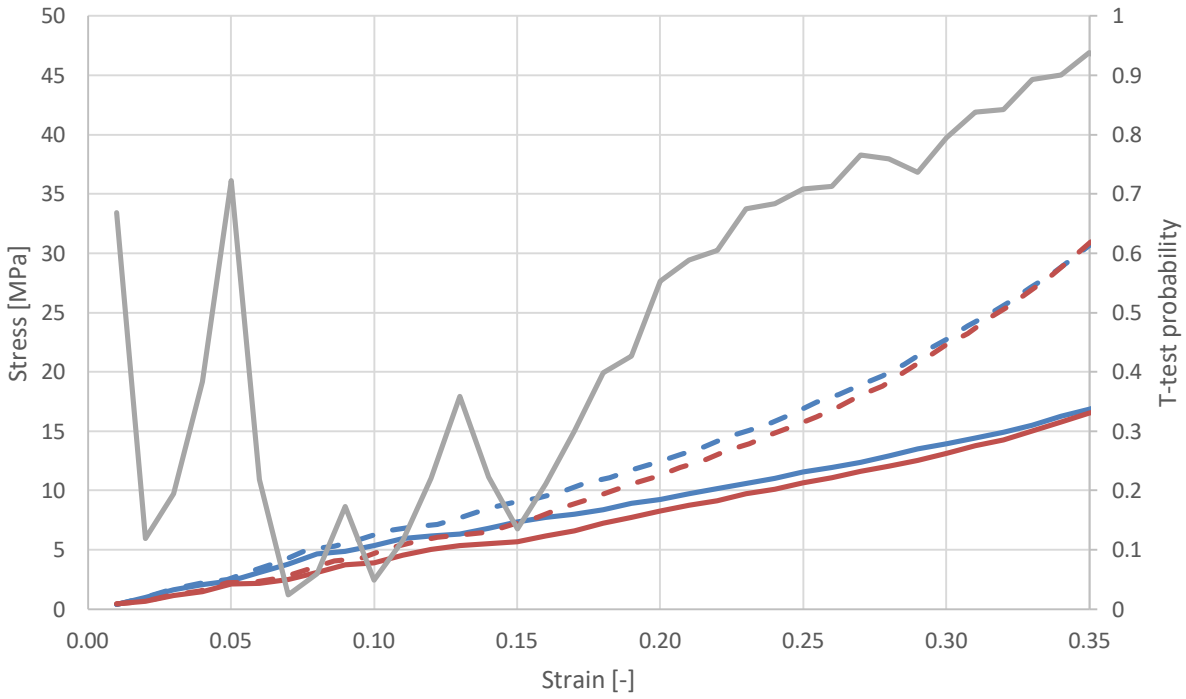


*Figure 77. The stress-strain graph for the high strain rate testing of the 0.73 solid loading HTPB-DOS-Melamine-Barium Sulphate samples, plotting both the engineering stress-strain curve (solid line) and the true stress-strain curve (dashed line). The LabRAM samples are in red and the planetary mixed samples are in blue. The T-Test probability is the grey line. The RAM and planetary mixed samples demonstrate consistency across the test*

*Table 42. Table comparing the high strain results of the full inert samples with literature*

| | | |
|---|---|---|
| **Source with summary of programme** | Chapter 5.4.2 | Behaviour of ammonium perchlorate-based propellants and a polymer-bonded explosive under impact loading, [Balzer et al, 2004] |
| **Material** | HTPB-DOS-Melamine- Barium Sulphate with solid loading levels of 0.66, 0.73 and 0.85. Sample sizes were 8 mm diameter and 2.7 mm length | Cast cured ammonium perchlorate (AP) propellant with HTPB binder. Has 80% solid loadings and 5% HMX |
| **Test Regime** | 7068 aluminium alloy input, output bars and striker, with respective lengths of 1500 mm, 1000 mm and 560 mm. | Standard SHPB set up. Striker bar propelled by a gas gun at a velocity of around 5 m $s^{-1}$ |
| **Results** | All samples had improved high strain rate compression behaviour when mixed via LabRAM. The 0.66 and 0.73 solid loading samples had little variation and provided no evidence that the null hypothesis could be rejected. The 0.85 solid loading sample had significant variation and provided sufficient evidence to indicate the samples are not statistically similar. The maximum stress, at 0.35 strain, was 15 MPa for the 0.66 solid loading sample, 22 MPa for the 0.73 solid loading sample and 50 MPa for the 0.85 solid loading sample. | The graph below is the true stress-strain graph for the AP propellant using a range of filler particle size and strain rates. The behaviour has a large amount of variation and does not demonstrate a consistent relationship. The 8 μm AP material demonstrates a maximum true stress of 12 MPa at 3.5 strain. |

| | | |
|---|---|---|
| | 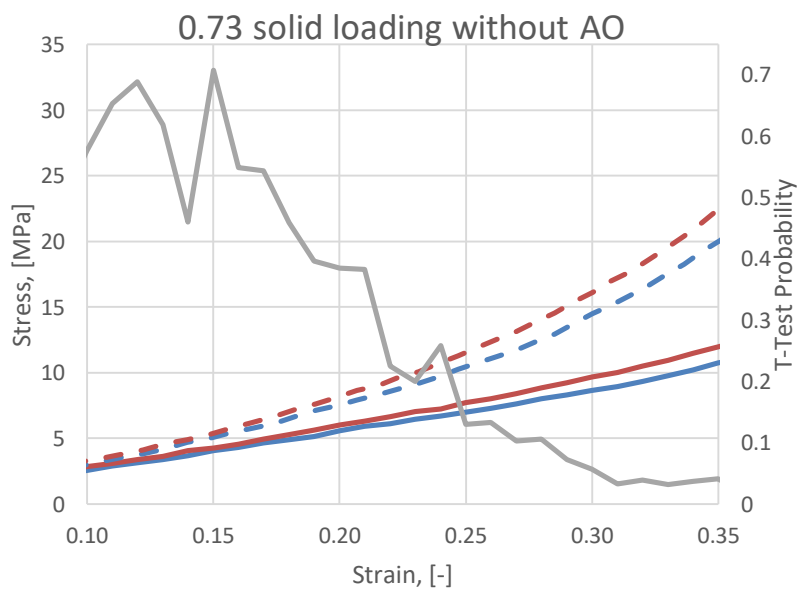 | 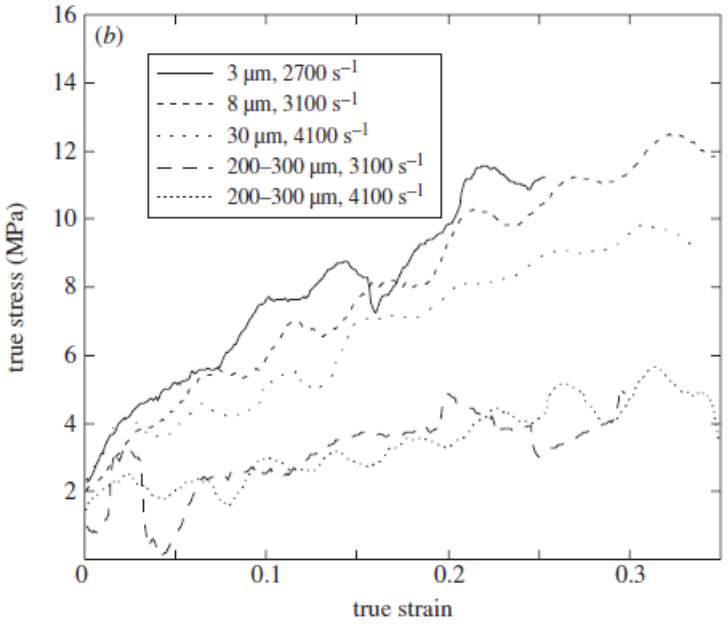 |
| **Comparison with this research programme** | All samples in the previous chapter had improved SHPB behaviour when mixed via LabRAM. These samples are less consistent with no relationship between mixing method and SHPB results. These samples had comparable maximum stresses: the 0.66 solid loading samples had 20MPa in this chapter compared to 15MPa in the previous and 0.73 solid loading had 25MPa compared to 22MPa. The highest solid loading samples were significantly weaker in this chapter, 31MPa, but the 50MPa was reported for the 0.85 solid loadings instead of 0.80 solid loadings. This would impact the material. | The compared sample in literature had the same solid loading as the 0.80 solid loading samples in this chapter and a comparable strain rate of $3100s^{-1}$ in comparison to $3300s^{-1}$. The maximum true stress seen in the literature was half that seen in this chapter. This is likely due to the monomodal filler system. However, the samples are within a comparable range and demonstrate that the results in this chapter are reasonable. |

### 6.4.3 DSC/TGA

The HTPB-Melamine samples in Chapter 3 underwent DSC testing, and there were no significant differences in the thermograms. As the thermogram detected only the melting temperatures of the two distinct components, it was not deemed necessary to test further compositions until the complete inert formulation. The full compositions were tested by DSC and TGA using a Mettler DSC1 running STARe software with 70 µl alumina open pans. A nominal mass of 5 mg was used and the test was run using a ramp rate of 10 °C $min^{-1}$. Two samples were run for each composition and mix method and the thermograms have been included in Figure 79 to Figure 84.

Thermogravimetric Analysis (TGA) is often associated with DSC as it also investigates the effect of temperature on a material. Using a single furnace, the sample is weighed whilst heated, in order to determine the percentage weight loss. This provides the key degradation points of the material. The sample has to be heated under an inert gas, typically nitrogen, in order to ensure that weight is not gained through reactions with oxygen [PerkinElmer, 2018]. Published research that investigates thermal behaviour typically consists of both tests, as it provides a more coherent overview of what is occurring whilst the sample is heated.

The style of the peaks can identify the transition that is occurring; in Figure 78 the thermograms are numbered from top to bottom and represent three different type of thermal transitions [Rawlinson, 2006]. Thermogram 1 is a pure, linear melting curve with a sharp peak which has the melting temperature defined as the curve onset. In comparison, thermograms 2 and 3 are for impure materials and exhibit a broader curve, with the potential for a second peak; the melting temperature is considered the peak of the curve. Thermograms 4 and 5 demonstrate a curve for a melting point followed by either an endothermic or exothermic decomposition.

*Table 43. Formulation table for the full inert compositions, with the percentage mass of the components*

| | | | | | |
|---|---|---|---|---|---|
| 0.66 solid loading | HTPB | AO | DOS | Melamine | Barium Sulphate |
| | 22.61 | 0.34 | 11.05 | 48.18 | 17.82 |
| 0.73 solid loading | HTPB | AO | DOS | Melamine | Barium Sulphate |
| | 17.955 | 0.27 | 8.775 | 53.29 | 19.71 |
| 0.80 solid loading | HTPB | AO | DOS | Melamine | Barium Sulphate |
| | 13.3 | 0.2 | 6.5 | 58.4 | 21.6 |

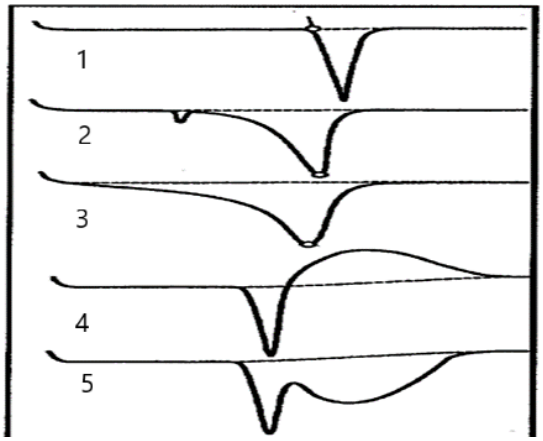


*Figure 78. Diagram demonstrating various thermogram peaks. From 1 to 5: pure melting, impure melting with a second peak, impure melting, melting with an exothermic decomposition, melting with an endothermic reaction [Rawlinson, 2006]*

*Table 44. Table with the percentage mass loss for the full inert compositions. The first mass loss is associated with the melamine component and the second the binder system. The two mixing methods demonstrate high levels of consistency*

| **Sample** | | **First Mass Loss** | **Second Mass Loss** | **Total Mass Loss** |
|---|---|---|---|---|
| 0.66 solid loading PM | 1 | 63.7% | 18.1% | 81.8% |
| | 2 | 63.9% | 18.1% | 82.0% |
| 0.66 solid loading LR | 1 | 65.0% | 17.9% | 82.9% |
| | 2 | 65.7% | 16.7% | 82.4% |
| 0.73 solid loading PM | 1 | 64.3% | 16.2% | 80.5% |
| | 2 | 59.5% | 19.7% | 79.2% |
| 0.73 solid loading LR | 1 | 64.8% | 15.7% | 80.5% |
| | 2 | 63.8% | 17.0% | 80.9% |
| 0.80 solid loading PM | 1 | 66.7% | 12.3% | 79.0% |
| | 2 | 65.6% | 12.3% | 77.9% |
| 0.80 solid loading LR | 1 | 66.3% | 12.5% | 78.8% |
| | 2 | 66.0% | 12.6% | 78.6% |

The tests exhibited two endotherms starting at 250 °C and 370 °C which were each accompanied by significant mass loss of 63 to 67% and 12 to 18% respectively. All samples had a total mass loss of around 80% regardless of the solid loading level, tabulated in Table 44; the remaining 20% is attributed to the barium sulphate. Barium sulphate is stable at high temperatures; the melting point is 1580 °C which is over double the highest temperature in

the testing regime. The composition has been included in Table 43 to serve as a reminder. The endotherm peaks are broad indicating a decomposition as opposed to a pure melting point and this is supported by the aforementioned mass loss. The first peak is associated with the decomposition and then sublimation of the melamine and the plasticiser; melamine begins to decompose at nominally 280 °C and then sublimes at 340 °C [UNEP Publications, 2019] [PubChem Open Chemistry Database, 2019]. In these formulations it is between 48 to 58% of the overall sample mass. DOS has a boiling point of 256 °C, which is the onset of the first peak and ranges from 6 to 11%. This causes a potential mass loss in the range of 59 to 64%, which is comparable to the 63 to 67% mass loss documented in Table 44. It is also likely that any available HTPB that has not been crosslinked into the overall network would decompose in this temperature range. The second peak is the decomposition of HTPB; the energy for this peak is within 20% of the energy for the first peak, which is the decomposition and sublimation of the plasticiser and the melamine as more energy is required to break the chemical bonds within the polymer.

The mass losses for all the compositions are tabulated in Table 44 and the samples do not have significant mass changes between the mixing methods. There is variation in some of the samples, but this occurs within the like mixing methods. Between the two separate mixing methods this variation is insignificant. As the thermograms looked similar, only one has been included for like samples. Figure 79 and Figure 80 are the 0.66 solid loading planetary mixed and LabRAM samples, Figure 81 and Figure 82 are the 0.73 solid loading samples and Figure 83 and Figure 84 are the 0.80 solid loading samples.

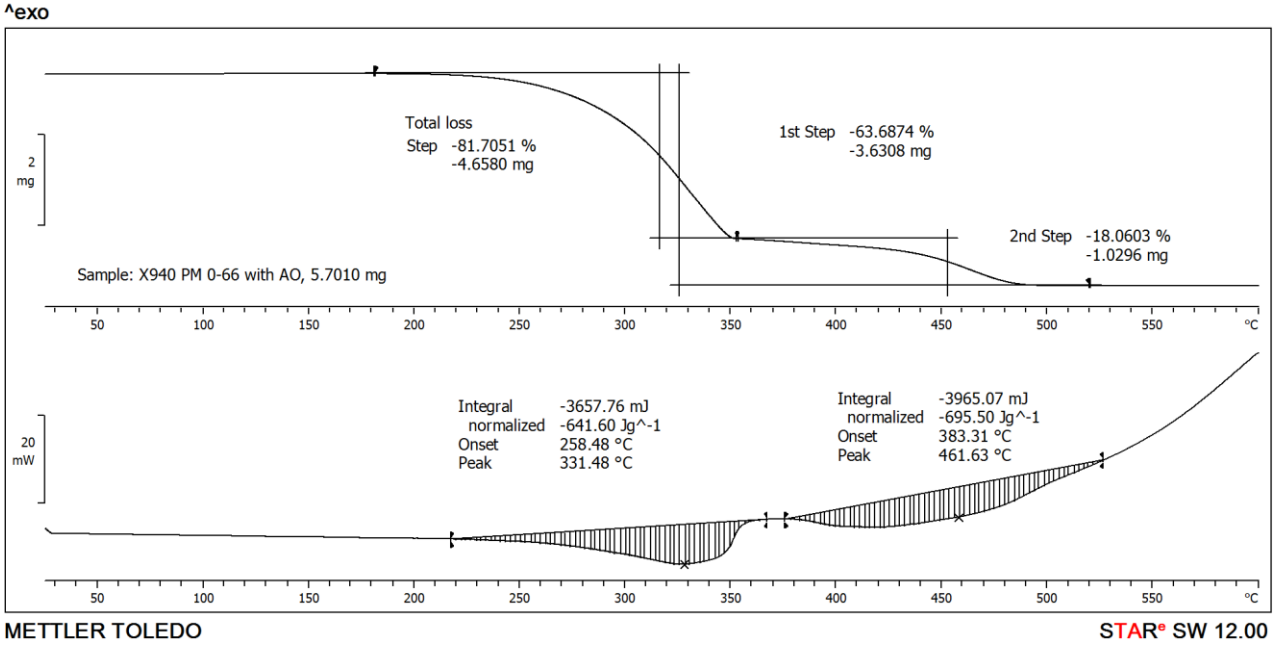


*Figure 79. DSC/TGA thermogram of 0.66 solid loading planetary mixed sample demonstrating two endothermic peaks due to the decomposition of the melamine and the binder system with the associated mass losses.*

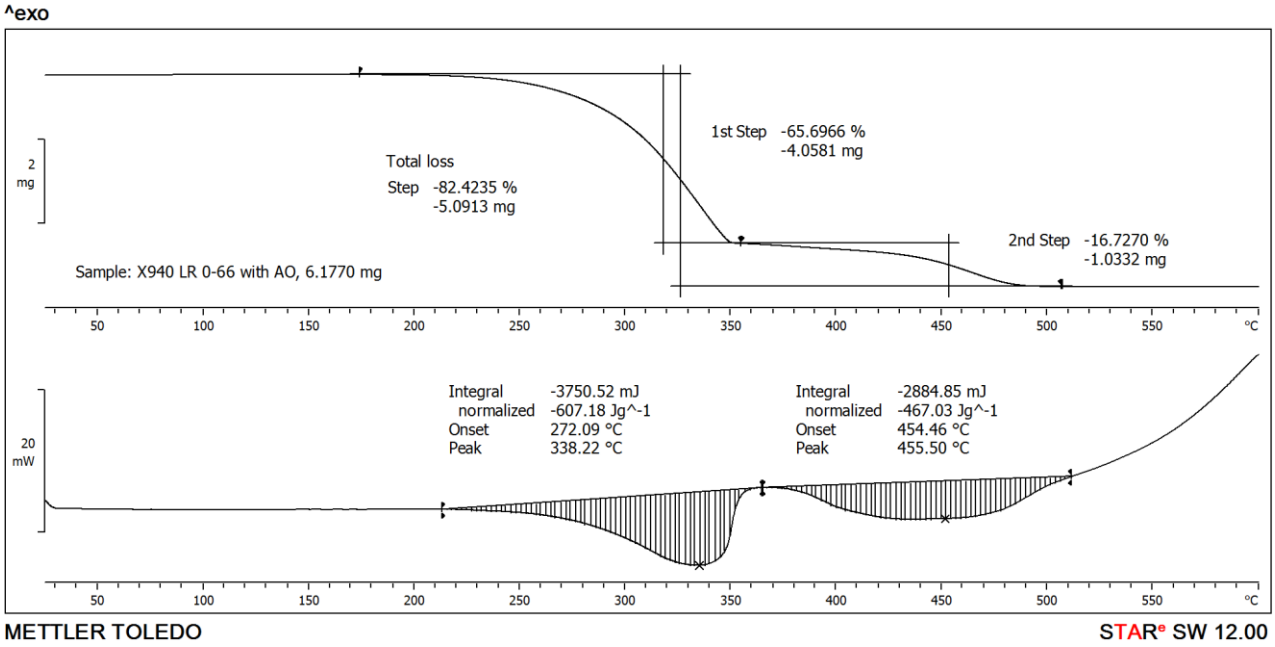


*Figure 80. DSC/TGA thermogram of 0.66 solid loading LabRAM sample demonstrating two endothermic peaks due to the decomposition of the melamine and the binder system with the associated mass losses*

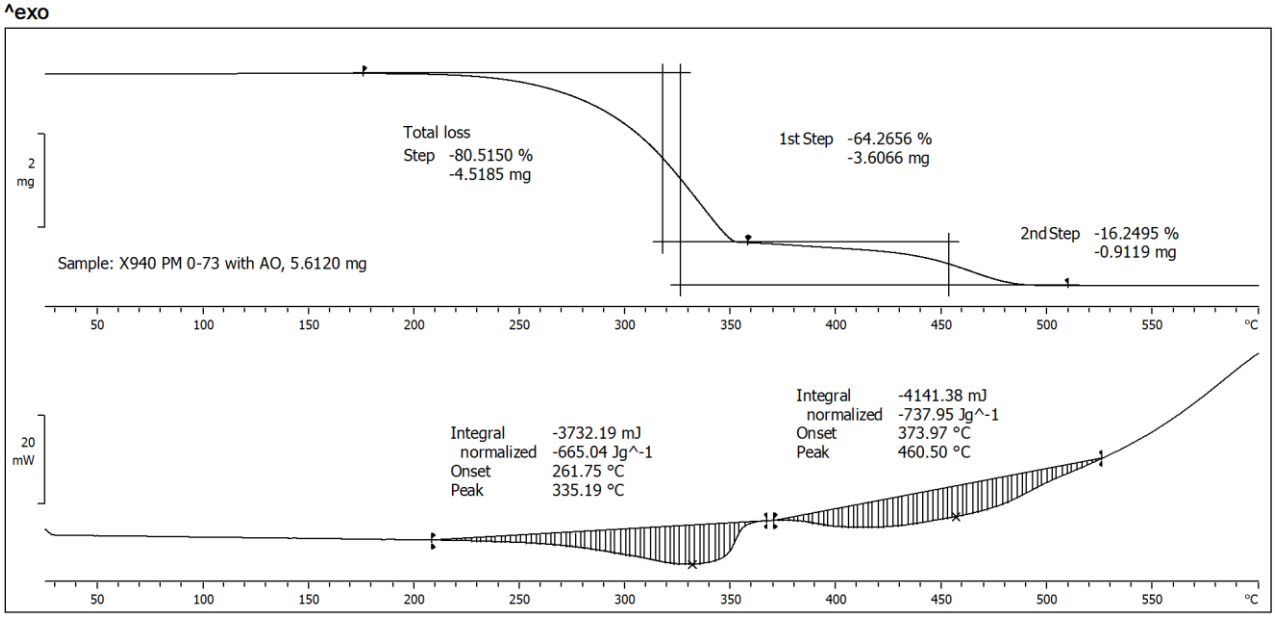


*Figure 81. DSC/TGA thermogram of 0.73 solid loading planetary mixed sample demonstrating two endothermic peaks due to the decomposition of the melamine and the binder system with the associated mass losses*

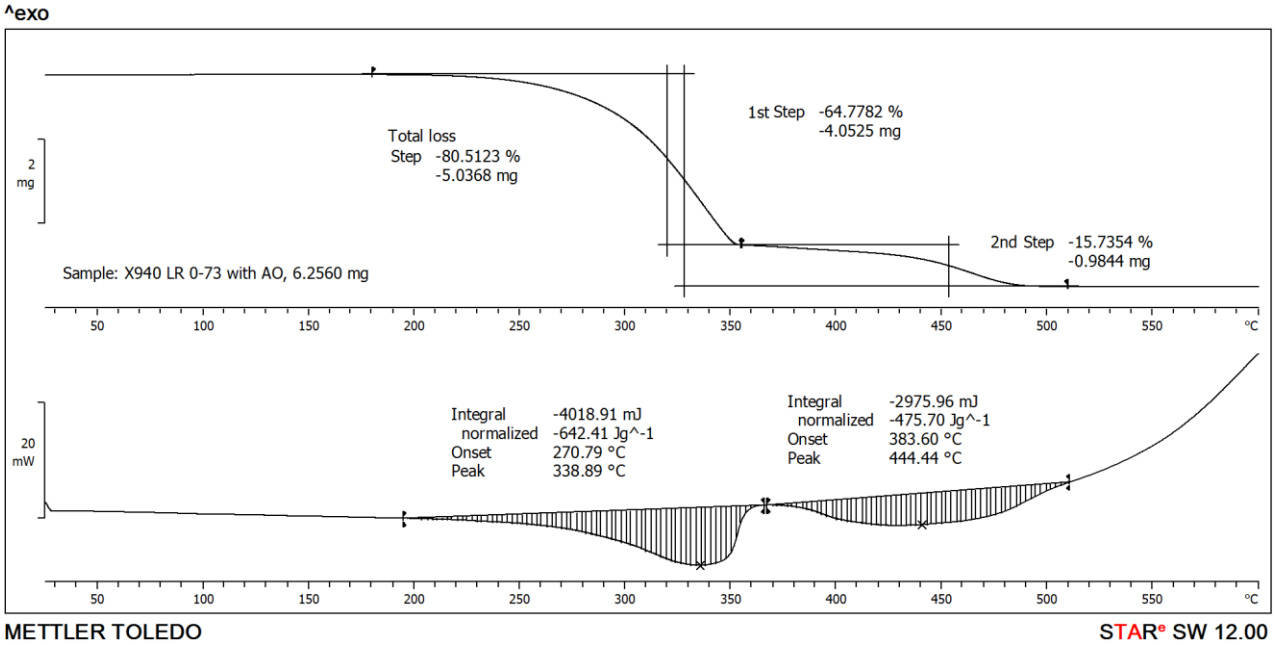


*Figure 82. DSC/TGA thermogram of 0.73 solid loading LabRAM sample demonstrating two endothermic peaks due to the decomposition of the melamine and the binder system with the associated mass losses*

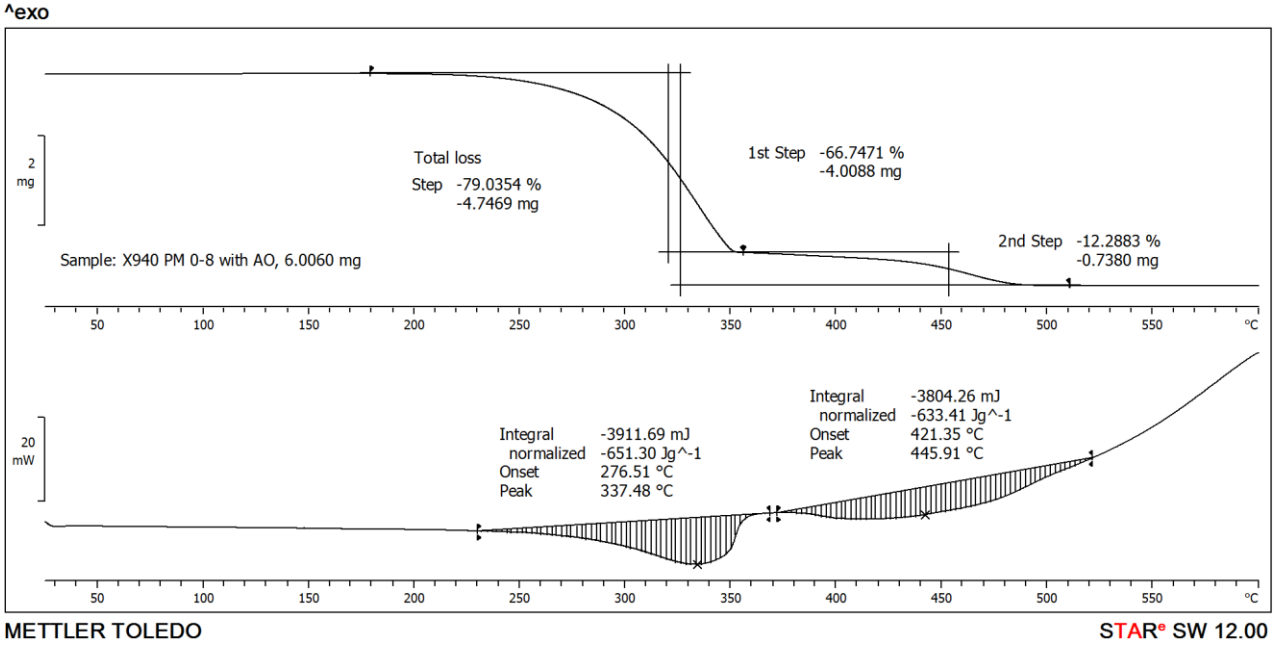


*Figure 83. DSC/TGA thermogram of 0.80 solid loading planetary mixed sample demonstrating two endothermic peaks due to the decomposition of the melamine and the binder system with the associated mass losses*

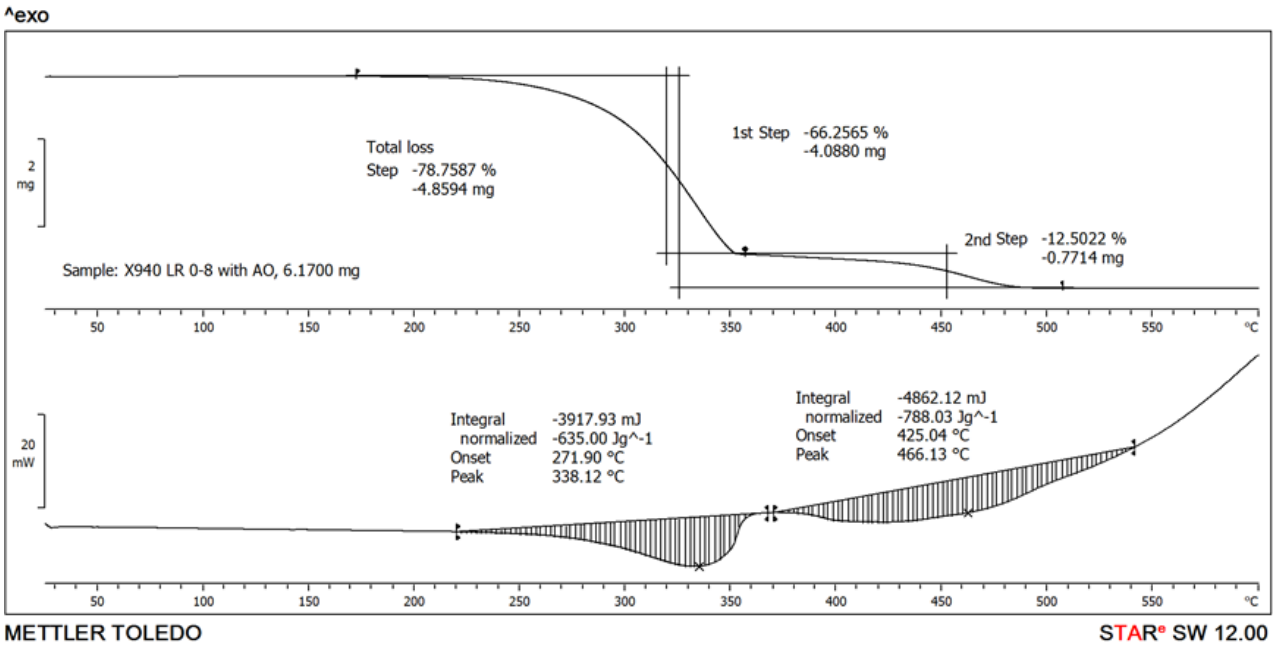


*Figure 84. DSC/TGA thermogram of 0.80 solid loading LabRAM sample demonstrating two endothermic peaks due to the decomposition of the melamine and the binder system with the associated mass losses*

### 6.4.4 NMR

NMR testing was undertaken to determine the chemical characteristics of the sample. Although the same formulation was used for both mixing methods, it was believed that

decomposition products or variations in HTPB could be present. A $CDCL_3$ and TTMS standard was used, and the samples were extracted overnight. Protonquant analysis was conducted to determine the quantity of individual components. More details on NMR can be found in Chapter 3.4.3.

Table 45 summarises the NMR results. Two samples were tested for each material, and an average was taken. The table also lists the added amount of each component in the composition. The HTPB is expected to be smaller than the added value as it is cured into the binder network. The HTPB measured is the extractable quantity; material not crosslinked and able to be dissolved out of the bulk. A lower value indicates a greater degree of curing, and would contribute to stiffer mechanical properties. The antioxidant (AO) will be depleted from the added value; previous compositions oxidised whilst curing at elevated temperatures and over time. These samples did not exhibit the same discolouration, indicating that some AO is consumed during processing of the sample. T-test analysis was conducted and reported in Table 46.

The results demonstrated consistency for the 0.66 solid loading samples; HTPB, DOS and AO had no significant variation and statistical analysis provided no evidence to reject the null hypothesis. HTPB had a value of 2.8%; 12.7% of the HTPB is not part of the larger binder network. Both sample sets had higher DOS concentration than expected indicating variation in the plasticiser distribution. This variation is insignificant. The LabRAM samples had a lower concentration indicating that distribution is more consistent when mixed via LabRAM. The AO concentration similarly had no significant variation demonstrating that samples are mixed and constituent parts are distributed throughout for both mixing methods.

The 0.73 solid loading samples demonstrated high variation; LabRAM samples had significantly higher HTPB and AO concentration with the AO providing enough statistical evidence to reject the null hypothesis. There was greater extractable HTPB and AO within the LabRAM sample due to poor crosslinking of the binder network indicating the curative was not distributed evenly throughout the sample. During curing there would be less oxidation of the cross-linked binder leading to lower consumption of AO. The DOS concentration was consistent between each mixing methods; however, was greater than the added value; indicating either poor plasticiser distribution or samples with above average binder concentration.

The 0.80 solid loading samples also demonstrated high variation with the HTPB and the AO concentration providing sufficient evidence to reject the null hypothesis and the samples are

statistically different. The HTPB and the AO have a higher concentration when mixed via LabRAM indicating that again there is inadequate cross-linking and poor isocyanate distribution throughout the sample. There was more DOS in the planetary mixed samples, but both the planetary mixed and the LabRAM samples indicate inconsistent binder distribution.

*Table 45. Table detailing the percentage composition of the extractable HTPB, DOS and AO from the NMR testing on the full inert samples*

| Sample | | Extractable HTPB | | | DOS | | | AO | | |
|---|---|---|---|---|---|---|---|---|---|---|
| | | Result | Average | Nominal | Result | Average | Nominal | Result | Average | Nominal |
| 0.66 PM | 1 | 2.58818 | 2.70702 | 22.61 | 11.969698 | 11.91559 | 11.05 | 0.20200 | 0.201305 | 0.34 |
| | 2 | 2.82586 | | | 11.86148 | | | 0.20061 | | |
| 0.66 LR | 1 | 3.04729 | 2.9009 | | 11.30874 | 11.43729 | | 0.20280 | 0.2065 | |
| | 2 | 2.75451 | | | 11.56583 | | | 0.2102 | | |
| 0.73 PM | 1 | 2.10673 | 2.14282 | 17.955 | 9.34813 | 9.361975 | 8.775 | 0.1544 | 0.15196 | 0.27 |
| | 2 | 2.17890 | | | 9.37582 | | | 0.14947 | | |
| 0.73 LR | 1 | 3.73447 | 3.3614 | | 9.5149 | 9.357935 | | 0.18175 | 0.177525 | |
| | 2 | 2.98832 | | | 9.20090 | | | 0.17330 | | |
| 0.80 PM | 1 | 1.97980 | 1.9814 | 13.3 | 6.7322 | 6.7895 | 6.5 | 0.0906 | 0.09022 | 0.2 |
| | 2 | 1.98300 | | | 6.68468 | | | 0.0897 | | |
| 0.80 LR | 1 | 3.60925 | 3.3799 | | 6.61589 | 6.5836 | | 0.14451 | 0.14353 | |
| | 2 | 3.15060 | | | 6.55124 | | | 0.14256 | | |

*Table 46. Table summarising the analysis of the NMR testing on the full inert samples, detailing the percentage change of the LabRAM results from the planetary mixed samples and the calculate T-Test value. The 0.77 and 0.80 solid loading samples demonstrate significant variation in the extractable HTPB and AO concentration demonstrating an inhomogeneous sample*

| Sample | Extractable HTPB | | DOS | | AO | |
|---|---|---|---|---|---|---|
| | % Change | T-Test | % Change | T-Test | % Change | T-Test |
| 0.66 solid loading | 7.16 | 0.411 | -4.01 | 0.076 | 2.58 | 0.302 |
| 0.73 solid loading | 56.87 | 0.083 | -0.04 | 0.982 | 16.82351 | 0.035 |
| 0.80 solid loading | 70.58 | 0.026 | -3.03 | 0.090 | 59.09 | 0.0004 |

### 6.4.5 Density

Density measurements were conducted on samples using a Quantachrome Ultrapyc 1200e, with a cell volume of 19.1460 cc. Details on density measurements are found in Chapter 4.4.3. The same parameters were used as in the previous section; helium was used with an automatic equilibrium time, with a target pressure of 19.0 psig; flow purge was 1.0 minute. Material was tested 3 times, and the average was taken and summarised in Table 47, with percentage change from planetary mixed to LabRAM samples. The standard deviation was below 0.0002 g $cc^{-1}$ for all materials and mixing methods.

*Table 47. Table detailing the density measurements of the full inert samples, with the percentage change of the LabRAM samples from the planetary mixed and the calculated T-Test value. There was no significant variation between the two mixing methods*

| Sample | Planetary Mixing | LabRAM | % Change | T-Test Probability |
|---|---|---|---|---|
| 0.66 solid loading | 1.3828 g $cc^{-1}$ | 1.3796 g $cc^{-1}$ | -0.23% | 0.266 |
| 0.73 solid loading | 1.4597 g $cc^{-1}$ | 1.4632 g $cc^{-1}$ | 0.24% | $7.45 \times 10^{-7}$ |
| 0.80 solid loading | 1.5486 g $cc^{-1}$ | 1.5448 g $cc^{-1}$ | -0.27% | $1.69 \times 10^{-8}$ |

Previous density measurements in Chapter 4.4.2 indicated insignificant changes in density of below 0.1%; however, the results for the full inert compositions had a much greater density change. Due to the very small variation in the like samples, the LabRAM results lie outside the 95% confidence boundaries for the planetary mixed samples. As such, there is statistically a variation between the results. There is less than 0.5% density change for all of the materials, with the 0.66 solid loading sample exhibiting the greatest variation with a density decrease of over 0.4%. The 0.73 and 0.80 sample had an increase of over 0.2%. All results were less than the ±2.5% variation allowed in PBX specifications and fall under the label of insignificant changes, as defined earlier in this programme. The results are inconsistent with each other; the LabRAM samples are less dense for the lowest and highest solid loading, but more dense for the 0.73 solid loading sample. As such, mixing materials via LabRAM will give a variation in the sample density but it will not be significant and it is not possible to predict whether the samples will be more or less dense.

Brief comparisons were made in the previous paragraph but Table 48 gives more detailed comparison with the previous chapter and existing literature. The results are highly comparable, indicating that the samples are within the expected range.

*Table 48. Table comparing the density measurements of the full inert samples with literature*

| **Source with summary of programme** | Chapter 4.4.3 | Formulation and Performance Studies of Polymer Bonded (PBX) Containing Energetic Binder Systems [Provatas, 2003] | Modeling of combustion and ignition of solid-propellant ingredients [Beckstead et al, 2007] |
|---|---|---|---|
| **Material** | HTPB- Melamine- Barium Sulphate with solid loading of 0.66, 0.73 and 0.80. | PBXs with a RDX loading ranging from 75 – 79% with a PolyGLYN binder system | Composite propellants with a polymer base and either AP, AN (ammonium nitrate) or KN (potassium nitrate) |
| **Test Regime** | Density measurements were conducted on the samples using helium pycnometry, using a Quantachrome Ultrapyc 1200e, with a cell volume of 19.1586 cc | Measurements taken on a Quantachrome Helium Ultrapycnometer 1000. | Modelling and simulation. |
| **Results** | Density ranged from 1.38 for the lowest solid loading to 1.55 g $cm^{-3}$ for the highest | 1.68 g $cm^{-3}$ | 1.2 – 2.0 g $cm^{-3}$ |
| **Comparison with this research programme** | The composition in this research programme has the same base as the research in the previous chapter; the additional plasticiser and antioxidant is not expected to change the density. The samples also have the same solid loading levels. The densities for each solid loading in this research are within 1.5% of the previous chapter, demonstrating that the densities are within the expected range. | The solid loadings in the literature are similar to the highest solid loading sample in this research programme. The density in literature is higher, but use a higher density binder. | The range of solid loading for composite propellants is much greater than that of PBXs and this is observed in the density range. The density range in the literature is consistent with the densities found in this research programme. |

### 6.4.6 **Moisture Diffusion**

The addition of the antioxidant is designed to reduce ageing so the diffusion experimentation was undertaken again. The same parameters were used as the samples tested in Chapter 5.4.3. As with the samples without AO the short duration samples did not have any relationship with the mixing methods over the first 4 and 24 hours.

After the HTPB-DOS-Melamine- Barium Sulphate samples, Dynamic Vapour Sorption (DVS) was conducted on samples in the hope of gaining more precise results as the sample mass is measured constantly on a sensitive balance with controlled humidity and temperature; however, several experiments were conducted and no results were achieved. The sample sizes were too small, several hundred milligrams, and the mass change was insignificant, due to the samples lack of hygroscopy. As such, the same experiment was conducted as with the previous composition. The 0.66 solid loading samples results are summarised in Table 49, Table 50 and Figure 85. The planetary mixed samples are more consistent over the test period indicating that the LabRAM samples have a large variation in the packing of both the binder system and the filler particles. During the first day, the LabRAM samples 1 and 2 lie both below and above the planetary mixed samples respectively. This indicates that sample 1 had a denser binder system and a smaller binder rich layer when compared to the planetary mixed samples; however, sample 2 had a looser and larger binder layer at the surface. Between day 2 and day 7 both sets of samples showed greater consistency, indicating that the packing density was comparable between mixing methods. After day 7 there was the same erratic behaviour that was seen with the previous composition where the behaviour is driven by erosion of the foil.

*Table 49. Mass increase, in grams, over the duration of the diffusion experiments on the 0.66 solid loading full inert samples*

| Time/days | Planetary Sample 1 | Planetary Sample 2 | LabRAM Sample 1 | LabRAM Sample 2 |
|---|---|---|---|---|
| 0 | 0.0000 | 0.0000 | 0.0000 | 0.0000 |
| 1 | 0.0046 | 0.0035 | 0.0026 | 0.0058 |
| 2 | 0.0049 | 0.0042 | 0.0032 | 0.0074 |
| 7 | 0.0072 | 0.0054 | 0.0055 | 0.0104 |
| 8 | 0.0303 | 0.0078 | 0.0064 | 0.0210 |
| 9 | 0.0300 | 0.0204 | 0.0134 | 0.0305 |
| 10 | 0.0348 | 0.0233 | 0.0163 | 0.0381 |

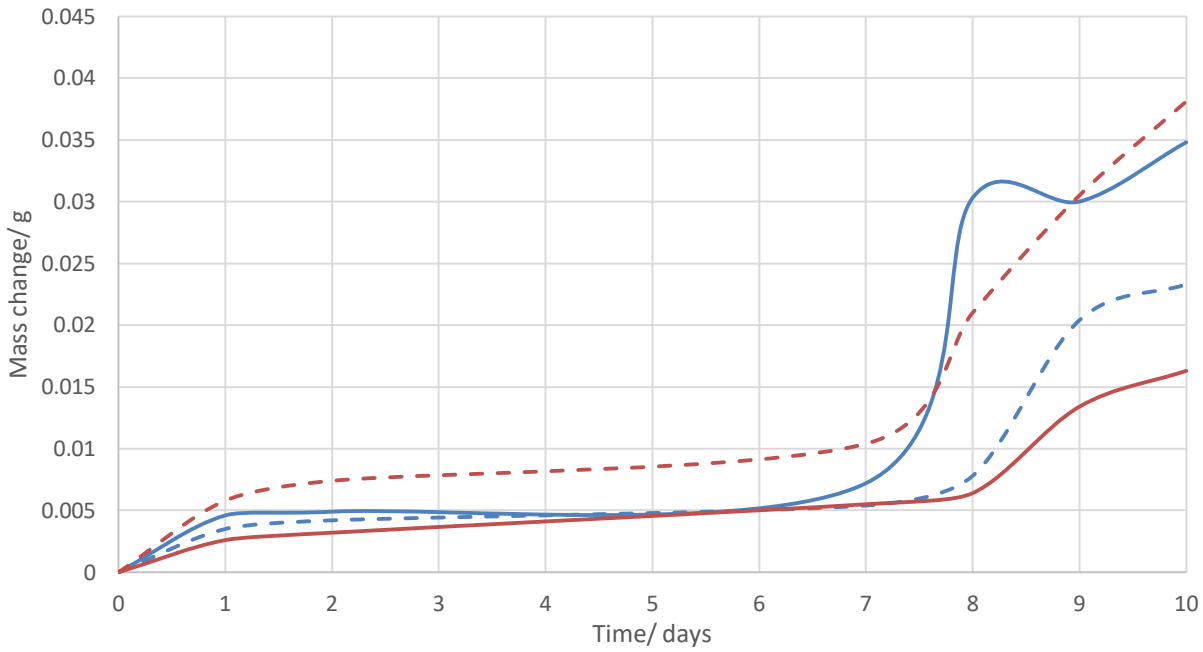


*Figure 85. Graph depicting the mass change during the diffusion experiments the for 0.66 solid loading full inert samples with the LabRAM samples in red and the planetary mixed samples in blue. The solid line is sample 1 and the dashed line is sample 2. The samples exhibit a larger increase over the first day, which plateaus out until day 8. After day 8 the samples exhibit an erratic mass increase attributed to corrosion of the aluminium tape. The RAM samples demonstrates larger variation in moisture absorption.*

*Table 50. Mass increase in grams for phase 1, the initial absorption, and phase 2, the bulk absorption, of the diffusion experiment for the 0.66 solid loading full inert samples*

| Duration | Planetary Sample 1 | Planetary Sample 2 | LabRAM Sample 1 | LabRAM Sample 2 |
|---|---|---|---|---|
| 0-1 day | 0.0046 | 0.0035 | 0.0026 | 0.0058 |
| 2-7 days | 0.0005 | 0.0002 | 0.0005 | 0.0006 |

The 0.73 solid loading samples, in Table 51, Table 52, and Figure 86, exhibit a varied behaviour between the two mixing methods. Over the first day, the LabRAM samples demonstrated less consistent moisture uptake as the samples had varying binder densities. However, the planetary mixed sample 2 demonstrated this initial moisture ingress until day 2 indicating that the binder rich layer was dramatically thicker than the LabRAM samples. After day 2, the LabRAM samples demonstrated a more consistent mass increase that is on average lower than the planetary mixed samples. This indicates that the LabRAM samples had a greater and more consistent packing density than the planetary mixed samples. As seen with all the other samples, the erratic behaviour begins during day 7.

*Table 51. Mass increase, in grams, over the duration of the diffusion experiments on the 0.73 solid loading full inert samples*

| Time/days | Planetary Sample 1 | Planetary Sample 2 | LabRAM Sample 1 | LabRAM Sample 2 |
|---|---|---|---|---|
| 0 | 0.0000 | 0.0000 | 0.0000 | 0.0000 |
| 1 | 0.0037 | 0.0034 | 0.0022 | 0.0054 |
| 2 | 0.0043 | 0.0107 | 0.0032 | 0.0061 |
| 7 | 0.0088 | 0.0120 | 0.0053 | 0.0091 |
| 8 | 0.0126 | 0.0202 | 0.0172 | 0.0115 |
| 9 | 0.0136 | 0.0377 | 0.0260 | 0.0180 |
| 10 | 0.0204 | 0.0442 | 0.0285 | 0.0213 |

*Table 52. Mass increase in grams for phase 1, the initial absorption, and phase 2, the bulk absorption, of the diffusion experiment for the 0.73 solid loading full inert samples*

| Duration | Planetary Sample 1 | Planetary Sample 2 | LabRAM Sample 1 | LabRAM Sample 2 |
|---|---|---|---|---|
| 0-1 days | 0.0037 | 0.0034 | 0.0022 | 0.0054 |
| 2-7 days | 0.0009 | 0.0003 | 0.0004 | 0.0009 |

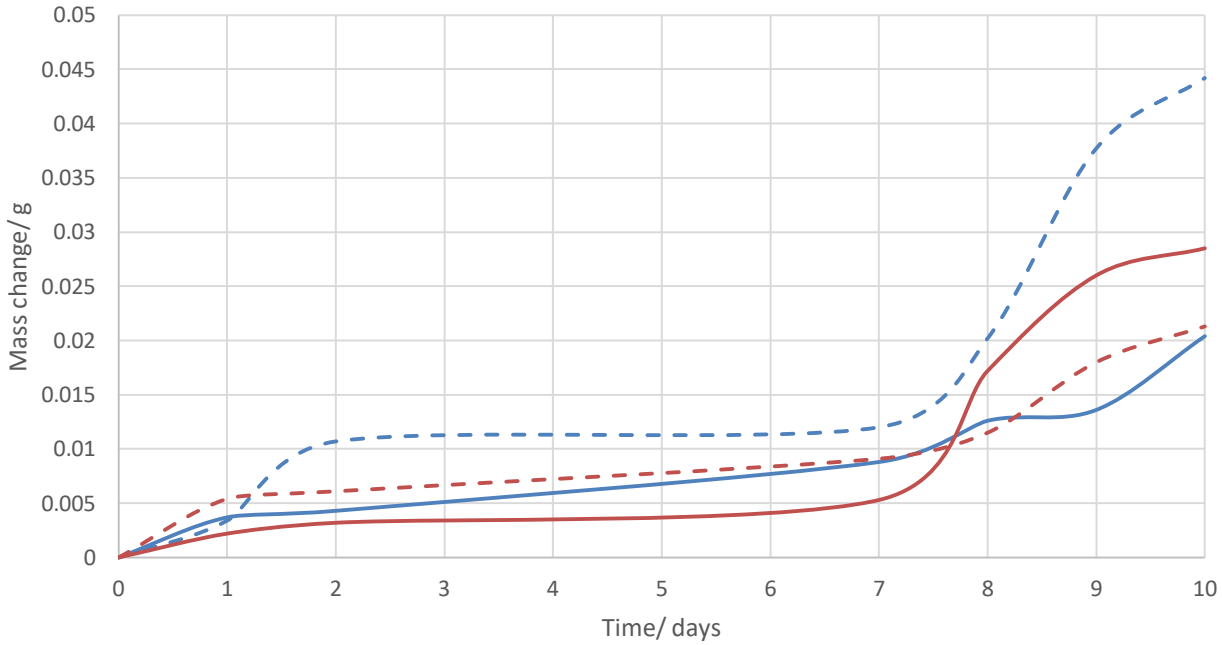


*Figure 86. Graph depicting the mass change during the diffusion experiments the for 0.73 solid loading full inert samples with the LabRAM samples in red and the planetary mixed samples in blue. The solid line is sample 1 and the dashed line is sample 2. The samples exhibit a larger increase over the first day, which plateaus out until day 8. After day 8 the samples exhibit an erratic mass increase attributed to corrosion of the aluminium tape. The planetary mixed and RAM samples demonstrate an overlap in the moisture absorption.*

The 0.80 solid loading samples have good consistency across the samples particularly when compared to the lower solid loading samples; the results are summarised in Table 53, Table 54, and Figure 87. Over the first day the LabRAM samples have greater variation when compared to the planetary mixed samples although they also have lower moisture ingress. From day 2 onwards the two mixing methods showed similar variation with the LabRAM samples having greater mass increase. This indicates that the LabRAM samples had a greater packing density for the filler particles but a less dense binder system. However, unlike

the lower solid loading samples these changes are negligible and the ageing behaviour is broadly similar.

*Table 53. Mass increase in grams for phase 1, the initial absorption, and phase 2, the bulk absorption, of the diffusion experiment for the 0.80 solid loading full inert samples*

| Duration | Planetary Sample 1 | Planetary Sample 2 | LabRAM Sample 1 | LabRAM Sample 2 |
|---|---|---|---|---|
| 0-1 days | 0.0037 | 0.0048 | 0.0041 | 0.0025 |
| 2-7 days | 0.0006 | 0.0010 | 0.0007 | 0.0012 |

*Table 54. Mass increase, in grams, over the duration of the diffusion experiments on the 0.80 solid loading full inert samples*

| Time/days | Planetary Sample 1 | Planetary Sample 2 | LabRAM Sample 1 | LabRAM Sample 2 |
|---|---|---|---|---|
| 0 | 0 | 0 | 0 | 0 |
| 1 | 0.0037 | 0.0048 | 0.0041 | 0.0025 |
| 2 | 0.004 | 0.0057 | 0.0046 | 0.0033 |
| 7 | 0.0069 | 0.0108 | 0.0083 | 0.0091 |
| 8 | 0.0152 | 0.014 | 0.0143 | 0.0154 |
| 9 | 0.0273 | 0.0152 | 0.03551 | 0.0334 |
| 10 | 0.0286 | 0.0141 | 0.0422 | 0.0298 |

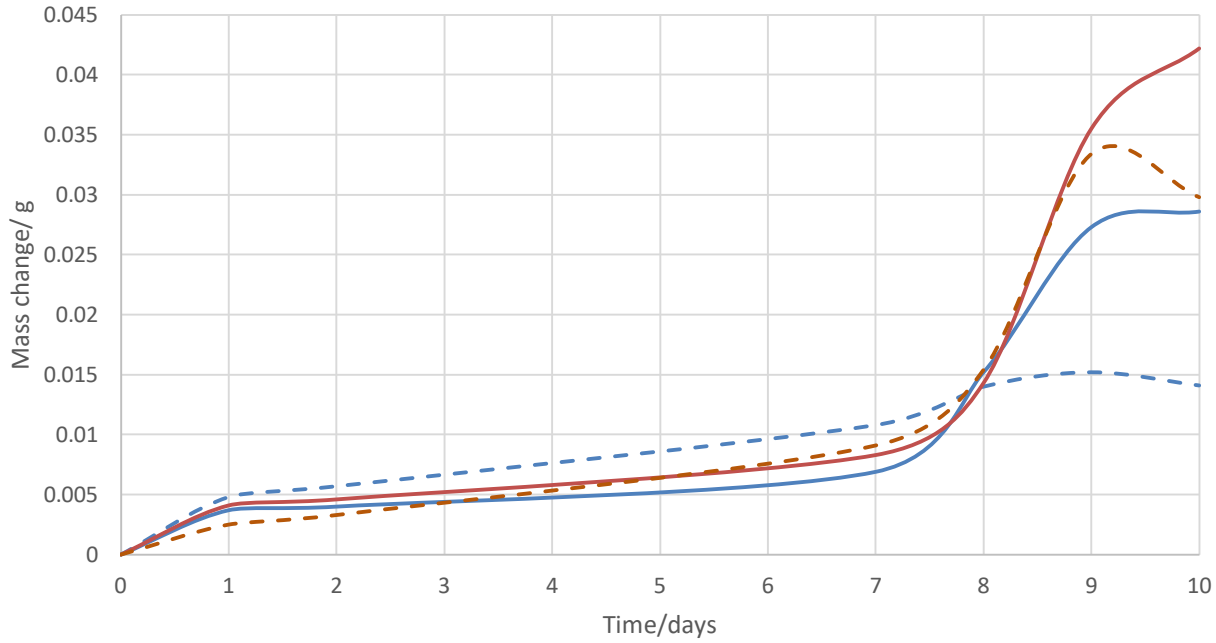


*Figure 87. Graph depicting the mass change during the diffusion experiments the for 0.80 solid loading full inert samples with the LabRAM samples in red and the planetary mixed samples in blue. The solid line is sample 1 and the dashed line is sample 2. The samples exhibit a larger increase over the first day, which plateaus out until day 8. After day 8 the samples exhibit an erratic mass increase attributed to corrosion of the aluminium tape. The planetary mixed samples demonstrates increased variation in moisture absorption.*

### 6.4.7 Optical Microscopy

Optical microscopy was conducted on the samples. These were prepared by cutting the samples with a craft knife at room temperature, inducing a ductile failure. Ductile failure causes deformation of the sample prior to failure, which would be observed in the binder system. This deformation causes a variation in height of the sample, so only one layer is in focus per picture. There are no obvious visual differences between the LabRAM and planetary mixed samples seen in Figure 88, Figure 89, and Figure 90, such as particle size or particle distribution throughout the matrix. There does not appear to be any chain scissoring or binder failure. The binder matrix is the majority of the picture, and the filler crystals can be observed as shiny, typically flat surfaces within it; examples have been circled on each image.

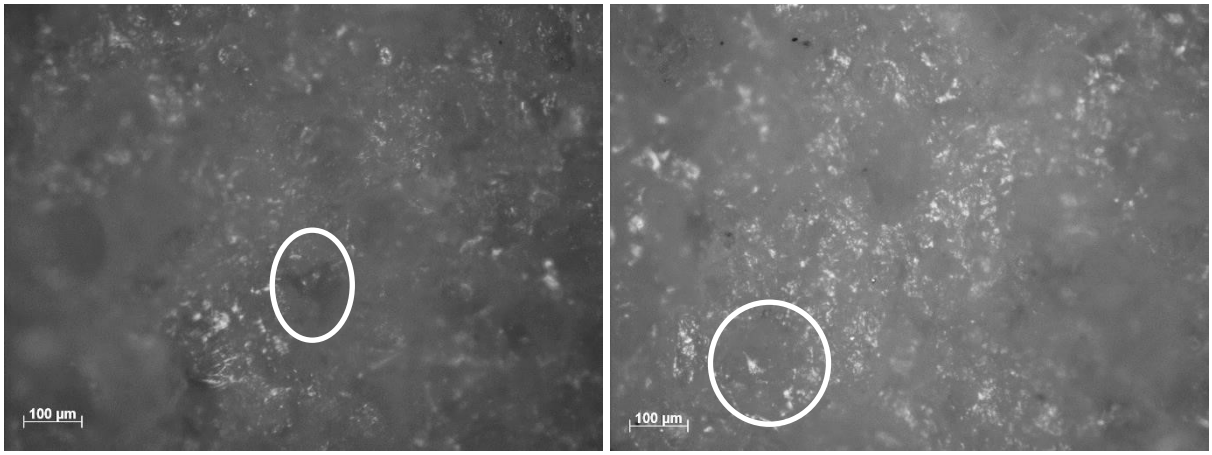


*Figure 88. Microscopy images of the 0.66 solid loading full inert samples mixed by LabRAM (left) and planetary mixing (right). The melamine and barium sulphate can be observed within the HTPB strands. The filler crystals do not appear to differ in either shape or size and the HTPB strands do not appear to be damaged or shorter when comparing the two mixing methods. Crystals have been circled in each image*

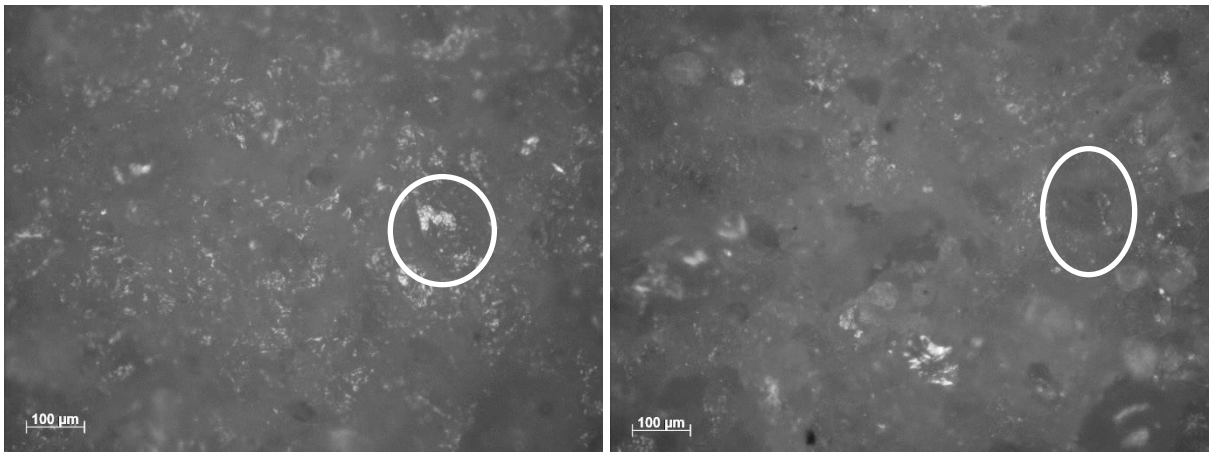


*Figure 89. Microscopy images of the 0.73 solid loading full inert samples mixed by LabRAM (left) and planetary mixing (right). The melamine and barium sulphate can be observed within the HTPB strands. The filler crystals do not appear to differ in either shape or size and the HTPB strands do not appear to be damaged or shorter when comparing the two mixing methods. Crystals have been circled in each image*

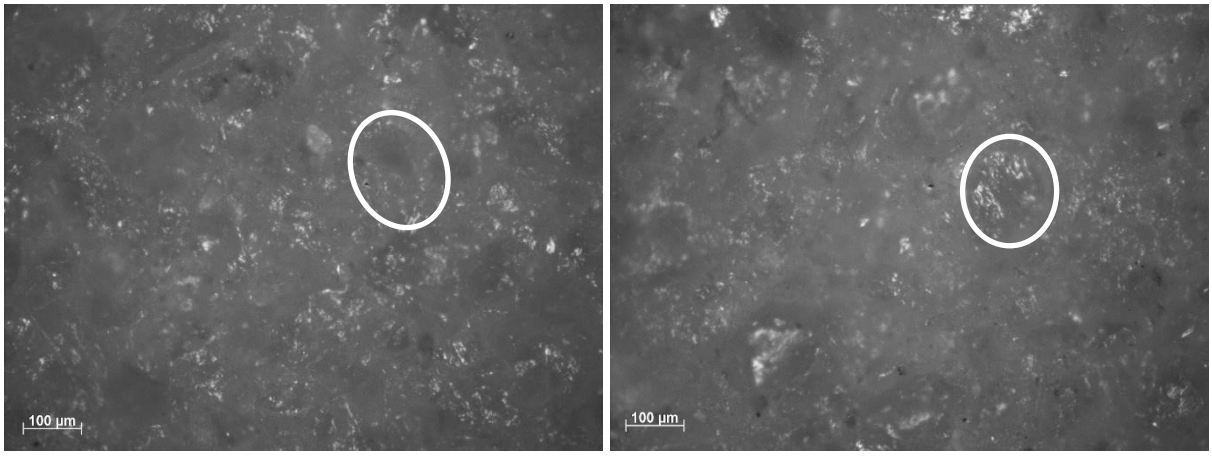


*Figure 90. Microscopy images of the 0.80 solid loading full inert samples mixed by LabRAM (left) and planetary mixing (right). The melamine and barium sulphate can be observed within the HTPB strands. The filler crystals do not appear to differ in either shape or size and the HTPB strands do not appear to be damaged or shorter when comparing the two mixing methods. Crystals have been circled in each image*

## 6.5 Discussion and Conclusions

The results produced from the inert full compositions support the other inert chapters in the assertion that for these materials there is no significant impact from mixing with LabRAM. The mechanical behaviour at low strain rates is primarily controlled by the binder system with the 0.73 and 0.80 solid loading samples having altered mechanical properties; assumed to be as a result of poor curing and isocyanate distribution. When testing at high strain rates statistical analysis was conducted and the average for like materials and the t-test results were plotted. The 0.66 and 0.80 solid loading samples had improved high strain rate mechanical properties when mixed by LabRAM although neither provided sufficient evidence to reject the null hypothesis. The 0.73 solid loading LabRAM sample had poorer mechanical properties and did provide sufficient evidence. The DSC results did not demonstrate variation between mixing methods, with the thermograms exhibiting two consistent endothermic peaks for the melamine and binder system. The NMR results did demonstrate a consistent increase in the amount of available and extractable HTPB when mixed via LabRAM which ranged from insignificant and with no evidence to reject the null hypothesis to significant variation that are statistically different. The density measurements demonstrated inconsistency between the solid loadings with the 0.66 and 0.80 solid loading samples being less dense when mixed via LabRAM and the 0.73 solid loading sample being denser. All the variation was insignificant with a maximum change of 0.27%. The 0.73 and 0.80 solid loading samples provided sufficient evidence to reject the null hypothesis, demonstrating the samples were statistically

different. Moisture permeation studies were conducted by two different experimental methods; DVS was not successful due to the small sample size. Single surface permeation experiments also demonstrated inconsistency with the results, with the 0.73 and 0.80 solid loading samples having a lower uptake in moisture when mixed via LabRAM. This was presumed to be due to a denser surface which limits the diffusion of moisture into the samples. The microscopy images do not demonstrate any variation in the results, and the samples had consistent levels of filler debonding during preparation indicating that the wetting and bonding of the filler within the binder system was consistent. The results are compared in Table 55, using the same methodology as before.

*Table 55. Table summarising the results of full inert characterisation. The DMA, SHPB and moisture permeation columns indicate the temperature range in which the results vary. The remaining results are percentage changes of the RAM samples from the planetary mixed samples. The colour coding indicates which sample had the higher results, with the planetary mixed samples being blue and the RAM samples being red. The results did demonstrate significant difference in available HTPB concentration for the 0.73 and 0.80 solid loading samples and in the high strain rate behaviour for the 0.73 solid loading sample.*

| | DMA | SHPB | Available HTPB | Density | Moisture Permeation |
|---|---|---|---|---|---|
| 0.66 solid loading | Negligible variations | Across whole range | 7.16% | 0.23% | Across whole range |
| 0.73 solid loading | -80 °C onwards | **Across whole range** | 56.8% | **0.24%** | Day 1 onwards |
| 0.80 solid loading | Inconsistent, negligible variation | 0.1 strain to 0.3 strain | **70.58%** | **0.27%** | Across whole range |

The 0.66 solid loading sample did not have significant or statistically varied behaviour when mixed by LabRAM. The LabRAM samples had stiffer behaviour, particularly for the high strain rate testing and were denser, indicating a superior filler packing density. The NMR results exhibited more available HTPB when mixed by LabRAM; curing was poorer for the LabRAM samples, likely due to isocyanate distribution. The increase in moisture permeation demonstrates the surface behaviour so does not tie in with the bulk material properties. As any variation is insignificant and provides no evidence that the null hypothesis could be rejected, there is no indication that mixing via LabRAM has impacted the material or its behaviour.

The 0.73 solid loading samples differ with a large variation in the mechanical properties, with enough evidence to reject the null hypothesis for the high strain rate testing. The LabRAM samples had weaker mechanical behaviour and a significant increase in available HTPB which would be expected. The LabRAM samples were denser and the results provided sufficient evidence to reject the null hypothesis, although the variation was not significant. It would be expected that the denser the sample the greater resistance to compression; however, due to the insignificant variation in density compared to the available HTPB, it indicates that the binder system has greater impact on the material. Like with the 0.66 solid loading the moisture permeation has no relationship with the bulk material properties. Mixing via LabRAM did impact the material, reducing the quality of the binder cure and impacting the mechanical behaviour.

The 0.80 solid loading samples also exhibited variation in the mechanical results; however, variation was insignificant and no evidence was provided to reject the null hypothesis. The low strain rate mechanical behaviour varied throughout indicating that there was inconsistency in the cure; this is supported through significant variation in available HTPB. The HTPB results provided sufficient evidence that the null hypothesis could be rejected and the samples were not statistically similar; however, the level of variation was not reflected in the mechanical behaviour. It would be expected that samples would demonstrate a greater deviation in stiffness due to the high change in available HTPB concentration. This was not reflected in the results indicating alternate mechanisms are dominating the mechanical behaviour of these samples. The samples did not have significant variation in density, although statistically were not similar with the planetary mixed samples being denser. Like the other samples, the moisture permeation does not link with the bulk material properties.

Mixing via LabRAM has caused a consistent increase in the amount of available HTPB in these materials demonstrating that the cure is less effective. This is most likely due to the distribution of isocyanate throughout. For the 0.73 solid loading samples this has affected the mechanical properties causing the LabRAM samples to be weaker; this has not significantly affected the other solid loading samples. Mixing via LabRAM has not affected the rest of the materials properties, indicating that as long as there is sufficient distribution of isocyanate, mixing via LabRAM has not significantly impacted these materials.

# 7 Explosive Formulation

The objective of this study was to identify any influence that resonant acoustic mixing had on explosives. Due to their hazardous nature, it was important that research was conducted on inert materials first. This entailed a systematic increase in sample complexity to mimic the composition of an in-use explosive. The same binder system was used in the inert formulation. The inert formulations used multiple loading levels representing composite propellants and polymer bonded explosives; however, for the energetic compositions the decision was made to focus on the higher loaded polymer bonded explosives with a solid loading of 80%.

## 7.1 Materials

The binder used was the same as that in Chapter 5.1; the HTPB, when combined with an isocyanate curing agent, forms the binder network with a plasticiser, DOS, addition to improve the mechanical properties. This binder is representative of a range of PBXs and composite propellants used both in research and in-service. The inert research highlighted that by using RAM the distribution of isocyanate within the sample varied.

The explosive filler chosen was RDX, Research Development Explosive; it is a commonly used high explosive crystalline ingredient, used as the standard for EMTAP (Energetic Materials Testing and Assessment Panel) testing [Defence Ordnance Safety Group, 2019]. It is well characterised and handled regularly by competent explosive workers. Developed in the UK in 1899, it was not introduced into service until after the First World War and eventually replaced a lot of TNT based systems. The chemical name is cyclotrimethylenetrinitramine; the structure is in Figure 91. There are two manufacturing methods and the UK uses both; the Bachman process produces around 10% HMX as a by-product but has a higher yield than the Woolwich method which produces pure RDX [Agrawal, 2010] [Teipel, 2005]. HMX is a variant of RDX, which was commonly used in US weapons developed in the 1950s to the 1970s and in early Composition B formulations. It is considered to be one of the fastest reported explosives. It has multiple potential names, including High Melting Explosive, Her Majesty's Explosive and octogen [Agrawal, 2010].

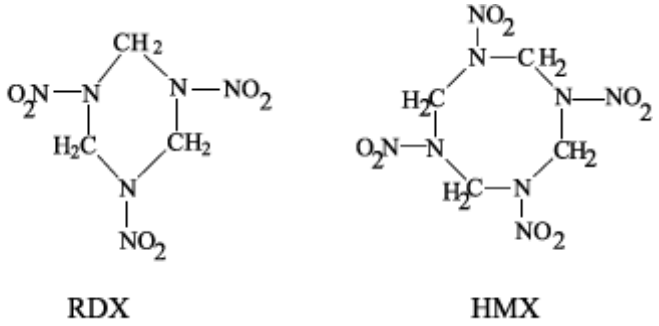


*Figure 91. RDX and HMX chemical structure*

RDX is a white powder, and as mentioned in previous chapters, is available in a range of classes. Material used in this programme are Class 1 and Class 5, both manufactured by the Bachman process. Some key properties are found in Table 56.

*Table 56. Explosive properties of HMX and RDX [Agrawal, 2010]*

| Property | RDX | HMX |
|---|---|---|
| Heat of formation/ kcal $kg^{-1}$ | 72.0 | 60.5 |
| Calculated detonation velocity/ m $s^{-1}$ | 8977 | 9320 |
| Calculated detonation pressure/ GPa | 35.17 | 39.63 |

## 7.2 Planetary Mixing

Samples were mixed using an IKA Planetron HKV-5 mixer, chosen due to increased blade clearance. Grinding or crushing of explosive crystals can cause initiation, and the blade clearance on the HKV-1 mixer was considered insufficient. The HKV-5 operates on the same principle but has a minimum capacity of 1 kg instead of 300 g. Two mixes were conducted; 1kg was mixed for the characterisation tests and 1.2 kg was manufactured for the functionality tests. A 0.1 bar to 0.2 bar vacuum was applied and blade speed varied between 11 and 18 rpm. The samples flowed with no external stimuli and cast into three types of moulds; 25 mm diameter tubes lined with greaseproof paper, DMA finger moulds and a simple square mould. After casting, the samples were cured in an oven at 50 °C for 1 week. The cured samples did not exhibit any voidage. The composition and mix notes are in Table 57.

*Table 57. Formulation table for the energetic planetary mixed samples with mixing notes*

| HTPB | DOS | RDX Coarse | RDX Fine | Planetary Mixing | Samples flowed without any external stimuli |
|---|---|---|---|---|---|
| 13.3 | 6.5 | 58.4 | 21.6 | | |

## 7.3 LabRAM Mixing

Mixing was conducted remotely in a suitably licenced explosive facility. The LabRAM was situated in the process room; all other equipment including the controlling computer and the vacuum pump were in the control room. As LabRAM is not ATEX approved samples were prepared in a different facility to prevent dust build up and the generation of an explosive atmosphere. ATEX is the European directive to control explosive atmospheres; equipment used in an explosive atmosphere should be tested and compliant with these regulations. [Hse.gov.uk, 2019]

The LabRAM vessel had a maximum mix capacity of 200 g; multiple batches were manufactured and combined into samples to produce sufficient quantity of material to test. Samples were mixed under a vacuum of 0.1 bar and used a layered approach. Premixed binder sandwiched the filler powder to reduce free powder movement. Mixing had three stages; half filler, addition of the remaining filler and the addition of the isocyanate, illustrated in Figure 92.

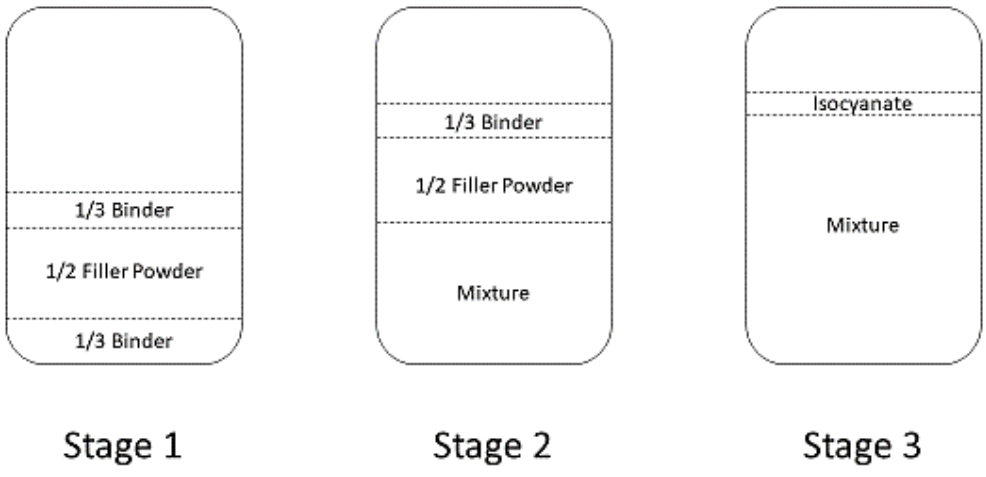


*Figure 92. The three stages for mixing explosives by LabRAM used in this programme. A layered approach was used to limit the likelihood of explosive powder being flung around the vessel and impact the vessel walls. Although it was not expected that this would be sufficient enough to cause a shock to detonation, it was decided that reducing the likelihood was the right choice.*

Like the planetary mixed samples, material was cast into a DMA mould, a block mould and VoD moulds. The samples appeared consistent and flowed out of the vessel without any external stimuli. Composition and the mix note can be found in Table 58.

*Table 58. Formulation table of energetic LabRAM samples*

| HTPB | DOS | RDX Coarse | RDX Fine | LabRAM | Samples flowed without any external stimuli |
|---|---|---|---|---|---|
| 13.3 | 6.5 | 58.4 | 21.6 | | |

### 7.3.1 Safety Consideration

Planetary mixing of explosives is well established and associated risks are well understood; risk reduction has undergone multiple iterations which has not yet happened with LabRAM. Prior to mixing energetic materials a safety case was produced which detailed all risk management that was conducted. The key risks and control measures are detailed in Table 59.

*Table 59. Table detailing the risks and control measures for mixing energetic samples via LabRAM*

| Risk | Likelihood and Severity | Control Measures |
|---|---|---|
| Static Charge | Static build due to rapid movement of explosive powders. RDX will initiate when subjected to an electrostatic discharge of 0.45 J | Sample vessel was grounded during mixing via an earthing cable to facilities grounding strip preventing build-up of static charge. Material was added in a layered approach with binder on the surface to reduce the likelihood of powder escaping the bulk material. |
| Temperature Increase | Temperature increase causing initiation. RDX has a temperature of ignition (TofI) of 215 °C | Temperature measurements were conducted on inert formulations; a maximum temperature increase of 20 °C was noted. Real time temperature measurements were taken; if the temperature exceeded 50 °C mixing would stop.<br>Note: maximum temperature seen whilst mixing these samples was 45 °C. |
| Powder Shock | Dry explosive powder impacting mix vessel lid causing initiation. | A layered approach was adopted where all explosive crystals were bound by binder layers, reducing the potential for explosive filler to move freely within the vessel and the likelihood of powder impacting the vessel lid. |
| Material Shock | Material de-bonding from the vessel and shocking material to initiation | The input power was gradually increased to ensure minimum power was inputted into the sample. Any erratic behaviour noted on the mix diagram or in the temperature measurements caused the mixing to stop. |
| Compatibility | Incompatible materials causing initiation | The formulation is based on well understood formulations that have already passed compatibility testing. The mix vessel was an untreated steel pot known to be compatible with RDX. |

## 7.4 Characterisation

Characterisation was based on the full inert composition undertaken in Chapter 5.4; testing was comprehensive and provided understanding on the effect of RAM on materials. Some tests were not included for the energetic samples as they were deemed not suitable or required. High strain rate testing was not conducted as the laboratory was not licenced for explosives at the time of testing. The diffusion behaviour did not demonstrate sufficient variation. However, DMA testing, density measurements, hardness, NMR and DSC/TGA were still conducted. This suite of tests will provide enough data to generate understanding of the impact of RAM on energetic materials. Hazard testing enabled understanding of handling and safety requirements. Functionality testing determined performance.

### 7.4.1 Hazard Testing

Hazard testing was conducted in accordance with the Energetic Material Testing Assessment Policy (EMTAP) manual [Defence Ordnance Safety Group, 2006]. This manual is a UK standard which provides instruction and guidance on small scale hazard testing. EMTAP testing determines the sensitiveness, the response of a material to unintended stimuli, of energetic materials and is a requirement when assessing the safety of energetic materials, particularly for UK service and use. All the tests are volumetric and use sub-gram quantities.

#### 7.4.1.1 EMTAP Test 1A

EMTAP Test 1A, or Rotter testing, tests the response of a solid material to an impact stimuli. It was initially designed to study the sensitiveness of crystalline secondary explosives and has since been developed to be applicable to a range of solid energetic materials. It uses 30 $mm^3$ of material. The design is simple; a 5 kg weight is dropped onto a sample enclosed within an anvil based system and the response is monitored. Ignitions are identified either through the production of gas or through secondary ignition criteria such as smoke or discolouration. Dependent on the samples properties, the drop height can be range from 5 cm up to 240 cm. A schematic has been included in Figure 93 to illustrate the equipment set up.

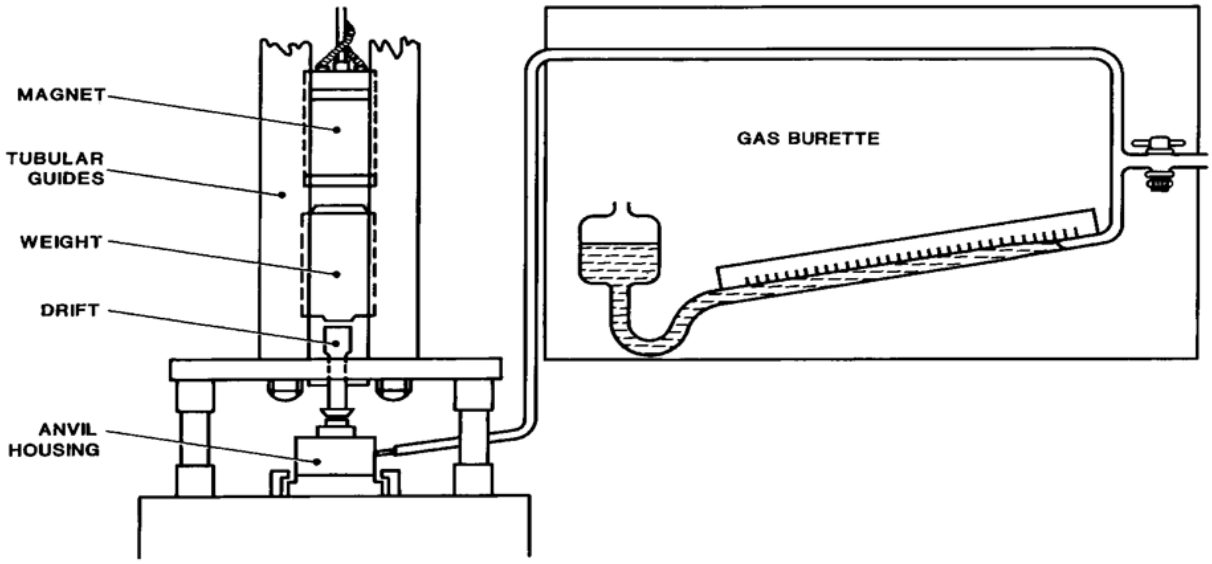


*Figure 93. Schematic detailing the test set up of EMTAP Test 1A, or the Rotter test. A 5kg weight is dropped from the magnet, and impacts the anvil housing which contains the explosive sample. The gas burette is connected to the anvil to measure the gas produced and determine whether an event has occurred. This test measures the impact sensitiveness of the material [Defence Ordnance Safety Group, 2006].*

The test is conducted using the Bruceton staircase procedure, which uses 50 tests conducted at predefined drop heights; an ignition, or go, involves a decrease in drop height and imparted energy and a lack of ignition, or no-go, results in an increase in drop height. After the 50 tests have been conducted the Figure of Insensitivity, or F of I, is calculated. The F of I is divided into three categories to identify the sensitiveness of the sample; Table 60 summarises these classes.

*Table 60. Table detailing the three sensitiveness categories that the Rotter results can fall into. These categories would require different handling approaches [Defence Ordnance Safety Group, 2006]*

| F of I | Classes |
|---|---|
| ≤ 30 | Very sensitive |
| 35 – 90 | Sensitive |
| ≥ 90 | Comparatively insensitive |

*Table 61. The rotter testing results comparing the planetary mixed sample, the LabRAM samples and the RDX standard accepted value. The samples are less sensitive than RDX with the RAM samples have greater sensitiveness to impact*

| | **Planetary Mixed Sample** | **LabRAM Sample** | **RDX Standard** |
|---|---|---|---|
| Rotter | 118 | 98 | 80 |
| Mean Gas Volume/ ml | 3.6 | 2.8 | N/A |

The results are in Table 61. Regardless of the mixing method, the material is classed as comparatively insensitive as both samples have an F of I above 90. Additionally, they are less sensitive than the RDX standard, which has an accepted F of I of 80. The binder system provides low vulnerability properties by absorbing some energy impacted through an unintended stimuli, which explains the popularity of polymer based explosives.

The rotter test has a variability of 15%, which is based off the RDX standard running mean specific for the machine. The F of I for the LabRAM sample was 17% lower than that of the planetary mixed sample, which is on the border of the significant variability. Potential inhomogeneity within the sample could cause deviations in F of I as areas with greater quantity of energetic crystals and less binder would have a lower F of I. Mixing via LabRAM has increased the sensitivity of the material, but there is insufficient evidence for this to be a significant change.

#### 7.4.1.2 **EMTAP Test 2**

EMTAP Test 2, the Mallet Friction testing, is designed to replicate the impact and friction a sample could experience during handling. This is done through a series of standardised mallets and anvils. The results are categorised into three categories, described in Table 62.

*Table 62. Table detailing the three sensitiveness categories that the mallet friction results can fall into. These categories would require different handling approaches [Defence Ordnance Safety Group, 2006]*

| | | |
|---|---|---|
| Very Sensitive | 100% ignitions on metal and at least 50% ignitions on Yorkstone and hardwood | Extreme care required handling these materials |
| Comparatively Insensitive | No ignitions on any surface combination | Friction and impact between materials harder than softwood is to be avoided |

| | | |
|---|---|---|
| Sensitive | Any other result | Blows between hard surfaces be avoided, but transfer between metal containers is allowed |

This test is conducted on a small sample, approximately 100 $mm^3$ for powdered material, which is spread onto an anvil; an operator uses either a standard wood, steel-tipped or nylon-tipped mallet to strike a glancing blow onto the sample. The mallets have a smooth surface profile through the use of rounded corners. The anvils are either softwood (yellow Norwegian pine), hardwood (oak), mild steel or Yorkstone. The combinations are as following: steel-tipped mallet/ steel anvil, nylon-tipped mallet/steel anvil, wood mallet/softwood, wood mallet/hardwood, or wood mallet/Yorkstone. Material that ignites on wooden surfaces are considered either very sensitive to fiction or sensitised by any abraded particles than can then act as a fuel.

The operator has to provide a fair glancing below. A cycle consists of five attempts or until an ignition occurs. An ignition consists of either sparks or flame, a crack as material reacts, or smoke or any indication of reaction. The results are reported as the number of ignitions occurring during 10 cycles.

The results from the test are in Table 63. The samples were not initiated under any conditions in this test and are classed as comparatively insensitive. There was no variation between the mixing methods as both sets of samples did not initiate. These samples are less sensitive than the RDX standard, due to addition of binder.

*Table 63. Table containing the mallet friction results comparing the planetary mixed sample, the LabRAM samples and the RDX standard accepted value. The samples are less sensitive than RDX and consistent between mixing methods*

| | **Planetary Mixed Sample** | **LabRAM Sample** | **RDX Standard** |
|---|---|---|---|
| Mallet Friction | 0 ignitions | 0 ignitions | 50-100 steel tipped mallet on mild steel anvil |

#### 7.4.1.3 **EMTAP Test 3**

EMTAP Test 3, Temperature of Ignition (T of I), determines the temperature at which an event occurs. An event is either a flame, explosion or rapid decomposition and is demonstrated by a

puff of smoke or visible flame; these are considered to be equal outcomes. Samples are placed in a borosilicate test tube and placed in a steel block. This block is heated at a steady rate and the test is monitored until an event occurs.

Typically, materials with results less than 140 °C are considered unsuitable for service. Materials with results between 140 °C and 170 °C should have a short service life and be monitored regularly.

*Table 64. Table containing the temperature of ignition results comparing the planetary mixed sample, the LabRAM samples and the RDX standard accepted value. The samples have a lower T of I than RDX but are consistent between mixing methods [Defence Ordnance Safety Group, 2006]*

| | **Planetary Mixed Sample** | **LabRAM Sample** | **RDX Standard** |
|---|---|---|---|
| Temperature of Ignition | 205 | 207 | 217 |
| Comments | Clouds of smoke | Clouds of smoke then flame | N/A |

The results are in Table 64. The LabRAM sample had a higher T of I by 2 °C, which is insignificant, indicating that mixing via RAM did not have an impact on the material. For a T of I test an error of ± 3 °C is accepted. The RDX standard has a higher T of I than the mixed composition; it is suspected that the plasticiser begins to degrade and reduces the T of I for this composition.

#### 7.4.1.4 **EMTAP Test 6**

EMTAP Test 6, Electric Spark test, distinguishes between materials that need a high electrostatic spark energy for ignition and materials that need a low energy. The material is tested at 3 levels; 0.045 J, 0.45 J and 4.5 J. These are based on the maximum electrostatic energy that can be accumulated on a person in the UK; this is 0.02 J. The energy is stored on one of three capacitors, 0.1 µF, 0.01 µF or 0.001 µF, which is charged to a potential of 9.5 kV. Sample is placed in a 3.2 mm thick polythene strip that has 4 holes with diameters of 6.35 mm. Along the bottom of the polythene strip is a self-adhesive copper foil that is 0.08 mm thick. The copper foil is also added to the top of each individual sample, forming electrodes. The setup is illustrated in Figure 94.

Testing begins at 4.5 J. Samples are tested for 50 runs or until an ignition occurs. If an ignition occurs the energy level is lowered and the samples are run again for another 50 runs

or until another ignition. An ignition is determined by audible or visual output not due to spark discharge. Results are summarised in Table 65. The planetary mixed and LabRAM samples were consistent with ignitions at 0.45 J but not at 0.045 J; this is the same as the RDX standard as well. The mixing method has not impacted the ESD properties of the material.

*Table 65. Table containing the electric spark results comparing the planetary mixed sample, the LabRAM samples and the RDX standard accepted value. The samples have a consistent ESD sensitiveness between mixing methods and with the RDX standard*

| | **Planetary Mixed Sample** | **LabRAM Sample** | **RDX Standard** |
|---|---|---|---|
| Electric Spark Test 6 | Ignitions at 0.45 and not at 0.045 J | Ignitions at 0.45 and not at 0.045 J | Ignitions at 0.45 and not at 0.045 J |

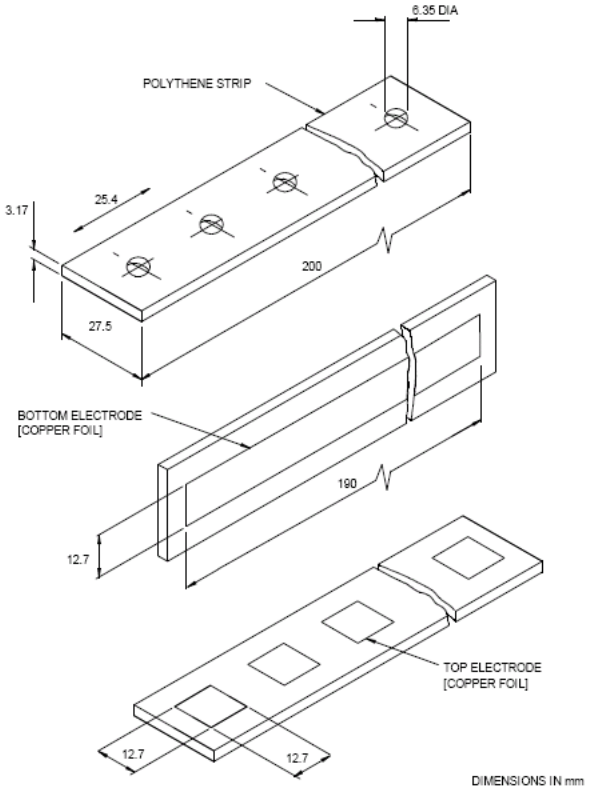


*Figure 94. Diagram demonstrating the sample set up for the ESD test, with a top before sample preparation, side and top after sample preparation view of the sample holder (top to bottom). Four samples can be arranged in the sample holder, going in the gaps seen in the top image. Copper foil is placed along the whole bottom side of the sample holder, and then individual pieces are placed on top each sample to form bottom and top electrodes [Defence Ordnance Safety Group, 2006]*

#### 7.4.1.5 **EMTAP Test 33**

EMTAP Test 33, Rotary Friction testing, is another friction test designed to replicate the friction a sample experiences during handling. Unlike the Mallet Friction, there is no impact component on the test. Mild steel wheels, with a nominal diameter of 70 mm, and mild steel blocks are both used with a standard ground surface finish. The wheel is attached to a flywheel which then rotates at speeds based on the logarithmic scale, with increments of 0.1 and passing through 100 rpm. Figure 95 illustrates the setup. A Bruceton staircase run is used, where 50 samples are tested and the speed is set on a go/no-go system. An ignition is characterised as a loud crack, the consumption of sample or evidence of combustion. From this Bruceton staircase a Figure of Friction (F of F) can be calculated. This ranges from 0 to ≥6. The results can be separated into three categories; these are detailed in Table 66.

*Table 66. Table detailing the three sensitiveness categories that the rotary friction results can fall into. These categories would require different handling approaches [Defence Ordnance Safety Group, 2006]*

| **Category** | **Result** |
|---|---|
| Very sensitive | <3 |
| Sensitive | ≥3 but <6 |
| Comparatively insensitive | ≥6 |

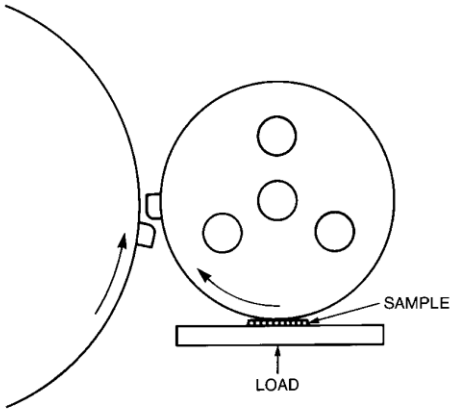


*Figure 95. Diagram demonstrating the rotary friction setup with the sample under the rotating flywheel [Defence Ordnance Safety Group, 2006]*

The results are in Table 67. RDX standard has an F of F of 3.0. In comparison, these compositions are comparatively insensitive. The binder system reduces the effects of the friction and the sensitiveness of the samples. This is also observed with the Mallet Friction

test. The mixing method has not impacted these samples as they have the same figure of friction (F of F) of >6.

*Table 67. Table containing the rotary friction results comparing the planetary mixed sample, the LabRAM samples and the RDX standard accepted value. The samples have a consistent sensitiveness between mixing methods and a significantly lower sensitiveness when compared to the RDX standard*

| | **Planetary Mixed Sample** | **LabRAM Sample** | **RDX Standard** |
|---|---|---|---|
| Rotary Friction | >6 | >6 | 3.0 |

### 7.4.2 DMA

DMA testing was conducted with the same conditions as Chapter 3.4.1; details on testing can be found there. It was performed on a Rheometrics RDAII dynamic mechanical analyser, testing from -110 °C to +80 °C with a nominal strain of 0.1 %. Samples were from the bulk and cut to size. A graph was produced, plotting storage modulus, G', loss modulus G'', and tan(delta). The red lines are LabRAM samples and the blue are the planetary mixed samples. Solid lines indicate G', dotted lines are G'' and dashed lines are tan(delta). Samples were prepared by cutting the appropriate sized bar out of bulk material.

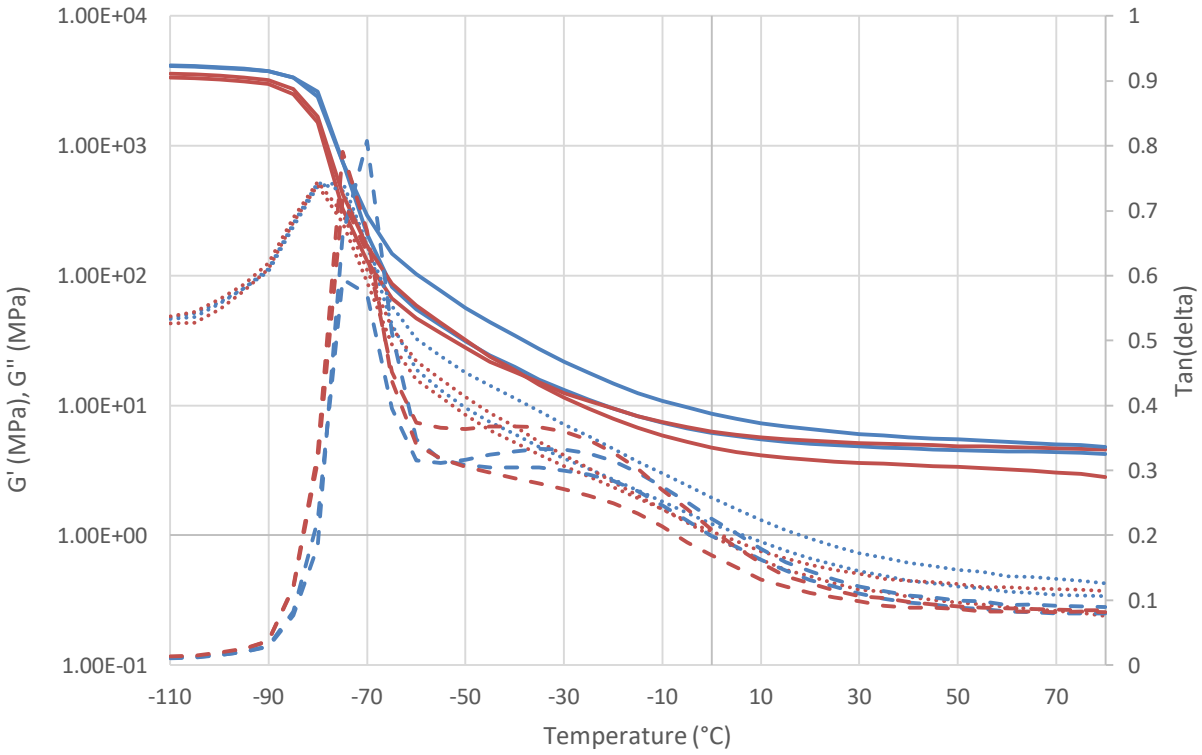


*Figure 96. DMA graph energetic samples plotting the elastic modulus or G' (solid line), loss modulus or G'' (dotted line) and tan(delta) (dashed line), and comparing the LabRAM samples (red) with the planetary mixed samples (blue). The samples demonstrate reasonable consistency between the mixing methods*

The energetic samples were the first samples mixed remotely, using the mix indicators detailed in Chapter 8.2. Samples, in Figure 96, showed a variation in their mechanical properties between like samples; this is likely due to sample preparation as samples were cut from bulk material. The planetary mixed samples had greater variation compared to the RAM samples. The LabRAM samples were less stiff in comparison to the planetary mixed samples for both moduli, indicating greater movement within the sample. This could be as a result of poor curing within the material, or variation in sample size. The behaviour variation was not significant.

The results are compared to research found in literature in Table 68. The results were consistent with the literature demonstrating that these samples behaved as expected.

*Table 68. A table comparing the DMA results of the energetic compositions with literature*

| **Source with summary of programme** | Chapter 6.4.1 | Studies on the Influence of Testing Parameters on Dynamic and Transient Properties of Composite Solid Rocket Propellant Using a Dynamic Mechanical Analyzer [Wani et al, 2012] |
|---|---|---|
| **Material** | HTPB – DOS – AO – Melamine - Barium Sulphate with solid loading levels of 0.66, 0.73 and 0.80 | High burning rate solid composite propellant consisting of an HTPB binder system, cured by toluene diisocayante (TDI), with an undisclosed solid loading of ammonium perchlorate with a tetra-modal distribution and aluminium. |
| **Test Regime** | Testing conducted on a Rheometrics RDAIIII with a 0.1% strain, and a temperature range of -110 °C to +80 °C. The temperature was incremented at 3 °C $min^{-1}$. | Testing conducted on a TA Instruments Dynamic Mechanical Analyser Q800 with a 0.01% oscillatory strain at 11Hz. A heating rate of 2°C/min |
| **Results** | The 0.80 solid loading samples, in the graph below, showed variation in mechanical properties between the two mixing methods. The LabRAM samples had higher stiffer mechanical behaviour before the glass transition temperature and weaker mechanical properties after. The moduli is approximately 3.5 GPa then drops to 1 MPa. The samples had a glass transition point at approximately -75 °C and a second tan(delta) peak at -25 °C. | A “standard” composite propellant DMA graph was plotted below. The tan(delta) has two peaks characteristic of an HTPB binder system. The glass transition temperature is at -60 °C and has an associated tan(delta) value of less than 0.5. The storage moduli is approximately 4.5 GPa, dropping after the glass transition temperature. The y-axis does not have a logarithmic scale which limits the clarity of the moduli at the higher temperatures. |

| | | |
|---|---|---|
| | 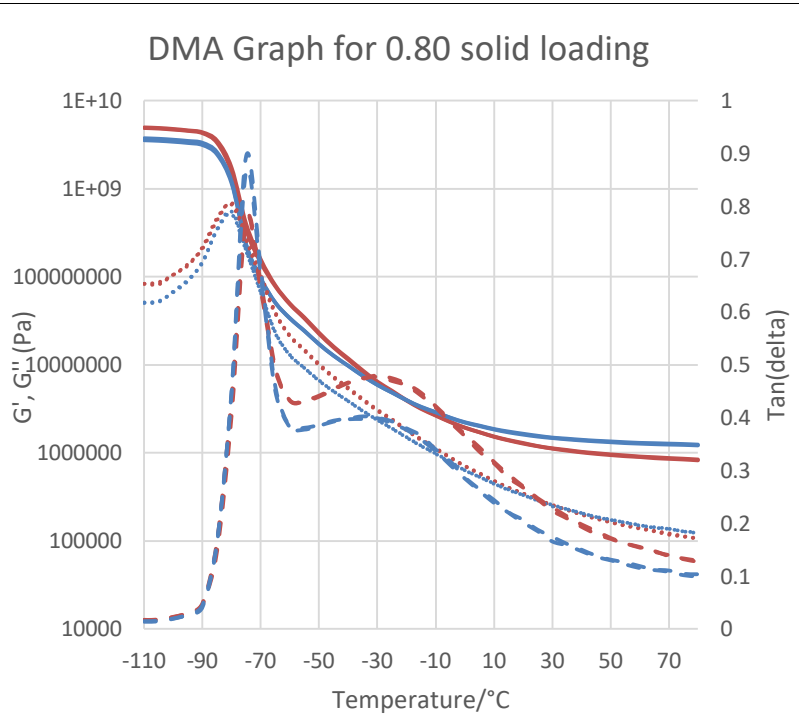 | 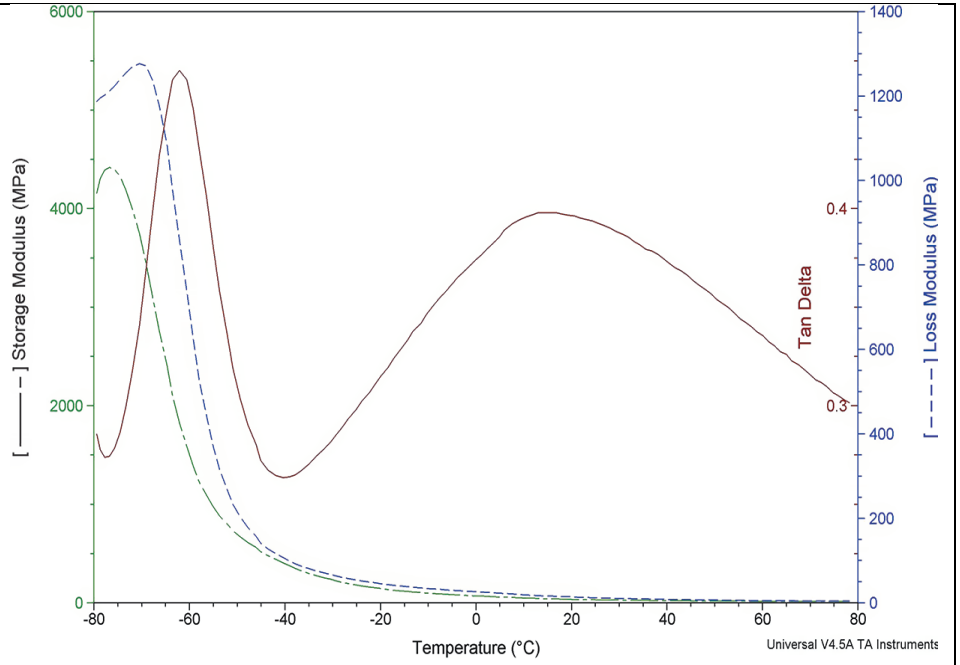 |
| **Comparison with this research programme** | The moduli is comparable between the literature and the samples in this chapter with an initial storage moduli of 3.5 GPa. The samples have similar glass transition temperatures of -75 °C. After the glass transition temperature the samples in this chapter were stiffer; however, they are within an order of magnitude. Overall, the samples in this chapter and the samples in literature are comparable indicating reasonable and expected results. | The samples in the literature had a higher storage moduli of 4.5 GPa instead of 3.5 but the variation is negligible. The glass transition temperature is higher for the sample in this literature by approximately 15 °C. This is likely due to the alternate curative. There are small differences between the samples in literature and in this chapter, but the results are consistent enough to prove that these samples behave as expected. |

### 7.4.3 NMR

NMR testing was conducted to the same principles as Chapter 3.4.3. A protonquant NMR was used to determine the mass percentage of the HTPB and DOS components. The HTPB is the extractable HTPB that has not been cured to form the wider binder network. NMR can demonstrate the level of curing that has occurred and the distribution of the binder within the sample.

The results are summarised in Table 69, with statistical analysis conducted in Table 70. When mixed via LabRAM the samples had a decrease in available HTPB concentration indicating either better curing of HTPB or greater variation of binder components within the material. The LabRAM samples had sufficient decrease to be a significant variation, with enough evidence to reject the null hypothesis. The DOS concentration for both sets of samples differed from the nominal expected value indicating variation within the sample. This could be either within the sample or within the binder system.

*Table 69. Table detailing the percentage composition of the extractable HTPB and DOS from the NMR testing on the energetic samples*

| Sample | | HTPB | | | DOS | | |
|---|---|---|---|---|---|---|---|
| | | Result | Average | Nominal | Result | Average | Nominal |
| Planetary Mixed | 1 | 2.75094 | 2.53442 | 13.0 | 5.98421 | 5.94363 | 5.7 |
| | 2 | 2.33677 | | | 5.89757 | | |
| | 3 | 2.51555 | | | 5.94911 | | |
| LabRAM | 1 | 1.85076 | 1.71966 | | 5.46619 | 5.41225 | |
| | 2 | 1.53364 | | | 5.03873 | | |
| | 3 | 1.77459 | | | 5.73184 | | |

*Table 70. Table summarising the analysis of the NMR testing on the energetic samples, detailing the percentage change of the LabRAM results from the planetary mixed samples and the calculated T-Test value. The samples demonstrate significant and statistical variation in the extractable HTPB concentration*

| Sample | HTPB | | DOS | |
|---|---|---|---|---|
| | % Change | T-test | % Change | T-Test |
| Explosive | -32.1 | 0.006 | -8.9 | 0.059 |

### 7.4.4 DSC/ TGA

DSC/TGA was conducted using a Mettler TGA/DSC with sample mass of ~1 mg; each sample was run in duplicate. Using a nitrogen atmosphere of 50 ml $min^{-1}$ and a temperature ramp of 5 °C $min^{-1}$ the samples were sealed in an aluminium crucible and the cap was

pierced. As these samples are energetic, the maximum temperature was 350 °C as opposed to 600 °C for the inert material. Further details on DSC/TGA can be found in Chapter 6.4.3.

The results are summarised in Table 71, and one thermogram is included for each test. Figure 97 is the planetary mixed sample and Figure 98 is mixed via LabRAM. The thermograms demonstrate a large sharp exothermic peak at ~215 °C. This coincides with a large weight loss of over 80 % indicating a decomposition. RDX has a melting temperature with decomposition of 205 °C [Gill, 2015] and makes up 80 % of this composition. The addition of the binder has increased the degradation by 10 °C due to the interactions between the binder and filler particles. When comparing the LabRAM and the planetary mixed samples there is no significant variation; samples have consistent weight loss and comparable exothermic peak temperatures.

*Table 71. Table containing the thermal peak (in Celsius) and the weight loss (percentage) of the energetic samples demonstrating consistency in the thermal degradation of the RDX between both mixing methods*

| Sample | Peak (°C) | Weight loss (%) |
|---|---|---|
| Planetary Mixed | 218.19 | 83.52 |
| | 217.72 | 82.87 |
| LabRAM | 216.27 | 82.71 |
| | 216.14 | 82.82 |

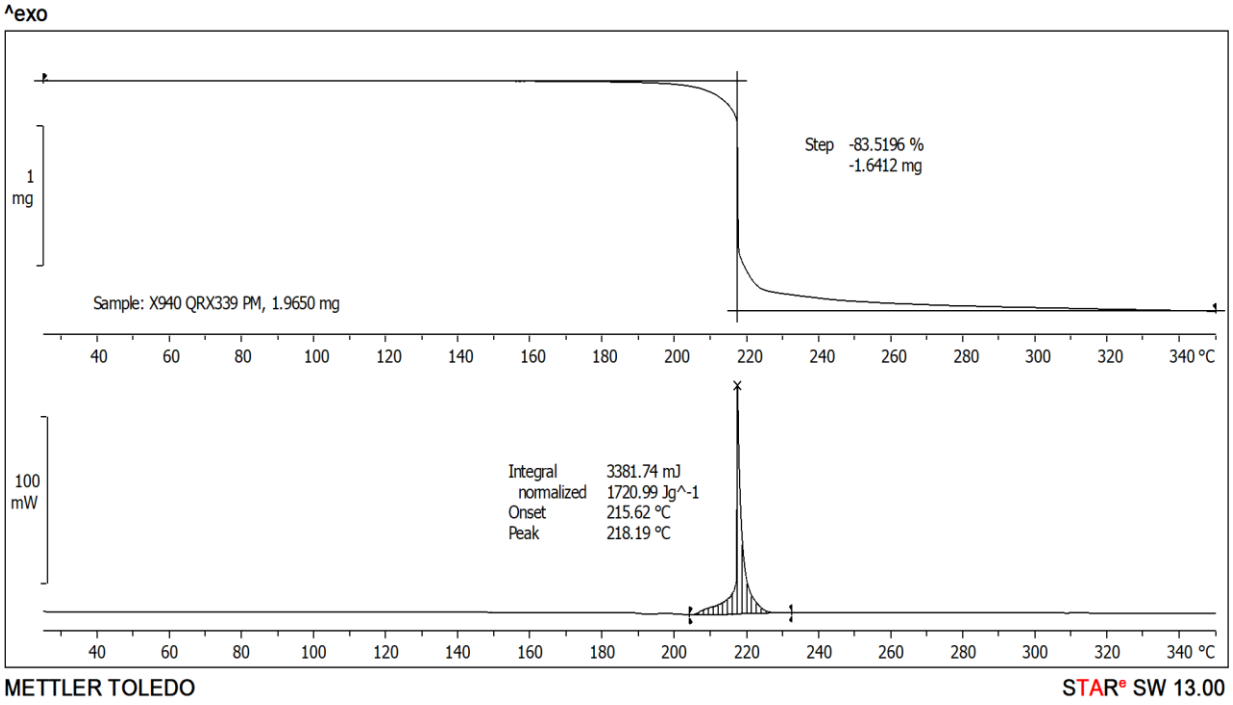


*Figure 97. Planetary mixed thermogram demonstrating a thermal peak at approximate 218 °C corresponding with a percentage mass loss of 83%. This coincides with the thermal degradation of RDX*

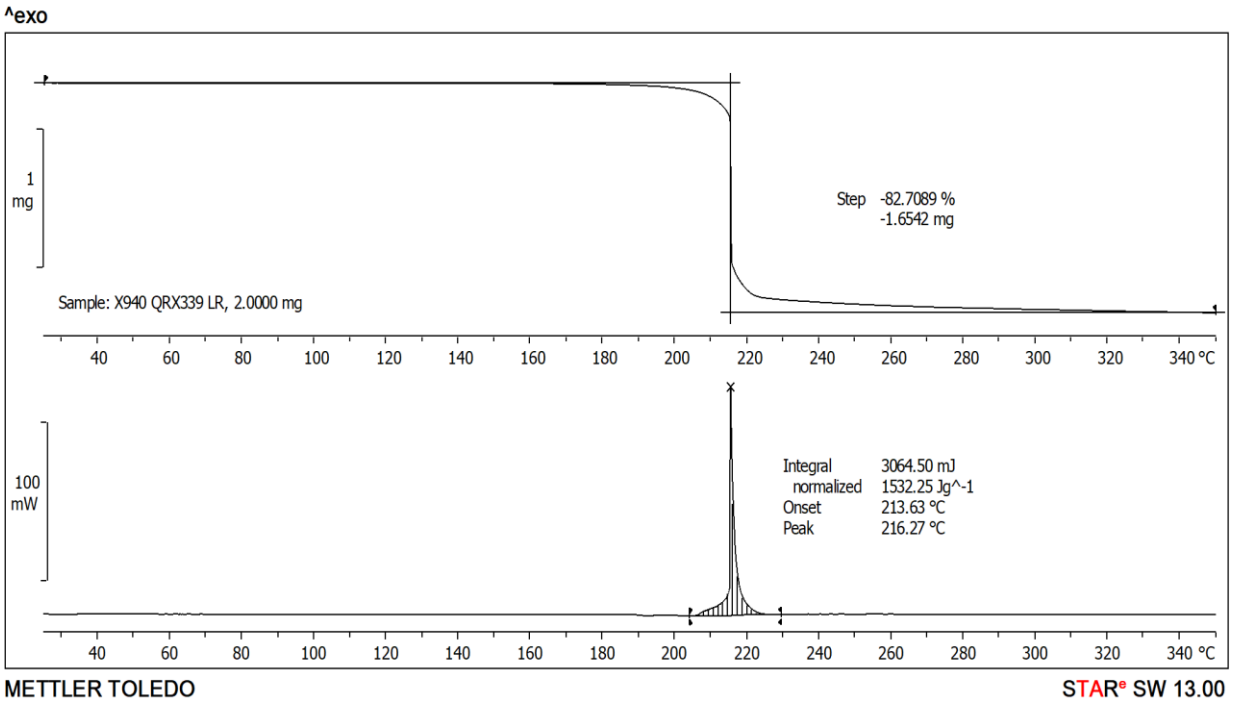


*Figure 98. LabRAM thermogram demonstrating a thermal peak at approximate 216 °C corresponding with a percentage mass loss of 82%. This coincides with the thermal degradation of RDX*

### 7.4.5 Density

As with the inert samples, density measurements were conducted on a Quantachrome Ultrapyc 1200e using helium pycnometry. Further details can be found in Chapter 4.4.3. Tests were conducted on 4 samples for each material; results are found in Table 72. Samples from the same mixing method have a small standard deviation and are highly consistent.

*Table 72. Table containing the results from the density testing on the energetic samples with the average result and the standard deviation. The samples showed good consistency.*

| Mixing Method | Results/ g $cc^{-1}$ | Average | Standard Deviation |
|---|---|---|---|
| Planetary Mixed | 1.5164 | 1.5160 | 0.0003 |
| | 1.5161 | | |
| | 1.5158 | | |
| | 1.5156 | | |
| LabRAM | 1.5125 | 1.5123 | 0.0002 |
| | 1.5123 | | |
| | 1.5121 | | |
| | 1.5122 | | |

*Table 73. Table detailing the density measurements of the energetic samples, with the percentage change of the LabRAM samples from the planetary mixed and the calculated T-Test value. There was no significant variation between the two mixing methods*

| Sample | Planetary Mixing | LabRAM | % Change | T-test probability |
|---|---|---|---|---|
| Explosive | 1.5160 g $cc^{-1}$ | 1.5123 g $cc^{-1}$ | -0.24% | $1.37 \times 10^{-6}$ |

The results were compared in Table 73; samples mixed via RAM had a decrease of 0.24% implying that either the filler packing density is greater or the binder is denser. This density change of 0.24% is insignificant by the definition in this study, less than 10%. The samples have high consistency with a standard deviation of 0.0003 or less. A t-test was applied and produced a probability of $1.37 \times 10^{-6}$ which provides sufficient evidence to reject the null hypothesis and that the samples are statistically different.

These have been compared with available literature to determine the reasonableness of these results and to provide context in Table 74. Chapter 4.4.3 used material specifications for comparison; the same material specifications are used for this chapter. The samples in this research programme had lower density than the PBXN-110 and PBXN-109 specifications; likely due to the decreased solid loading.

*Table 74. Table comparing the density measurements of the energetic samples with literature*

| | | |
|---|---|---|
| **Source with summary of programme** | Explosive, Plastic-Bonded, Cast PBXN-110, MIL-DTL-82901A [Naval Sea Systems Command, 2002] | Explosive, Plastic-Bonded, Cast PBXN-109, MIL-DTL-82886 [Naval Sea Systems Command, 1993] |
| **Material** | PBXN-110 (HTPB based with a solid loading between 86 – 89%) | PBXN-109 (HTPB based with a solid loading of RDX between 62 – 66% and aluminium between 18 - 22%) |
| **Test Regime** | Two samples weighing between 10 g – 20 g tested on an analytical balance equipped for underwater weighing with an accuracy of 0.1 mg. Testing shall occur at 25 °C. | Two samples weighing between 10 g – 20 g tested on an analytical balance equipped for underwater weighing with an accuracy of 0.1 mg. Testing shall occur at 25 °C. |
| **Results** | 1.62 – 1.70 g $cc^{-1}$ | 1.60 – 1.70 g $cc^{-1}$ |
| **Comparison with this research programme** | As with the samples in the previous chapter, the samples in this literature are denser than this material due to higher solid loading. | Samples in this literature have a greater filler loading and density when compared to samples in this research programme. |

### 7.4.6 Hardness

Hardness testing was conducted on the bulk material, as with the inert samples in Chapter 4, using a ProviTesting Standard portable Shore A hardness tester. Five tests were taken at various points within the sample on cut surfaces, and the average was calculated.

Results are summarised in Table 75 and Table 76. The planetary mixed samples had larger hardness results, but also had greater spread, when compared to the LabRAM samples. The LabRAM samples had a decrease in hardness of 3.5%, which is not significant as defined by this study. The t-test probability did not indicate sufficient evidence to reject the null hypothesis. By mixing via LabRAM, there was neither a statistical or significant change within the hardness of these samples.

*Table 75. Table detailing the results from the hardness test conducted on the energetic samples. The samples had a hardness between 65 and 73 Shore A*

| Sample | Results/ Shore A | Average | Standard Deviation |
|---|---|---|---|
| Planetary Mixed | 73.0 | 70.2 | 3.23 |
| | 69.1 | | |
| | 65.2 | | |
| | 72.8 | | |
| | 71.1 | | |
| LabRAM | 67.5 | 67.8 | 1.28 |
| | 68.9 | | |
| | 66.4 | | |
| | 69.3 | | |
| | 66.8 | | |

*Table 76. Table detailing the average hardness result in Shore A for the energetic samples, the percentage change of the LabRAM results from the planetary mixed results and the calculated T-Test probability. The variation between the RAM and the planetary mixed samples was not significant*

| Sample | Planetary Mixing/ Shore A | LabRAM/ Shore A | % Change | T-Test Probability |
|---|---|---|---|---|
| Explosive | 70.2 | 67.8 | -3.5% | 0.151413 |

These samples were compared with the PBXN-110 and PBXN-109 specifications in Table 77. The specifications allow for great variation within the results, and these samples lie within the boundaries set, indicating reasonable and comparable results.

*Table 77. Table comparing the energetic hardness results with literature*

| | | |
|---|---|---|
| **Source with summary of programme** | Explosive, Plastic-Bonded, Cast PBXN-110, MIL-DTL-82901A [Naval Sea System Command, 2002] | Explosive, Plastic-Bonded, Cast PBXN-109, MIL-DTL-82886 [Naval Sea System Command, 1993] |
| **Material** | PBXN-110 (HTPB based with a solid loading of HMX between 86 – 89%) | PBXN-109 (HTPB based with a solid loading of RDX between 62 – 66% and aluminium between 18 - 22%) |
| **Test Regime** | Shore A hardness testing with a 15 second delay. Tested at 25 °C using a Type A-2 durometer. | Shore A hardness testing with a 30 second delay. Tested at 25 °C using a Type A-2 durometer. |
| **Results** | Minimum 15 | Minimum 30 |
| **Comparison with this research programme** | A large range is allowed in the PBXN-110 specification, and these samples fall within that range. | Like with the PBXN-110 specification, the PBXN-109 specification allows for large variation. These samples are within this range. |

### 7.4.7 Functionality

Functionality is the key output for explosive materials; therefore velocity of detonation (VoD) trials were conducted. Detonation is a very fast chemical reaction within explosive material that produces a shock, or detonation, wave. The wave front contains high temperatures and pressure gradients which, along with the continuing chemical reactions, sustains the detonation as it travels through the material. This shock wave will have a constant speed associated with it, known as the velocity of detonation, which is dependent on the density and composition of the material [Agrawal, 2010].

Three VoD samples were manufactured for each mixing method. 25 mm diameter moulds were used with greaseproof paper lining on the inside to enable sample removal; this resulted in two lips on opposite sides of each sample where the greaseproof paper met. The dimensions, mass and density of each sample is detailed in Table 78. The samples are pictured in Figure 99 to Figure 105. All the samples appeared high quality with the exception of the LabRAM sample 3 which exhibited voidage throughout. The voidage in LabRAM Sample 3 can be seen in Figure 104 and Figure 105. The densities were comparable with less than 5% variation. Samples were initiated by a 25 mm diameter tetryl pellet, with an approximate mass of 20 g, and an RP-80 detonator which is fired with a 4 kV firing voltage. The set up can be seen in Figure 106.

*Table 78. Table containing the sample variables for the velocity of detonation samples. The samples had a nominal diameter of 2.5 cm. The LabRAM sample 3 was shorter than the other samples and had one of the lowest densities*

| Sample | | Diameter/ cm | Length/ cm | Mass/ g | Density/ g $cm^{-3}$ | Shot Number |
|---|---|---|---|---|---|---|
| Planetary Mixed | 1 | 2.50 | 20.6 | 156.2 | 1.549 | 2871 |
| | 2 | 2.45 | 20.5 | 150.4 | 1.554 | 2873 |
| | 3 | 2.49 | 20.1 | 150.3 | 1.537 | 2874 |
| LabRAM | 1 | 2.47 | 20.0 | 144.1 | 1.508 | 2872 |
| | 2 | 2.46 | 19.6 | 141.9 | 1.529 | 2875 |
| | 3 | 2.43 | 16.0 | 111.7 | 1.509 | 2870 |

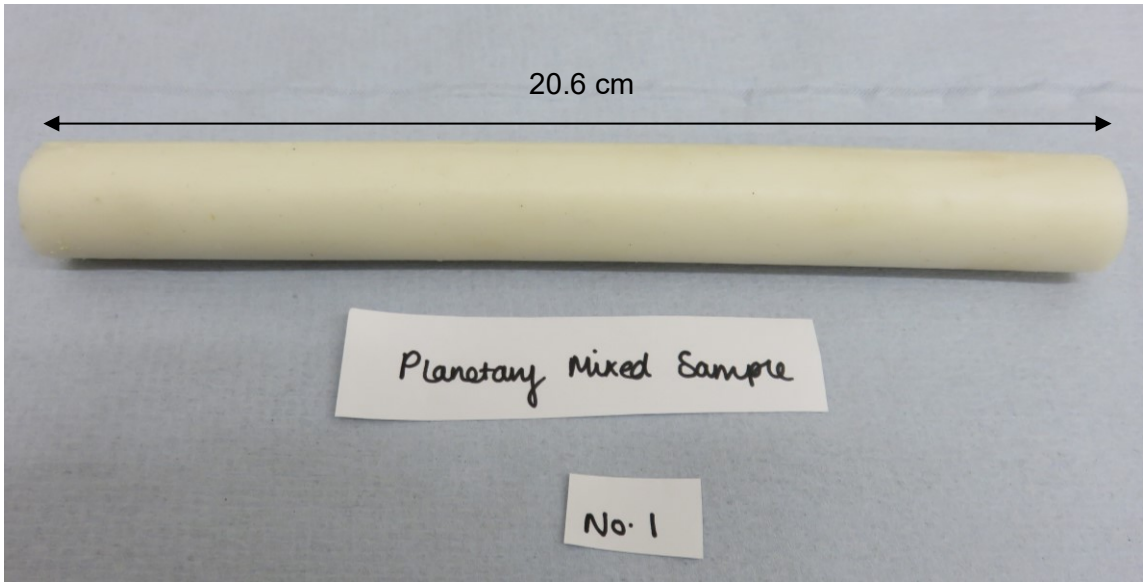


*Figure 99. Photo of planetary mixed VoD sample 1 demonstrating a cylindrical sample with a 20.6 cm length. The sample appears consistent*

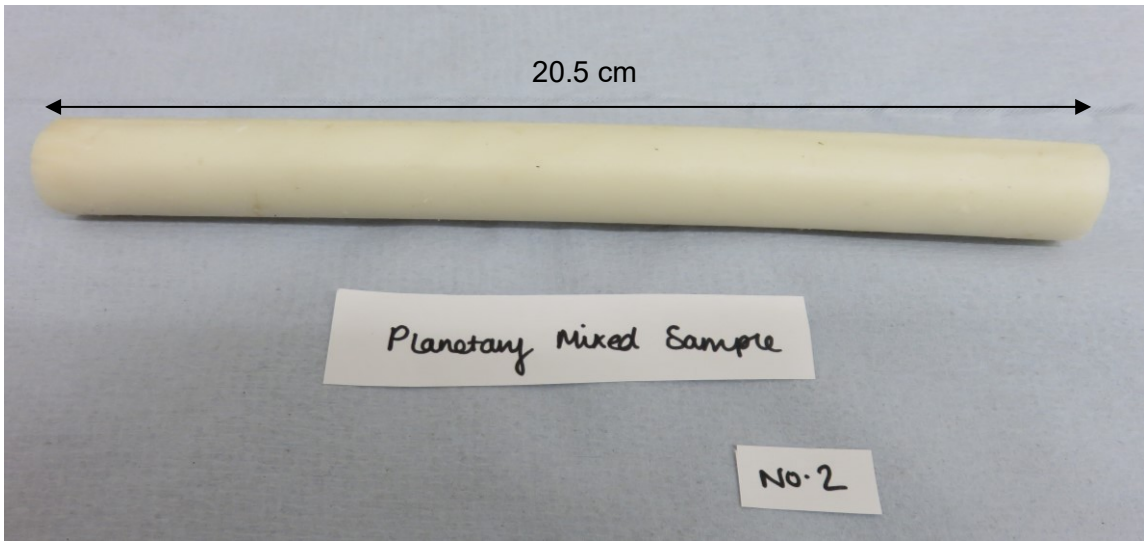


*Figure 100. Photo of planetary mixed VoD sample 2 demonstrating a cylindrical sample with a 20.5 cm length. The sample appears consistent*

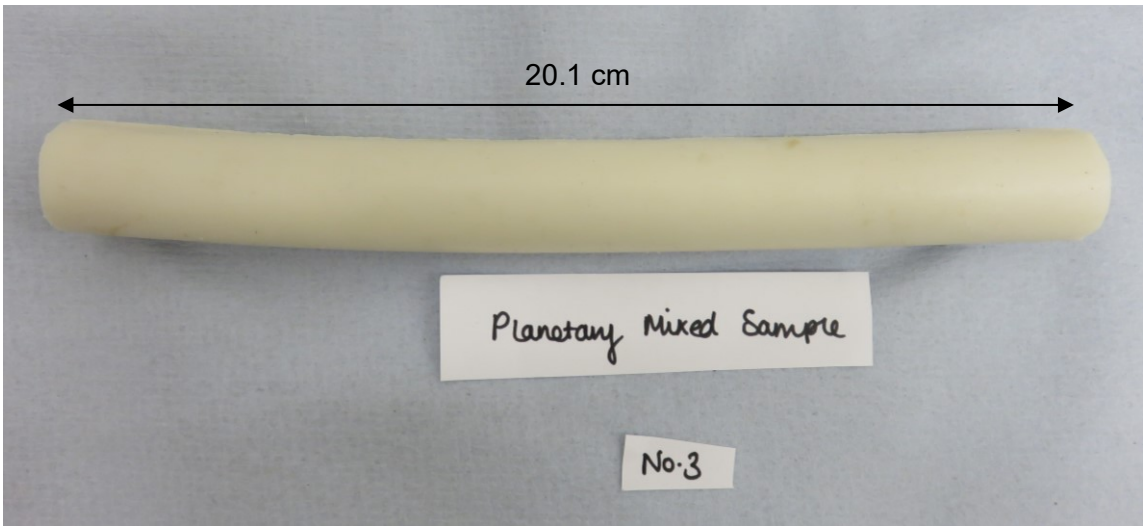


*Figure 101. Photo of planetary mixed VoD sample 3 demonstrating a cylindrical sample with a 20.1 cm length. The sample appears consistent although there is a bit of deformation at the left hand side of the sample*

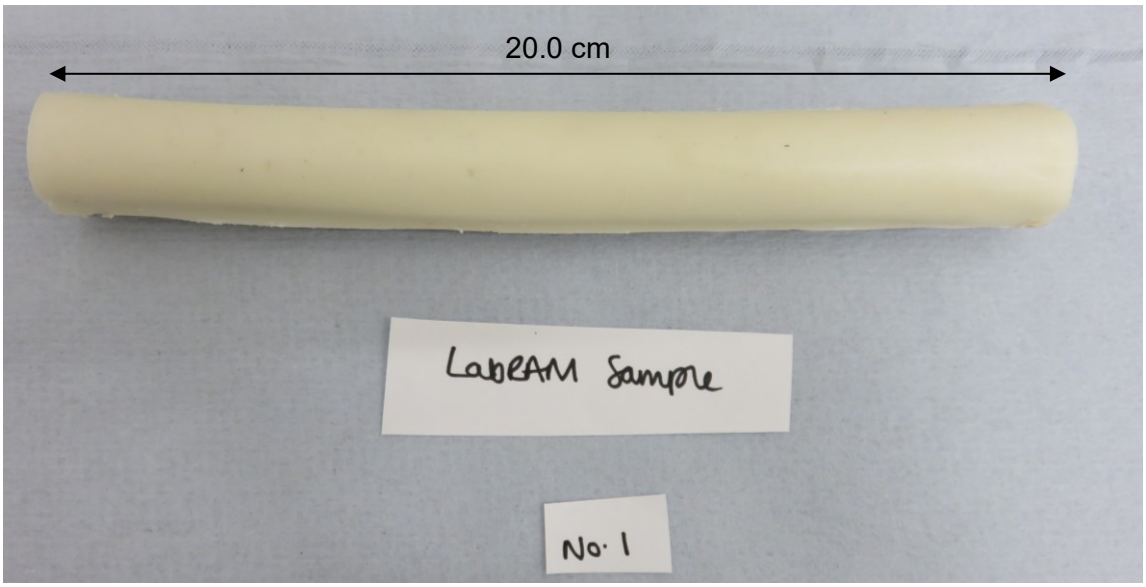


*Figure 102. Photo of LabRAM VoD sample 1 demonstrating a cylindrical sample with a 20.0 cm length. The sample appears consistent although does appear to be deforming at the ends, resembling a banana*

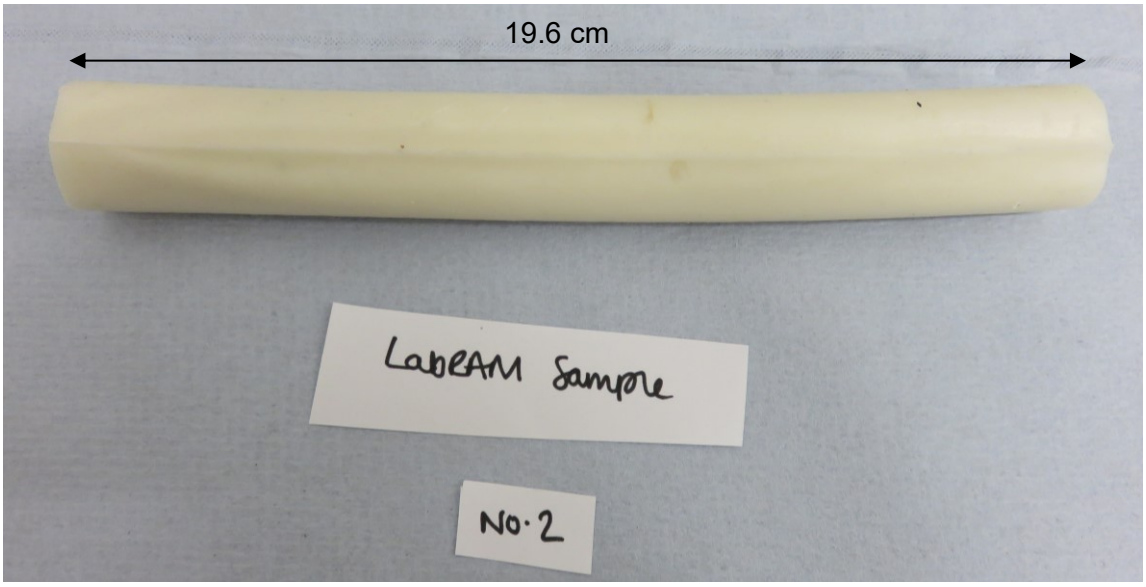


*Figure 103. Photo of LabRAM VoD sample 2 demonstrating a cylindrical sample with a 19.6 cm length. The sample appears consistent*

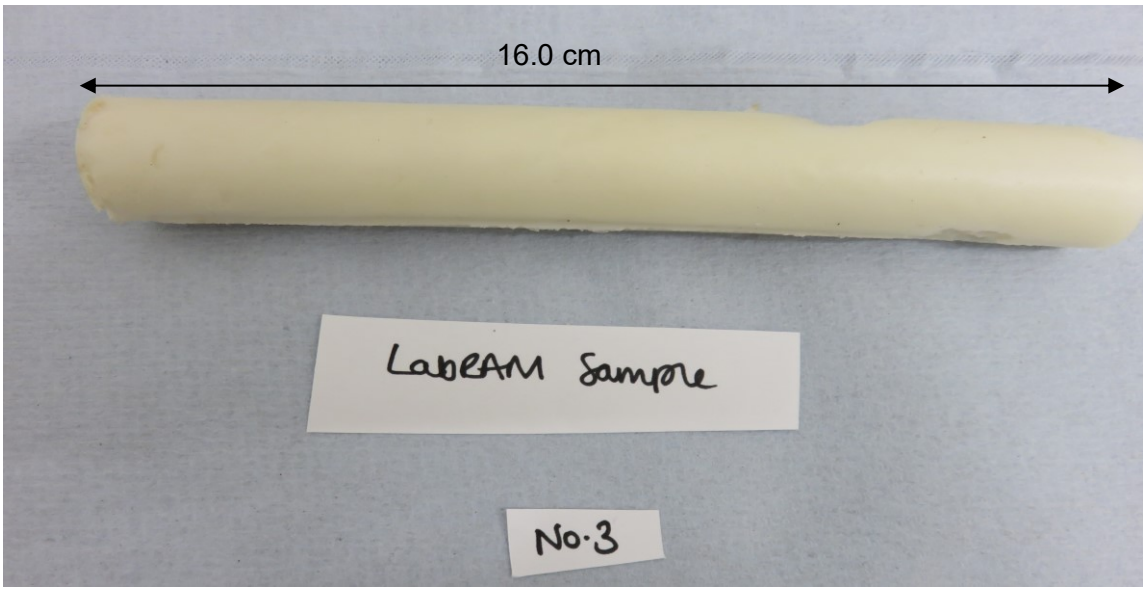


*Figure 104. Photo of LabRAM VoD sample 3 demonstrating a cylindrical sample with a 16.0 cm length. The sample is shorter than the other VoD samples, and exhibits significant voidage towards the right of the sample*

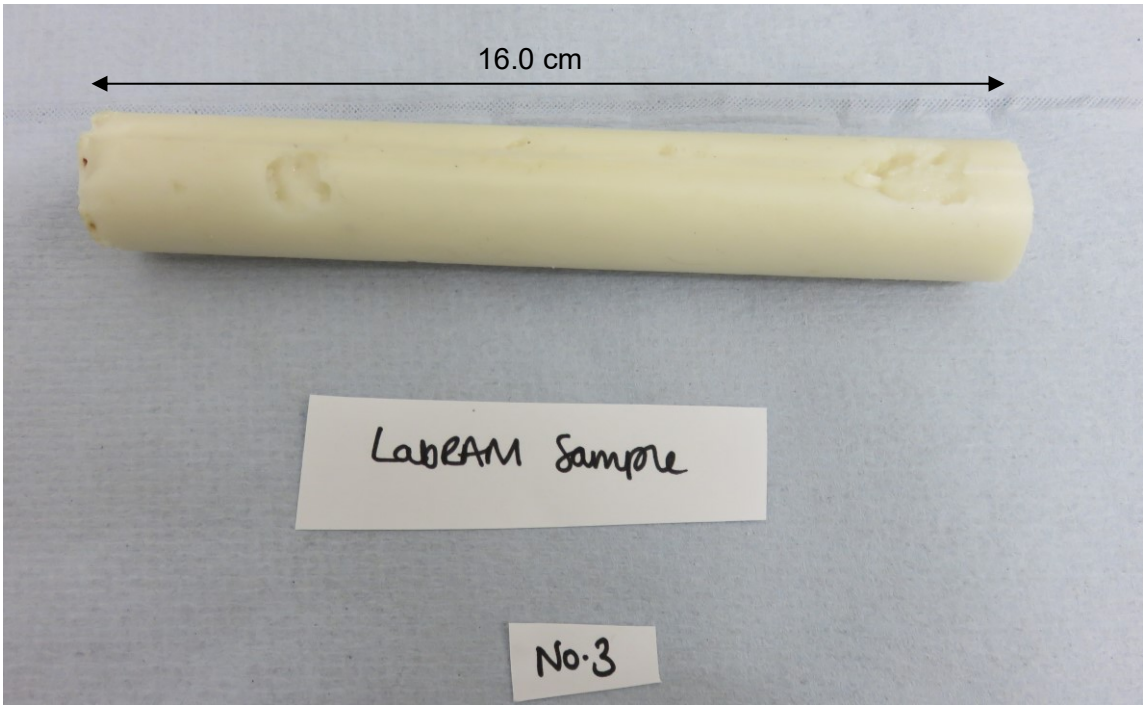


*Figure 105. Photo of LabRAM VoD sample 3 demonstrating a cylindrical sample with a 16.0 cm length. The sample exhibits significant voidage along the length of the sample*

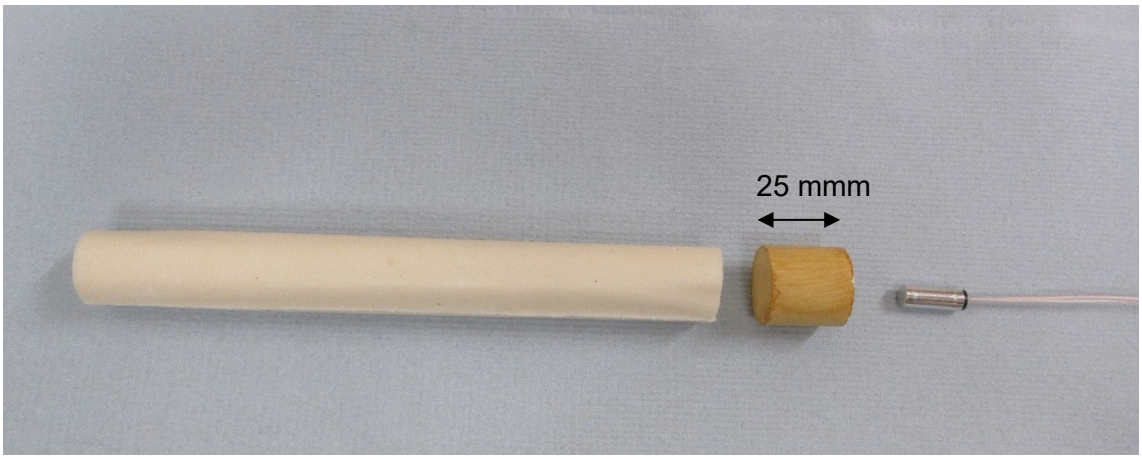


*Figure 106. Photo illustrating the set-up of the explosives for the trial. The VoD sample is placed next to the 25 mm tetryl booster pellet (in contact) and the detonator is placed next to the booster pellet (in contact)*

VoD trials were conducted at the firing range at QinetiQ Fort Halstead. A Cordin streak camera was used; a rotating mirror records light output onto wet film which is then developed in a dark room. The speed of the mirror is 667 μs revolution$^{-1}$, or 6mm μs$^{-1}$. The camera was situated outside of the firing chamber; a mirror was used to reflect the image through a porthole. Chamber set up is seen in Figure 107.

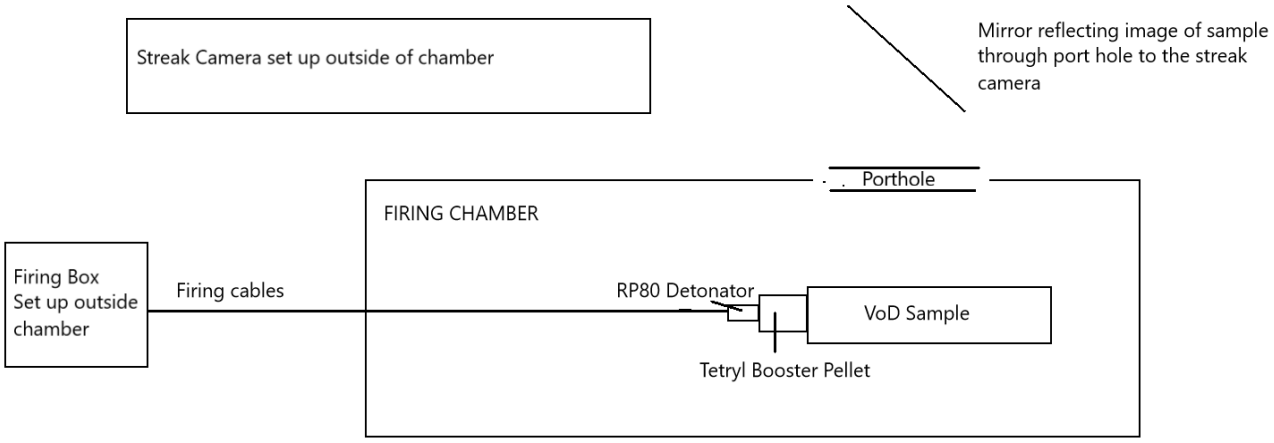


*Figure 107. Chamber set up demonstrating the explosive train contained in the firing chamber with the instrumentation, including the firing box and the streak camera, located safely outside the chamber*

Firings were not done sequentially. Due to voidage in the LabRAM sample 3, it was fired first, Shot 2870, to confirm successful set up so no witness plate was used. Planetary mixed sample 1 was fired next, Shot 2871, and used a 10 mm steel witness plate. Although the sample did not puncture the plate there was damage with a large indentation and spalling at the back of the plate. All further shots used a 5 mm steel witness plate which punctured cleanly. The witness plates are seen in Figure 108, Figure 109 and Figure 110.

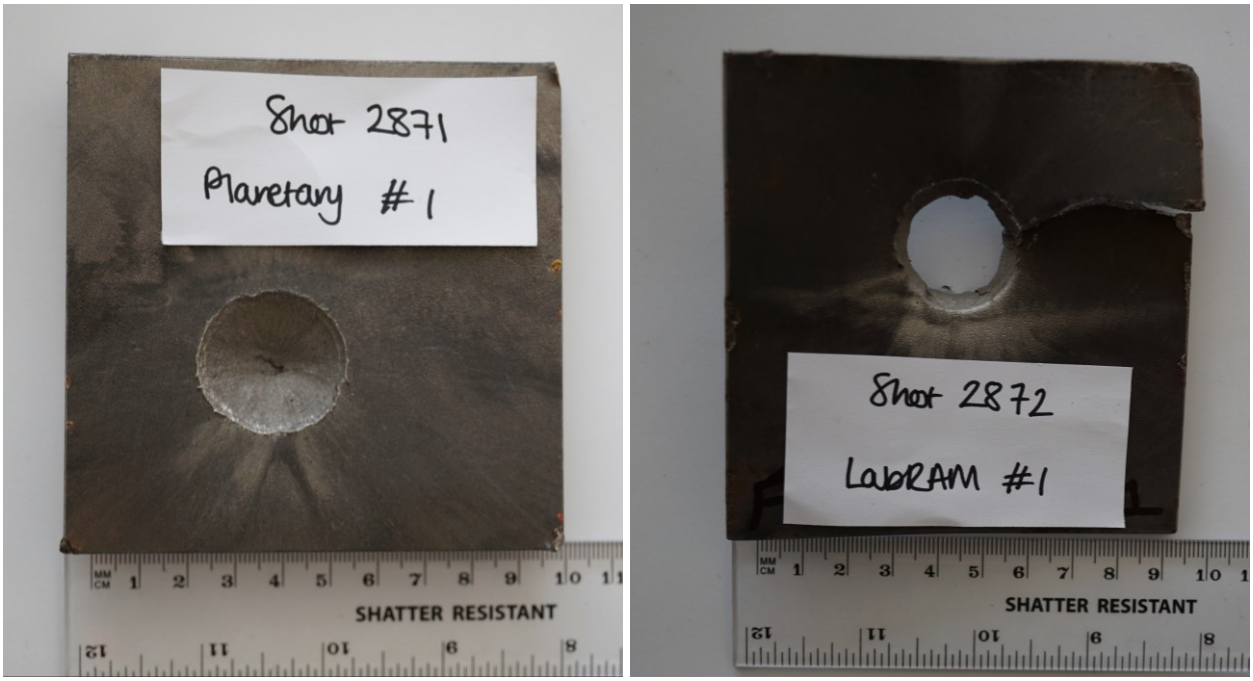


*Figure 108. Witness plates for shots 2871 (PM #1) and 2872 (LR#1). The witness plate for Shot 2871 was 10 mm steel; the charge did not puncture the witness plate. Shot 2872 used a 5 mm steel witness plate; the charge penetrated the plate cleanly.*

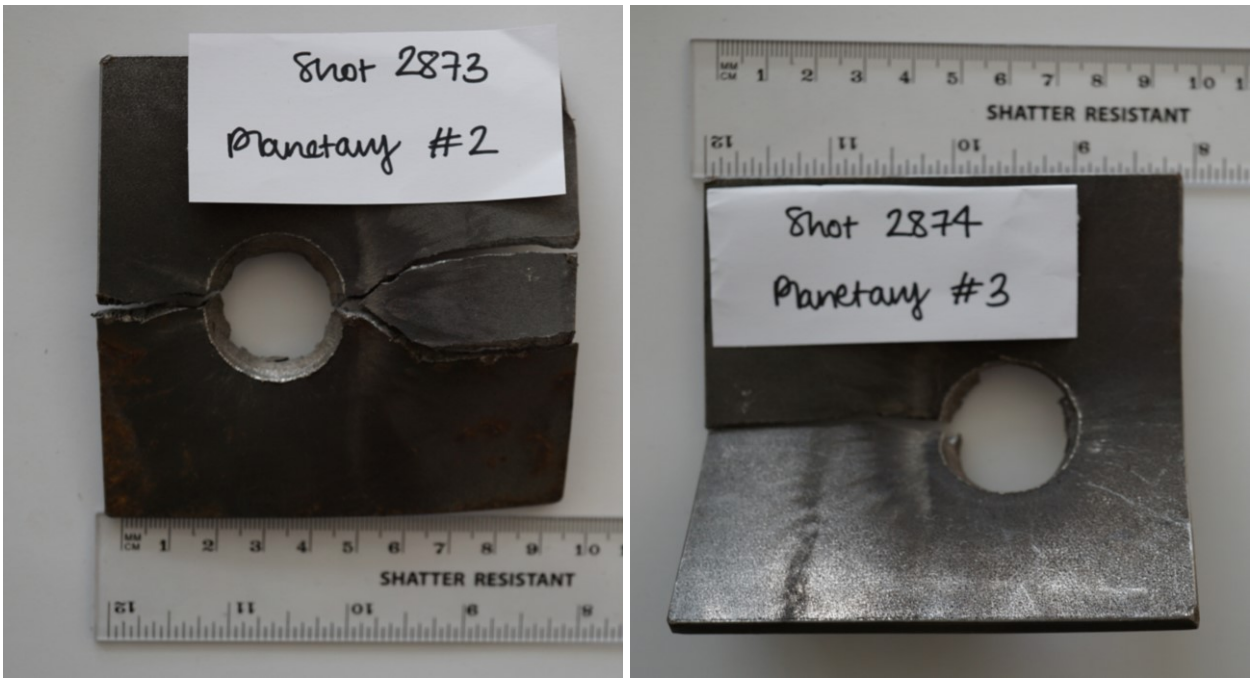


*Figure 109. Witness plates for shots 2873 (PM #2) and 2874 (PM #3). Both samples use a 5mm steel witness plate which have been cleanly punctured by the charges.*

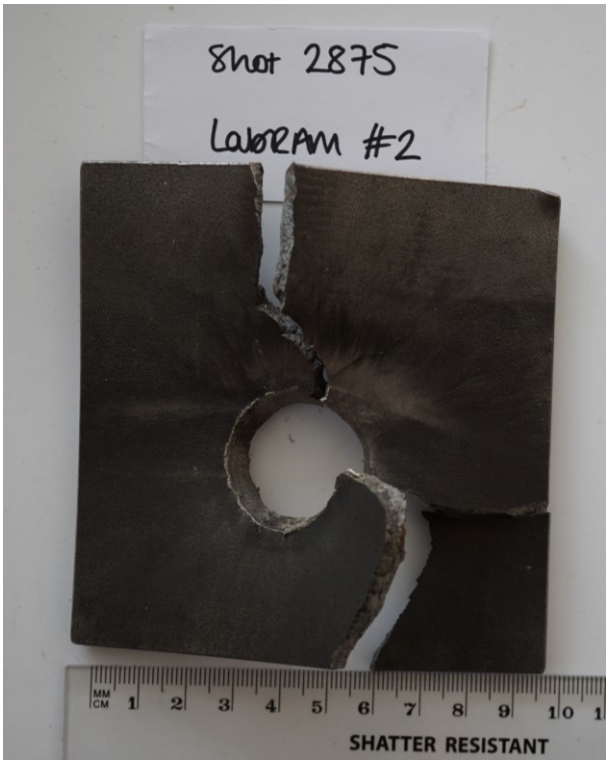


*Figure 110. Witness plate for shot 2865 (LR #2). The 5mm steel witness plate is cleanly punctured by the charge.*

The results were calculated from the Cordin film, seen from Figure 111 to Figure 116 and tabulated in Table 79. The planetary mixed samples had an average VoD of 7716 m $s^{-1}$; the LabRAM samples had a decrease of 0.25% for an average VoD of 7696 m $s^{-1}$. Both sets of samples had a consistent spread of results and the t-test did not provide any evidence to reject the null hypothesis. From these results, mixing via LabRAM did not impact the VoD. The results were compared with literature in Table 80, and demonstrated that these results are appropriate and expected.

*Table 79. Table detailing the velocity of detonation results for the RAM and planetary mixed explosive samples. There was no variation in the results*

| Mixing Method | Sample Number | VoD/ m $s^{-1}$ | Average | % Change | T-Test |
|---|---|---|---|---|---|
| Planetary Mixed | 1 | 7778 | 7716 | -0.25 | 0.92 |
| | 2 | 7788 | | | |
| | 3 | 7583 | | | |
| LabRAM | 1 | 7355 | 7696 | | |
| | 2 | 7859 | | | |
| | 3 | 7876 | | | |

*Figure 111. Streak camera film of Shot 2870 (LR 3). A static image of the sample is observed on the left hand side. As the mirror rotates within the streak camera at 6 mm $\mu s^{-1}$ the light from the sample detonation is projected onto the film. The VoD is calculated from the hypotenuse of the light using the known mirror speed and the length of the sample. Shot 2870 had a sample length of 16.0 cm*

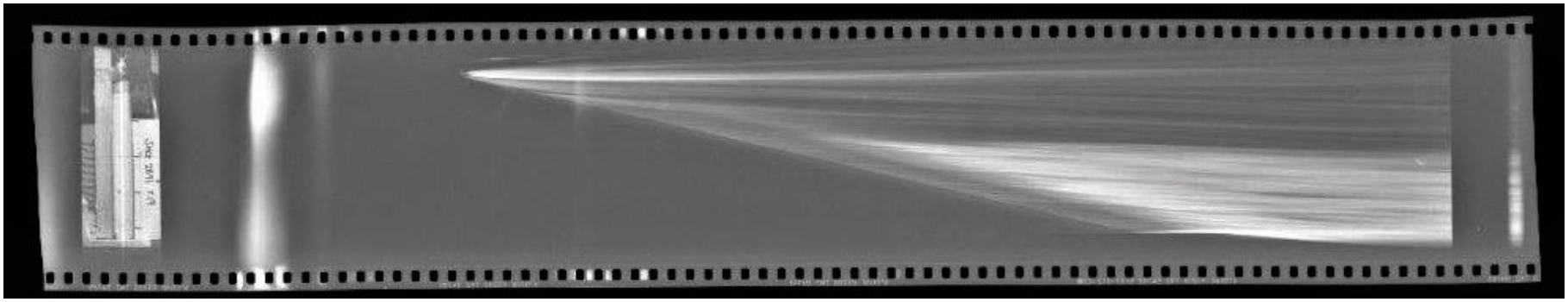

*Figure 112. Streak camera film of Shot 2871 (PM 1). A static image of the sample is observed on the left hand side. As the mirror rotates within the streak camera at 6 mm $\mu s^{-1}$ the light from the sample detonation is projected onto the film. The VoD is calculated from the hypotenuse of the light using the known mirror speed and the length of the sample. Shot 2871 had a sample length of 20.6 cm*

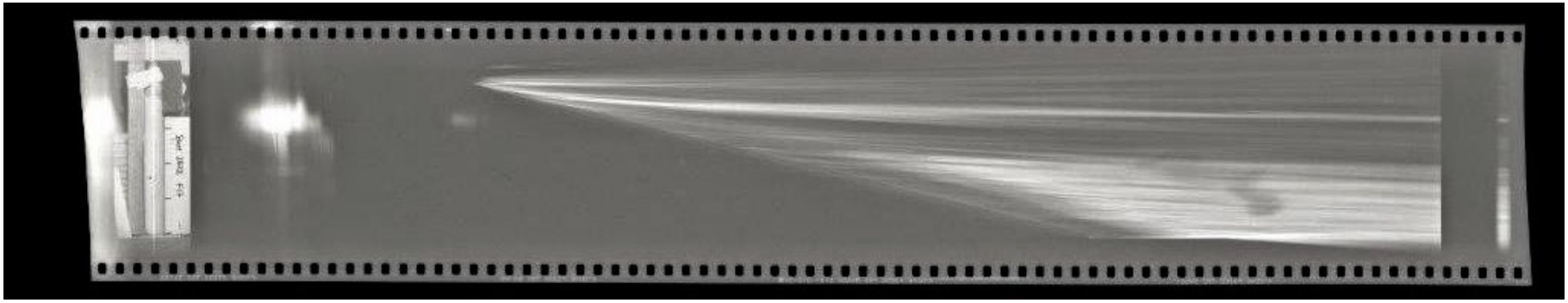

*Figure 113. Streak camera film of Shot 2872 (LR 1). A static image of the sample is observed on the left hand side. As the mirror rotates within the streak camera at 6 mm $\mu s^{-1}$ the light from the sample detonation is projected onto the film. The VoD is calculated from the hypotenuse of the light using the known mirror speed and the length of the sample. Shot 2872 had a sample length of 20.0 cm*

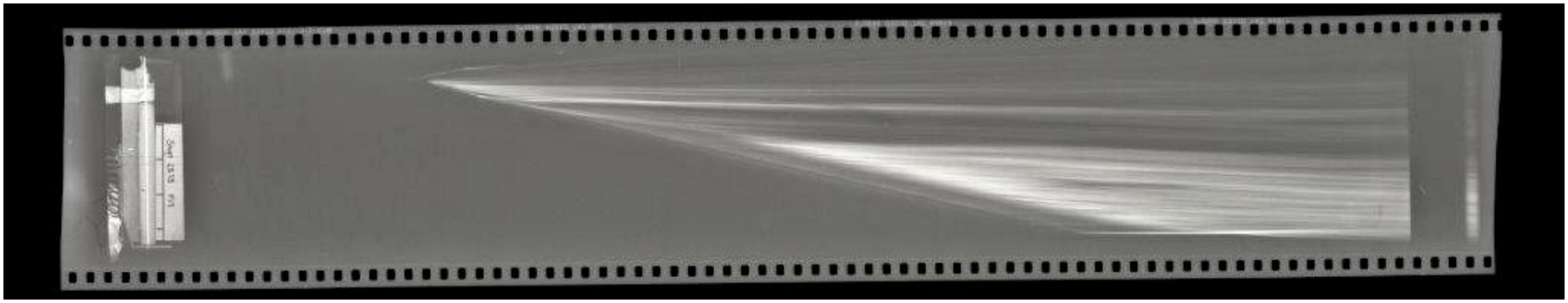

*Figure 114. Streak camera film of Shot 2873 (PM 2). A static image of the sample is observed on the left hand side. As the mirror rotates within the streak camera at 6 mm $\mu s^{-1}$ the light from the sample detonation is projected onto the film. The VoD is calculated from the hypotenuse of the light using the known mirror speed and the length of the sample. Shot 2873 had a sample length of 20.5 cm*

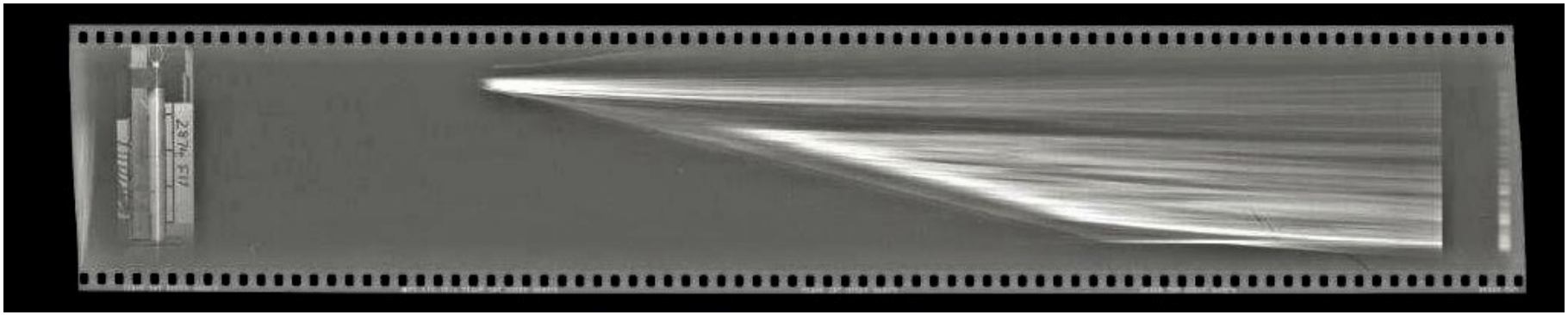

*Figure 115. Streak camera film of Shot 2874 (PM 3). A static image of the sample is observed on the left hand side. As the mirror rotates within the streak camera at 6 mm $\mu s^{-1}$ the light from the sample detonation is projected onto the film. The VoD is calculated from the hypotenuse of the light using the known mirror speed and the length of the sample. Shot 2874 had a sample length of 20.1 cm*

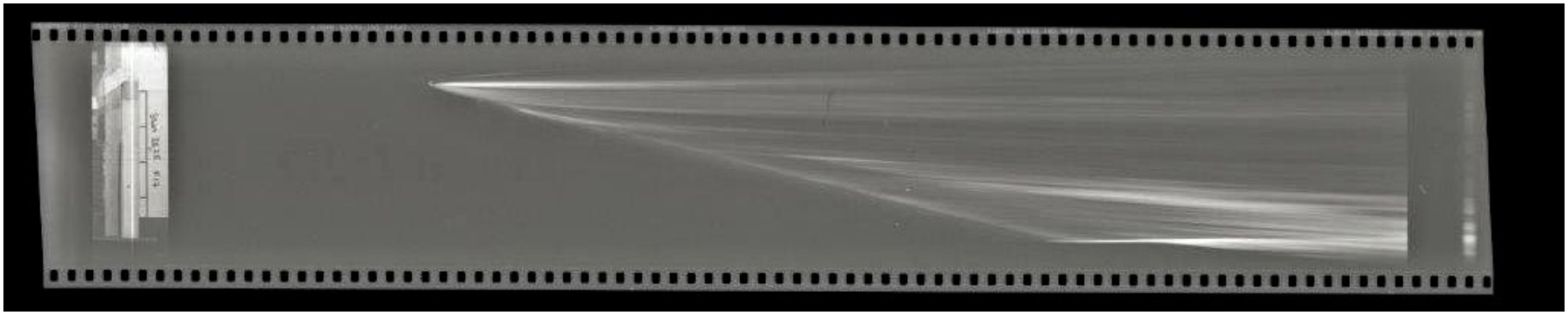

*Figure 116. Streak camera film of Shot 2875 (LR 2). A static image of the sample is observed on the left hand side. As the mirror rotates within the streak camera at 6 mm $\mu s^{-1}$ the light from the sample detonation is projected onto the film. The VoD is calculated from the hypotenuse of the light using the known mirror speed and the length of the sample. Shot 2875 had a sample length of 19.6 cm*

*Table 80. Table comparing the VoD results with literature*

| | | |
|---|---|---|
| **Source with summary of programme** | Cast composite explosives based on hexogen with the maximum detonation parameters, Gordana Antic, Vesna Dzingalasevic [Antic et al, 2003] | Influence of Aluminium on Performance of HTPB-based Aluminised PBXs, Vinay Prakash et al [Prakash et al, 2004] |
| **Material** | PBX-7 with 80% solid loading and an HTPB binder system mixed via a Planetron HKV vertical mixer. Samples have a density of 1.569 g $cm^{-3}$ | PBX based on RDX and HTPB with 85% solid loading mixed in a planetary mixer. Samples had a density of 1.578 g $cm^{-3}$. Samples were 30 mm diameter and 150 mm length |
| **Test Regime** | Measured in the steady-state detonation zone with an electric counter. Method SNO 1475 was quoted but no further details were provided. | Measured by pin oscillographic technique |
| **Results** | 7870 m $s^{-1}$ | Experimental: 7658 m $s^{-1}$ Theoretical: 7750 m $s^{-1}$ |
| **Comparison with this research programme** | The results in literature are within 10% of the results in this chapter. Despite having the same solid loading, the samples in literature have a higher VoD and density. However, this variation is not significant and demonstrates that the results are within range. | The results in this chapter are comparable with the results in this literature. The samples had a 5% higher solid loading which would be expected to provide a higher experimental VoD. The samples in this chapter performed better than the literature and just below the theoretical VoD. |

## 7.5 Conclusion

The energetic samples have not demonstrated any significant change in behaviour due to LabRAM mixing when compared to the baseline planetary mixed samples. The results were consistent for the mechanical, thermal and functionality behaviour. For previous chapters, the material was grouped together to explain material behaviour and highlight the impact, if any, of mixing via LabRAM. As there was only one composition in this chapter it was deemed unnecessary to tabulate the results, and as characterisation variation was insignificant there is no impact on the material and its behaviour.

The DMA results varied within mixing method, likely due to sample preparation. The samples were taken from the bulk causing inconsistent sample size. When comparing the mixing method the planetary mixed samples were stiffer than LabRAM samples possibly indicating poorer HTPB cross-linking in the LabRAM samples. However, the variation was insignificant. Likewise, the hardness testing did not demonstrate significant variation, with the LabRAM samples decreasing in hardness by 3.5% compared to the planetary mixed samples. Hardness testing is highly variable with location of testing and surface defects having a large impact. The results did not provide any evidence to reject the null hypothesis. The density measurements did provide sufficient evidence to reject the null hypothesis due to the high reliability of the test; however, the variation was insignificant with the LabRAM samples demonstrating a decrease of 0.24%. This demonstrates that mixing via LabRAM has not impacted the filler packing, binder density or overall density of the sample.

The DSC and TGA results did not demonstrate any variation between mixing methods; both are dominated by the RDX transition point. The mass loss was nominally 80%, which is the mass percentage of RDX within the composition, and decomposition occurred at 215 °C.

Hazard data tested the response to a range of stimuli, including friction, impact, thermal and electrostatic. All results bar the rotter and temperature of ignition were identical between mixing methods demonstrating no variation in the sensitiveness of the material. The temperature of ignition and the rotter testing, whilst not identical, were consistent and demonstrated no significant variation. The functionality test demonstrated that there was no impact to the functionality of the material, and although there was a decrease in the velocity of detonation of the LabRAM samples it was not significant nor was there any evidence to reject the null hypothesis.

Although the other properties demonstrated no significant variation, the NMR results for LabRAM samples demonstrated lower extractable HTPB concentration implying greater

cross-linking. By the definition of this study this was both a significant variation, greater than 10%, and provided sufficient evidence to reject the null hypothesis. The null hypothesis states that there is no statistical variation between the LabRAM and the planetary mixed samples. The DOS concentration also varied between the LabRAM and the planetary mixed samples. It demonstrated that there was inhomogeneity in both sets of samples, regardless of mix method, but the variation was insignificant.

The NMR results indicate that the samples should be softer for the planetary mixed samples but the mechanical behaviour is consistent between the mixing methods. The NMR samples were taken from a different location within the bulk material to the DMA samples for both mixing methods, demonstrating variability in the behaviour of either sample set. As all other results are consistent, it is not possible to conclude which sample is variable. However, although the NMR results demonstrate inconsistency between the planetary mixed and the LabRAM samples, the other material properties are consistent between the two mix methods. As such, there is no evidence to suggest that mixing via LabRAM has significantly impacted these materials.

# 8 Mixing Theory

This study highlighted that the application of appropriate sample specific mix parameters is the greatest limitation of this technique. LabRAM has a bulk mixing zone and smaller multi-mixing zones throughout which encourages greater mix efficiency in a shorter duration; however, there is dependency on viscosity, input and the presence of a vacuum, as well as countless other variables. Conventional planetary mixing uses intrusive mix blades which force flow and reduce variability in input. In the literature review in Chapter 2.3 there is no consistency between mixing parameters and materials, implying the mix theory is still not well understood. This is one of the main hindrances to the scale up and industrialisation of LabRAM. This chapter has the following format: identifying remote mixing parameters, identifying the influence of variables on mixing and identifying mixing mechanisms for a range of materials.

## 8.1 Observed Mixing Mechanisms

Throughout this programme there have been four key mixing mechanisms observed that enable mixing in different material types. These are particular for viscous slurries. These are:

1. Macro-mixing
2. Micro-mixing
3. Volcano effect
4. Sample debonding

Macro- and micro-mixing has been discussed in the literature [Bickley, 2009] [Tanaka et al, 2016]. Macro-mixing is movement through the bulk of the material, and is what would be observed in conventional mixing techniques. It is good for distributing components so that large areas of sample are consistent. However, it is not as effective at the smaller localised areas. In comparison, micro-mixing does mix these small highly localised regions, typically around 50 microns [Bickley, 2009]. Figure 117 illustrates both these mechanisms.

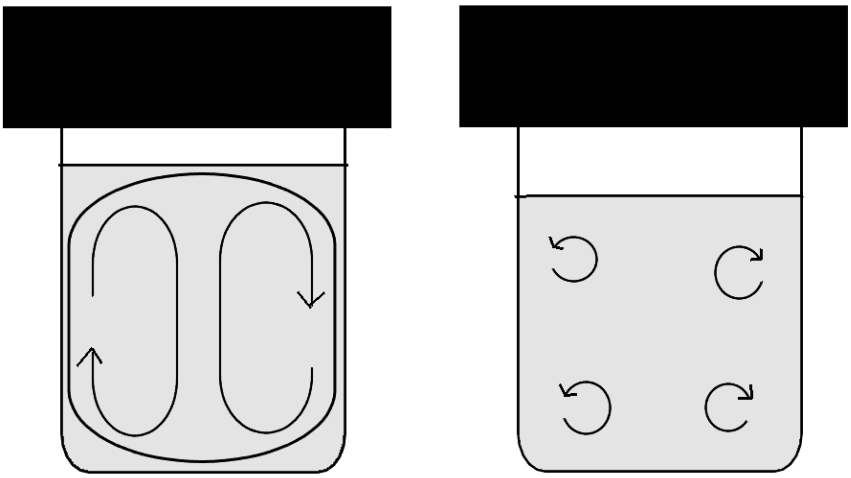

*Figure 117. Diagram demonstrating the macro- and micro-mixing mechanisms. Macro-mixing, on the left, mixes the bulk of the material, whereas micro-mixing, on the right, mixes small localised zones*

The volcano effect is a version of the macro-mixing mechanism. The material flows from each side of the bottom of the vessel into the centre, upwards to the surface and outwards to the edges of the vessel, mimicking a volcano. It ensures the entire bulk of the material flows within the vessel. Debonding has been reported in the literature [du Plessis, 2016] and was used as a way of mixing viscous slurries. The sample, typically at high acceleration, forms a cohesive mass and debonds from the mix vessel. It usually moves throughout the vessel impacting the vessel walls and does not enable flow within the material. These mechanisms are pictured in Figure 118.

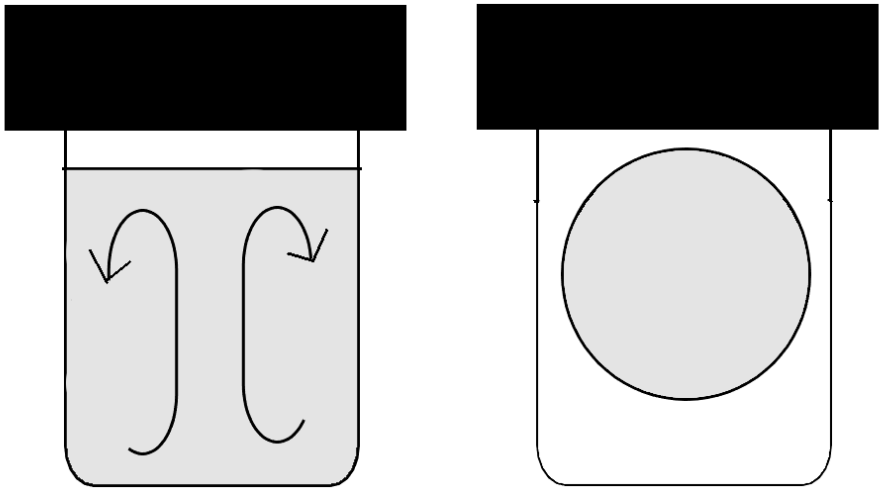

*Figure 118. Diagram demonstrating the volcano effect and the debonding mechanisms. The volcano effect, on the left, draws material up through the centre of the vessel and forces it down along the edges. In comparison, the debonding on the right hand side causes the material to detach from the vessel*

## 8.2 Mixing Indicators

During this study, input was controlled manually. During the inert phase, clear plastic pots were used and the mixes were conducted in the same room; flow was visually observed within the vessel.

Mixing of energetics was conducted remotely and in opaque pots so indicators were used to assess mixing. A 2-phase composite with a low viscosity liquid and pre-dispersed powder was mixed in a clear polystyrene pot and a relationship was seen between mixing, the frequency and temperature rise. Figure 119 is the mixing diagram and the acceleration was set at 40 G. Whilst the sample was stationary and there was no flow and mixing the frequency, power input and temperature remained constant on the mixing diagram. Once the sample started to flow the frequency fluctuated causing changes in the power input. This occurred at 43 minutes. The temperature also increased as a result of friction as the sample flows. These mixing indicators can be determined remotely which has positive safety and scale up implications. There is no “one solution fits all” with this technology, as was seen quite clearly throughout the literature review. Therefore throughout this study an understanding of the mixing behaviour through the mix diagram is a necessity.

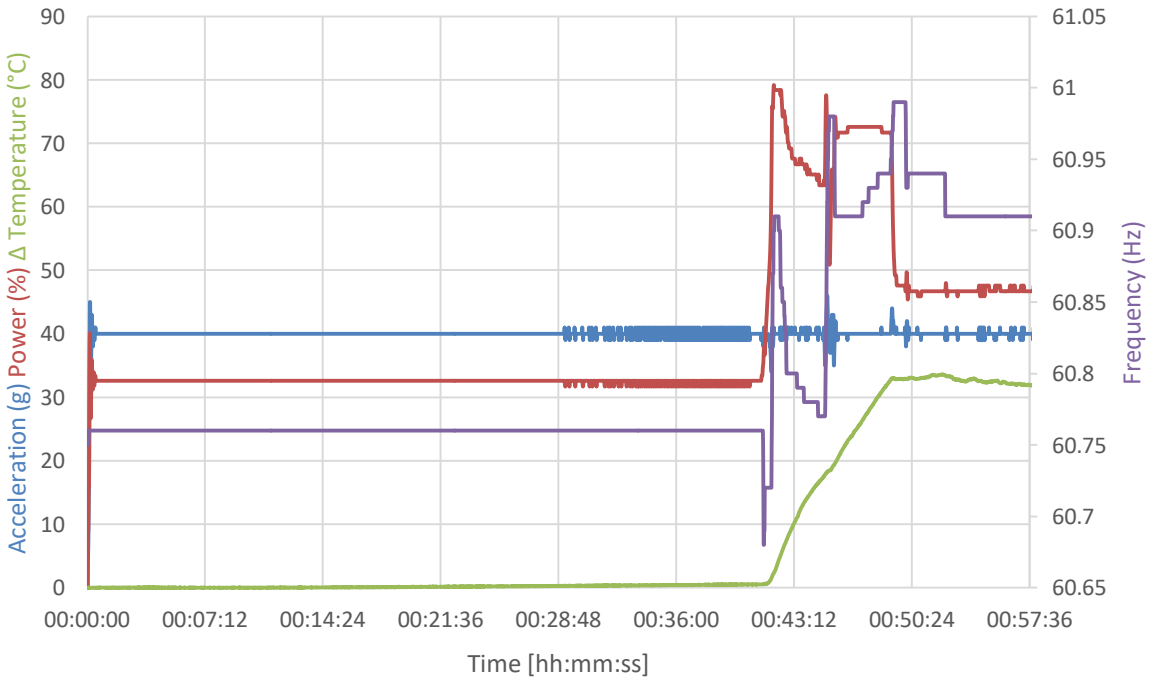


*Figure 119. Mixing diagram- visual mixing coincided with frequency and temperature changes*

## 8.3 Variable Influence

Three key variables have been identified that are suspected to have the most impact on mixing; mass, vacuum and acceleration. Experiments were conducted with the aim of providing an understanding on how they interact and defining a relationship.

### 8.3.1 Influence of mass

Using a clear cylindrical 8 oz polystyrene pot, with a nominal internal diameter of 6.5 cm and height of 8.5 cm, various masses, with the same composition as Chapter 8.2, were tested. A simple mix regime was applied; starting at 10 g, the acceleration was incrementally increased by 10 G until 70 G. Each acceleration was applied for 3 minutes and observations were recorded. Masses tested were 100 g, 125 g, 150 g, 175 g and 200 g. In this phase, de-bonding is material inconsistently flowing along the vessel wall, as opposed to viscous de-bonding where the sample had no contact with the vessel.

Several mixing mechanisms were observed; bubbling, volcano effect, flow, climbing up vessel walls and de-bonding. The mixing mechanisms are described in Chapter 8.1. Bubbling is primarily observed in the liquid binder system when vacuum is applied. The vacuum degasses and dries the sample causing gas to move upwards through the sample. These gas bubbles can vary in size depending on the sample, from sub-millimetre diameters to several centimetres and more. The volcano effect was material flowing up the centre of the vessel and down the vessel walls. Flow is a catch-all term for any movement of material within the vessel; with these samples the most common example of flow was material moving downwards along the vessel walls. Climbing up the vessel walls was characterised as material moving upwards along the vessel walls. Although the majority of this was observed with material breaking away from the bulk, it was also noticed with the bulk sample. Finally, debonding was the material detaching itself from the vessel. This can either be viscous debonding, where the material detaches forming a ball which then bounces within the vessel or non-viscous debonding where the material continues to flow within the vessel but is no longer completely in contact with the vessel walls. The latter was the most common example of debonding.

Table 81 lists the observations for the 100 g sample with the mix diagram plotted in Figure 120. Mixing occurred at 20 G with visible flow. At the 10 G level the sample was stationary. At 30 G and 40 G there was no visual flow of the bulk sample but there were micro-mixing zones in the sample. At these levels mixing is poor. At the highest acceleration the sample debonded and the material was disengaging from the bulk, moving up the walls. The mix

diagram indicates that mixing occurs at 20 G but is unable to differentiate between the mix mechanisms.

*Table 81. Table detailing the mix observations for 100 g sample with testing from 10 G to 70 G. Mixing was observed at 20 G*

| Mass= 100 g | | | | | | |
|---|---|---|---|---|---|---|
| | Bubbling | No movement | Volcano Effect | Flow | Climbing up vessel walls | De-bonding |
| 10 G | X | X | | | | |
| 20 G | X | | X | X | | |
| 30 G | X | | | | | |
| 40 G | X | | | | | |
| 50 G | | | X | X | | |
| 60 G | X | | X | X | X | X |
| 70 G | X | | X | X | X | |

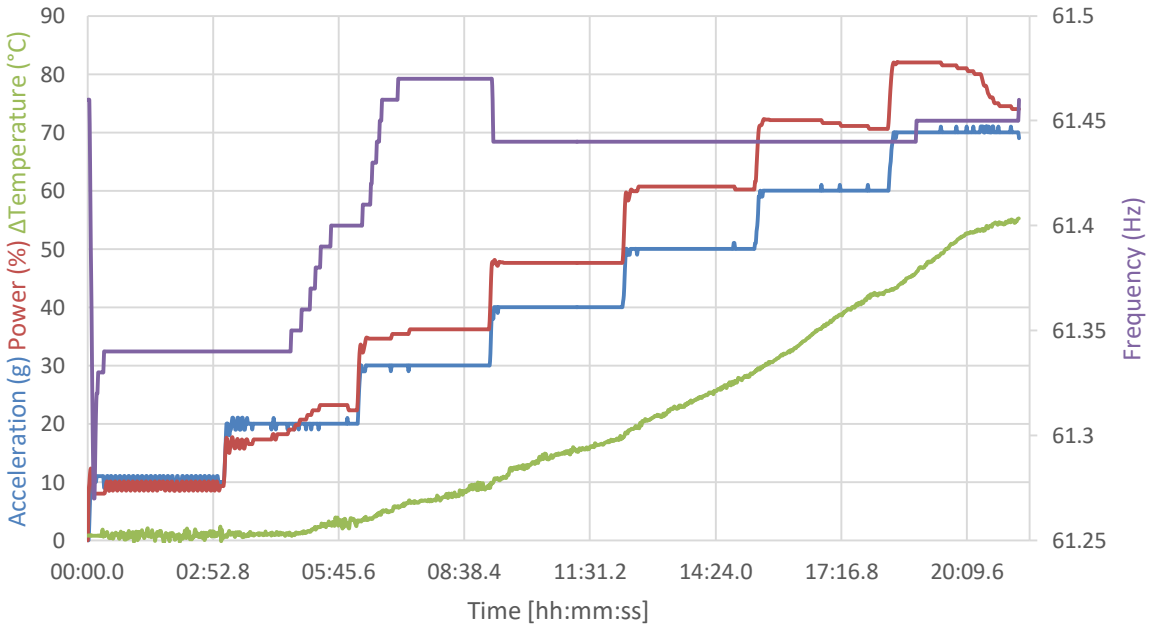


*Figure 120. Mixing diagram for 100 g sample with increases in the power %, frequency and temperature demonstrating mixing at approximately 20 G*

The mass was increased to 125 g and the mixing results summarised in Table 82 and Figure 121. Micro mixing began at 40 G. Prior to this the sample was stationary in the vessel. From

50 G onwards mixing occurred at the macro-level with clear flow and the observed volcano effect. Temperature rise was noted at the 40 G set point but the frequency and power did not increase until the end of the 40 G interval.

*Table 82. Table detailing the mix observations for 125 g sample with testing from 10 G to 70 G. Mixing was observed at 50 G*

| Mass= 125 g | | | | | | |
|---|---|---|---|---|---|---|
| | Bubbling | No movement | Volcano Effect | Flow | Climbing up vessel walls | De-bonding |
| 10G | | X | | | | |
| 20G | | X | | | | |
| 30G | | X | | | | |
| 40G | X | | | | | |
| 50G | X | | X | X | X | X |
| 60G | X | | X | X | | X |
| 70G | X | | X | X | | |

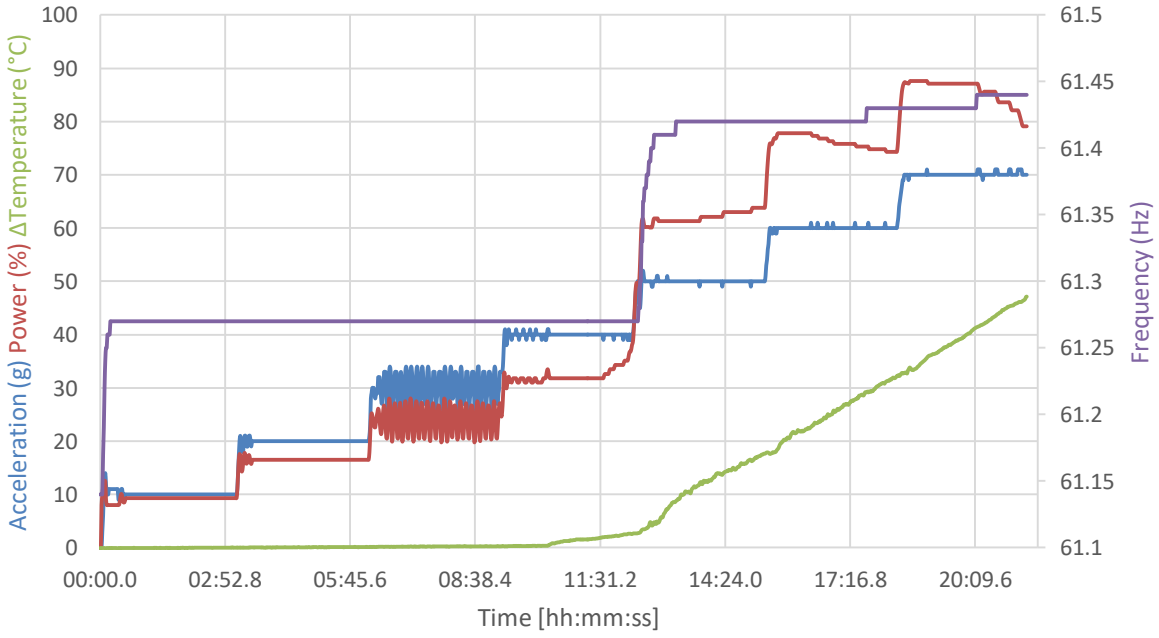


*Figure 121. Mixing diagram for 125 g sample with increases in the power %, frequency and temperature demonstrating mixing at approximately 40 G*

The 150 g sample is summarised in Table 83 and Figure 122. Below 40 G the sample did not mix or flow. Mixing occurred at 40 G when the sample exhibited both flow and the characteristic volcano effect. The mix diagram indicated mixing began at the beginning of the 40 G interval.

*Table 83. Table detailing the mix observations for 150 g sample with testing from 10 G to 70 G. Mixing was observed at 40 G*

| Mass= 150 g | | | | | | |
|---|---|---|---|---|---|---|
| | Bubbling | No movement | Volcano Effect | Flow | Climbing up vessel walls | De-bonding |
| 10 G | X | X | | | | |
| 20 G | | X | | | | |
| 30 G | | X | | | | |
| 40 G | X | | X | X | X | |
| 50 G | | | | X | X | |
| 60 G | | | X | X | | |
| 70 G | | | X | X | X | |

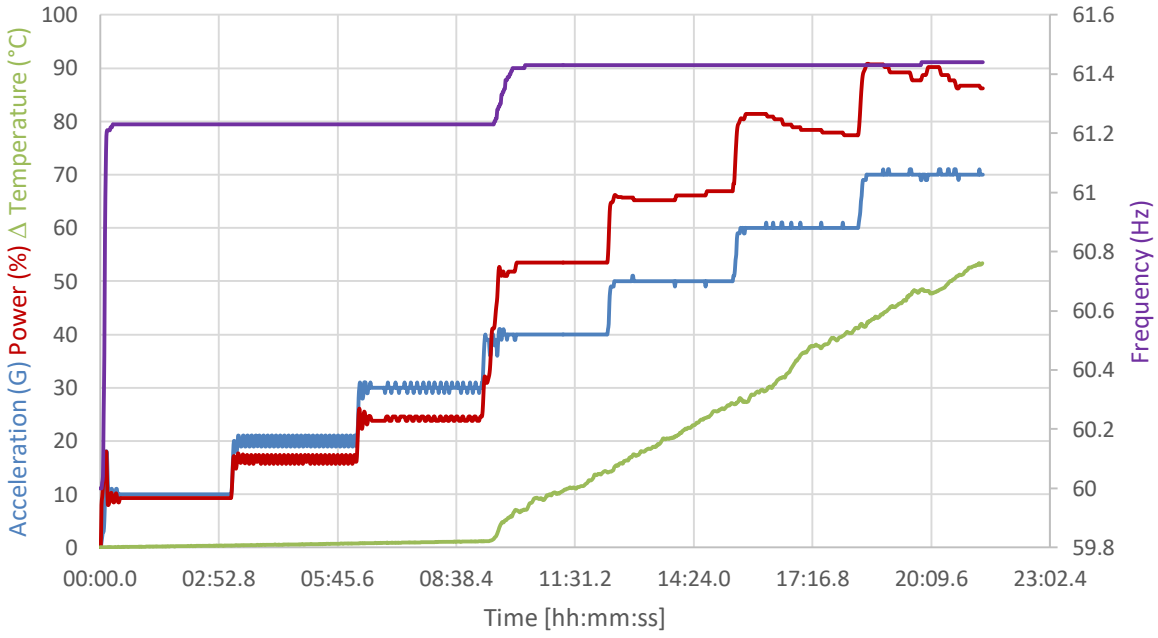


*Figure 122. Mixing diagram for 150 g sample with increases in the power %, frequency and temperature demonstrating mixing at approximately 40 G*

Table 84 summarises the mix observations for the 175 g sample; there was no mixing or mix indicators, in Figure 123, observed throughout the experiment which concluded at 70 G. The LabRAM could not mix this composition at this mass. There was no visual flow, the temperature did not rise throughout the test and the power input was significantly lower than the acceleration set point.

*Table 84. Table detailing the mix observations for 175 g sample with testing from 10 G to 70 G. Mixing was not observed*

| Mass= 175 g | | | | | | |
|---|---|---|---|---|---|---|
| | Bubbling | No movement | Volcano Effect | Flow | Climbing up vessel walls | De-bonding |
| 10 G | | X | | | | |
| 20 G | | X | | | | |
| 30 G | | X | | | | |
| 40 G | | X | | | | |
| 50 G | | | | | X | |
| 60 G | | X | | | | |
| 70 G | | X | | | | |

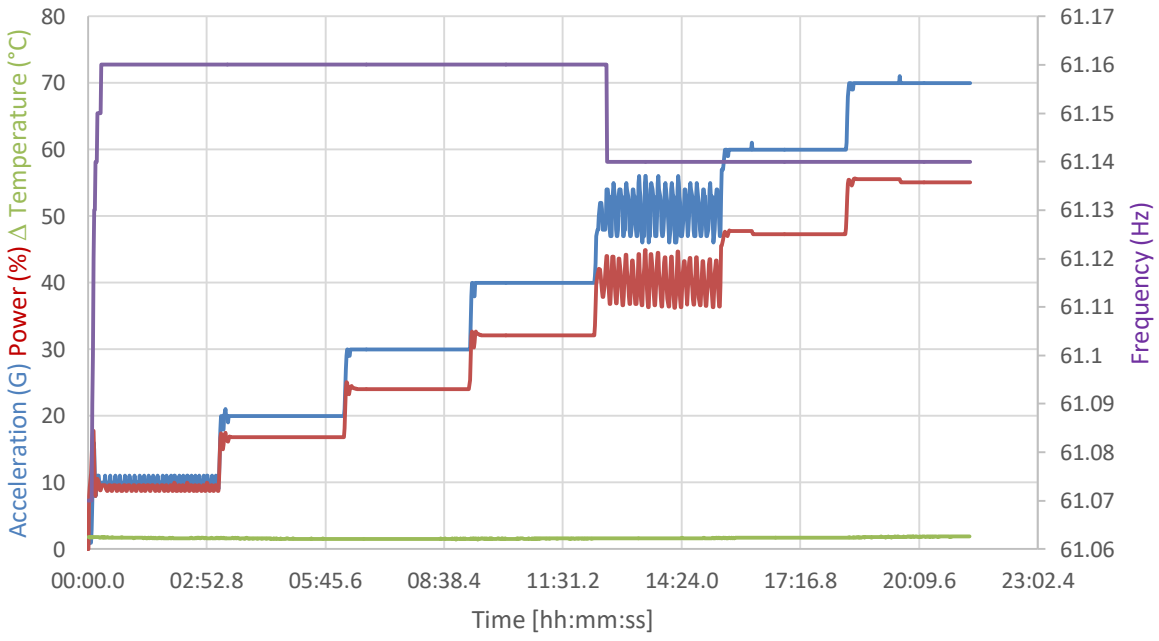


*Figure 123. Mixing diagram for 175 g sample with no indicators for mixing*

As the 150 g sample demonstrated mixing earlier compared to the 125 g sample, an additional increment was added. Table 85 summarises the mix observations for the 200 g sample; there was no mixing or mix indicators, in Figure 124, observed throughout the experiment which concluded at 70 G. Like the 175 g sample, it is concluded that LabRAM cannot mix this composition at this mass.

*Table 85. Table detailing the mix observations for 200 g sample with testing from 10 G to 70 G. Mixing was not observed*

| Mass= 200 g | | | | | | |
|---|---|---|---|---|---|---|
| | Bubbling | No movement | Volcano Effect | Flow | Climbing up vessel walls | De-bonding |
| 10 G | | X | | | | |
| 20 G | | X | | | | |
| 30 G | | X | | | | |
| 40 G | | X | | | | |
| 50 G | | X | | | | |
| 60 G | | X | | | | |
| 70 G | | X | | | | |

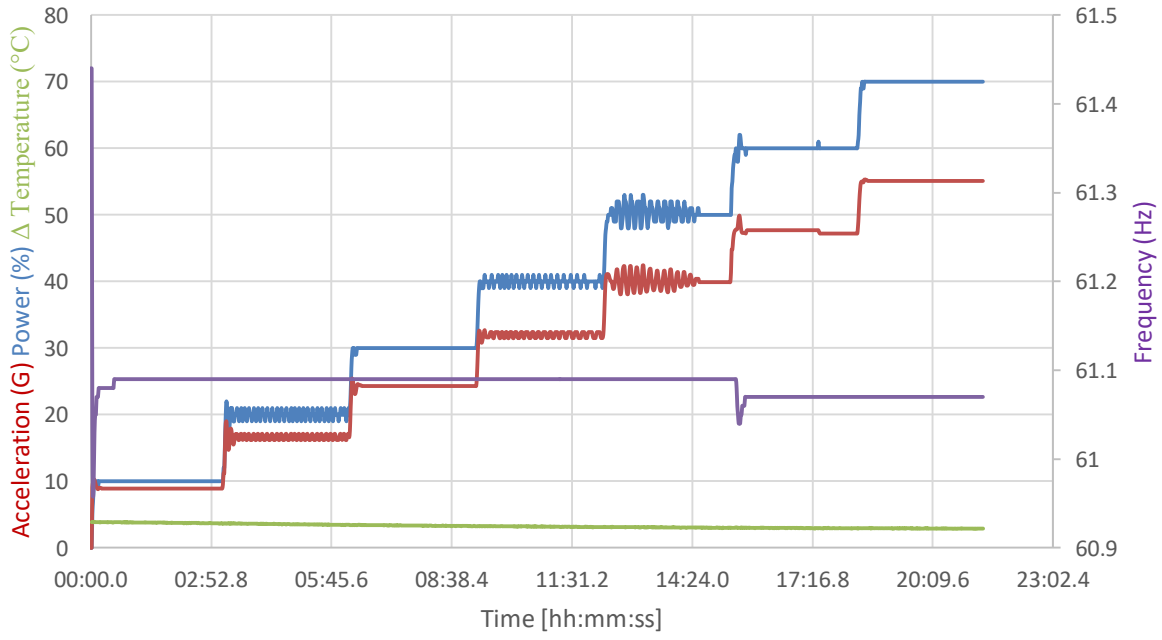


*Figure 124. Mixing diagram for 200 g sample with no indicators for mixing*

The results from these experiments demonstrated the effect of mass on mixing parameters required. The increased mass required higher input to encourage flow within the sample. The smallest mass, 100 g, exhibited mixing at 20 G input whereas 175 g and 200 g did not exhibit any mixing or flow. The results were plotted in Figure 125. A linear relationship was found with the acceleration required for mixing being 0.4 the mass of the sample. This had a positive correlation with an $R^2$ value of 0.75. This is for a specific composition so allowances must be made for alternative materials; however, the greater the amount of sample the greater required input.

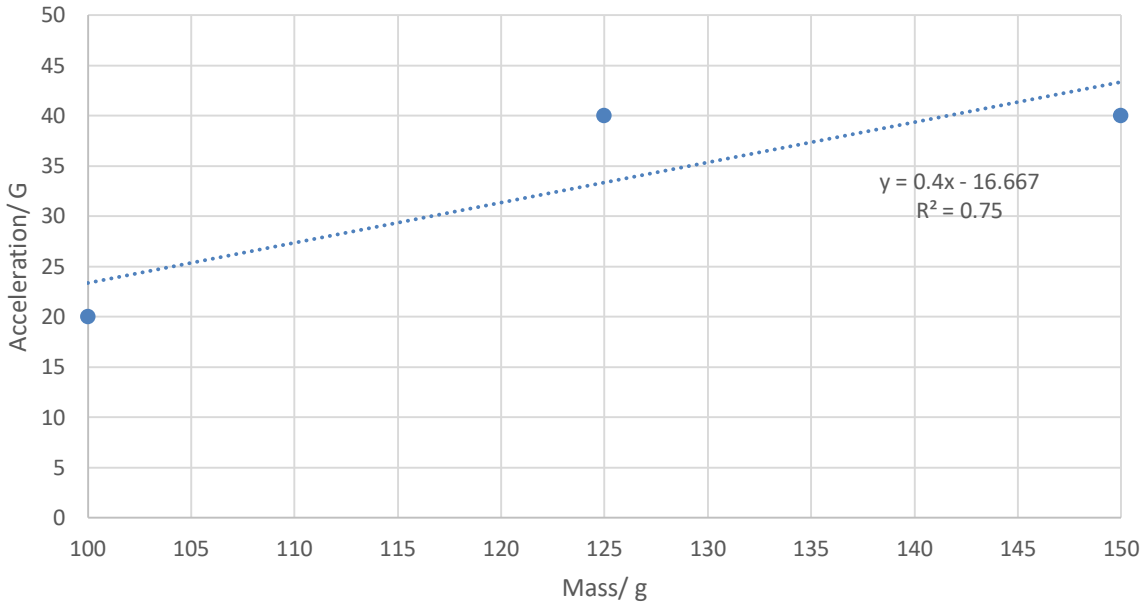


*Figure 125. Graph comparing the acceleration required for mixing to the mass of the sample*

### 8.3.2 Influence of vacuum

The presence of a vacuum is important for enabling flow and mixing. The same composition used in Chapter 8.2 and 8.3 was tested with varying vacuum levels to characterise behaviour and determine the mixing transition. A constant acceleration input of 40 G was used. Several experiments were conducted with each experiment undertaken at least twice; as the results were consistent one mixing diagram and one set of mixing notes for each are included. The four different types of experiments were: no vacuum to full vacuum, 0.3 bar to 0.2 bar, full vacuum to no vacuum and full vacuum with anti-bumping granules added. The sample mass was 125 g.

The first experiment ran from no vacuum to full vacuum (0.005 bar) and is summarised in Figure 126 and Table 86. The vacuum was incrementally decreased with steps of nominally

0.1 bar. No mixing occurred until 0.2 bar, at which point the sample exhibited aggressive mixing with the sample debonding from the vessel.

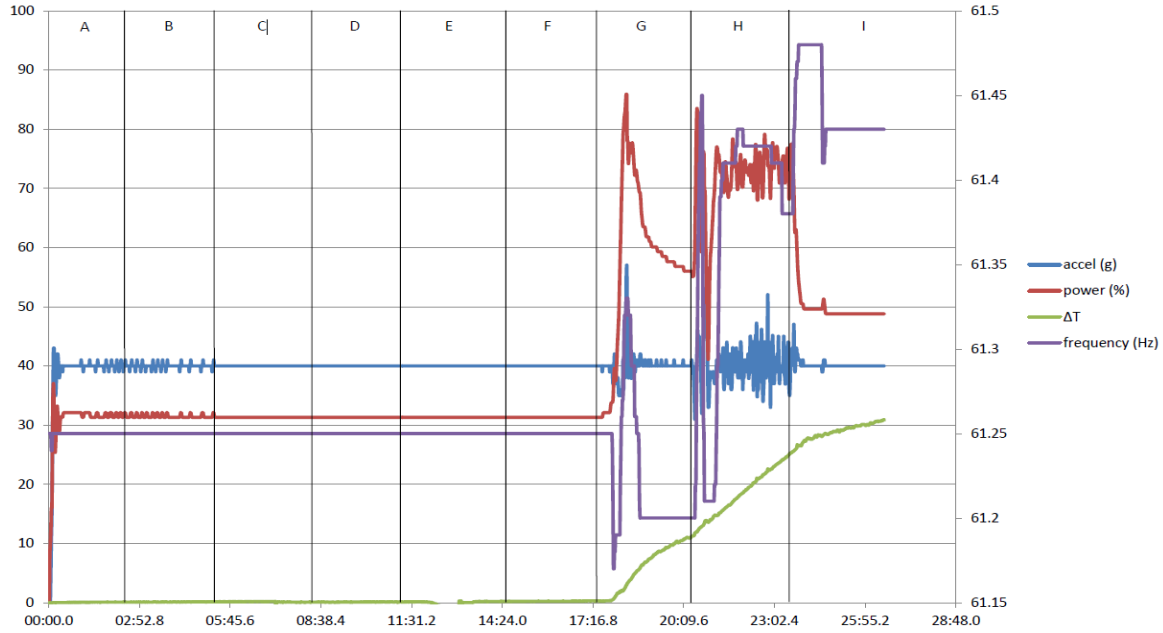


*Figure 126. Mix diagram for a 125 g sample mixed at 40 G, with vacuum applied throughout the mix. Mixing occurred at 0.2 bar*

*Table 86. Mixing notes for mixing experiment run from no vacuum to full vacuum. Mixing occurred at 0.2 bar*

| Section | Vacuum/ bar | Notes |
|---|---|---|
| A | 0.985 | No flow/movement. No bubbling |
| B | 0.727 | No flow/movement. No bubbling |
| C | 0.605 | No flow/movement. No bubbling |
| D | 0.504 | No flow/movement. No bubbling |
| E | 0.403 | No flow/movement. No bubbling |
| F | 0.304 | No flow/movement. No bubbling |
| G | 0.203 | Bubbling. De-bonding. Lots of flow. Variation in height. |
| H | 0.113 | Variation in vac level. Fast flow. De-bonding from vessel. Little bit of jumping |
| I | 0.005 | Vac fully closed. Lots of flow. Stopped jumping and erratically de-bonding. Bulk stationary as vac dropped. Took a while for vac to drop effectively. |

As 0.1 bar is a large increment to determine the go/ no go point an experiment was conducted between 0.3 and 0.2 bar. As can be seen in both Figure 127 and Table 87, there was no mixing until 0.271 bar, at which point the sample immediately experiences flow. Like the no vacuum to full vacuum, mixing was aggressive with rapid flow and debonding of the sample.

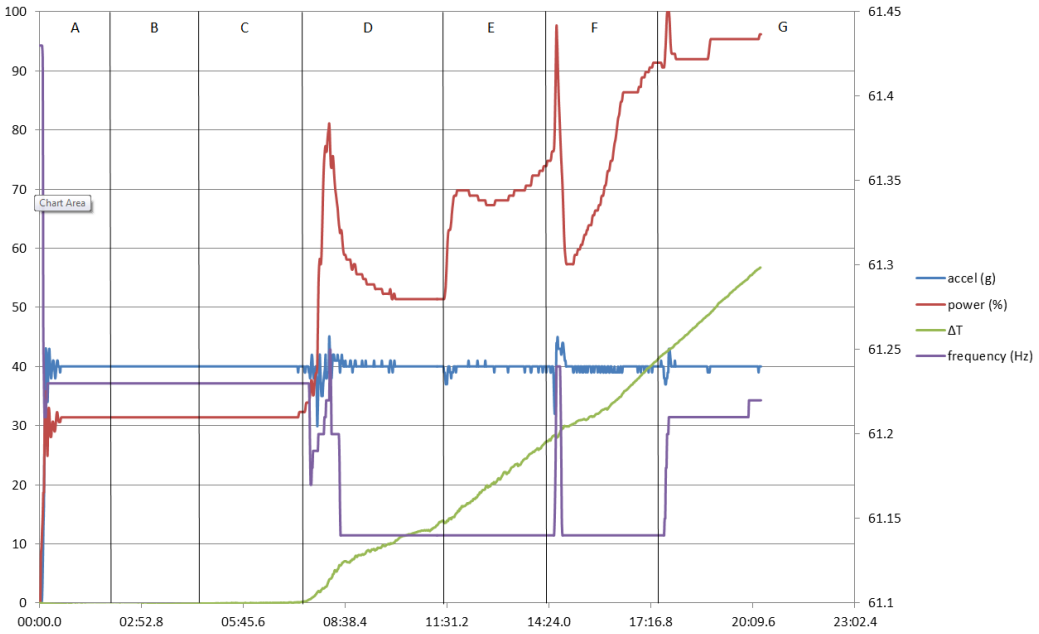


*Figure 127. Mix diagram for a 125 g sample mixed at 40 G, with vacuum ranging from 0.3 to 0.2 bar throughout the mix. Mixing occurred at 0.27 bar*

*Table 87. Mixing notes for mixing experiment run from 0.3 bar to 0.2 bar. Mixing occurred at 0.27 bar*

| Section | Vacuum | Notes |
|---|---|---|
| A | | Vac settling. No bubbling. No flow/movement. |
| B | 0.306 | No bubbling. No flow/movement. |
| C | 0.287 | No bubbling. No flow/movement. |
| D | 0.271 | Immediate flow. Bubbling. Slight de-bonding from walls. Slight variation in vac level (up to 0.28). |
| E | 0.227 | More rapid flow. More de-bonding at bottom of vessel. Little bit of turbulent motion. Occasional jumping |
| F | 0.21 | More rapid flow. Bubbling. |
| G | 0.172 | Very rapid flow. Slight jostling in pot. |

For the next experiment, in Table 88 and Figure 128, a vacuum was applied before the mixer started. Throughout the experiment, the material remained stationary and the sample did not

mix. As previous samples have mixed at these levels of vacuum, as have samples with a clear divide between solid and liquid loadings, it demonstrate that a nucleation point or sufficient density variation is required to initiate mixing. By applying the vacuum before mixing the sample was fully degassed and did not have a nucleation point.


*Figure 128. Mix diagram for a 125 g sample mixed at 40 G, with vacuum released throughout the mix. Mixing did not occur*

*Table 88. Mixing notes for mixing experiment run from full vacuum to no vacuum. No mixing was observed*

| Section | Vacuum | Notes |
|---|---|---|
| A | 0.003 | No bubbling. No flow/movement. |
| B | 0.194 | No bubbling. No flow/movement. |
| C | 0.295 | No bubbling. No flow/movement. |
| D | 0.412 | No bubbling. No flow/movement. |
| E | 0.564 | No bubbling. No flow/movement. |
| F | 0.725 | No bubbling. No flow/movement. |
| G | 0.986 | No bubbling. No flow/movement. |

The full vacuum test had been repeated several times and was found to be consistent; as a result, modifications were made to the sample to introduce defects. Powder was pre-distributed throughout the polymeric matrix and the sample had been degassed prior to the

mix so there was no density variation or nucleation points. Small quantities of anti-bumping granules, non-spherical granules with a nominal diameter of a couple of mms, were added. The addition of these granules enabled flow within the sample. The results are summarised in Table 89 and Figure 129

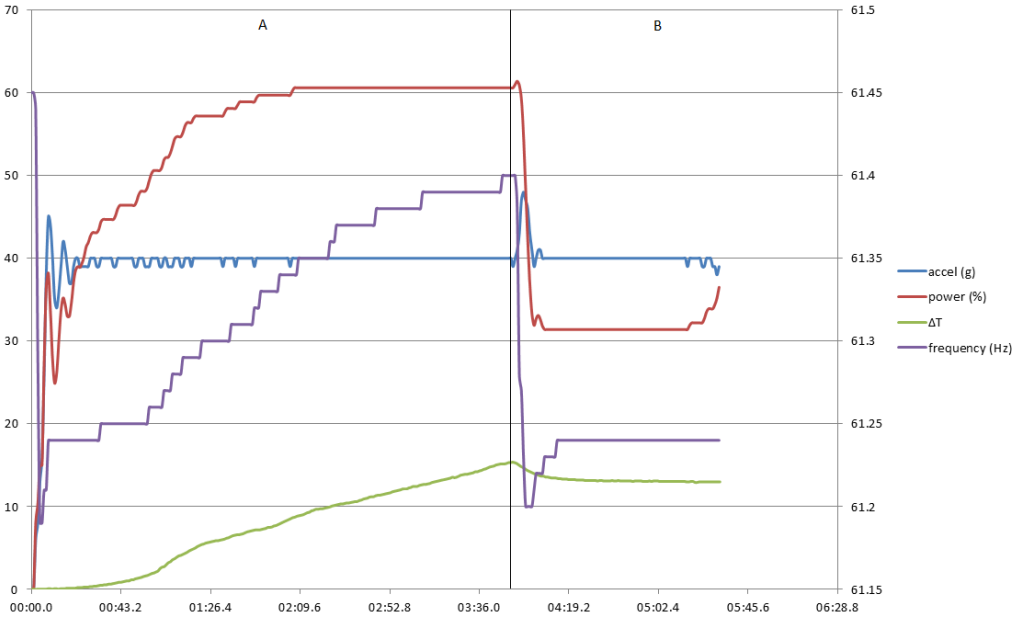


*Figure 129. Mix diagram for a 125 g sample mixed at 40 G with anti-bumping granules, with vacuum ranging from full vacuum to 0.14 bar. Mixing stopped when the vacuum was released*

*Table 89. Mixing notes for mixing experiment with anti-bumping granules run from full vacuum to 0.14 bar. The sample stopped flowing once the vacuum was released*

| Section | Vacuum | Notes |
|---|---|---|
| A | 0.002 | Good flow. Bubbling appearing along walls. Decoupling where bubbles occur. |
| B | 0.137 | Variation in vac levels (from 0.167 to 0.011). Initially still rapid flow. Flow then stopped. No movement |

These experiments are summarised in Table 90 and reiterate this technique's dependency on sample variation. When vacuum was applied during mixing, the sample started to flow at nominally 0.27 bar. When the sample had been fully degassed, no mixing occurred until defects were added. These experiments demonstrate the need for a mix nucleation point, whether that is degassing points, density variation or defects.

*Table 90. Table summarising the four vacuum tests and detailing when mixing occurred*

| **Test** | No vacuum to full vacuum | 0.3 bar to 0.2 bar | Full vacuum to no vacuum | Full vacuum with defects |
|---|---|---|---|---|
| **Summary** | Mixing occurred at 0.2 bar | Mixing occurred at 0.27 bar | No mixing occurred | Mixing occurred immediately and stopped at 0.137 bar |

### 8.3.3 Influence of acceleration

Acceleration experiments were conducted over 10 minutes with still images taken at 10 seconds, 30 seconds, 1 minute, 2 minutes, 5 minutes and 10 minutes. Three acceleration levels were applied: 10 G, 35 G and 70 G. The experiments used 75 ml of coloured sand and HTPB, with the powder added on top of the binder; it typically sunk and congregated forming a binder-powder sandwich, see Figure 130. When acceleration was applied, any powder on the surface was flung around the vessel before it integrated into the material bulk. As stated in the safety case in Chapter 7.3.1, this is a safety issue as material could be repeatedly shocked against the vessel walls.

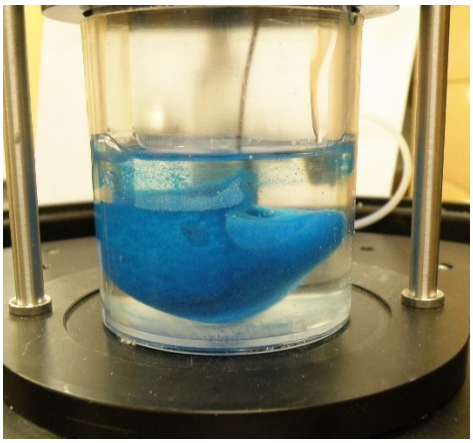

*Figure 130. The sample for mixing liquid-filler composite consisting of HTPB and fine sand prior to mixing. The sand was added on top of the binder but sunk through so when mixing started the sand was already within the HTPB.*

*Table 91. Table detailing the mixing at set intervals for the liquid-sand composite at 10 G. After 10 minutes the sample appeared visually consistent.*

| **10 G** | | |
|---|---|---|
| At 10 seconds | At 30 seconds | At 1 minute |
| 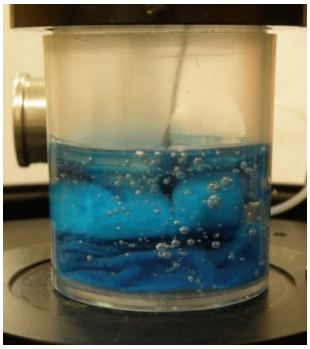 | 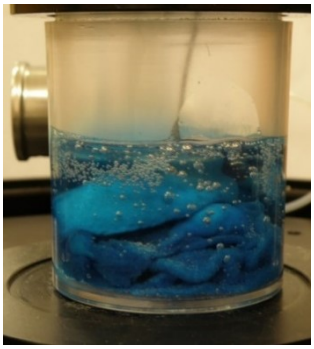 | 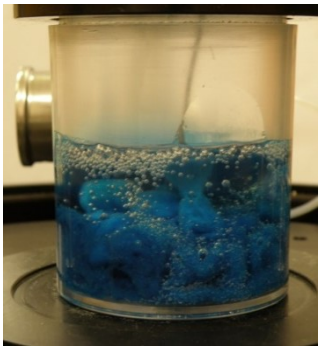 |
| After 10 seconds powder separated out of a large consolidated mass and moved throughout the binder system. | The powder sunk to the bottom of the vessel and the bulk has separated into independently moving phases. A micro-mixing zone can be identified in the bottom right corner. The powder has not integrated within the binder system. | There was distribution throughout the bottom of the sample. The top remains pure binder. |
| At 2 minutes | At 5 minutes | At 10 minutes |
| 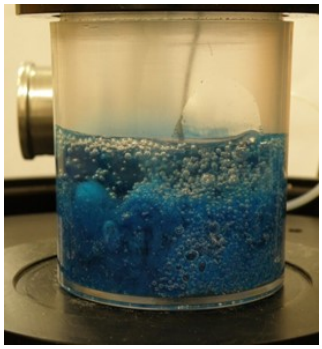 | 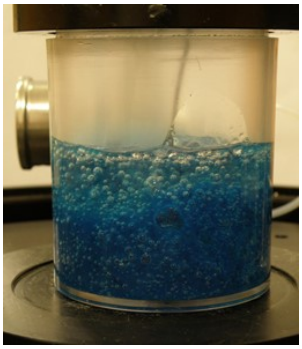 | 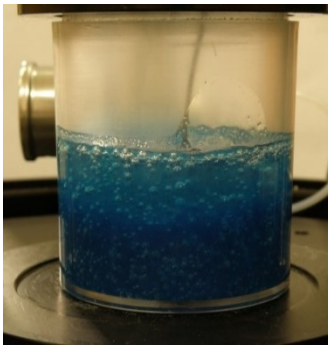 |
| The bottom half of the sample exhibited a greater degree of mix as binder and powder are no longer distinct phases. The sample top has not changed. | The powder dispersed throughout the binder system with a gradient. The bottom of the vessel appears to have more powder. | The powder dispersed more effectively throughout the binder; the sample still has a large gradient of powder concentration though |

*Table 92. Table detailing the mixing at set intervals for the liquid-sand composite at 35 G. After 2 minutes the sample appeared visually consistent.*

| **35 G** | | |
|---|---|---|
| At 10 seconds | At 30 seconds | At 1 minute |
|  | 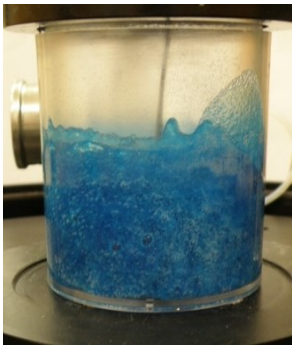 | 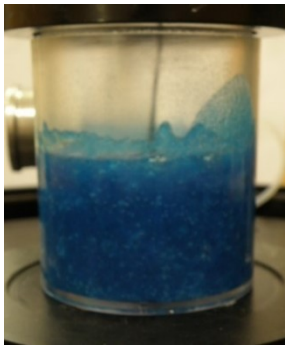 |
| The bulk powder began to disperse throughout the sample and formed multiple phases | Powder has integrated within the binder and there are no distinct phases. However, there is variation within the sample | The sample appears mostly mixed after a minute. There is minor variation with a powder gradient throughout. |
| At 2 minutes | At 5 minutes | At 10 minutes |
| 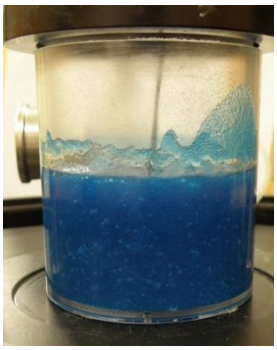 |  | 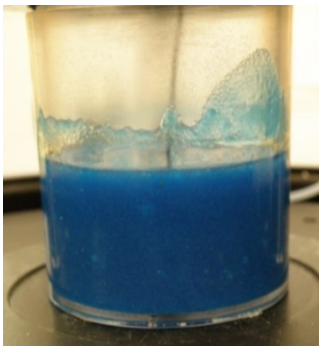 |
| The sample appears fully mixed. | There are no observable changes in the sample after an additional 3 minutes | The powder is fully distributed after mixing for 10 minutes at 35 G. |

*Table 93. Table detailing the mixing at set intervals for the liquid-sand composite at 70 G. After 2 minutes the sample appeared visually consistent.*

| **70 G** | | |
|---|---|---|
| At 10 seconds | At 30 seconds | At 1 minute |
| 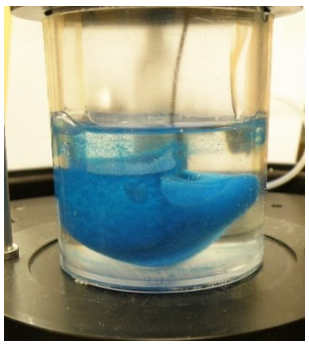 | 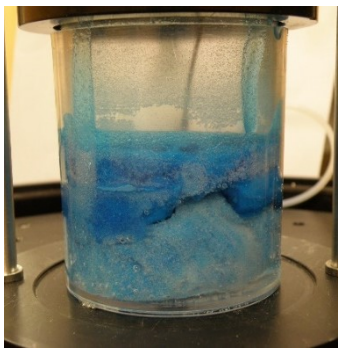 | 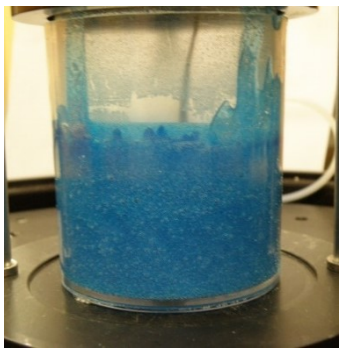 |
| Bulk powder remained a distinct phase within the binder system and mixing had not started | The consolidated powder began to separate and two powder phases dispersed through binder were observed | The powder was dispersed throughout the binder with visible variation in the centre |
| At 2 minutes | At 5 minutes | At 10 minutes |
| 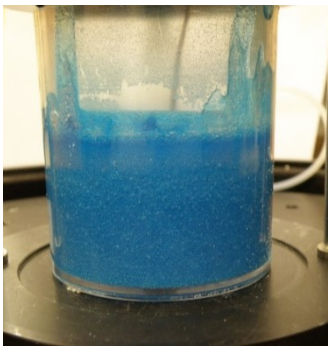 | 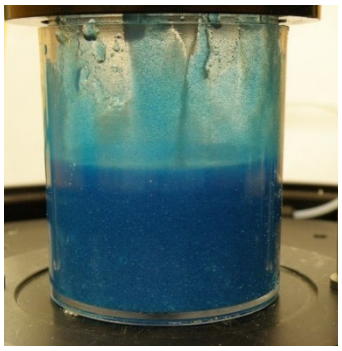 | 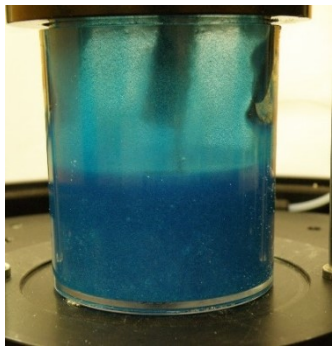 |
| The variation in the centre has gone and the sample appears consistent | Sample remains consistent but mixing has been aggressive- material is observed along the walls | Sample remains consistent but material is spread up the walls, out of the main bulk |

The 10 G, 35 G and 70 G results are tabulated in Table 91, Table 92 and Table 93 respectively. 10 G did not provide sufficient energy to successfully mix the sample. At the end of the 10 minutes there was a powder gradient within the vessel, with a greater concentration of powder at the bottom. The 35 G sample demonstrated greater effectiveness, with the sample being visually mixed after 2 minutes. Likewise, the 70G also appeared visually mixed after 2 minutes. The 70 G mix was a more aggressive process, with more material separated from the bulk sample and smeared up the vessel walls.

## 8.4 Mixing Mechanisms

Material comparison in previous chapters highlighted a specific issue with diffusion of products throughout the bulk material, noticeably the isocyanate. Research was conducted to characterise the mixing mechanisms throughout the sample whilst mixing different materials via LabRAM. High speed video was initially intended to be used; however, trial runs indicated that mix duration was too long so normal video was chosen. Samples were run at a consistent 35 G acceleration input, with each phase having 75 ml volume. Stills were taken from various points in the video and tabulated with a time stamp and a description of the observed behaviour. Mixing was conducted on filler, liquid and filler-liquid systems.

### 8.4.1 Filler

Powder mixing was conducted on two different variables; like particles and unlike particles. Powder testing was conducted in a polyethylene pot without vacuum or thermal measurements. There were three different grain sizes; small, medium and large. The small particle size was sand and was more representative of energetic particle sizes. It has a nominal grain size of 100 microns. The medium grain size were Tesco's "Hundreds and Thousands" which have an average diameter of 1.2 mm. The large grain size are sugar pearls which have an average diameter of 3.5 mm.

#### 8.4.1.1 Like filler

The small grain sizes were the first samples mixed and are summarised in Table 94. During mixing these smaller grain sizes utilised the micro-mixing mechanism leading to potentially large areas with inhomogeneous mix where components have not successfully diffused out of their immediate area. Macro-mixing does occur but at a much slower rate in comparison to the micro-mixing. Mixing took over 2 minutes.

*Table 94. Table detailing the mixing experiment for the fine powder sample using a 35 G acceleration. The sample exhibited the micro-mixing mechanism and appeared consistent at 121 seconds.*

| | | |
|---|---|---|
|  |  | 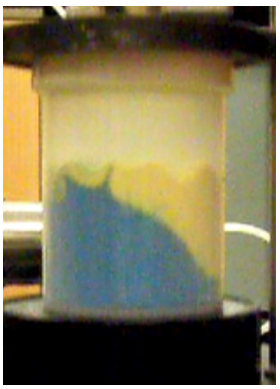 |
| $T_0$<br>Sample has two clear phases before input is applied | $T_0$ + 5 seconds<br>Acceleration is applied and sample exhibits wave like mixing at top of sample as micro-mixing zones are identified | $T_0$ + 7 seconds<br>Sample is starting to mix. The bottom layer has congregated to the side of the vessel and is starting to diffuse upwards into the upper layer |
|  |  |  |
| $T_0$ + 8 seconds<br>The bottom layer diffuses into the top layer with a wave like pattern in several points. These micro-mixing zones are clearly visible in the top left | $T_0$ + 9 seconds<br>The wave like behaviour has started to integrate the two layers, again focusing on the top left of the sample | $T_0$ + 13 seconds<br>More of the bottom layer has migrated to the top and there is an increased area of mixed material, indicated by the green colour. |

$T_0$ + 18 seconds

The sample is more integrated; however, there are still patches of distinct materials from each layer. Macro-mixing zones are now becoming important as larger areas have yet to be consolidated within the bulk

$T_0$ + 25 seconds

The bulk of the visible material is mixed, but pockets of unmixed materials exist in the bottom corners of the image. Larger mixing zones are visible around the edges of the unmixed material

$T_0$ + 29 seconds

The bulk material is still mixing, and the areas of unmixed material are decreasing in size

$T_0$ + 39 seconds

The bulk material is moving around the vessel and areas of unmixed powder are now visible to the left

$T_0$ + 53 seconds

Small macro-mixing areas are observed in the centre of the yellow powder. The bulk still shows marbling indicating that it is not consistently mixed

$T_0$ + 64 seconds

The unmixed zones continue to decrease in size and the marbling appears to be reducing

$T_0$ + 75 seconds
The unmixed material has decreased dramatically in size. A small patch remains in the bottom right corner. The bulk demonstrates that marbling pattern which indicates variation in mixing.

$T_0$ + 84 seconds
The bulk now shows no large areas of unmixed materials, although the sample is not consistently mixed as indicated through the marbling pattern

$T_0$ + 121 seconds
The sample is consistently mixed, and the colour is a blended green

The medium grain sizes, summarised in Table 95, mixed after a minute and a half, and exhibited a range of mixing mechanisms. Unlike the small particle size, the medium sample demonstrated debonding and more effective macro-mixing. The micro-mixing zones could be observed at various points within the sample and have the biggest positive impact on the homogeneity of the sample. Although debonding is a potential hazard when mixing energetics, it was an effective tool for this sample.

*Table 95. Table detailing the mixing experiment for the medium grain sample using a 35 G acceleration. The sample exhibited both the macro- and micro-mixing mechanisms and appeared consistent at 86 seconds.*

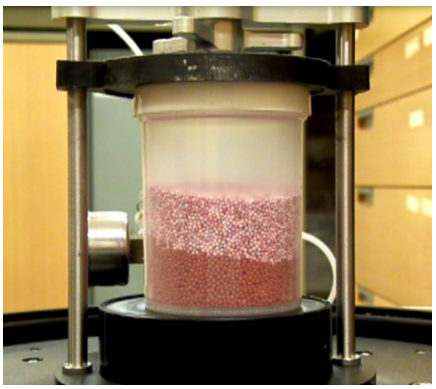

$T_0$

Sample has two clear phases before input is applied

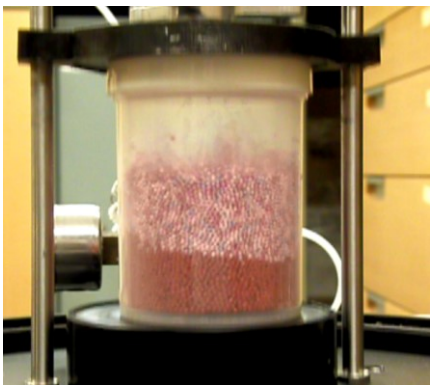

$T_0$ + 3 seconds

Input is applied and sample debonds with the top layer scattering into the empty space at the top of the vessel

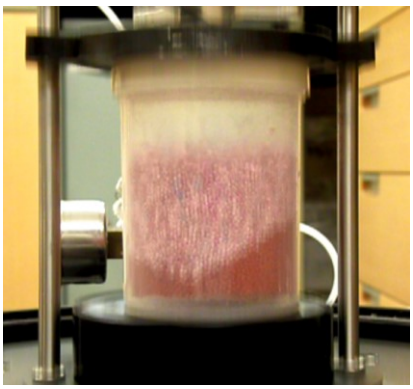

$T_0$ + 5 seconds

Sample is starting to mix on the left hand side of the vessel with the top layer diffusing into the bottom layer

$T_0$ + 7 seconds

Top layer is moving downwards and towards the left of the vessel and the bottom layer is migrating to the right and upwards

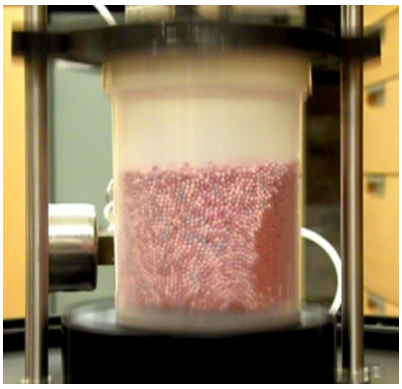

$T_0$ + 9 seconds

The bottom layer has almost fully migrated to the right hand side of the vessel

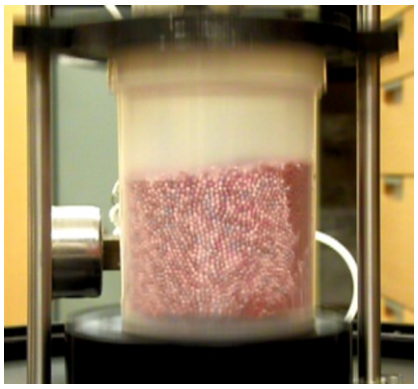

$T_0$ + 13 seconds

The top layer of sample is most of the visual bulk material as the sample moves around the vessel. There appear to be no micro-mixing zones or dispersion of the two phases

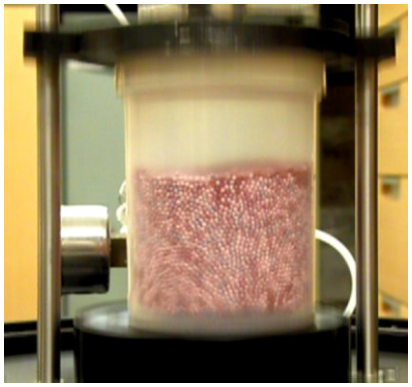

$T_0$ + 18 seconds

The top layer of the sample is now the bulk of the visually available sample. The beginning of a micro mixing zone can be observed at the top

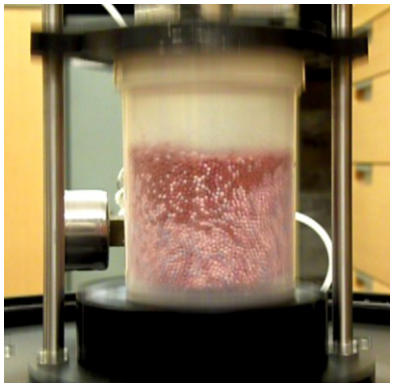

$T_0$ + 21 seconds

The two phases are slowly starting to combine as the original top layer (the pink phase) is diffusing into the other. Micro-mixing zones can be seen in the middle of the sample

$T_0$ + 25 seconds

Mixing is occurring as the phases are diffusing into each other. The micro-mixing zones have provided the greatest level of mixing in comparison to the rest of the sample

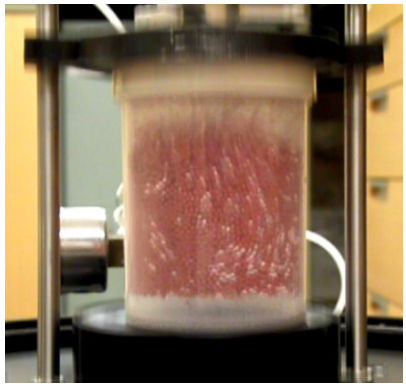

$T_0$ + 35 seconds

The sample is de-bonding from the vessel although the majority of the material remains within the bulk sample.

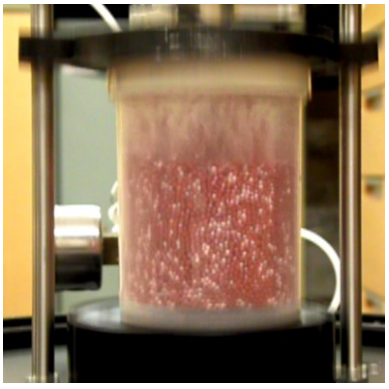

$T_0$ + 53 seconds

The sample continues to debond with material breaking off from the bulk of the sample. This is causing some degree of mixing; however, is much less efficient when compared to the micro- and macro-mixing zones observed previously

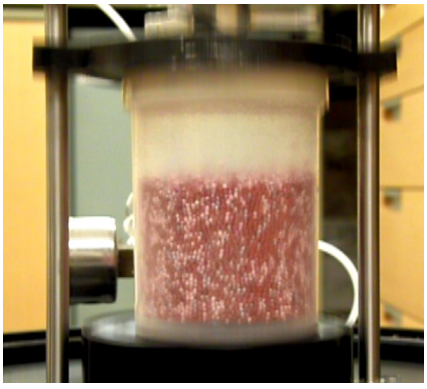

$T_0$ + 86 seconds

Mixing is stopped. It took longer to mix via the debonding method, and there are still areas with more of each phase.

The large grain size did not exhibit the same micro-mixing as the previous samples. Macro-mixing was the key driver for these materials. Diffusion was slow as the large particles blocked potential movement and flow within the vessel. After 3.5 minutes mixing had occurred and the phases were distributed; however, the sample is not uniformly mixed with uninterrupted groups of either phase 1 or phase 2. Results are summarised in Table 96.

*Table 96. Table detailing the mixing experiment for the large grain sample using a 35 G acceleration. The sample exhibited the macro-mixing mechanism and appeared consistent at 219 seconds.*

| | | |
|---|---|---|
|  | 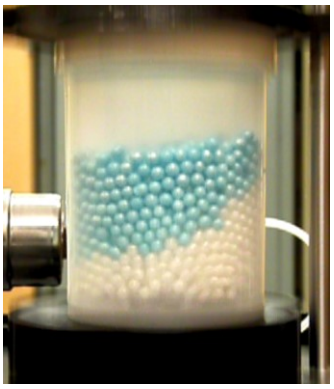 |  |
| $T_0$<br>Sample has two clear phases before input is applied | $T_0$ + 6 seconds<br>After input has been applied it takes 6 seconds before samples start to move within the bulk | $T_0$ + 11 seconds<br>Bulk mass is starting to jump, see gap at bottom of vessel, and the top layer is starting to migrate towards the bottom of the sample |

$T_0$ + 23 seconds
The visual bulk consists of mostly the top layer as the bottom layer has moved around the sample vessel

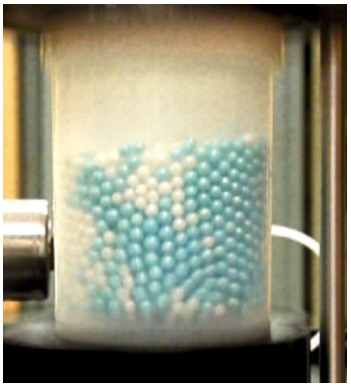

$T_0$ + 40 seconds
The bulk sample is rotating in the vessel as it mixes and the two layers are starting to diffuse into one another

$T_0$ + 65 seconds
The bulk sample is still rotating within the vessel, but there is greater diffusion between the two layers

$T_0$ + 97 seconds
The rotation of the bulk material continues and further diffusion of the phases within each other. This is occurring through the macro-mixing mechanism.

$T_0$ + 119 seconds
Individual parts of phase 1 have diffused through the bulk of phase 2 but the overall phases still remain separate

$T_0$ + 149 seconds
As the bulk sample rotates more of phase 1 is visible. There is diffusion of the phases; however, the bulk remains separate.

$T_0$ + 190 seconds
The phases are becoming more integrated, although there are still clear patches where the bulk is either phase 1 or phase 2

$T_0$ + 219 seconds
Distribution of the phases has occurred but the sample is not uniformly mixed

#### 8.4.1.2 **Unlike powder**

The like powder demonstrated the micro- and macro-mixing zones and the effect the particle size has on mixing. A monomodal system is rarely used in energetics so the same experiments were conducted with bimodal phases. Using the 35 G acceleration set point and 75 ml of each phase. Attempts were made to mix the small grain sizes with both the medium and large fillers. Mixing was not successful due to the large size discrepancy. With the larger grain size, the smaller grains sunk to the bottom of the vessel and during mixing the phases did not mix and the small grains remaining at the bottom. When mixing with the medium grains, the phases did move around the vessel but remained distinct; see Figure 131 and Figure 132.

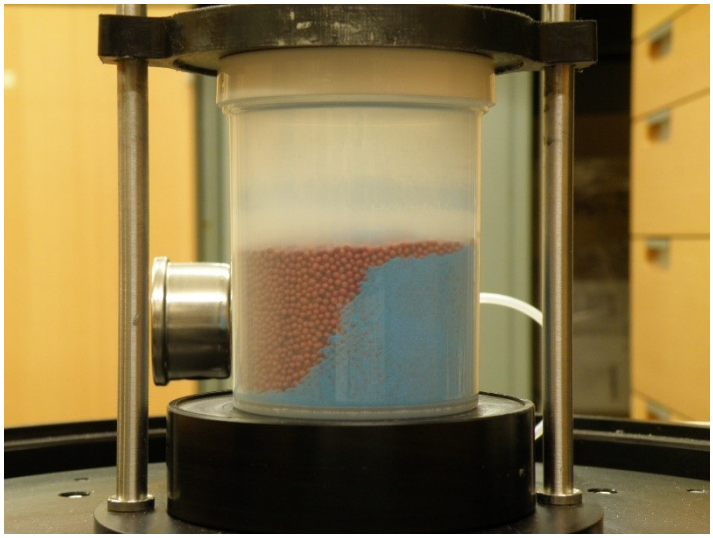

*Figure 131. Side view of the small-medium filler sample after mixing. The two phases were unable to disperse throughout, due to the fineness of the sand.*

*Figure 132. Aerial view of the small-medium filler sample after mixing. The two phases were unable to disperse throughout, due to the fineness of the sand.*

The large-medium diffusion experiment were conducted with the large particles at the bottom of the vessel, see Table 97, and then on the top, see Table 98. Most mixing occurred through either micro-mixing at the phase interface or through sample debonding from the vessel. The sample had greater mix efficiency, particularly at the beginning of the mix, when the larger grains were on top as they debonded, allowing movement between phases.

*Table 97. Table detailing the medium-large filler diffusion experiment with the large filler at the bottom of the vessel. The sample exhibited debonding and macro-mixing. The two phases were dispersed within each other after 109 seconds.*

| | | |
|---|---|---|
|  |  |  |
| $T_0$<br>Sample has two distinct phases before input was applied | $T_0$ + 5 seconds<br>The two layers are starting to integrate between each other, | $T_0$ + 9 seconds<br>The phases are still distinct, and are rotating around the vessel |
|  |  |  |
| $T_0$ + 21 seconds<br>The phases have separated so they are no longer horizontal in the vessel, but vertical. They continue rotating around the vessel. Only one phase is currently visible | $T_0$ + 27 seconds<br>The sample continues rotating and the larger particle sizes are returning to the front of the vessel. There is some dispersion between the two phases. | $T_0$ + 30 seconds<br>The powder is debonding from the sample vessel. The smaller particles are more affected. Some of the larger particles are sinking through the smaller phase. |

$T_0$ + 38 seconds
Mixing is occurring between the two phases, with the larger particles dispersing through the smaller phase

$T_0$ + 51 seconds
The bulk sample continues to rotate within the vessel. More of the larger grain size phase is now visible

$T_0$ + 64 seconds
The larger grain size appears less clumped and more dispersed within the smaller phase; however, the mix is not consistent

$T_0$ + 71 seconds
The samples experience debonding from the vessel again, with the smaller grain size being more affected

$T_0$ + 90 seconds
The debonding has had a greater impact on the mixing then the other mechanisms as the larger grain phase appears more distributed in the material.

$T_0$ + 109 seconds
The phases are dispersed throughout the sample, although the sample does not have a consistent mix.

*Table 98. Table detailing the medium-large filler diffusion experiment with the medium filler at the bottom of the vessel. The sample exhibited debonding and macro-mixing. The two phases were dispersed within each other after 86 seconds.*

| | | |
|---|---|---|
|  |  |  |
| $T_0$<br>The two phases are distinct, with the larger grain on top | $T_0$ + 3 seconds<br>The larger grain phase is diffusing into the other phase and the sample is debonding from the vessel | $T_0$ + 3 seconds<br>The sample continues to debond from the vessel and the larger grain phase continues to diffuse |
| 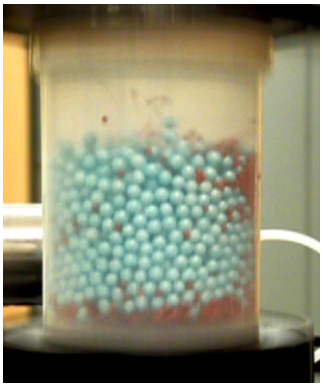 |  |  |
| $T_0$ + 6 seconds<br>The larger grain phase has diffused throughout the sample and is visually dominating the front of the sample vessel | $T_0$ + 12 seconds<br>The sample begins to rotate within the vessel and demonstrates the staggered diffusion of the larger grain phase | $T_0$ + 12 seconds<br>The sample is debonding, with the smaller grain being more affected. The larger grains are dispersed throughout the smaller grains but it is not consistent |

$T_0$ + 27 seconds
Debonding from the vessel continues, and as the sample rotates more of the smaller grain phase is visible indicating large areas of just that phase

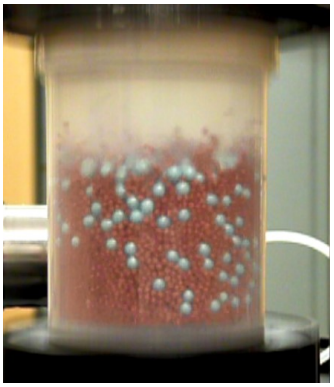

$T_0$ + 35 seconds
The sample continues to rotate and the larger grain continues to diffuse into the smaller grain phase.

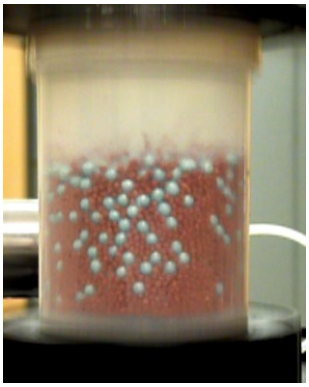

$T_0$ + 45 seconds
Mild debonding continues with the smaller grain phase being most affected. The larger grain continues to mix and the sample appears more consistent

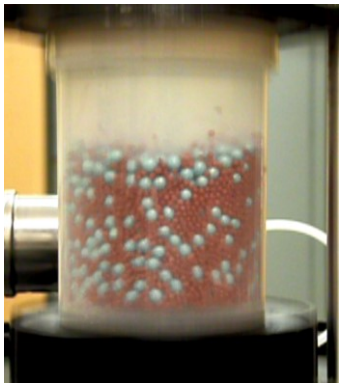

$T_0$ + 56 seconds
The samples exhibit greater degree of mixing and a greater consistency. The phases are not fully distributed.

$T_0$ + 86 seconds
After 86 seconds the sample appears mixed and although it is not highly consistent, the phases are dispersed

### 8.4.2 **Liquid**

The liquid experiments were conducted on liquids with contrasting viscosities; HTPB R45HTL0 has a viscosity of 5000 mPa s at 30 °C, whereas water has a viscosity of 0.7978 mPa s. Water based sucrose solution was used due to its colour. 75 ml phase sizes were

used to keep consistency between the experiments. The HTPB was added first but the sucrose solution sunk to the bottom of the vessel when added, see Figure 133.

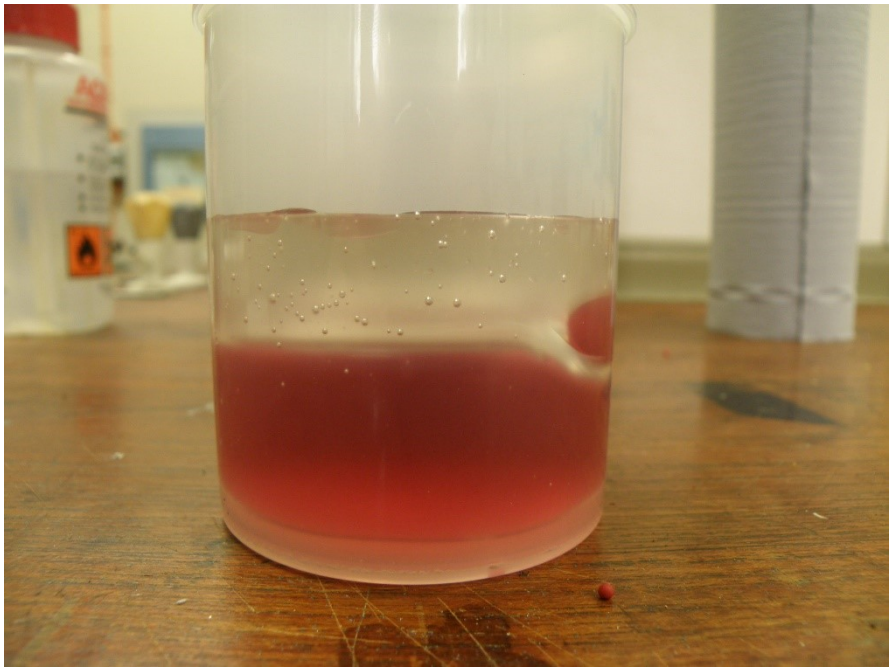

*Figure 133. The liquid mixing experiment sample. Two different liquids were used; high viscosity HTPB and low viscosity water based sucrose solution. The water based sucrose solution was added after the HTPB but sunk through the HTPB to the bottom of the vessel*

Initial experiments were conducted with no vacuum, and no mixing occurred. When a vacuum was applied the samples exhibited mixing with turbulent flow and excessive debonding, see Table 99. Mixing depended primarily on the macro-mixing mechanism and degassing of the phases. During mixing, the sample appeared fully mixed at 49 seconds with consistent colour and viscosity. However, when mixing was stopped the sample experienced phase separation with the HTPB flocculating and creaming. An image of the material after mixing is found in Figure 134.

*Table 99. Table detailing the various mix points of the liquid-liquid mix experiments. Viscous HTPB and low viscosity water based sucrose solution was used. The samples main mixing mechanisms were micro-mixing and sample debonding. Although the sample appeared consistent whilst mixing, when the mixer was stopped the sample returned as two distinct phases.*

| | | |
|---|---|---|
|  |  |  |
| $T_0$<br>The phases are distinct with the sucrose solution at the bottom | $T_0$ + 3 second<br>Mixing has begun but the phases remain separate | $T_0$ + 13 second<br>After 13 second the sucrose solution begins to degas, initiating in the bottom right corner |
|  |  | 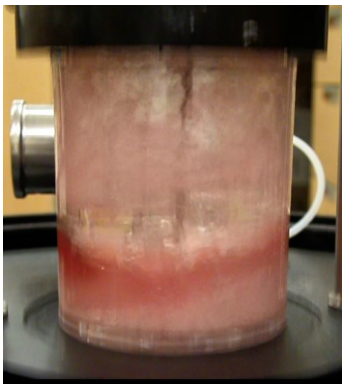 |
| $T_0$ + 14 second<br>Degassing causes the sucrose solution to bubble. The interface between the two phases is disrupted | $T_0$ + 15 second<br>The bubbling continues and the sucrose solution begins to demonstrate turbulent motion. At the right side of the vessel the sucrose solution has broken through the HTPB layer and has debonded from the vessel | $T_0$ + 15 second<br>The sample is debonding and causing turbulent motion within the vessel. The two phases begin to diffuse into each other |

$T_0$ + 19 second

The sample is demonstrating a greater degree of mix. The colour appears to be more consistent, although large lumps of HTPB can be observed throughout the sample

$T_0$ + 24 second

The HTPB agglomerations have been broken and distributed more evenly throughout the sample

$T_0$ + 35 second

Areas of HTPB can still be spotted at the bottom of the sample, but the mix appears more consistent

$T_0$ + 49 second

The sample appears consistent and there are no visible agglomerations of HTPB

$T_0$ + 223 second

After 223 seconds the sample looks consistent. The sample is lighter indicating that a greater degree of aeration.

$T_0$ + 226 second

Mixing was stopped and the sample began to separate with the HTPB flocculating and creaming at the surface

$T_0$ + 228 second
The HTPB continues to cream and flocculate, increasing the phase separation. The sample is returning to the two distinct phases.

$T_0$ + 229 second
The HTPB layer is compressing demonstrating that the sample was not successfully mixed. This indicates that the HTPB and the sucrose solution were not compatible.

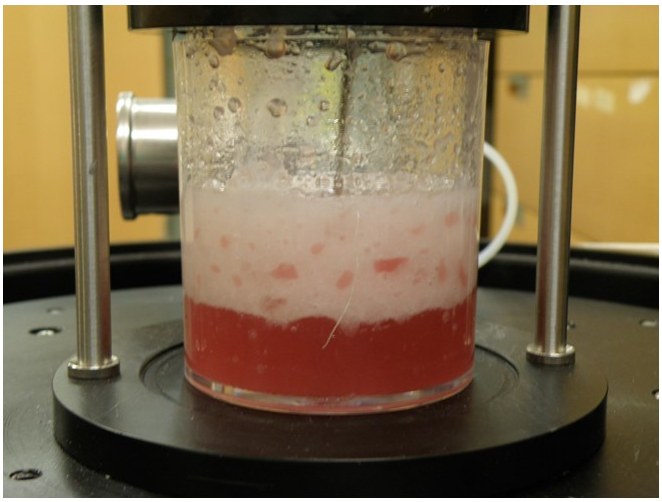

*Figure 134. The liquid-liquid mixing experiment, using a viscous HTPB and low viscosity water based sucrose solution, was mixed at 35G. Despite visually appearing consistent during mixing, once the mixer was stopped the sample returned to two distinct phases. The HTPB, which appears as a white foamy layer on top, appeared to cream and flocculate. The sample was not effectively mixed.*

### 8.4.3 Binder and powder

The binder and powder experiments were used to identify any variation in mixing the filler with binder. For all of the grain sizes the same mixing mechanisms as the pure filler dominated mixing; the larger grain sizes primarily used macro-mixing, the medium grain sizes used a

combination of macro- and micro-mixing with debonding of the sample from the vessel, the small grain sizes was dominated by the micro-mixing at phase interfaces. Mixing experiments were conducted with the binder and then filler on top. When the filler was on top of the binder the samples exhibited a greater degree of debonding with the filler escaping into the vessel head space. As previously mentioned this could have a safety impact when mixing explosive materials. When the binder was on top of the filler the filler was trapped in location but the vibrational energy caused the bulk to separate and fracture. This is seen most clearly in the small grain size samples; see Table 105.

The large grains were summarised in Table 100 and Table 101. Table 100 had the binder on top whereas Table 101 had the binder on the bottom. The sample was primarily controlled by the macro-mixing with the filler diffusing into the binder phase. This was consistent for both set ups. Mixing was more aggressive when the filler was on top of the binder. Mixing occurred in less than 1.5 minutes for both experiments.

*Table 100. Table detailing the liquid-large filler diffusion experiment with the large filler at the bottom of the vessel. The sample exhibited macro-mixing. The two phases were dispersed within each other after 96 seconds.*

| | | |
|---|---|---|
| 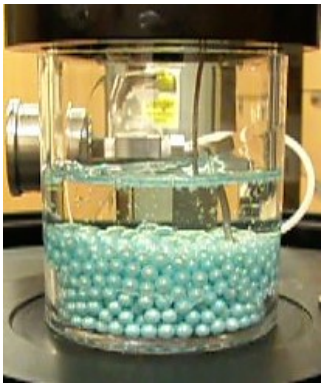 |  |  |
| $T_0$<br>The sample has two distinct phases with the binder visible on top of the filler. Binder is starting to soak through and wet the top layer of filler. | $T_0$ + 1 second<br>Binder continues to soak through and wet the filler particle. | $T_0$ + 3 seconds<br>The binder continues to soak through and the filler particles are vibrating |

$T_0$ + 5 seconds

Filler particles are vibrating at a greater rate, and the binder is slowly wetting the filler

$T_0$ + 6 seconds

The filler is separating and the binder continues to flow down and wet the filler. Bubbling begins to occur at the binder surface

$T_0$ + 7 seconds

Filler particles in the centre begin to move upwards. The filler is not fully wetted yet

$T_0$ + 10 seconds

Filler particles continue to move upwards and towards the middle of the vessel. The binder continues to soak through

$T_0$ + 23 seconds

Binder is bubbling and the filler particles begin to flow within the sample

$T_0$ + 33 seconds

Filler is fully wetted as the binder has diffused into the filler phase

$T_0$ + 53 seconds

A layer of binder remains at the surface, but the rest of the sample is distributed throughout

$T_0$ + 96 seconds

The two phases are interdispersed after 1.5 minutes of mixing

*Table 101. Table detailing the liquid-large filler diffusion experiment with the liquid at the bottom of the vessel. The sample exhibited debonding and macro-mixing. The two phases were dispersed within each other after 72 seconds.*

$T_0$

The two phases are distinct; however, the filler has begun to sink down in the binder

$T_0$ + 1 second

Filler is debonding from the bulk material, and continues to sink into the binder system

$T_0$ + 2 seconds

Filler continues to debond from the bulk and the right hand side of the sample is moving upwards

$T_0$ + 18 seconds
Binder begins to bubble. The filler continues to debond, although a small amount of binder has been incorporated to the debonding mass causing the filler to consolidate

$T_0$ + 27 seconds
The bulk filler continues to sink into the binder

$T_0$ + 33 seconds
The binder is bubbling in the right hand corner of the and the sample is beginning to flow

$T_0$ + 34 seconds
Flow continues within the sample and the filler is being integrated into the binder

$T_0$ + 37 seconds
Filler is climbing up the thermoprobe. Filler is still being integrated into the binder

$T_0$ + 43 seconds
The filler is more integrated within the binder; however, there is still a patch of pure binder along the bottom of the sample

$T_0$ + 54 seconds
The binder patch has now been integrated within the bulk material

$T_0$ + 66 seconds
Sample appears mixed with the filler and binder equally distributed

$T_0$ + 72 seconds
After 72 seconds the sample appears consistently mixed

The medium grains were summarised in Table 102 and Table 103. When the filler was on top of the binder the sample exhibited consistent behaviour with the large grain sizes. The filler distributed into the binder and mixing occurred within 1.5 minutes. Mixing was initiated by bubbling of the binder which caused macro-mixing. Once the filler was mostly distributed within the binder mixing began to occur at the micro-mixing scale. When the binder was on top of the filler the sample demonstrated unusual behaviour. The binder debonded from both the filler and the vessel. Mixing only occurred once the binder settled back into the vessel and flowed down the vessel edges. Unlike the other experiments, the binder diffused into the filler. Mixing was slower, with the binder not settling until 18 seconds in. Mixing took over 2.5 minutes.

*Table 102. Table detailing the liquid-medium filler diffusion experiment with the medium filler at the bottom of the vessel. The sample exhibited debonding and macro-mixing. The two phases were dispersed within each other after 165 seconds.*

| | | |
|---|---|---|
|  |  | 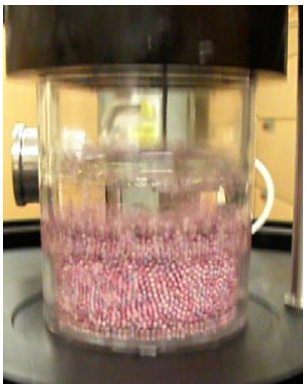 |
| $T_0$<br>The two phases are distinct. Binder has soaked the top of the filler phase | $T_0$ + 3 seconds<br>The phases still remain distinct but the filler particles vibrate and debond from the vessel. They remain trapped by the binder layer | $T_0$ + 4 seconds<br>Small quantities of filler begin to diffuse upwards into the binder |
| 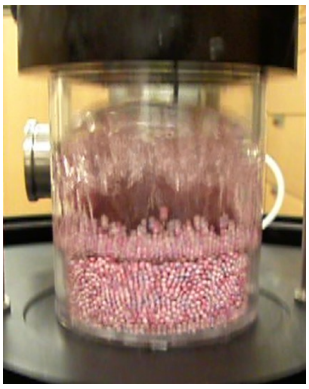 |  |  |
| $T_0$ + 4.5 seconds<br>The binder has debonded and risen within the mixing vessel as a result of the vacuum. More filler has diffused into the binder | $T_0$ + 5 seconds<br>The binder continues to rise forming a dome as the vacuum pulls. The filler remains in place at the bottom of the vessel | $T_0$ + 5.5 seconds<br>The binder bubble reached the top of the vessel and broke, dropping back down in the mix vessel |

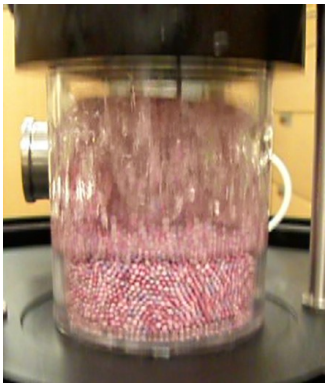

$T_0$ + 6 seconds

The binder continues to rise and fall within the sample vessel, integrating more filler each time

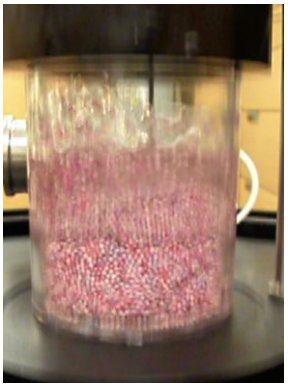

$T_0$ + 18 seconds

The binder and filler mixture at the top of the sample settles and begins to exhibit macro-mixing. Some filler at the top of the sample remains unintegrated and bounces within the vessel head space

$T_0$ + 24 seconds

As the mixed sample at the top flows, it wets the edges of the filler and integrates them into the bulk. The majority of the filler remains separate and vibrates in place

$T_0$ + 35 seconds

The binder continues to wet the filler with the mixed phase flowing downwards in the volcano effect. Unmixed filler phase reduces in size as more is constituted into the mix zones

$T_0$ + 36 seconds

The sample continues to flow with only a minor amount of unmixed filler left. The sample is not mixing, merely wetting the pure filler.

$T_0$ + 41 seconds

As the remaining filler is integrated into the bulk the sample exhibits slow macro-mixing. As the sample flows down the vessel walls minor debonding occurs, resulting in the dark patches

| | |
|---|---|
|  |  |
| $T_0$ + 78 seconds<br>The sample continues to flow; however, there has been separation and the layer at the bottom of the sample vessel is stationary | $T_0$ + 165 seconds<br>After 165 seconds the sample appears consistent with all material enclosed within the bulk |

*Table 103. Table detailing the liquid-medium filler diffusion experiment with the liquid at the bottom of the vessel. The sample exhibited debonding, macro-mixing and the specific volcano effect. The two phases were dispersed within each other after 90 seconds.*

| | | |
|---|---|---|
| 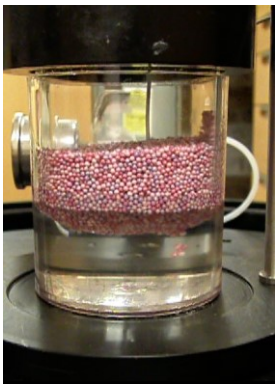 |  |  |
| $T_0$<br>The two phases are distinct with the filler on top. A small amount of filler has sunk into the right hand side of the binder | $T_0$ + 2 seconds<br>Filler is vibrating with the bottom layer beginning to sink into the binder | $T_0$ + 8 seconds<br>Filler is debonding with most remaining as a bulk mass. Small quantities of filler are bouncing in the free head space of the vessel. |

$T_0$ + 24 seconds
Binder begins to bubble, using the previously mentioned filler in the right hand side of the binder as a nucleation point

$T_0$ + 31 seconds
Binder continues to bubble and filler is dropping into the binder

$T_0$ + 35 seconds
The bubbling allows more filler to sink into the binder and the sample begins to exhibit flow and mixing

$T_0$ + 41 seconds
As the filler starts to wet it forms a bulk material which then integrates more material. The sample experiences bulk mixing exhibiting the volcano effect

$T_0$ + 54 seconds
The bulk mixing continues with most of the sample mixed into a consistent composite. A small batch of pure binder remains in the lower left hand corner of the sample. Sample debonds from the vessel wall whilst flowing producing the dark patches

$T_0$ + 90 seconds
The pure binder corner has now been integrated into the bulk material and the sample exhibits the classic macro-mixing, volcano effect.
The sample appears consistent

The small grain material, in Table 104 and Table 105, utilised the micro-mixing mechanism which was particularly noticeable and effective at the filler-binder interfaces. Like with the medium grain size, when the binder was on top of the filler it debonded and took 9 seconds to

settle. However, unlike the medium grain size mixing was significantly shorter when the filler was on top with a mix time of over 2 minutes, instead of nearly 4 minutes.

*Table 104. Table detailing the liquid-small filler diffusion experiment with the small filler at the bottom of the vessel. The sample exhibited debonding and micro-mixing. The two phases were dispersed within each other after 139 seconds.*

| | | |
|---|---|---|
| 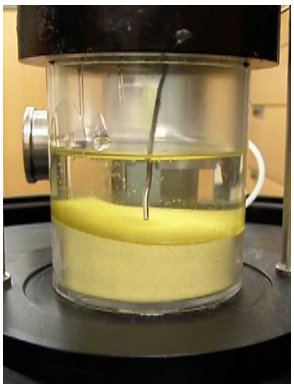 |  |  |
| $T_0$ | $T_0$ + 2 seconds | $T_0$ + 3 seconds |
| Sample has two phases with the binder on top. The top layer of the filler is already wetted by the binder | A bubble initiates from just below the filler surface on the left hand side of the sample, dragging filler up away from the bulk | The bubble moves to the surface leaving a column of filler within the binder system |

$T_0$ + 4 seconds

As the binder bubble pops, the filler gets dragged upwards into the binder

$T_0$ + 6 seconds

The binder layer bubbles with some filler entrapped in the bottom of the binder. The bulk filler is not affected

$T_0$ + 9 seconds

As the binder drops back down, turbulent motion causes the binder and entrapped filler to begin mixing. This is on the micro-mixing scale. The bulk filler at the bottom of the vessel begins to vibrate

$T_0$ + 12 seconds

As the binder begins to settle the bulk filler begins to integrate within the binder. Some filler has debonding and can be seen in the vessel head space

$T_0$ + 18 seconds

The sample is flowing within the vessel. More filler is being consistently integrated into the mix. There is still filler debonding at the top of the sample

$T_0$ + 35 seconds

As more filler is assimilated into the bulk, the sample begins to demonstrate macro-mixing.

$T_0$ + 56 seconds
Sample has stopped flowing. Some material has detracted from the bulk and can be seen in the top left corner

$T_0$ + 61 seconds
Sample rises and falls several times as if degassing but still does not demonstrate any flow

$T_0$ + 98 seconds
Sample begins to demonstrate inconsistent flow. This can be identified in the bottom right corner

$T_0$ + 139 seconds
Mixing is occurring utilising voids within the sample to initiate micro-mixing, seen in the lower left corner. After 139 seconds the sample appears consistent.

*Table 105. Table detailing the liquid-small filler diffusion experiment with the liquid at the bottom of the vessel. The sample exhibited debonding and micro-mixing. The two phases were dispersed within each other after 225 seconds.*

| | | |
|---|---|---|
|  |  |  |
| $T_0$<br>Sample has two phases. The filler, on top, has begun to sink into the binder system | $T_0$ + 5 seconds<br>The filler is exhibiting micro-mixing with acoustic waves visible on the surface. Filler is debonding from the bulk, seen in the vessel headspace. Some filler has sunk into the binder | $T_0$ + 27 seconds<br>No mixing has occurred but the filler continues to sink within the binder. |
|  |  |  |
| $T_0$ + 35 seconds<br>Filler continues to sink and micro-mixing is visible at the filler-binder interface | $T_0$ + 43 seconds<br>Mixing is occurring using the micro-mixing mechanism. This is particularly noticeable in the filler and at the interface | $T_0$ + 48 seconds<br>Micro-mixing zones are integrating the remainder of the binder into the sample |

$T_0$ + 58 seconds
Sample is demonstrating a greater degree of mix but is also climbing up the vessel wall and the thermoprobe

$T_0$ + 85 seconds
Sample is mostly mixed. A small patch of unintegrated filler remains in the left hand side of the sample

$T_0$ + 143 seconds
Sample appears mostly consistent although there are patches of variation. Mixing is very slow and not efficient.

$T_0$ + 225 seconds
Sample appears consistent and well mixed, although there is bubbling throughout.

## 8.5 Conclusion

Understanding the mix parameters allows operators to produce more consistent samples and increase quality control. Throughout this study this has been a consistent issue, leading to samples with poor distribution of isocyanate and poor curing of the binder. The aims of this chapter was to identify mixing mechanisms, indicators and determine the influence of mass, vacuum and acceleration on mixing.

The first set of experimentation identified indicators to determine whether mixing was occurring when operating the mixer remotely. The experiment demonstrated that a variation in frequency and an increase in temperature and power input coincides with sample mixing. As the sample mixes it will cause the frequency of the system to vary, which is linked to a variation in the power input required to deliver a set acceleration. As the sample flows, the material will experience internal friction which causes a significant temperature increase.

The second set of experimentation determined the impact of three variables on mixing; mass, vacuum and acceleration. As expected, an increase in mass required a change in the mix parameters. Above 175 g the experiment, which had a maximum acceleration of 70 G, did not induce flow within the sample. Vacuum experimentation demonstrated that without sufficient vacuum and a nucleation point, mixing would not occur. For this material, successful mixing occurred when a vacuum of less than 0.27 bar was applied after mixing had begun. When the sample was degassed prior to mixing there was not a suitable nucleation point for mixing. Finally, acceleration was tested at 3 levels; 10 G, 35 G and 70 G. Mixing occurred at both 35 and 70 G, although the mixing was more aggressive at the higher level. Mixing did not occur at 10 G.

The final set of experimentation identified the mixing mechanisms and the diffusion of components within a sample. Sand was the small grain sized materials and utilised the micro-mixing mechanisms. This was most effective at phase interfaces, but the material struggled to mix the overall sample unless there was a degree of debonding. The debonding disrupted the larger sample and provided diffusion of the phases. The medium grain size was Tesco's Hundreds and Thousands, which provided the most efficient combination of mixing mechanisms. Micro-mixing still occurred at points within the sample; however, the sample also exhibited macro-mixing and debonding. This enabled the phases to distribute easily throughout the sample and achieve a consistent mix. The large grain size sample used sugar pearls. Mixing was dominated by macro-mixing, which has limited effectiveness. The phases dispersed but the samples still demonstrate variation. The grain size was too large to enable micro-mixing.

This chapter illustrates that successful mixing is highly dependent on the parameters chosen, and is more sensitive in this respect than conventional planetary mixing. It is demonstrated that there is a limited parameter space for optimised mixing. When mixing polymer based energetics, there are some areas to be addressed. The energetic filler has a typical crystal size most similar to the sand, so distribution of the energetic fill is dominated by the micro-mixing zones. This has been proven to be an effective mixing mechanism for the powders;

however, was less efficient for HTPB- sand composites which helps explain the poor distribution of isocyanate observed in samples throughout this study.

# 9 Discussion

This study was designed to build on research already published within this field. As discussed in the introduction in Chapter 1 this study aims to answer a simple question: is the material impacted because of mixing via RAM. The interest for this technique grows due to its clear advantages: quicker mix time, significantly less clean up, potential to mix in case and the potential to mix materials that would not be easily mixed with current techniques. Papers have been summarised in the literature review, in Chapter 2.3, where they were categorised as either technique analysis, mixing effectiveness or materials characterisation.

The two main industries that have published the most research relevant to this programme are pharmaceuticals and energetics. The pharmaceuticals have primarily published the mixing parameters and the effectiveness of the mixes, whereas the major drive of the research in the energetics industry has been investigations into the materials functionality and key behaviour. The energetics industry is missing a published comprehensive analysis of the impact on the overall material and its behaviour looking at a range of material properties to fully understand the impact of the mixing method on the material.

This programme started with the simplistic HTPB-Melamine composites, in Chapter 3. As these materials are highly complex with multiple component interactions, it was decided that starting with the full composition would be too complicated to determine the cause of any potential issues. The starting mix parameters were based on the literature summarised in the technique analysis and mixing effectiveness. Research conducted on various viscous solid-liquid systems used accelerations ranging from 40 G upwards [Lucon, 2009] [Hope et al, 2015] [Wilgeroth et al, 2018] [Davey et al, 2019] and intensities in similar ranges [du Plessis, 2016] [Nelson et al, 2012] [Rumeau et al, 2015]. Multiple research papers [Nelson et al, 2012] [Rumeau et al, 2015] [Wilgeroth et al, 2018] [Davey et al, 2019] used a ramping system where the mixing parameters were incrementally increased during the mix. For this research, the mixing started at a low intensity percentage was incrementally increased until the sample exhibited mixing, at 45% intensity. This remains consistent with the range seen in the literature.

Characterisation of the samples covered the mechanical, thermal and chemical properties. The literature found primarily tested the tensile properties of materials mixed by RAM [Bluestone et al, 2010] [Coguill et al, 2014] [Nelson et al, 2012] [Rumeau et al, 2015] [Smith et al, 2019] with the samples having either similar or improved mechanical properties when compared to the conventional planetary mixed samples. BAE have used DMA but as a

thermal technique instead of a mechanical technique [Davey et al, 2019]. DMA offers a better understanding of the mechanical behaviour over a temperature range. Unlike the mechanical testing results in literature, the DMA results demonstrated minor variation with the LabRAM samples behaving worse than the planetary mixed. The highly loaded, 0.80 solid loading, sample demonstrated a transition in the glass transition tan(delta) peak, which supported by the significant variation in the NMR results, is due to either poor cross-linking of the HTPB network or poor distribution of the binder throughout the sample. It demonstrates that although the mixing parameters were within the range seen in the literature, the mixing was not sufficient and the mechanical properties were affected as a result.

Where DMA testing has not been reported, DSC, the chosen thermal technique for this composition, has been tested as it demonstrates all the key thermal transition points, such as melting and crystallisation temperatures [Nelson et al, 2012] [Wilgeroth et al, 2018] [Davey et al, 2019]. The thermal transition peaks were not affected in either the literature or this research; there was the expectation that any potential changes due to mixing would be overshadowed by the components thermal behaviour, which is the dominant mechanism.

The simplistic composites proved that when they were sufficiently mixed there was no impact on the material; as such, the composition was increased in complexity. The HTPB-Melamine-Barium Sulphate samples, in Chapter 4, used the mixing method from the previous compositions and adjusted the parameters to improve the mix quality. The key issue appeared to be the distribution of the isocyanate throughout the sample, so greater time was taken during the final stage of mixing when the isocyanate had been added. The characterisation was built from the HTPB-Melamine samples, as part of an iterative process. DMA testing was kept, and remained as a crucial technique throughout this study, as it provided a good indication of the mechanical behaviour of the material and data on the mechanical behaviour over a range of temperatures, which as noted before, is not prevalent within the literature. In addition, hardness, density and thermomechanical testing was conducted. DMA testing focuses on the viscoelastic component or the reversible deformation whereas hardness investigates the localised permanent deformation. The density measurements demonstrate the loading and the packing of the sample, which would impact the materials ability to deform. The DMA testing exhibited consistent behaviour, demonstrating that the additional mixing time for the isocyanate addition ensured a consistent mix. The hardness and density testing, both of which has been reported as being consistent in literature [Wilgeroth et al, 2018] [Davey et al, 2019], demonstrated that there is no significant variation between the mixing method. The next stage of the thermal testing was the investigation of expansion over a temperature range; it has already been proven that the

various thermal transition points were not affected due to the mixing method. Thermal expansion has not been investigated in the literature; however, the variation with these samples were insignificant.

In Chapter 5, the addition of the plasticiser allowed higher solid loadings to be successfully mixed and cast. As with the other samples, DMA testing was conducted and the results were highly consistent, demonstrating a uniform mixing. This stage also investigated additional parameters that have not been reported throughout literature. High strain rate testing is of key interest to determine the materials response during functional use; Split Hopkinson Pressure Bar measured the compressive stress-strain. The highly loaded, 0.85 solid loading, samples demonstrated a significant and statistically different increased stress to strain with the RAM samples. This means greater stress is required to deform the RAM samples compared to the planetary mixed samples.

The other parameter that hadn't been investigated was the impact on the ageing behaviour. The energetic components are chemically stable and do not typically exhibit decomposition over time. The binder system is the most susceptible to ageing, as the polymeric chains can oxidise and damage. As such, the permeation of moisture throughout the sample is a key indicator to the aged behaviour. The moisture diffusion experiments did not demonstrate any significant variation through the material.

The next composition is the full inert composition resembling a PBX mimic, in Chapter 6. The anti-oxidant hinders the ageing process and provides a longer shelf life for the material. As this was the final stage of the inert research a comprehensive characterisation programme was conducted. This had a combination of tests already conducted in literature, hardness, density, and DSC, and the novel testing that has not been reported, DMA, NMR, SHPB, TGA and moisture diffusion. The DMA testing demonstrated consistency between the 0.66 and 0.80 solid loadings. The 0.73 solid loading RAM sample had a lower elastic moduli demonstrating a softer material, likely due to poor curing of the polymer matrix. Likewise, the SHPB samples had consistent behaviour for the 0.66 and 0.80 solid loading samples but the 0.73 solid loading RAM sample had a significant decrease in the stress. The density also did not demonstrate any significant variation, demonstrating that the packing of the sample was consistent between the two mixing methods, like in literature [Wilgeroth et al, 2018].

The DSC, similar to the HTPB-Melamine composition and the literature [Nelson et al, 2012] [Wilgeroth et al, 2018] [Davey et al, 2019], demonstrated the same thermal transition peaks between the two mixing methods. TGA was conducted with the DSC testing, to determine

mass loss during heating. The mass loss peaks were associated with the thermal peaks for the decomposition of the melamine and binder system.

Chemical analysis was conducted via NMR to quantify the distribution of components within the material. It was found that there was a high level of inconsistency between the RAM and planetary mixed samples with the distribution of the extractable HTPB and the anti-oxidant. It indicates that there is variation either in the isocyanate distribution and therefore the curing of the polymeric binder or the mix quality.

Like with the HTPB-DOS-Melamine-Barium Sulphate, the moisture diffusion experiments measured the mass change over time in a high moisture environment to determine the rate of the most likely degradation route. The full inert compositions did not demonstrate variation in the materials ability to diffuse moisture throughout the sample

The energetic composition, in Chapter 7, used a combination of coarse and fine RDX as the filler. Due to the nature of the materials, alongside the characterisation there were also functionality testing. A standard five suite of hazard tests were chosen, representing a range of potential stimuli, to determine the initiation characteristics of the material. The stimuli were friction, temperature, impact and electrostatic discharge. When working with energetics hazard data is an important part of the safety case, as such it has been covered in the literature [Wilgeroth et al, 2018] [Smith et al, 2019]. The hazard data in this programme, and in the literature, did not demonstrate any significant variation in the materials response to stimuli. In addition to the hazard testing, the velocity of detonation was tested. The samples were fired at the QinetiQ Fort Halstead ranges, using an RP80 detonator and a tetryl booster pellet. A streak camera measured the light output produced by the detonation and a witness plate was placed at the end of the sample. The results were highly consistent between mix methods, and corroborates literature [Davey et al, 2019].

With regards to material properties, the mechanical behaviour when tested by DMA and hardness testing showed no significant difference between the RAM and planetary mixed samples, which is consistent with the inert research in this programme and literature [Wilgeroth et al, 2018] [Davey et al, 2019]. Similarly, the density showed no variation between the two mix methods which is consistent with the literature [Wilgeroth el al, 2018] [Davey et al, 2019].

The DSC/TGA results had one exothermic peak at ~ 215 °C, due to the degradation of the RDX. This was accompanied by a mass loss of approximately 82%. There was no significant variation between the two mix methods, although there was a consistent 2 °C decrease in the

peak temperature for the RAM samples. The previous compositions, and literature, both demonstrated consistency between RAM and planetary mixed samples when tested by DSC [Nelson et al, 2012] [Wilgeroth et al, 2018] [Davey et al, 2019].

The NMR results showed a significant change in the concentration of extractable HTPB. The DOS concentration remained consistent between the two mixing methods, indicating that it is not the distribution of the binder system, but more a variation in the cross-linking. The RAM samples had a decrease of 32%, indicating that the RAM samples had greater cross-linkage than the planetary mixed samples.

This study progresses the field in several ways. One, as alluded to earlier, was characterisation that has not been reported in literature; testing included DMA, SHPB, moisture diffusion, and TGA. However, the real novelty comes from linking these results together to form a greater idea about the material. In most cases, the variation between mixing methods was negligible; however, there are two samples that did not behave consistently.

The first one is the 0.80 RAM HTPB-Melamine sample, which when tested via DMA demonstrated a shifted tan(delta) peak and variation in the moduli. Additional experimentation via NMR proved that the extractable HTPB concentration, which is the amount of HTPB that can be easily removed from the sample, varied greatly within the like RAM samples. Combined with the mechanical behaviour, this demonstrates variation within the cross linking of the sample.

The full inert composition with the 0.73 solid loading also demonstrated variability between the two mixing methods. The RAM samples had a significant decrease in the elastic moduli when tested via DMA meaning the material was softer. Likewise, the high strain rate testing had both a significant and statistical decrease in the stress to strain. There was no variation in the DSC/TGA, as the results are dominated by the thermal transitions of the components. The density was consistent which demonstrates that the decrease in mechanical behaviour is not related to the packing density of the material. Chemical analysis, via NMR, proved that the RAM samples had a significant increase in the extractable HTPB concentration which demonstrates poor curative, most likely as a result of poor isocyante distribution.

In both of these samples, the cause for the behaviour variability was the poor distribution of isocyanate which meant poor curing of the binder system. This poor curing limited the effectiveness of the polymeric chains leading to the decrease in the mechanical behaviour.

This has been observed in literature [Davey et al, 2019] where, for their samples, using an acceleration below 50 G did not distributed the isocyanate sufficiently.

This research has demonstrated that, assuming consistent distribution of isocyanate through the material, the mixing method does not impact the materials behaviour or properties. Although a potentially dull conclusion, it is a positive outcome for the wider industry. RAM is more efficient, both with time and material, and has the possibility to mix novel materials in case. This not only reduces the cost per munition, but opens up whole new avenues for optimising materials and performance, manufacturing materials that previously just weren't feasible.

As the isocyanate distribution was the limiting factor within this study Chapter 8 focused on determining the various parameters that influence the materials ability to mix. The first thing defined was the various mixing mechanisms; in literature micro-mixing is mentioned for fluids [Bickley et al, 2009], and debonding is used for powders [Lucon, 2009]. Four different mechanisms were observed in this literature; the micro- and macro-mixing, the volcano effect and debonding. These mixing mechanisms have different properties and are only effective for certain materials. Experimentation tracking the mixing of a range of powders and liquids proved that the most efficient mixing combination was utilising both the macro- and micro-mixing mechanisms; the sample would distribute the two phases throughout the bulk material but localised mixing helped ensure that the sample was consistent on a finer scale.

When processing explosives, mixing has to be conducted remotely, as such indicators were identified to determine whether mixing was occurring when operating the mixer remotely. The experiment demonstrated that a variation in frequency and an increase in temperature and power input coincides with sample mixing. As the sample mixes it will cause the frequency of the system to vary, which is linked to a variation in the power input required to deliver a set acceleration. As the sample flows, the material will experience internal friction which causes a significant temperature increase.

In Chapter 4.3 there is a diagram that indicates the influence of acceleration on RAM mixing; too low and the material will not flow and too high and the material will debond. The next stage of experimentation determined the impact on how the sample mixes with varying mass, vacuum and acceleration. As expected, the greater the mass the greater the acceleration required. The impact of vacuum was highlighted as material would not flow without sufficient vacuum; this can also be seen indirectly in literature [Davey et al, 2019] where samples mixed without vacuum had a high level of variation. The acceleration experiments demonstrated that

a sufficient acceleration was required to force the material to flow; mixing at 10 G did not produce a consistent material after 10 minutes, whereas the 35 and 70 G did.

# 10 Conclusion

This study investigated the influence of resonant acoustic mixing on energetic materials. RAM is a novel mixing method for explosives which utilises acoustic waves to initiate flow within a sample sealed in a mix vessel. It was divided into three research areas; the first investigated the effect on inert materials based on composite propellants and polymer bonded explosives. Starting with simplistic two-phase composites consisting of HTPB and melamine, the samples underwent a range of testing with an emphasis on mechanical behaviour. Testing included DMA to characterise the low strain rate behaviour at a range of temperatures, DSC to determine thermal transition points, density to determine the packing of the material, SHPB to understand the high strain rate mechanical behaviour and moisture diffusion to begin to identify any impact on the ageing behaviour.

The HTPB-Melamine samples, in Chapter 3, had consistent thermal behaviour, but variation in the mechanical performance for the highly loaded samples due to variable curing. The NMR results demonstrated inconsistent extractable HTPB concentration, proving that the isocyanate was not properly distributed. The HTPB-Melamine- Barium Sulphate samples, in Chapter 4, had consistent mechanical and thermal behaviour as well as consistent density. With the addition of the plasticiser, in Chapter 5, the samples had consistent low strain rate mechanical properties and consistent moisture permeation, but exhibited improve high strain rate mechanical behaviour when mixed via LabRAM. The full inert compositions, in Chapter 6, had variation in the mechanical properties, both at low and high strain rates, which was accompanied by greater extractable HTPB concentration for the RAM samples. The thermal characterisation, density measurements and moisture permeation remained consistent. With the inert compositions, mixing via RAM did not have any significant impact on the material or its behaviour. When variation occurred, it was due to poor isocyanate distribution throughout the sample and subsequently poor curing.

The second phase, in Chapter 7, mixed and tested energetic material. The samples had 0.80 RDX loadings and underwent similar characterisation as the inert material with additional functionality tests. The functionality, mechanical and thermal behaviour was not altered by the mixing method. The extractable HTPB concentration, again, was affected with the LabRAM samples having less extractable HTPB, indicating inhomogeneity within the sample and inconsistent cross-linking of the binder. This variation was significant but did not impact any other behaviour of the material. Further detail on this testing and conclusions can be found in the individual chapters.

Due to the poor distribution of isocyanate within the material, research was conducted on diffusion of material and identifying the impact of variables on the mixing, in Chapter 8. The first set of research identified mixing indicators to determine whether mixing occurred when operated remotely. Using a slurry consisting of a low viscosity binder and pre-dispersed filler, recorded observations were compared with the mix diagram. There was a correlation between temperature increase, frequency fluctuation, an increase in power input required and flow within the sample. These indicators informed the following stages of research. Additional experimentation demonstrated that an increase in mass required increased energy to initiate flow and induce mixing. It also demonstrated the requirement of initiation points to induce mixing or flow through the determination of the go/no-go zones with vacuum. Finally, research was conducted on the mixing mechanisms for various materials. The small grain sized material used the micro-mixing mechanisms between phase interfaces to distribute material throughout the sample, whereas the large grain sizes depended on the macro-mixing within the sample.

As stated, this study was a comparison to determine if mixing with RAM had an impact on the material, so the planetary mixing methodology was applied directly to the RAM mixes. When processing via planetary mixing, isocyanates are the last addition due to limited pot life of curing material. Once added the sample will exhibit a gradual increase in viscosity reducing the processing capability, and if left, can cure within the pot. RAM has significantly shorter timescales enabling isocyanate to be added earlier in the mix process. The variation found throughout this study was as a result of poor curing caused by poor isocyanate distribution. This is a procedural artefact which will be optimised with continued use of the RAM.

This body of research has proved that resonant acoustic mixing has not impacted the material, and that processing these materials with either mix methods can be used interchangeably with no impact.

# 11 Future Work

As with all research, there was an aim for this study to be as comprehensive as possible; however, this is not always feasible. Future work is an area that needs to be addressed and this study identifies recommendations for further research.

1. The high strain rate experimentation is dominated by the sample size and shape. A decision was made to not machine these samples, due to the time and cost impact. As such, the samples were prepared by hand which can cause variability in size and shape. It is expected that greater consistency in sample size will reduce the spread in high strain rate results. As such, it would be of value to test machined samples.
2. This study focused on polymer bonded composites; nitrate ester based propellants and pyrotechnics did not feature and this study should be repeated for these materials. These materials are different, and although the results from this study suggests that there will not be an impact, there is no published evidence to support that. An emphasis should be made on the ageing behaviour, particularly with propellants.
3. Having proven that the LabRAM does not significantly impact the material, ensuring the product is consistent is the next technical challenge. Continuation of the mix theory research in Chapter 8 with an emphasis on appropriate mix parameters is recommended. As highlighted previously, in order to conduct a fair comparison between planetary mixing and LabRAM, methodology was kept consistent. Research was conducted to try and address the issues regarding methodology and mix theory with the LabRAM, but further research should be undertaken. A recommendation is made to focus on areas such as material addition and optimisation of mix parameters.
4. The research conducted in this study utilised the LabRAM which has less than 1 kg mix capability. To be able to use this in an industrial setting, a scale up study should be conducted. Initial research [Coguill et al, 2014] demonstrated that although the material was mixed in similar time scales on the LabRAM, RAM 5 and RAM 55, there was greater consistency in mechanical behaviour when the sample was mixed by LabRAM. Ensuring that this technique scales up without having a detrimental effect on the quality is important; quality assurance is still within its infancy for this technique. Additionally, thought needs to be given to the implementation; facility set up, environmental impact, and health and safety procedures would need to be developed.

# 12 References


Aaker, P.E. 2017. Material Engineering Expert. [online] Engineering Services LP. Available at: http://www.engineering-experts.com/materials-casting-engineering-expert.html [Accessed Jan. 2017].

Agrawal, J.P. 2010. High Energy Materials. Wiley-VCH.

Akhavan, J. 2012. The chemistry of explosives. Cambridge: Royal Soc. Of Chemistry.

am Ende, D.J., Anderson, S.R., Salan, J.S., 2014. Development and Scale-Up of Cocrystals Using Resonant Acoustic Mixing. Organic Process Research & Development 18, 331–341.

Andrews, M.R., Collet, C., Wolff, A., Hollands, C., 2020. Resonant Acoustic Mixing: Processing and Safety. Propellants, Explosives, Pyrotechnics 45, 77–86.

Antic, G., Dzingalasevic, V., 2003. Cast composite explosives based on hexogen with the maximum detonation parameters. Scientific Technical Review 3.

Balzer, J.E., Siviour, C.R., Walley, S.M., Proud, W.G., Field, J.E., 2004. Behaviour of ammonium perchlorate-based propellants and a polymer-bonded explosive under impact loading. Proceedings of The Royal Society of London A, 781–806.

Banerjee, B., Adams, D.O., 2002. Micromechanics-Based Prediction of Thermoelastic Properties of High Energy Materials. Presented at the 15th ASCE Engineering Mechanics Conference, Columbia University, New York, NY.

Barnwell.co.uk. 2019. Shore A Hardness / What is a Shore A Hardness and why is it important? : Barnwell. [online] Available at: https://www.barnwell.co.uk/shore-a-hardness/

Beckstead, M.W., Puduppakkam, K., Thakre, P., Yang, V., 2007. Modeling of combustion and ignition of solid-propellant ingredients. Progress in Energy and Combustion Science 33, 497–551.

Bickley, J,. 2009. Resonant Acoustic Mixing RAM Technical White Paper, Resodyn Acoustic Mixers, 2009

Bluestone, S., Heister, S.D., Son, S.F., Austin Jr, B.L., 2010. Development of Composite Solid Propellants Based on Dicyclopentadiene Binder. Presented at the 46th AIAA/ASME/SAE/ASEE Joint Propulsion Conference & Exhibit, Nashville, TN.

Bohn, M.A., Cerri, S., 2010. Ageing behaviour of composite rocket propellent formulations investigated by DMA, SGA and GPC, in: International Progress in Insensitive Munitions and Eneretic Materials. Presented at the NDIA 2010 Insensitive Munitions and Energetic Materials Technology Symposium, Munchen, Germany.

Callister Jr, W.D. 2007. Materials Science and Engineering An Introduction. John Wiley & Sons Inc.

Cegla, M., Zmywaczyk, J., Koniorczyk, P., 2018. Thermo-mechanical analysis of heterogeneous solid rocket propellant. WITU 147, 105–121.

Charles Ross & Son. 2011. For the Production of Low to High Viscosity Adhesives Applications.

chemringnobel.no. 2019. Chemring Nobel. [online] Available at: https://chemringnobel.no/produkter/base-products/hmx/ [Accessed May 2019].

chemringnobel.no. 2019b. Chemring Nobel. [online] Available at: https://chemringnobel.no/produkter/base-products/rdx/ [Accessed May 2019(b)]

Coguill, S.L., Farrar, L.C., 2014. Resonant acoustic mixing of PBX. 40th International Pyrotechnics Seminar

Coguill, S.L., Martineau, Z.R., 2012. Vessel geometry and fluid properties influencing mix behaviour of resonant acoustic mixing processes. The 38th International Pyrotechnics Seminar.

Cooke, E.D., Beckel, E.P., Anderson, P.E., Paraskos, A.J., 2016. Optimizations of High Energy Explosives Utilizing JMP. Presented at the JMP Discovery Summit, Cary, NC.

Cray Valley, accessed 2018. Hydroxyl-Terminated Polybutadiene Resins and Derivatives- Poly bd and Krasol.

Daniel, M.A., 2006. Polyurethane Binder Systems for Polymer Bonded Explosives (No. DSTO-GD-0492). Weapons Systems Division, Defence Science and Technology Organisatio, Australian Government, Department of Defence.

Daumann, B., Nirschl, H., 2008. Assessment of the mixing efficiency of solid mixtures by means of image analysis. Powder Technology 182, 415–423.

Davenas, A. 1993. Solid rocket propulsion technology. Oxford: Pergamon Press.

Davey, R.J., Wilgeroth, J.M., Burn, A.O., 2019. Processing Studies of Energetic Materials using Resonant Acoustic Mixing Technology. Presented at the IMEMTS, BAE Systems Land UK, Seville.

Defence Ordnance Safety Group. 2019. Energetic Materials Testing and Assessment Policy Committee Manual of Tests.

Dey, A., Sikder, A.K., Athar, J., 2017. Micro-structural Effect on Hydroxy Terminated Poly Butadiene (HTPB) Prepolymer and HTPB Based Composite Propellant. Molecular Nanotechnology & Nanomedicine 1.

Drodge, D.R., Williamson, D.M., 2015. Understanding damage in polymer-bonded explosive composites. Journal of Materials Science 51, 668–679.

du Plessis, R. 2016. Resonant Acoustic Mixing- Small scale and scale-up. SSSG Early Careers Symposium

Edward, P.L., Atiemo-Obeng, V.A. and Kresta, S.M. 2004. Handbook of Industrial Mixing: Science and Practice.

Ehrenstein, G.W., Riedel, G. and Trawiel, P. (2004). Thermal analysis of plastics: theory and practice. Hanser Gardner Publications.

Fan, J.T., Weerheijm, J., Sluys, L.J., 2015. Dynamic compressive mechanical response of a soft polymer material. Materials and Design 79, 73–85.

Fenner, R.T. 1970. Extruder Screw Design. The Plastics Industry.

Gill, P. 2015. Manufacturing and Material Properties of Explosives, lecture notes, Cranfield University Defence Academy of the United Kingdom, delivered 12-16 October 2015

Hamshere, B.L., Lochert, I.J., Dexter, R.M., 2003. Evaluation of PBXN-109: the Explosive Fill for the Penguin Anti-Ship Missile Warhead (No. DSTO-TR-1471). Weapons Systems Division, Defence Science and Technology Organisation, Australian Government, Department of Defence.

Hardnesstesters.com. 2016. Hardness Testing Basics. [online] Available at: https://www.hardnesstesters.com/test-types/hardness-testing-basics.

Harnby N and Al, E. 1992. Mixing in the process industries. Oxford: Butterworth-Heinemann.

HBM. 2017. Split-Hopkinson Bar Material Tests. [online] Available at: https://www.hbm.com/en/2996/split-hopkinson-bar-material-tests/ [Accessed 1 August 2017].

Hope, K.S., Lloyd, H.J., Ward, D., Michalchuk, A.A.L., Pulhman, C.R., 2015. Resonant Acoustic Mixing: Its applications to energetic materials. Presented at the New Trends in Research of Energetic Materials, Czech Republic.

Hse.gov.uk. 2019. ATEX and explosive atmospheres - Fire and explosion. [online] Available at: https://www.hse.gov.uk/fireandexplosion/atex.htm.

Humboldt Universitat zu Berlin, 2015. Investigation of Polymers with Differential Scanning Calorimetry. Humboldt Universitat zu Berlin, Mathematisch-Naturwissenschaftliche Fakultat I Institut fur Physik.

Ide, K.M., n.d. Thermal and Fracture Behaviour of Rocket Motor Materials (PhD). University of Adelaide.

Inchem.org. 2019. In Chem Melamine. [online] Available at: https://www.inchem.org/documents/sids/sids/108781.pdf. [Accessed April 2019].

ITA Labs. 2019. Pycnometry | ITA Labs UK. [online] Available at: https://www.italabs.co.uk/services/pycnometry/ [Accessed April 2019]

Jordan, J.L., Montainge, D., Gould, P., Neel, C., Sunny, G., Molek, C., 2016. High Strain Rate and Shock Properties of Hydroxyl-Terminated Polybutadiene (HTPB) with Varying Amounts of Plasticizer. Journal of Dynamic Behavior of Materials 2, 91–100.

Kang, T.G., Ahn, S., Chung, S.H., Chung, S.T., Kwon, Y.S., Park, S.J., German, R.M., 2012. Modeling and simulation of metal injection molding (MIM), in: Handbook of Metal Injection Molding. Woodhead Publishing Limited, pp. 197–234.

Keeler, J., 2002. Understanding NMR Spectroscopy. Wiley, University of Cambridge, Department of Chemistry.

Kimura, T., Moriya, S., Takahashi, M., 2017. Effects of Cu-alloy Material Properties on Lifetime of a Combustion Chamber with or without a Thermal Barrier Coating. Presented at the 7th European Conference for Aeronautics and Space Sciences (EUCASS), Milan.

Lattin, W., Arbon, R., Bickley, J., Lucon, P., 2010. Acoustic mixing and treatment of organic waste Results of proof of principle.pdf. Presented at the WM2010, Phoenix, Arizona.

Leung, D.H., Lamberto, D.J., Liu, L., Kwong, E., Nelson, T., Rhodes, T., Bak, A., 2014. A new and improved method for the preparation of drug nanosuspension formulations using acoustic mixing technology. International Journal of Pharmaceutics 473, 10–19.

Li, M., Dave, R.N., Bilgili, E., 2015. An Intensified Vibratory Milling Process for Enhancing the Breakage Kinetics during the Preparation of Drug Nanosuspensions. AAPS PharmSciTech 17.

Liang, J., Zhan, Z., Yang, Y., Li, X., Shi, T., 2016. A numerical investigation of the effects of blade's geometric parameters on the power consumption of the twin-blade planetary mixer. Advances in Mechanical Engineering 8, 1–12.

Liu, Z.-K., Shang, S.-L., Wang, Y., 2017. Fundamentals of Thermal Expansion and Thermal Contraction. Materials 10.

Lucon, P., Farrar, L.C., 2009. Low frequency acoustic mixing of complex and multiphase systems. Resodyn Acoustic Mixers.

Mahanta, A.K., Pathak, D.D., 2012. HTPB-Polyurethane: A Versatile Fuel Binder for Composite Solid Propellant, in: Zafar, F. (Ed.), Polyurethane. InTech.

Matthews, G. 1982. Polymer Mixing Technology. Applied Science Publishers.

Matweb.com. 2019. Shore Durometer Hardness Testing of Rubber and Plastics. [online] Available at: http://www.matweb.com/reference/shore-hardness.aspx.

Menard, K.P. 2002. Dynamic Mechanical Analysis, A Practical Introduction. CRC Press.

Merck Sharp & Dohme Corp. 2015. Medical Milling Process for the Manufacture of Active Pharmaceutical Ingredients in Propellants.

Ministry of Defence. 2006. Environmental Handbook for Defence Materiel.

Molina-Jorda, J.M., 2015. Nano- and micro- / meso- scale engineered magnesium diamond composites: Novel materials for emerging challenges in thermal management. Acta Materialia 96, 101–110.

Mol-Instincts. (2017). Antioxidant 2246 Structure - C23H32O2 - Over 100 million chemical compounds. [online] Available at: https://www.molinstincts.com/structure/Antioxidant-2246-cstr-CT1000766117.html [Accessed 2017]

Mukdadi, O. 2004. Biomedical Ultrasound. [online] Available at: http://www.colorado.edu/MCEN/MCEN4228/index_files/biomedicalultrasound.pdf.

Musanic, S.M., Suceska, M., 2013. Dynamic Mechanical Properties of Artificially Aged Double Base Rocket Propellant and the Possibilities for the Prediction of Their Service Lifetime. Central European Journal of Energetic Materials 10, 225–244.

Muthaiah, R., Manjari, R., Krishnamurthy, V.N., Gupta, B.R., 1993. Rheology of HTPB propellant: Effect of mixing speed and mixing time. Defence Science Journal 43, 167.

Muthiah, R., Krishnamurthy, V.N., Gupta, B.R., 1996. Rheology of HTPB Propellant: Development of Generalized Correlation and Evaluation of Pot Life. Propellants, Explosives, Pyrotechnics 21, 186–192.

NATO Standardization Agency. 2008. Explosives, Nitrocellulose Based Propellants, Stability Test Procedures And Requirements Using Stabilizer Depletion.

Naval Sea Systems Command. 1993. Explosive, Plastic-Bonded, Cast PBXN-109.

Naval Sea Systems Command. 2002. Explosive, Plastic-Bonded, Cast PBXN-110.

NavSea, 2015. RAM Technology provides Safer and Cheaper Manufacturing of Energetic Materials (No. A2575). NavSea.

Nellums, R.R., Terry, B.C., Tappan, B.C., Son, S.F., Groven, L.J., 2013. Effect of Solids Loading on Resonant Mixed Al-Bi2 O3 Nanothermite Powders. Propellants, Explosives, Pyrotechnics 38, 605–610.

Nelson, A., Cross, T., 2012. Processing Benefits of Resonance Acoustic Mixing on High Performance Propellants and Explosives.

Osorio, J.G., Muzzio, F.J., 2015. Evaluation of resonant acoustic mixing performance. Powder Technology 278, 46–56.

Patil, M.S., Singh, H., 1988. Ballistic and mechanical properties of HTPB based composite propellants. Journal of hazardous materials 19, 271–278.

Perez, D., Ramohalli, K., 1990. A Scientific Approach to Composite Propellant Processing. Presented at the American Institute of Aeronautics and Astronautics 26th Joint Propulsion Conference, Orlando, Florida.

PerkinElmer, 2014. Differential Scanning Calorimetry (DSC), A Beginner's Guide, Frequently Asked Questions.

PerkinElmer, 2018. Thermogravimetric Analysis (TGA).

Peterson, P.D., Fletcher, M.A., Roemer, E.L., 2003. Influence of Pressing Intensity on the Microstructure of PBX 9501. Journal of Energetic Materials 21, 247–260.

Prakash, V., Phadke, V.K., Sinha, R.., Singh, H., 2004. Influence of Aluminium on Performance of HTPB-based Aluminised PBXs. Defence Science Journal 54, 475–482.

Provatas, A., 2003. Formulation and Performance Studies of Polymer Bonded Explosives (PBX) Containing Energetic Binder Systems. Part I. (No. DSTO-TR-1397). Weapons Systems Division, Defence Science and Technology Organisation, Australian Government, Department of Defence.

Pslc.ws. 2019. Differential Scanning Calorimetry. [online] Available at: https://pslc.ws/macrog/dsc.htm. [Accessed 31 August 2017]

PubChem. 2019(b). [online] Nih.gov. Available at: https://pubchem.ncbi.nlm.nih.gov/compound/barium_sulfate [Accessed April 2019].

PubChem. 2019. Melamine. [online] pubchem.ncbi.nlm.nih.gov. Available at: https://pubchem.ncbi.nlm.nih.gov/compound/melamine [Accessed January 2019].

Quincot, G., Azenha, M., Barros, J., Faria, R., 2011. Use of salt solutions for assuring constant relative humidity conditions in contained environments (No. PTDC/ECM/099250/2008). Fundacao para a Ciencia e a Tecnologia, Ministerio de ciencia, tecnologia e ensino superior.

Rawlinson, C., 2006. Differential Scanning Calorimetry "Cooking with Chemicals."

Resodyn Acoustic Mixers, 2010. Resonant acoustic mixing for lithium ion battery manufacture. Resodyn Acoustic Mixers.

Resodyn Acoustic Mixers. 2016. Home. [online] Available at: https://resodynmixers.com [Accessed 2016].

Resodyn Acoustic Mixers. 2017. How RAM Mixes. [online] Available at: http://resodynmixers.com/technologies/ [Accessed January 2017].

Ripani, E., Frioni, M., Marcelli, G., Squeo, E.A., Cianfanelli, S., Lillo, F., 2017. Dynamical Characterization of Propellant using the DMA. Presented at the 7th European Conference for Aeronautics and Space Sciences (EUCASS), Politecnico di Milano - Campus Bovisa Milano.

Rumeau, N., Threlfall, D., Wilmet, A., 2015. Resonant acoustic mixing Processing and formulation challenges for cost effective manufacturing. Roxel.

Sigmaaldrich.com. 2016. DOS. [online] Available at: https://www.sigmaaldrich.com/catalog/product/sial/84818?lang=en&region=GB [Accessed 2016]

Sigmaaldrich.com. 2016b. Isophorone diisocyanate 317624. [online] Available at: https://www.sigmaaldrich.com/catalog/product/aldrich/317624?lang=en&region=US [Accessed 2016].

Simić, D., Petković, J., Milojković, A., Brzić, S., 2013. Influence of Composition on the Processability of Thermobaric Explosives. Scientific Technical Review 63, 3–8.

Singh, P.P., Bhattacharya, B., 2015. Application of Twin Screw Extrusion for Continuous Processing of Energetic Materials. Central European Journal of Energetic Materials 12, 507–522.

Sinha, Y.K., Sridhar, B.T.N., Santhosh, M., 2015. Thermal decomposition study of HTPB solid fuel in the presence of activated charcoal and paraffin. Journal of Thermal Analysis and Calorimetry 119, 557–565.

Smith, P.C., Dahlberg, J., Huf, J.P., Williams, C.A., 2019. Rocket Propellant comparison_ Traditional planetary mixing and resonant acoustic mixing.

Sritharan, K., Strobl, C.J., Schneider, M.F., Wixforth, A., Guttenberg, Z., 2006. Acoustic mixing at low Reynold's numbers. Applied Physics Letters 88, 054102.

Sturman, R., 2012. The Role of Discontinuities in Mixing, in: Advances in Applied Mechanics. pp. 51–90.

Substech.com. 2020. [online] Available at: https://www.substech.com/dokuwiki/lib/exe/fetch.php?cache=cache&media=powder_pressing.png [Accessed April 2020].

Tadros, T.F. 2013. Emulsion Formation and Stability. Wiley-VCH.

Tanaka, R., Takahashi, N., Nakamura, Y., Hattori, Y., Ashizawa, K., Otsuka, M., 2017. In-line and Real-time Monitoring of Resonant Acoustic Mixing by Near-infrared Spectroscopy Combined with Chemometric Technology for Process Analytical Technology Applications in Pharmaceutical Powder Blending Systems. Analytical Sciences, The Japan Society for Analytical Chemistry 33.

Tanaka, R., Takahashi, N., Nakamura, Y., Hattori, Y., Ashizawa, K., Ostuka, M., 2016. Verification of the mixing processes of the active pharmaceutical ingredient, excipient and lubricant in a pharmaceutical formulation using a resonant acoustic mixing technology. RSC Advances 6, 87049–87057.

Teipel, U. 2005. Energetic Materials. Wiley VCH.

Tekchandaney. 2012. Mixing expert : Mixer Design for Explosives and Composite Propellants. [online] Available at: http://mixing-expert.com/mixer-design/. 22 August 2012

Tucker, J., 2012. A whole life assessment of extruded double base propellants (PhD). Cranfield University.

Turker, L., 2016. Thermobaric and enhanced blast explosives (TBX and EBX). Defence Technology 12, 423–445.

UNEP Publications (2019). SIDS INITIAL ASSESSMENT PROFILE Melamine, STRUCTURAL FORMULA CONCLUSIONS AND RECOMMENDATIONS. [online] Available at: http://www.inchem.org/documents/sids/sids/108781.pdf [Accessed January 2019].

Vadhe, P.P., Manickam, S., Rahujade, N., Kondra, A., Prasad, U., Sinha, R.K., 2015. Studies on Tungsten Based High Density Cast Polymer Bonded Explosive (PBX) Formulations. Central European Journal of Energetic Materials 12, 497–506.

Vanarase, A., Osorio, J., Muzzio, F.J., Coguill, S.L., Lucon, P., 2010. Resonant acoustic mixing Uniform distribution of minor materials during powder mixing.pdf. Presented at the JANNAF 36th Propellant and Explosives Development and Characterization Joint Subcommittee Meeting.

Wani, V., Mehilal, M., Jain, S., Prakash, P., Bhattacharya, B., 2012. Studies on the Influence of Testing Parameters on Dynamic and Transient Properties of Composite Solid Rocket Propellants Using a Dynamic Mechanical Analyzer. Journal of Aerospace Technology and Management 4, 443–452.

Watt, D.S., Cliff, M.D., 1998. TNAZ Based Melt-Cast Explosives: Technology Review and AMRL Research Directions (No. DSTO-TR-0702). Weapons Systems Division, Defence Science and Technology Organisation, Australian Government, Department of Defence.

web.calce.umd.edu. 2018. Hardness. [online] Available at: https://web.calce.umd.edu/TSFA/Hardness_ad_.htm [Accessed June 2018].

Webb, S., 2014. Acoustic mixing forms cocrystals. C&EN.

Wilgeroth, J. M., Davey, R. J., Burn, A. O., 2018, Resonant, in-case mixing of a polymer-bonded explosive shaped charge, BAE Systems, Land UK, 2018

Wingborg, N., 2004. Improving the mechanical properties of composite rocket propellants. Stockholm, Department of Fibre and Polymer Technology, Royal Institute of Technology.

www.chemicalbook.com. 2019. Ammonium perchlorate | 7790-98-9. [online] Available at: https://www.chemicalbook.com/ChemicalProductProperty_EN_CB9259751.htm [Accessed May 2019].

www.gordonengland.co.uk. 2017. Hardness Testing. [online] Available at: https://www.gordonengland.co.uk/hardness/ [Accessed 25/08/2017].

www.labdepotinc.com. 2019. Archimedes' Principle and Density Determination. [online] Available at: https://www.labdepotinc.com/articles/archimedes-principles.html [Accessed May 2019].

www.omega.com. 2018. Resources. [online] Available at: https://www.omega.com/temperature/z/pdf/z103.pdf [Accessed 1 May 2018].

Xiao, Y., Sun, Y., Wang, Z., Xu, Z., Su, T., 2017. Uniaxial Dynamic Compressive Properties of HTPB Casting Explosives. Presented at the 21st International Conference on Composite Materials.

Zhang, W., Tian, Y., Zhou, H., Yang, Z., Luo, G., Zong, H., 2008. Process Monitoring of Cast Explosive Solidification Molding by on-line Multichannel Ultrasonic Measurement. Presented at the 17th World Conference on Nondestructive Testing, Shanghai, China.